The Hydrodynamics of Gulf St. Vincent, South Australia

Henry Charles Powell Ellis
Adelaide University Shool of Mathematical Sciences

May 2019

page left blank intentionally

Copyright and DAI Statement

'I hereby grant the University of Adelaide or its agents the right to archive and to make available my thesis or dissertation in whole or part in the University libraries in all forms of media, now or here after known, subject to the provisions of the copyright act 1968. I retain all property rights, such as patent rights. I also retain the right to use in future works (such as articles or books) all or part of this thesis or dissertation.

I also authorise University Microfilms to use the 350 word abstract of my thesis in Dissertation Abstracts International.

I have either used no substantial portions of copyright material in my thesis or I have obtained permission to use copyright material; where permission has not been granted I have applied/will apply for a partial restriction of the digital copy of my thesis or dissertation.'

Signed:

Date: 28/05/2019

Authenticity Statement

'I certify that the Library deposit digital copy is a direct equivalent of the final officially approved version of my thesis. No emendation of content has occurred and if there are any minor variations in formatting, they are the result of the conversion to digital format.

Signed:

Date: 28/05/2019

Originality Statement

I certify that this work contains no material which has been accepted for the award of any other degree or diploma in my name, in any university or other tertiary institution and, to the best of my knowledge and belief, contains no material previously published or written by another person, except where due reference has been made in the text. In addition, I certify that no part of this work will, in the future, be used in a submission in my name, for any other degree or diploma in any university or other tertiary institution without the prior approval of the University of Adelaide and where applicable, any partner institution responsible for the joint-award of this degree.

I give permission for the digital version of my thesis to be made available on the web, via the University's digital research repository, the Library Search and also through web search engines, unless permission has been granted by the University to restrict access for a period of time.

I acknowledge the support I have received for my research through the provision of an Australian Government Research Training Program Scholarship

Signed:

Date: 28/05/2019

Dedication

Dedicated to Evie Jean Ellis, the light of my life, and her beautiful mother Ria.

Acknowledgments

There are many people I wish to thank for their support and advice throughout the course of my project.

First and foremost I would like to thank my beautiful wife Ria, who not only supported me wholeheartedly in quitting my previous job to pursue extra studies, but also financially and emotionally supported me throughout the entire process. Without her support, material and emotional, I would never have been able to complete this project.

Secondly I would like to thank John Middleton, my principle supervisor, who not only encouraged me to pursue this project but also lent his extensive knowledge and expertise throughout.

John Luick provided immense practical programming and modeling knowledge making the learning process involved, which can often be a daunting process, much smoother.

Trent Mattner, my internal Adelaide University supervisor, provided invaluable 'outsider' critique and general numerical modeling advice.

Charles James at SARDI was a constant source of coding and modeling support and helped expand my understanding of ROMS and modeling in general exponentially.

Finally, the entire expanded oceanography team at SARDI, who made me feel right at home from day one and provided as a good working environment as anyone could ask for.

Abstract

The hydrodynamics of Gulf St. Vincent (GSV) are investigated through the use of several numerical models based on the Regional Ocean Modeling Suite (ROMS). Idealised models which investigate tides, wind forcing and thermohaline forcing are undertaken, as well as a fully forced qausi-realistic hindcast model. The model domain encompasses Investigator Strait, GSV and Backstairs Passage, as well as some of the shelf to the south-east.

The tidal model incorporates a new method for estimating the quadratic coefficient of drag which accounts for depth and benthic type. Results of the tidal model indicate that the presence of seagrass meadows are significant for bottom friction and the estimation of tidal elevations and currents. This is a particularly important result for GSV, as the health and distribution of seagrass meadows is a key environmental factor.

The idealised wind-forced and geostrophically adjusted models indicate that the wind-stress direction and magnitude is critical in determining the connectivity of the gulf with the shelf, where thermohaline circulation is less important. Results of the idealised models indicate that during summer, when winds are dominated by south-easterlies, gulf waters are largely recirculated and salinity increases as a result. During winter the winds become dominated by south-westerlies, which induce a gulf wide clockwise circulation which draws in fresher shelf waters via Investigator Strait and expels salty gulf water via Backstairs Passage. A volume averaged salt balance for the quasi-realistic model supports this finding, indicating that salinity increases whilst under summer wind conditions and decreases for winter wind patterns. This is due to the excess of evaporation over precipitation year round.

Flushing time scales for summer and winter conditions are also explored based on the results of the quasi-realistic model, and indicate that the interior of the gulf is flushed more slowly during summer than winter. Investigator Strait and Backstairs Passage exhibit little seasonal variability. Passive Lagrangian float tracer studies are also conducted, and further support the finding that summer conditions show reduced connectivity between the shelf and gulf when compared to winter. In the weather band, periods of enhanced exchange between the shelf and gulf are shown to coincide with wind-stresses from the west, while periods of reduced exchange coincide with wind-stresses from the east.

page left blank intentionally

Contents

List of Figures **xi**

List of Tables **xv**

Nomenclature **xvi**

1 Introduction **1**

1.1 About Gulf St. Vincent 1

1.2 Existing Hydrodynamic Knowledge of Gulf St. Vincent 3

1.3 Objectives 5

1.4 Thesis Outline 5

1.5 Major Findings 6

2 Methods and the ROMS model **7**

2.1 The ROMS Model and Parameterisation 7

2.2 The High-Resolution Gulf St. Vincent Model (GSVM) Domain 8

2.2.1 Resolution 9

2.2.2 Open Boundaries 10

2.2.3 Topographic Data 10

2.3 The SAROM Parent Model 11

2.4 The BRAN 2015 Global Model 12

2.5 Available Data 12

3 Tidal Model **14**

3.1 Summary 14

3.2 Introduction 15

3.3 ROMS Configuration for the GSVM Tidal Model 15

3.4 Theoretical Considerations 16

3.4.1 Neap/Dodge Tides and Resonance 16

3.4.2 Bottom Friction: The Role of Benthos 17

3.5 Available Data and Tidal Model Validation (Method) 20

3.6 Tidal Model Validation (Results) 23

4 Wind Forcing **27**
4.1 Summary . . . 27
4.2 Introduction . . . 28
4.3 Barotropic Experiments . . . 30
4.3.1 Cross-Gulf South-Easterly (Summer) Wind-Stress . . . 30
4.3.1.1 Key Features . . . 30
4.3.1.2 Dynamics . . . 34
4.3.2 Up-Gulf SW (Winter) Wind-Stress . . . 38
4.3.2.1 Key Features . . . 38
4.3.2.2 Dynamics . . . 41
4.3.3 Net Transport via wind-stress . . . 44
4.4 Coastal Trapped Waves . . . 45
4.4.1 Summary . . . 45
4.4.2 Introduction . . . 45
4.4.3 Methods . . . 46
4.4.4 Results . . . 46

5 Geostrophically Adjusted Thermohaline Circulation **48**
5.1 Summary . . . 48
5.2 Introduction . . . 49
5.3 Summer Conditions . . . 49
5.3.1 Thermohaline Structure . . . 49
5.3.2 Depth-Integrated Density Distribution . . . 50
5.3.3 Sea Level . . . 51
5.3.4 Depth-Integrated Velocity . . . 53
5.4 Winter Conditions . . . 55
5.4.1 Thermohaline Structure . . . 55
5.4.2 Depth-Integrated Density . . . 55
5.4.3 Sea Level . . . 57
5.4.4 Depth-Integrated Velocity . . . 57
5.5 The Effect of Thermohaline Circulation on Connectivity . . . 60

6 The GSV Model: Methods, Validation and Physical Drivers **61**
6.1 Summary . . . 61
6.2 Introduction . . . 62
6.3 Model Configuration . . . 62
6.3.1 Initial Conditions . . . 62
6.3.2 Implementation of Boundary Forcing . . . 62
6.3.3 Local Forcing Surface Fluxes . . . 63
6.3.3.1 Wind-Stress Data . . . 63
6.3.3.2 Thermal Flux . . . 63
6.3.3.3 Salt Flux . . . 67
6.4 Model Calibration . . . 68
6.4.1 Bottom Friction Coefficients . . . 68

6.4.2 Heat Flux Calibration - SST Nudging . . . 68
6.5 Model Validation and Physical Drivers . . . 69
6.5.1 Daily Mean Animation: Introduction . . . 70
6.5.2 Validation - Filtered Currents: Tides Removed . . . 73
6.5.3 Sea Surface Height at Pt. Stanvac . . . 79
6.5.4 Temperature . . . 81
6.5.4.1 Weatherband . . . 81
6.5.4.2 Long Term . . . 82
6.5.5 Salinity . . . 85
6.5.5.1 Idealised Salt Model . . . 86

7 Connectivity and Flushing of GSV 88
7.1 Summary . . . 88
7.2 Seasonal Depth-Integrated Velocities . . . 89
7.2.1 Mean Depth-Integrated Summer Velocities . . . 89
7.2.2 Mean Depth-Integrated Winter Velocities . . . 91
7.3 Flushing Gulf St. Vincent: Small Local Scale . . . 93
7.4 Flushing of GSV: Large Scale . . . 97
7.4.1 Mechanism . . . 97
7.4.2 Long Term Salinity Balance . . . 99
7.5 Lagrangian Float Tracer Studies . . . 101
7.5.1 Seasonal Mean Depth-Integrated Velocity . . . 102
7.5.1.1 Mean Summer Depth-Integrated Flow: 1st December 2010 - 1st March 2011 . . . 102
7.5.1.2 Mean Depth-Integrated Flow: 1st June - 1st September . . . 106
7.5.1.3 Summer vs. Winter Results . . . 106
7.5.2 Quasi-Realistic 1.5 Daily Mean Velocity Fields . . . 110
7.5.2.1 Summer time Particle Distribution . . . 110
7.5.2.2 Winter time Particle Distribution . . . 112

8 Conclusions and Recommendations for Future Work 115
8.1 Key Findings . . . 115
8.1.1 Tidal Circulation . . . 115
8.1.2 Wind-stresses: The Dominant Force in Subtidal Circulation of GSV . . . 116
8.1.3 The Temperature Front: A False Flag . . . 116
8.2 Limitations and Future Work . . . 117
8.2.1 Flood Modeling . . . 117
8.2.2 Domain Extents . . . 117
8.2.3 Additional Connectivity and Flushing Studies . . . 117
8.2.4 Further Data Collection and Model Validation . . . 117

A Additional Tidal Modeling Results 118

B Additional Wind Modeling Results **129**
B.1 Additional Barotropic Experiments 129
B.2 Baroclinic Experiments 130
B.3 Coastal Trapped Waves 143

C Additional Geostrophic Modeling Results **145**
C.1 Mean Summer Cross Sections 145
C.2 Mean Winter Cross Sections 148

D Additional GSVM Calibration Information **151**

E Index of Electronic Appendix/DVD **153**

Bibliography **155**

List of Figures

1.1 Gulf St. Vincent location and key geographical features. 2

2.1 Domain extents and depths (m) for high-resolution Gulf St. Vincent ROMS model. 9
2.2 SAROM domain depth, GSV high-resolution model domain outlined. 11
2.3 BRAN model domain for southern Australian region depth, SAROM model domain outlined 12

3.1 Bottom type and dimensionless quadratic coefficient of drag distribution 20
3.2 Position of ANTT stations used in validation of the tidal GSVM 22
3.3 Sea level predictions at Pt. Stanvac for GSVM tidal model and ANTT data 25
3.4 Maximum simulated depth integrated tidal velocities for GSVM. 26

4.1 Mean summer and winter seasonal wind-stresses for GSV 28
4.2 Sea level for south-easterly cross-gulf (summer) wind-stress idealised model 31
4.3 Depth-averaged velocity field for south-easterly cross-gulf (summer) wind-stress idealised model 33
4.4 Force balance solutions for line B1-B2 for idealised SE (summer) wind-stress model 36
4.5 Dynamical force balance vector diagram for idealised SE (summer) wind-stress model . . 37
4.6 Sea level for south-westerly up-gulf (winter) idealised wind-stress model. 38
4.7 Velocity field for south-westerly up-gulf (winter) idealised wind-stress model. 40
4.8 Force balance solutions for line A1-A2 for SW (winter) idealised wind-stress model 42
4.9 Dynamical force balance vector diagram for idealised SW (winter) wind-stress model . . . 43
4.10 Transport across mouth of gulf (M1-M2) for idealised SE (summer) and SW (winter) wind-stress models 44
4.11 SSH and depth integrated velocity for GSV for passage of CTW 47

5.1 Thermohaline climate for mean summer conditions 50
5.2 Depth-integrated density anomaly for the mean summer conditions. 51
5.3 Geostrophically adjusted sea level for typical summer thermohaline structure. 52
5.4 Geostrophically adjusted depth-averaged flow field for mean summer conditions. 54
5.5 Thermohaline climate for mean winter conditions. 55
5.6 Depth-integrated density anomaly for mean winter conditions. 56
5.7 Geostrophically adjusted sea level for mean winter conditions. 57
5.8 Geostrophically adjusted depth-integrated velocity field for mean winter conditions. 59

6.1 Downward shortwave radiation transmission by Jerlov water types. Reproduced from Stewart (2006). The left panel indicates the transmittance of light of different wave lengths through 1 m of sea water. The right panel indicates the total amount of sunlight to reach given depths for different Jerlov water types. Type 9, or dark coastal water, is absorbed entirely within the first ∼5 m. 64
6.2 2011 Heat flux components and net heat flux for Pt. Stanvac 66
6.3 Daily mean evaporation, precipitation and resultant salt flux for Pt. Stanvac for 2011. . . 67
6.4 Temperature sensitivity to nudging strength (dQdSST) 69
6.5 Animation displaying the daily mean bottom salt (top left), bottom temperature (top right), speed and current direction (middle left), sea level (middle right) and domain averaged heat flux, salt flux and wind-stress (bottom 3 panels). Animation Location: Electronic Appendix/Daily Mean Animation.avi 71
6.6 Current axis orientation for Pt. Stanvac model and observation comparisons. 74
6.7 Time series comparison for Pt. Stanvac band pass filtered depth-integrated current velocity. 76
6.8 Mean Sea Level Pressure (MSLP) maps for (a) 19th August 2010 showing pressure gradients inducing SW winds, (b) 14th October 2010 showing pressure gradients inducing S winds and (c) 27th November 2010 showing pressure gradients inducing SE winds for GSV. Sourced from Bureau of Meteorology. 76
6.9 Monthly mean alongshore current velocities for the GSVM and observations at Pt. Stanvac 78
6.10 Weatherband sea level GSVM vs observations comparison for 2010 at Pt. Stanvac. 79
6.11 Seasonal sea level 2010-2011 time series comparison for Pt. Stanvac, Outer-Harbor and Pt. Giles, observations and GSVM. 81
6.12 Band pass filtered temperature anomaly for temperature observations from Pt. Stanvac and GSVM results. 82
6.13 Idealised model configuration 83
6.14 ROMS depth averaged temperature vs. idealised model predicted depth averaged temperature for several locations throughout GSV. 85
6.15 Salinity comparisons at Pt. Stanvac for GSVM results and SA Water observations. 87

7.1 Mean summer time depth-integrated velocity field. 90
7.2 Mean winter time depth-integrated velocity field. 92
7.3 Estimated flushing timescales for Summer. 95
7.4 Estimated flushing timescales for Winter. 96
7.5 Example of salt pulse expulsion from system under SW wind-stresses 98
7.6 2011 Volume averaged salt balance for GSV proper 100
7.7 Initial positions for the 10,000 Lagrangian floats used in LTRANS models. Zone 1 is the interior the gulf as defined by the line M1-M2 (Figure 1.1) with particles seeded in this zone shown as black. Zone 2 is the majority of the model domain, including the interior of the gulf (Zone 1). Particles which are seeded within Zone 2 but outside Zone 1 are shown in red. Model domain is outlined. 101
7.8 Animation displaying the paths and distribution of Lagrangian particles under a fixed, depth-integrated and seaonsally averaged flow field for summer time. Animation Location: Electronic Appendix/LTRANS animations/Seasonal Fixed Summer.avi 103

7.9 Percentage of particles with initial position within the gulf (Zone 1) remaining in Zone 1 (black line) and Zone 2 (red line) vs time in days for the fixed mean depth-integrated velocity field for summer. Slow decline in percentage for particles remaining in Zone 1 (black line) indicates weak connectivity between GSV and IS/BP. Extremely slow decline for Zone 2 (red line) indicates extremely weak gulf-shelf connectivity. 104
7.10 Particle distribution for summer using fixed mean depth-integrated velocity (see Figure 7.1) after 60 days of simulation time. A clear front is visible roughly across the mouth of the gulf, keeping intruding shelf waters and gulf waters separate. A weak outflow of gulf particles can be seen in the upper portion of IS. A small number of 'strait' particles can be seen to have made their way in to GSV proper. A high concentration of particles on the open boundary shows particles which have left the domain and become 'stuck' such that they do not re-enter the model. 105
7.11 Animation displaying the paths and distribution of Lagrangian particles under a fixed, depth-integrated and seaonsally averaged flow field for winter time. Animation Location: Electronic Appendix/LTRANS animations/Seasonal Fixed Winter.avi 107
7.12 Percentage of particles with initial position within the gulf (Zone 1) remaining in Zone 1 (black line) and Zone 2 (red line) vs time in days for fixed winter mean depth-integrated velocity field (see Figure 7.2). Steep decline in percentage for Zone 1 (black line) indicates strong connectivity for GSV and IS/BP. Matching decline for Zone 2 (red line) suggests strong gulf-shelf connectivity. 108
7.13 Particle distribution for winter using fixed mean depth-integrated velocity (see Figure 7.2) after 60 days of simulation time. Very few particles remain within IS and the southern coast of BP, indicating the strong intrusion and throughflow of shelf waters. A high concentration of particles on the open boundary (especially on the eastern boundary) shows particles which have left the domain and become 'stuck' such that they do not re-enter the model. 109
7.14 Animation displaying the paths and distribution of Lagrangian particles under a depth-integrated one and-a-half day mean flow field for summer time. Animation Location: Electronic Appendix/LTRANS animations/1.5 Daily Mean Summer.avi 111
7.15 LTRANS particle tracking for summer months and associated westerly wind-stress component. 112
7.16 Animation displaying the paths and distribution of Lagrangian particles under a depth-integrated one and-a-half day mean flow field for winter time. Animation Location: Electronic Appendix/LTRANS animations/1.5 Daily Mean Winter.avi 113
7.17 LTRANS particle tracking for winter months and associated westerly wind-stress component. 114

A.1 Sea level predictions for GSVM tidal model versus ANTT predictions for Ardrossan . . . 119
A.2 Sea level predictions for GSVM tidal model versus ANTT predictions for Cape Jervis . . 120
A.3 Sea level predictions for GSVM tidal model versus ANTT predictions for Edithburgh . . 121
A.4 Sea level predictions for GSVM tidal model versus ANTT predictions for Kingscote . . . 122
A.5 Sea level predictions for GSVM tidal model versus ANTT predictions for Outer Harbour 123
A.6 Sea level predictions for GSVM tidal model versus ANTT predictions for Peneshaw . . . 124
A.7 Sea level predictions for GSVM tidal model versus ANTT predictions for Port Giles . . . 125
A.8 Sea level predictions for GSVM tidal model versus ANTT predictions for Port Noarlunga 126

A.9 Sea level predictions for GSVM tidal model versus ANTT predictions for Pt. Stanvac . . 127
A.10 Sea level predictions for GSVM tidal model versus ANTT predictions for Port Vincent . 128

B.1 Velocity sea level fields for idealised barotropic wind-stress model under NE wind. 129
B.2 Velocity sea level fields for idealised barotropic wind-stress model under NW wind. 130
B.3 Water column profiles for temperature and salinity used in baroclinic wind-stress model initialisation 131
B.4 Sea level for south-westerly along-gulf wind-stress and stratified water column. 132
B.5 Depth-integrated velocity for south-westerly along-gulf wind-stress and stratified water column. 133
B.6 Force balance solutions on line A1-A2 for south-westerly along-gulf wind-stress and stratified water column. 134
B.7 Sea level for south-easterly cross-gulf wind-stress and stratified water column. 137
B.8 Depth-integrated velocity for south-easterly cross-gulf wind-stress and stratified water column. 138
B.9 Force balance solutions for line B1-B2 for south-easterly cross-gulf wind-stress and stratified water column. 139
B.10 Velocity sea level fields for idealised baroclinic wind-stress model under NE wind. 140
B.11 Velocity sea level fields for idealised baroclinic wind-stress model under NW wind. 140
B.12 Transport across mouth (line M1-M2) for baroclinic up-gulf and cross-gulf wind models. . 142
B.13 GSV sea level results for passage of a CTW. 144

C.1 Cross sections for mean seasonal summer temperature, salinity and density for section W1-W2. 146
C.2 Cross sections for mean seasonal summer temperature, salinity and density for section E1-E2. 147
C.3 Cross sections for mean seasonal winter temperature, salinity and density anomaly for section W1-W2. 149
C.4 Cross sections for mean seasonal winter temperature, salinity and density anomaly for section E1-E2. 150

D.1 Monthly mean, 10 yr climatology and nudging SST values for Pt. Stanvac 152

List of Tables

2.1 Model parameters common to all GSVM simulations. For full definitions and mathematical explanations please refer to Hedström (2010) 8

2.2 Sigma coordinate stretching parameters used within all GSV modeling. For full definitions and mathematical explanations please refer to Hedström (2010) . Please note that in reference to sigma coordinate stretching critical depth refers to the maximum allowable layer thickness before discretisation is required, rather than the ROMS definition of critical depth which refers to wetting and drying of a cell. 10

2.3 Observed data for Gulf St. Vincent used for model validation and calibration. 13

3.1 Benthic type quadratic drag multiplier value 19

3.2 Final values for tuning parameters used to calibrate tidal model. 19

3.3 Tidal model validation 24

6.1 Open boundary conditions for child model 62

Nomenclature

GSV - Gulf St. Vincent

GSVM - Gulf St. Vincent Model

SAROM - South Australian Regional Ocean Model

IS - Investigator Strait

BP - Backstairs Passage

SG - Spencer Gulf

KI - Kangaroo Island

CTW(s) - Coastal Trapped Wave(s)

SE - South Easterly wind (i.e. wind originating from the south east and blowing toward north west). This terminology is used for all winds, e.g. SW = wind from south west blowing north east

Chapter 1

Introduction

1.1 About Gulf St. Vincent

Gulf St. Vincent (herein known as GSV) is a shallow, semi-enclosed gulf located in South Australia (Figure 1.1). The topography of GSV is roughly triangular in shape, bounded at the mouth by Kangaroo Island (KI). GSV is connected to the shelf waters via Investigator Strait (IS) to the west and Backstairs Passage (BP) to the south east. IS is bordered on the northern shore by Yorke Peninsula, which resembles a foot with the heel on the gulf side and toe on the shelf side.

Taking a line from Cape Jervis to Edithburgh or 'the heel' as the mouth, GSV is approximately 120 km from mouth to head on the western coast, 160 km from mouth to the head on the eastern side and 60 km wide along the mouth. GSV gradually narrows toward the head. IS is approximately 40 km wide and quite uniform in width along its 70 km length, while BP is only around 14 km wide and 20 km long.

GSV is quite shallow, reaching a maximum depth of $\sim$ 40 m in a central basin to the north of Cape Jervis (see Figure 2.1). IS and BP reach maximum depths of approximately 50 m and 40 m respectively. GSV has an average depth of approximately 21m and area of 6,800 km^2, for total volume of approximately 143 km^3 (Bye & Kämpf, 2006).

GSV has few sources of freshwater, and none that contribute significant amounts of freshwater to the system on an ongoing basis (Pattiaratchi & Jones, 2005). Due to the excess of evaporation over precipitation, GSV is classed as an inverse estuary (Nunes et al., 1990; Kämpf et al., 2009), experiencing greater maximum salinity levels than the neighbouring shelf waters. GSV shares this property with neighbouring Spencer Gulf (SG) which lies to the west, and as such it has been widely assumed that GSV has many similar circulation properties to SG.



Figure 1.1: Gulf St. Vincent location and key geographical features. The gulf is bounded to west by Yorke Peninsula and to the south east by the Fleurieu Peninsula. Kangaroo Island restricts the mouth of the gulf to the south, and its presence creates Investigator Strait connecting the gulf and shelf to the west and Backstairs Passage in the south east. The line M1-M2 was chosen as the mouth, which separates the interior of the gulf (herein referred to as 'the gulf' or GSV) from IS/BP.

1.2 Existing Hydrodynamic Knowledge of Gulf St. Vincent

Gulf St. Vincent presents an interesting region for oceanographers as a partially obstructed inverse estuary, and has been the focus of many previous studies, chiefly focussing on tides and seasonal scale hydrodynamics. This thesis aims to fill gaps in the knowledge left by these previous studies.

The key studies to date which focus on GSV are outlined below, in addition to their shortfalls which are addressed by this thesis.

Kämpf et al. (2009) This study employs a three-dimensional COHERENS model forced with monthly mean climatology (as oppsed to 3 hourly within this thesis). The model and interrogation are focused on the distribution of brine discharge from a proposed desalination plant rather than the key drivers of circulation. Results of the study indicate that there is density driven discharge through both IS and BP, which is not found in the results of this thesis. The study also indicates the formation of a temperature front across the western end of IS during summer, which is supported by the results of this thesis.

Petrusevics (1993) This study is based on observations which indicate the presence of temperature front during summer at western end of IS in agreement with Kämpf et al. (2009) and this thesis.

Deltares (2016) In this technical report supplied by Deltares to SA Water, a high resolution non uniform three dimensional Delft model forced with 3 hourly meteorology is employed. The report is non peer-reviewed and focussed on seagrass health and habitat rather than key drivers of circulation. The report is centred around the Adelaide metropolitan coastline and uses data from single point (Adelaide airport) for wind-stress applied to entire domain. Crude boundary conditions are employed (no momentum exchange and spatially homogeneous temperature) which do not adequately represent the shelf dynamics.

Noye (1999) The Noye (1999) study was focused on the dispersion of prawn larvae due to advective and diffusive processes within the gulf for an 8 week period from late December as modelled by a three-dimensional model driven by tides and winds. The findings suggest larvae, seeded throughout the centre of the gulf, tend to settle in the north-western region of the gulf. The study also indicates that advective processes are much more important in particles distribution than diffusive. The study is however very limited in duration and does not include thermal fluxes of any kind. It also uses diurnal prawn larvae movement modelling rather than passive particles, which skews the interpretation of hydrodynamics via float distribution.

de Silva Samarasinghe (2003) This study employs a depth integrated model driven by monthly mean climatology over the summer-autumn period. Results suggest density driven circulation is strong due to high levels of evaporation in upper gulf resulting in dense waters and is in agreement with Kämpf et al. (2009) in regards to formation of temperature front during summer. This study suggests that the formation of a temperature front restricts density driven exchange between shelf and gulf, rendering circulation susceptible to wind-driven currents. Results of this thesis suggest that the temperature front is the result of wind-driven currents however. Results of this study show that under SW wind-stresses the gulf tends to a gulf-wide clockwise circulation, which is in agreement with the results of this thesis.

Sharobeam and Sag (1977) This study employes a depth-integrated model of short duration storm event to investigate sea surface height (SSH) under high wind-stress events. Results suggest that strong wind-stresses from SW induce large SSH set up in northern reaches of the gulf and gulf-wide clockwise circulation, in agreement with de Silva Samarasinghe et al. (2003) and this thesis.

Teixeira (2010) The Teixeira thesis employs a three dimensional ROMS model focused on circulation within Spencer Gulf, but the domain also includes GSV. However, no calibration for physical properties of GSV was made, only SG, nor was any detailed analysis of GSV results undertaken. The model results indicated limited connectivity between SG and GSV, showing potential for saline discharges from SG to enter GSV via IS under westerly wind-stresses.

Kämpf (2006) and Bye and Kämpf (2006) In this study two estimates of flushing times (the time taken to replace a body of water with 'fresh' oceanic water) using formulas and empirical data found the gulf to have flushing times of 3 and 4 months respectively. For upper regions of GSV the flushing timescales can be substantially longer.

Other published models were restricted to tidal forcing (Bowers et al., 1991), depth-integrated (de Silva Samarasinghe et al., 2003), conceptual (Sharobeam & Sag, 1977; Bowers et al., 1991), or are in non-peer reviewed technical reports focused on specific portions or processes in GSV (Pattiaratchi & Jones, 2005). There have also been coarser-resolution models of the larger South Australian shelf which included GSV but were not designed or validated for investigations of GSV (Middleton & Platov, 2003, 2005; Teixeira, 2010).

A recent review of the oceanography of Gulf St. Vincent (Kaempf & Bye , 2008) identified advective flushing of GSV as a major unresolved question and recommended hydrographic modeling as the means to address it.

Currently there is no information for the relationship between the hydrodynamics of the gulf and their influence on the biogeochemical balance within the gulf. This leaves unresolved questions about the sources and sinks of nutrients within the gulf and the lower trophic system. Anthropogenic sources of nutrients (such as storm water runoff and wastewater treatment discharge) and the fundamental role the lower trophic ecosystem plays in biogeochemical cycling on water quality and ecosystem health in the gulf remains unresolved. While this is not a key focus of study within this project, a better understanding of the physical hydrodynamics of GSV allows for much greater investigation in this area in the future.

Each chapter includes a self contained literature review and exploration of existing knowledge of the hydrodynamic porperties discussed.

1.3 Objectives

The project aims to achieve the following objectives:

- Create a functional high-resolution model of Gulf St. Vincent, the Gulf St. Vincent Model (GSVM);
- Couple this model with existing coarse-resolution model of the adjacent ocean;
- Calibrate and validate the GSVM with existing recorded oceanic data;
- Address the relative importance of physical drivers (e.g. wind, thermohaline, tides) on the circulation and flushing of the gulf; and
- Determine the roles of the expected summertime front in the lower GSV in reducing gulf-shelf connectivity.

The project aims, at a minimum, to answer the following research questions:

- What are the major ocean dynamics of Gulf St. Vincent? In particular, what are the horizontal momentum balances at sub-tidal frequencies, and what are the major drivers of horizontal and vertical exchange at different parts of the gulf?
- Does a summer time temperature front reduce exchange between GSV and the shelf, and if so to what extent?
- What are the major pathways, mechanisms and strength of winter time exchange with the shelf?
- What is the effect, if any, of Ekman transport in lower GSV and through IS and BP? If present, how important is this effect on the circulation of GSV and exchange of gulf waters with shelf waters?
- What are the practical implications of the thesis results for fisheries, industry, recreational users, local councils, and other users? For example, does it tell us anything about the population dynamics of certain marine species (e.g. larval dispersal) and the impact of anthropogenic sources (i.e. WWTP and desalination) on the gulf system?

1.4 Thesis Outline

This thesis has been written in 8 chapters including this introductory chapter. Each chapter has its own literature review (where applicable) and summary.

Chapter 2 introduces the Regional Ocean Model Suite (ROMS) which forms the methodological basis for the thesis. It also details the model set up and parameterisation.

Chapter 3 details the idealised tidal model and results. The model forcing was provided through the global tidal model Topex Poseidon Crossover Solution (TPXO) and the calibrated using adjustment of the bottom friction. Final calibration was achieved using a method which accounted for the effect of both depth and benthic type, specifically seagrass meadows, on bottom friction coefficients. Model results were compared with Australian National Tide Table (ANTT) data.

Chapter 4 investigates the circulation induced by idealised wind-stress regimes in the absence of any other forcing. The effects of directionality of wind-stress on circulation patterns was investigated through the use of up-gulf and cross-gulf wind-stress models. Dynamic balances of the momentum equation are

used to explain the resultant circulation. The effects of coastal trapped waves on GSV circulation are also investigated.

In chapter 5 geostrophically adjusted models were used to ascertain typical circulation patterns for expected seasonal thermohaline structures in the absence of other forcing fields.

Chapter 6 examines the combination of all forcing fields in order to form a quasi-realistic GSV Model (GSVM) which aims to reproduce circulation observed within the model domain throughout the period of the 2010-2011 calendar years. This was achieved as a result of the better understanding gained through the proceeding chapters. The GSVM was calibrated using the same bottom friction described in Chapter 3 and nudging to NOAA sea surface temperature monthly mean records. The model is validated against available long term observations at Pt. Stanvac and is shown to provide good reproduction of the physical circulation and thermohaline structures within the gulf.

Chapter 7 uses the results of the GSVM in order to explain the major modes of gulf-shelf connectivity and their seasonal variability. This is achieved through the examination of mean depth-integrated velocity fields, calculation of flushing timescales, passive Lagrangian particle tracking and the examination of a volume averaged salt balance. Additionally, the effect of accurately resolving shelf boundary conditions on circulation and salinity within GSV is investigated.

Finally, chapter 8 summarises the findings of this thesis and provides avenues for further research for Gulf St. Vincent and its surrounding regions.

1.5 Major Findings

The key findings of this thesis include;

1. The presence and distribution of seagrass meadows appears to impact that propagation of tidal signals throughout GSV. In turn, seagrass meadows have an effect on the larger gulf-wide dynamics as well as the near shore.

2. Seasonal wind-stresses appear to be the dominant factors in large scale hydrodynamics of the gulf. The highly seasonal nature of wind direction and strength are the key drivers in either recirculating or flushing gulf waters with fresher shelf water.

3. The temperature front which has been identified and studied in previous works appears to be a result of the wind-driven circulation of the gulf, and not a primary factor in the restriction of summertime shelf-gulf connectivity. It is a symptom, rather than a cause, of the lack of summer connectivity.

Chapter 2

Methods and the ROMS model

The basis of this thesis is the use of ROMS numerical models which aim to reproduce the physical processes which drive the circulation throughout GSV, IS, BP and nearby shelf. To achieve this an open-source modeling package known as the Regional Ocean Modeling Suite (ROMS) was used (www.myroms.org). ROMS is a flexible modeling package which allows for high levels of customisation and is the basis for all models used in this thesis to investigate the hydrodynamics of GSV. The flexibility of ROMS allows for the creation of specific model environments which can be tailored to investigate separate facets of circulation.

Theoretical models were created by isolating forcing fields (such as wind-stress, tidal elevations etc.), as well as quasi-realistic models which attempt to implement all forcing fields which are expected to have an effect on the circulation of the gulf under realistic natural conditions. Theoretical models can also be tweaked, or even fully forced, through the manipulation of boundary conditions alone.

For the quasi-realistic models (Chapter 6) and for some theoretical models, nesting the GSV Model (GSVM) within 'parent' models is required. This is achieved by running models with larger domains (and typically lower resolution) and using the results of these models to enforce hydrodynamic state variables at the open boundaries of the GSVM. The GSVM in this case was nested inside a parent model known as Southern Australian Regional Ocean Model (SAROM), which in turn is forced at its open boundaries by a global model Bluelink ReANalysis (BRAN 2015, www.cmar.csiro.au/staff/oke/BRAN.htm).

2.1 The ROMS Model and Parameterisation

ROMS is a free-surface, terrain following, finite-difference fully non-linear ocean model that solves the Reynolds-averaged Navier Stokes equations with the Boussinesq and hydrostatic approximations. ROMS has been used extensively for oceanographic studies (Capet et al., 2007; Hinckley et al., 2009; MacReady & Geye, 2001; Middleton et al., 2014; Winsor & Chapman, 2004), including in shelf and coastal zones (Blaas et al., 2007; Penven et al., 2006; Kumar and Feddersen., 2015; Liu et al., 2009). Model domains within ROMS are discretised using a boundary fitted, orthogonal curvilinear coordinates on a staggered Arakawa C-grid (Arakawa & Lamb, 1977).

The model uses a split-explicit time stepping scheme to separately calculate the free-surface and vertically integrated momentum for baroclinic and barotropic components. Momentum transfer and mixing occur along sigma surfaces. Volume conservation and constancy of tracers within ROMS are

maintained via a time-stepping constraint. More detail about the nonlinear algorithms ROMS employs can be found in Shchepetkin & McWilliams (2003) and Shchepetkin & McWilliams (2005). Horizontal mixing of tracers was set to occur along geopotential surfaces. Horizontal buoyancy and shear are smoothed in order to reduce introduction of instabilities. Vertical mixing of tracers is calculated using the Mellor-Yamada 2.5 turbulence scheme (Warner et al., 2005) and Kantha-Clayson stability function (Kantha & Clayson, 1994). Density based Laplacian with spline reconstruction of vertical profiles was implemented for accurate reproduction of the baroclinic pressure gradient (Shchepetkin & McWilliams, 2003).

The model has several parameters which represent physical properties of fluid mechanics. The parameters listed in Table 2.1 are consistent throughout all model runs, theoretical and realistic. These are generally basic properties of the fluid mechanics which are required to remain constant across models runs to allow meaningful comparisons as they fundamentally alter the simulated circulation.

Parameter	Value
Horizontal Eddy Viscosity	20 m^2 s^{-1}
Vertical Mixing Scheme	Mellor-Yamada 2.5
Horizontal Tracer Eddy Diffusion	2.0 m^2 s^{-1}
Vertical Tracer Diffusion	1.0^{-6} m^2 s^{-1}
Bottom Friction Scheme	Quadratic Drag Function (See Chapter 3)
Vertical Momentum Mixing	1.0^{-5} m^2 s^{-1}
Maximum Depth	100 m
Minimum Depth	4 m

Table 2.1: Model parameters common to all GSVM simulations. For full definitions and mathematical explanations please refer to Hedström (2010)

Horizontal eddy viscosity was set at the mimimum value which resulted in a stable model. Lower values resulted in sea surface level instabilities, especially through Backstairs Passage. Smagarinsky formulation was similarly avoided for stability reasons.

Minimum depth for all models was set at 4 meters as a necessary compromise between accurate topography and computational cost. For those areas with depth less than 4 meters the minimum depth of 4 meters was set in the model. This concession affects little of the model domain with the exception of the far northern reaches of the gulf, which is shallow in some regions. This compromise was necessary in order to avoid the use of 'wet-dry' or flood modeling which is computationally expensive and hence unreasonable for use in long term modeling. It is expected that the exclusion of flood modeling will perhaps have implications for ocean conditions within those flood zones but, due to their insignificantly small proportion of the total water mass of the gulf, little impact on the overall circulation is expected.

2.2 The High-Resolution Gulf St. Vincent Model (GSVM) Domain

The basis for all GSV modeling within this thesis is a high-resolution, twice-nested ROMS model described below. This model is known as the Gulf St. Vincent Model, or GSVM. The GSVM domain is shown in Figure 2.1.

2.2.1 Resolution

The model resolution must be fine enough to accurately resolve the physical processes occurring within the model domain. ROMS allows for the model domain to be gridded on curvilinear coordinates to accommodate the curvature of the Earth's surface. Horizontal grid discretisation is therefore determined by defining separation of grid points by longitude and latitude. The grid used for all GSVM simulations (see Figure 2.1) was built upon point separation of ~0.0047 degrees longitude and ~0.0038 degrees latitude, which equates roughly to a horizontal resolution of 500 x 500 m. The model domain in the horizontal spans from the south-western most tip of Yorke Peninsula in the west to the Coorong in east. In the vertical it spans from the head of the gulf to the south coast of Kangaroo Island. Whilst the domain includes a small portion of Spencer Gulf, this zone is flagged as land within the model and ignored in all terms of ocean dynamics.

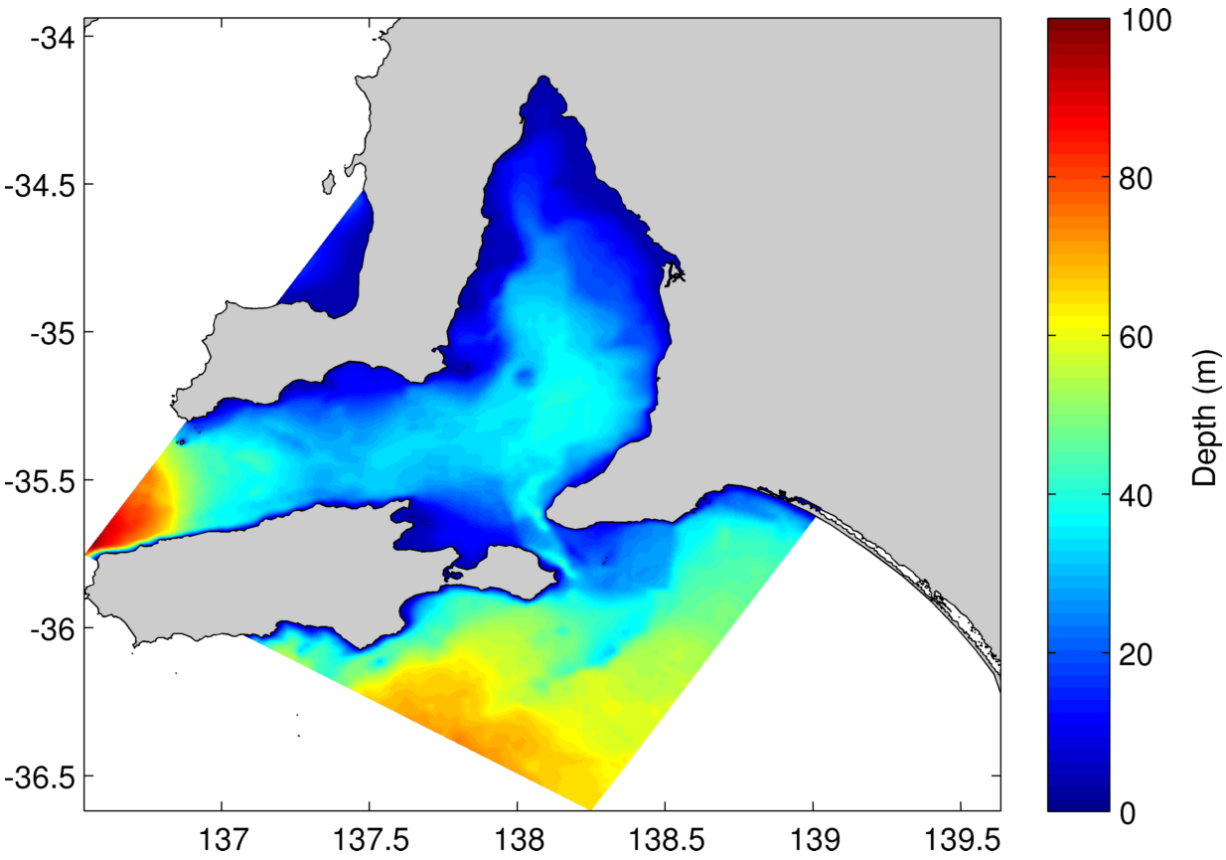

Figure 2.1: Domain extents and depths (m) for high-resolution Gulf St. Vincent ROMS model. The interior of the gulf is mostly quite shallow, with a deeper (~ 40 m) basin in the south eastern portion of the gulf. At the western boundary the depth rapidly increases in IS, and slowly increases on the shelf to the south of KI in the east.

The grid is separated in to 15 vertical layers using a terrain-following sigma coordinate system, which allows for concentration of levels at the surface and bottom of the water column, which are typically the most dynamically important zones. It also allows for high vertical resolution in shallow regions, which is a major benefit over fixed depth systems wherein shallow regions are often modeled as a single layer. In this case 15 vertical layers were selected, as this both adequately resolves vertical stratification and also matches the parent SAROM model from which the open boundary conditions are derived. As with

the horizontal resolution, the number of vertical layers chosen is always a trade off between realism and computational time. In this case 15 layers was deemed adequate in resolving the hydrodynamics of the system whilst allowing for practical computational time. The sigma coordinate stretching parameters are listed in Table 2.2.

Parameter	Value
Transformation Equation	2
Stretching Function	4
Surface Stretching Parameter	8.0
Bottom Stretching Parameter	4.0
Critical Depth	20 m

Table 2.2: Sigma coordinate stretching parameters used within all GSV modeling. For full definitions and mathematical explanations please refer to Hedström (2010) . Please note that in reference to sigma coordinate stretching critical depth refers to the maximum allowable layer thickness before discretisation is required, rather than the ROMS definition of critical depth which refers to wetting and drying of a cell.

2.2.2 Open Boundaries

The correct implementation of Open Boundary Conditions (OBCs) is vital in numerical modeling such that perturbations created within the model domain may leave it without deterioration of the model solution whilst allowing for the inward introduction of external information which may be important to the realistic representation of the physical environment within the model domain (Roed & Cooper, 1986; Marchesiello et al., 2001). The open boundaries must be located such that they are both far enough away from the internal dynamics of GSV proper, and also oriented in such a way to minimise edge effects when incorporating boundary forcing from a parent model. This was done by rotating the grid by approximately 32° from true north such that the southern boundary runs parallel to isobaths and the eastern boundary perpendicular to isobaths. The western boundary runs across IS between the south-western tip of Yorke Peninsula and the north-western tip of KI.

2.2.3 Topographic Data

Due to the high resolution nature of the model, accurate bottom topography is critical. The grid depths were constructed through a combination of Geosciences Australia 2009 (GA2009) data and depth sounding information from the Australian Royal Hydrographic Service (AHS). This was due to inaccuracies in the GA2009 data for the near shore (<10 m depths), where the AHS depth soundings were more accurate. This was also true for BP, where the GA2009 data seemed to suffer from over-smoothing which unrealistically reduced the depths in that region. Smoothing was applied to the combined data sets to form the final model topography in order to eliminate model stability issues which can arise from sudden changes in depth (Figure 2.1).

The topography of GSV has a few notable features. The first is a central basin which forms the deepest region of the gulf at approximately 40 m deep. There is also a central channel which runs from this basin to the head of the gulf. The very head of the gulf is dominated by a region of shallow water. There is another area of shallow water on the north coast of Kangaroo Island in the region of American River. At the western boundary the depth of Investigator Strait dramatically increases from ∼50 m to 100 m. For the most part, the depth of IS does not exceed 40 m. Backstairs Passage contains a deep channel on

the Kangaroo Island side, which expands to a shallow shelf region to the east. To the south of Kangaroo Island the depth gradually increases towards the open ocean.

2.3 The SAROM Parent Model

The Southern Australian Regional Ocean Model (SAROM) is a 2.5 km horizontal resolution model which covers the wider regional area of the South Australian coast, stretching from Fowler's Bay in the west to Portland in the east. This model is used to force the GSV model at the open boundaries. The SAROM model uses the same sigma coordinate system and parameters as the high-resolution GSVM as listed in Table 2.2. The SAROM model is forced at its open boundaries using the BRAN 2015 model. The SAROM model reproduces the circulation of the ocean and shelf waters to a depth of 5000 m all the way to the shallow waters within SG and GSV.

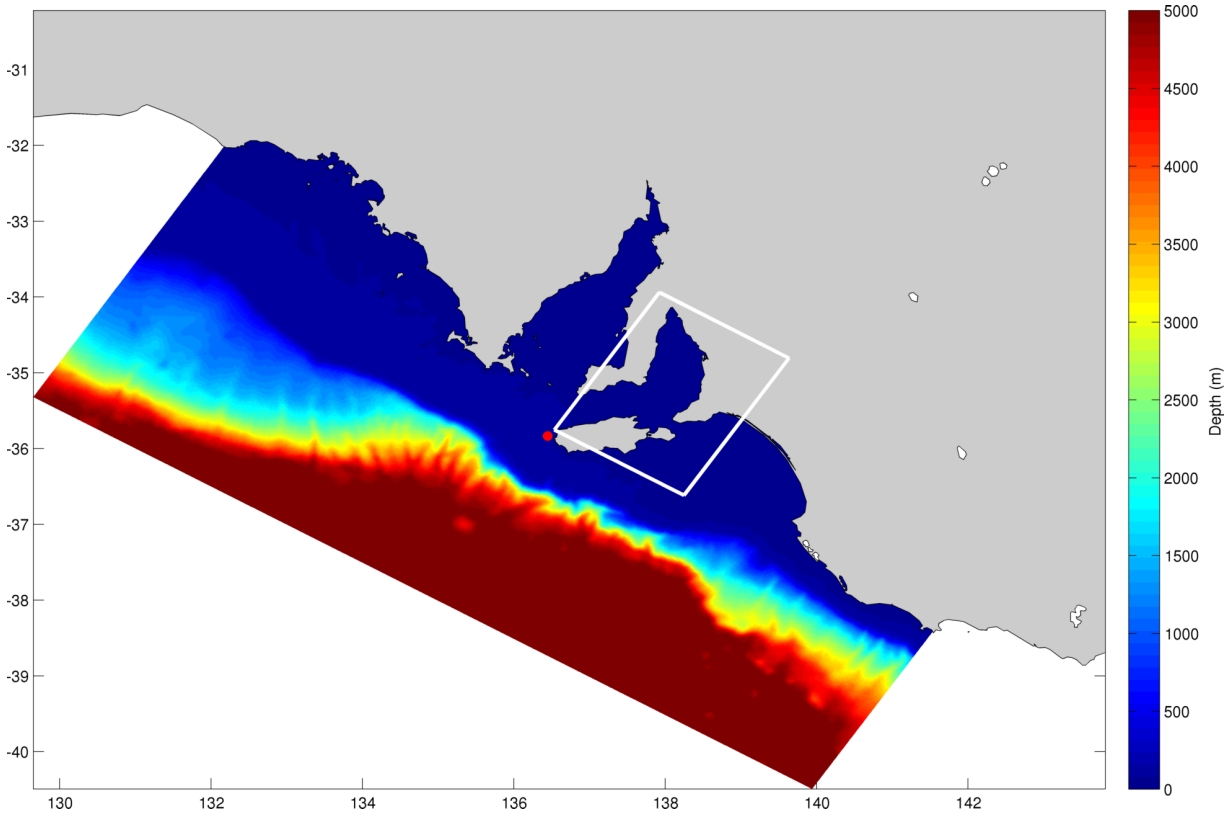

Figure 2.2: SAROM domain depth, GSV high-resolution model domain outlined. Isobaths shown for 50, 100 and 200m. Red marker indicates location of Kangaroo Island reference station. Depth rapidly increases to the south of KI at the shelf break, dropping from $\sim$ 200 m to over 5000 m in a short distance.

The SAROM model was validated for the gulf regions using data from the Kangaroo Island reference station (Middleton et al., 2016), indicated in Figure 2.2. The model accuracy as indicated by the validation against the KI reference station shows that the SAROM model reliably simulates circulation along the South Australian shelf waters (Middleton et al., 2016). This makes it ideal for providing boundary conditions for the high-resolution GSVM.

2.4 The BRAN 2015 Global Model

The global model which has been adopted by SARDI for nesting regional models is known as the Bluelink ReANalysis (BRAN 2015, http://www.cmar.csiro.au/staff/oke/BRAN.htm) model. BRAN 2015 output covers a temporal period from 2009 to mid-2015 making it suitable for modeling GSV during the 2010-2011 period when the greatest abundance of observations within the gulf are available for calibration and validation. BRAN 2015 is a data-assimilating model, meaning it integrates observations with model results to give better point by point agreement with observations by sacrificing some of the model dynamic's autonomy. The base model upon which BRAN is built is the Ocean Forecast Australia Model (OFAM) developed by BOM and CSIRO.

OFAM has been shown to adequately replicate large scale oceanic processes for the southern Australian region (Oke et al., 2012), and BRAN has been shown to strike a good balance between the artificial adjustments required to successfully assimilate data and allow suitable dynamic autonomy of the model under the supplied forcing fields (Oke et al., 2012).

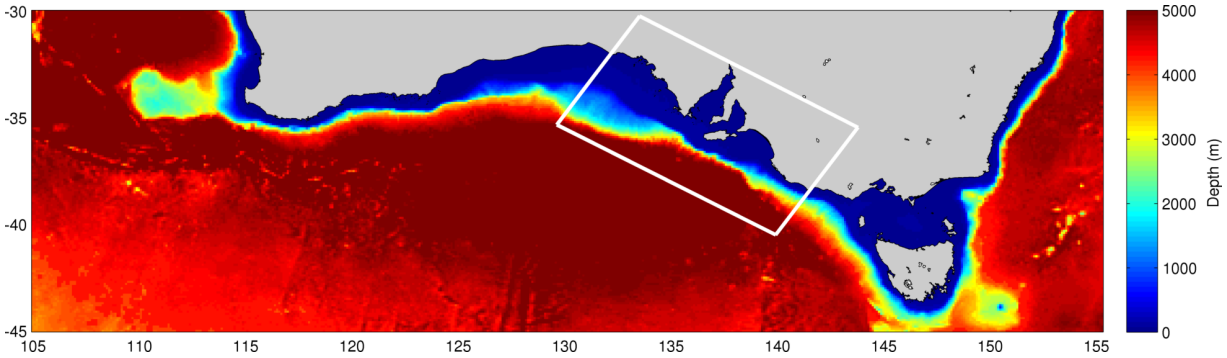

Figure 2.3: BRAN model domain for southern Australian region depth, SAROM model domain outlined

The BRAN model results have been used to create boundary conditions for the regional SAROM model, which in turn was used to create boundary conditions for the high-resolution GSVM. As such, the BRAN data is important in replicating circulation within the SAROM model, but unlikely to directly impact on the GSVM due to the distances between the GSV and SAROM model boundaries. Nesting the SAROM model within the BRAN model does ensure though that any global scale circulation patterns which may influence circulation within the gulf are not neglected.

2.5 Available Data

The time period which was chosen for the GSV modeling to encompass was based largely on the richness of observed data available within that period, as the more data allows for better calibration and validation of the model. The data which were used during calibration and validation of the model are outlined in Table 2.3.

Location (Source)	Data Types	Date Range
Pt. Stanvac (BOM)	SL	Jan 2010 - Nov 2010
Pt. Stanvac (SARDI)	SL, T, u, v	July 2010 - Dec 2011
Pt. Stanvac (SA Water)	T, S	May 2010 - Dec 2011
Pt Giles (PSMSL)	SL (monthly mean)	1995 - 2015
Outer Harbor (PSMSL)	SL (monthly mean)	1940 - 2015

Table 2.3: Observed data for Gulf St. Vincent used for model validation and calibration. SL is Sea Level, T is Temperature, S is Salinity, u and v are depth integrated current velocities. Sources of data are: the Bureau of Meteorology (BOM); South Australian Research and Development Institute (SARDI); SA Water and the Permanent Service for Mean Sea Level monitoring (PSMSL)

Chapter 3

Tidal Model

3.1 Summary

The tidal circulation in Gulf St. Vincent is simulated using the GSVM, forced at the boundaries using amplitudes and phases of 9 major tidal constituents from the global tidal model TPXO 8.1 (Egbert et al., 1994; Egbert & Erofeeva, 2002). While GSV has been the focus of previous tidal models, the model created here incorporates a new implementation of friction coefficients by depth and benthic type; specifically the presence of seagrass meadows. This inclusion resulted in more accurate reproduction of tides when compared to a 'traditional' constant domain wide assumed coefficient of friction, and may prove to be a useful tool in impleneting better tidal models for other systems. It also implies that seagrass health and distribution can have a direct impact on the tidal reponse of the gulf, and hence changes in seagrasses may have far reaching implications for not only the biology of the gulf but also hydrodynamics.

The results of tidal models are validated comparing the Sea Surface Height (SSH) predictions based on amplitude and phase of the 9 modeled constituents with data from the Australian National Tide Tables (ANTT) for 12 locations within GSV. Model results compare very favourably with ANTT data, indicating a reliable tidal model with mean squared correlation (R^2) of 0.95 for SSH predictions for the locations considered, i.e. 95% of variance is explained by the model.

In this chapter: Theoretical impacts of dodge tides and resonance on tidal waves are considered. An investigation on the effects of varying depth and spatially variable benthic environments on quadratic coefficient of friction (C_D) is undertaken through sensitivity testing, and a new method for estimating C_D is developed accounting for both depth and benthic environment. A new tidal model using the best fit depth and benthos dependent spatially variable C_D is employed, forced at the open boundaries by the global TPXO tidal model. The results of the new tidal model are validated against ANTT tidal gauge data and shown to improve model domain averaged squared variance (R^2) from 0.84 for a 'traditional' fixed C_D value of 0.0025 to $R^2 = 0.95$ using the results of the calibrated spatially variable benthic and depth dependent C_D.

3.2 Introduction

Though tides are seldom dominant factors in long-term net transport, they play an especially important role in mixing (or not in case of neap tides) and therefore the destruction (or creation) of stratification. This is especially true for GSV, where the gulf acts as a near quarter-wave resonator (Bowers & Lennon, 1990), greatly amplifying tidal signals towards the head of the gulf. An accurate tidal model is necessary in replicating this cycle of stratification and mixing which can have significant impact on the thermohaline structure of the body and hence the potential to influence long-term transport.

The southern coast of Australia presents an unusual tidal system, in which the principle semi-diurnal tidal constituents, M_2 and S_2, are almost equal in magnitude and phase. This results in the occurrence of 'dodge' tides when the M_2 and S_2 constituents become out of phase with one another, canceling each other out approximately every 15 days (Chapman, 1892; Easton, 1978; Bowers & Lennon, 1990). As the principle diurnal tides, K_1 and O_1, are relatively weak in comparison, there is very little tidal movement during these dodge tides. A key result of the occurrence of dodge tides in terms of circulation is the lack of mixing during these periods, presenting the opportunity for stratification to occur as found for SG by Nunes et al. (1990). Even though the magnitude of the dominant tidal constituents (M_2, S_2, K_1 and O_1) in South Australia are relatively small on the shelf, the topography of GSV lends itself to magnification of the semi-diurnal constituents' (M_2 and S_2) amplitudes through resonance (Bowers & Lennon, 1990; Bye, 1976). This leads to tidal magnification of up to a factor of 4 from western Investigator Strait (IS) to the head of GSV (Bowers & Lennon, 1990). This phenomenon, coupled with the relatively narrow and shallow flow paths of Investigator Strait (IS) and Backstairs Passage (BP) indicate that tidal variability, currents, mixing and shear dispersion are likely to be important processes in the circulation and connectivity of GSV waters. The Bowers & Lennon (1990) study indicated that there is roughly a 60/40 split of tidal volume flux for GSV between IS and BP respectively.

3.3 ROMS Configuration for the GSVM Tidal Model

For the tidal model, ROMS was run in a barotropic two-dimensional mode. Sensitivity tests perfomed after calibration resulted in neglible changes in dynamics between two-dimensional and three-dimensional models, indicating that two-dimensional models were suitable for model calibration. It has also been previously demonstrated that different vertical mixing schemes have minimal impact on key flow dynamics (Umlauf and Burchard, 2003; Warner et al., 2005; Wijesekera et al., 2003), and hence have not been further explored in this study.

Tidal amplitudes and phases for 9 major constituents (M_2, S_2, K_1 , O_1, Q_1, P_1, K_2, S_2 and M_4) from the TPXO 8.1 model (Egbert et al., 1994; Egbert & Erofeeva, 2002) were used to force the model at the open boundaries. Amplitudes and phases were linearly interpolated to the model domain from the TPXO 8.1 model results (supplied at $\frac{1}{30}$ degree resolution) (Egbert et al., 1994; Egbert & Erofeeva, 2002). TPXO 8 has recently been demonstrated to be one of the best available global tidal models, especially for shelf regions and shallow waters (Stammer et al., 2014).

Chapman and Shchepetkin (Chapman, 1985; Shchepetkin, 2007) boundary conditions were applied to the sea level and two-dimensional momentum fields respectively at all open boundaries. The time step was set to 10 seconds. No heat or fresh water fluxes were applied and hence the density field remained constant during modeling. Tidal models were run over a period of 90 days with a 3 day ramp up period from 0 to actual value for amplitude to avoid introducing instabilities.

The bottom friction was calibrated using a new approach to determining the quadratic coefficient of drag, taking account of both depth and benthic environment, detailed in section 3.4.2.

3.4 Theoretical Considerations

3.4.1 Neap/Dodge Tides and Resonance

The theory behind the neap tide is simply explained by Equation 3.1, which describes the superposition of the M_2 and S_2 tidal constituents when they have equal amplitude and phase difference φ.

$$sin\left(\omega_{S_2}t\right) + sin\left(\omega_{M_2}t + \varphi\right) = 2cos\left(\Delta\omega t - \frac{\varphi}{2}\right) sin\left(\omega t + \frac{\varphi}{2}\right) \tag{3.1}$$

where $\omega = \frac{\left(\omega_{M_2}+\omega_{S_2}\right)}{2}$, $\Delta\omega = \frac{\left(\omega_{M_2}-\omega_{S_2}\right)}{2}$ and ω_{M_2} and ω_{S_2} are the frequencies of the M_2 and S_2 tidal constituents. As the period $2\pi/\Delta\omega$ is 29.6 days, the superposition of the two semi-diurnal tidal constituents results in a tidal signal with amplitude modulated over a period of 14.8 days. The canceling of the principal M_2 and S_2 tidal signals at the neap is known as a "dodge tide" in South Australia. When the dodge tide also coincides with an equinox then the tidal range is even more muted over an extended period, as the K_1 and O_1 tidal amplitudes also tend to zero (Noye & Grzechnik, 1995). The dodge tide is a unique feature of the South Australian gulfs due to the near identical amplitudes of the semi-diurnal tides.

GSV, much like SG, has been shown in the past to be effectively a quarter wave resonator for the M_2 and S_2 tidal constituents (Bowers & Lennon, 1990). Previous studies have shown that the tidal constituent resonance for a theoretical idealised semi-enclosed gulf can be simply represented (Platov & Middleton, 2000). Assuming a narrow gulf with constant depth h_0, length L and forced oscillations at the open mouth an estimate of sea level η can be given:

$$\eta = \eta_0 cos\left(\omega t\right) \tag{3.2}$$

$$\eta = \frac{1}{2}A\left[cos(kx - \omega t) + cos\left(kx + \omega t\right)\right] \tag{3.3}$$

or simplified

$$\eta = Rcos(\omega t - \delta) \tag{3.4}$$

where $A = \frac{\eta_0}{cos(kL)}$, $R = Acos(kx)$, $k = \frac{\omega}{(gh_0)^{\frac{1}{2}}}$, x is distance seaward along the gulf, h_0 is mean depth, $\omega = \frac{2\pi}{T}$ is the frequency, T is period and δ is the phase, equal to zero. In this idealised case Coriolis effects are ignored. Resonance for different wave numbers will occur for a gulf of length L when:

$$L = \frac{\left(n + \frac{1}{2}\right)\pi}{k},\ n = 0, 1, 2, ... \tag{3.5}$$

where n is the wave number. Quarter-wave resonance will occur when the wave number $n = 0$, or $kL = \frac{\pi}{2}$ which gives Equation 3.6.

$$L = \frac{\pi\left(gh_0\right)^{\frac{1}{2}}}{2\omega} \tag{3.6}$$

where ω is the frequency of free oscillations at the open boundary. For GSV, previous observations show that the period for oscillations is approximately 12 hours within IS and BP (Bowers & Lennon, 1990). Assuming an average depth of 21 m (Bye & Kämpf, 2006) and applying Equation 3.6, we would expect quarter-wave resonance to occur perfectly for a gulf of length 155 km. This compares well with the length of GSV, which taken from the head of the gulf to the tip of Cape Jervis is approximately 165 km, or 120 km from the head of the gulf to the south-east tip of Yorke Peninsula for an average of approximately 140 km, indicating a strong preference for quarter-wave resonance.

As shown in both this study and numerous others Bowers & Lennon (1990); Bye (1976); Bye & Kämpf (2006); Chapman (1892); Noye & Grzechnik (1995), this tidal resonance is shown to occur within GSV and results in much larger tidal amplitudes at the head of the gulf than the mouth.

Applying Equation 3.6 to the diurnal tidal constituents with wave number $n = 1$, the ideal length of a gulf for resonance at the same frequency and average depth is given as 465 km, substantially longer than GSV. Hence we would expect very little resonance and magnification to occur for the diurnal tides.

3.4.2 Bottom Friction: The Role of Benthos

The drag experienced by tidal waves due to bottom friction plays a critical role in the manner that the tidal signals propagate (Backhaus et al., 2008; Chunyan et al., 2004; Spitz & Klinck, 1998; Zhang et al., 2011). Coefficients of friction vary with depth and bottom type (Bao et al., 2000; Chunyan et al., 2004; Koch & Gust, 1999; Luhar & Nepf, 2013; Spitz & Klinck, 1998). Differences between benthic environments can have a significant impact on friction, and as GSV has many benthic environments (Tanner, 2005), the coefficient of drag is expected to vary spatially. This is especially true for the presence of sea-grass meadows, which often neighbour bare sand, two benthic environments of greatly differing drag.

In this model a quadratic drag approach is adopted. To estimate the effect of bottom drag on momentum, a quadratic coefficient of drag (C_D) is estimated. The coefficient of drag is important as it represents the frictional effect of turbulent flow on the bottom boundary layer which is of too small a scale to be resolved in the relatively course (compared to scale of frictional turbulance) model grid. In order to best determine the distribution and magnitude of quadratic coefficient of drag, a sensitivity analysis was performed in which several experiments using different approaches were conducted, the results of which were compared with the ANTT data in order to test their predictive ability. These experiments included constant domain wide C_D (the 'traditional' approach), depth dependent C_D models and finally depth and benthos dependent C_D models. The results of these experiments (not shown) showed both depth and distribution of benthic type are key factors in the formulation of C_D at a given point, and these models gave the best fit to ANTT data.

Previous studies (Chunyan et al., 2004; Spitz & Klinck, 1998; Ullman & Wilson, 1998; Lu & Zhang , 2006) have shown that there is a correlation between water depth and C_D, increasing for shallower water, and has previously been applied to modeling GSV (Cheng et al., 1993; Samarasinghe et al., 2003). This is due to the Ekman bottom layer being proportionally larger on the total water column in shallow water than in deeper water, and bottom stress is parallel and opposite to the vertically averaged current. In deeper waters fully geostrophic flows form, whereby the current flows perpendicular to the pressure gradient, and bottom stress is independent from depth (Mofjeld, 1988). Therefore an assumption for the tidal model was made whereby C_D for a given cell is proportional to the relative depth of that cell to the

maximum depth in the model domain:

$$C_D \propto \frac{D_{max}}{D_{i,j}} \tag{3.7a}$$

Where D_{max} is the maximum depth within the model domain and $D_{(i,j)}$ is the depth of the cell at position i, j.

It has also been shown that seagrasses exhibit substantially higher effective C_D than substrates such as bare sand (Luhar & Nepf, 2013; Nepf and Ghisalberti, 2009; Gils & Erftemeijer, 2016). Therefore an additional assumption was made here where the depth dependent C_D should be modified by a factor F_b which accounts for differing benthic environments:

$$C_D \propto F_b \in [1, 2] \tag{3.7b}$$

The inclusion of the proportionality of (3.7a) and (3.7b) in this study led to a simple new, and more accurate, approach for estimating C_D based on:

$$C_{D_{(i,j)}} = \min \left\{ C_{D_{base}} + F_{b_{(i,j)}} * f_d * \left(\frac{D_{max}}{D_{(i,j)}} \right),\ C_{D_{max}} \right\} \tag{3.7c}$$

Where $C_{D_{(i,j)}}$ is the coefficient of friction for a given grid cell, F_b is a factor dependent on bottom type, f_d is a tuning parameter which scales the influence of depth variation and benthic environment on C_D and $C_{D_{max}}$ is a maximum allowable coefficient of friction. The model was calibrated based on the non-spatially varying parameters $C_{D_{base}}$, f_d and $C_{D_{max}}$ and finalised through sensitivity experiments wherein these parameters where tuned in order to obtain the best possible fit to ANTT data. It is important to note that the value of D_{max} is arbitrary and could have been incorporated in to the other tuning parameters. The importance is in that C_D varies with depth. $C_{D_{base}}$ was chosen such that the resultant minimum $C_{D_{min}} = C_{D_{base}} + f_d$ (where $\left(\frac{D_{max}}{D_{(i,j)}} \right) = F_b = 1$) was close to the 'traditional' value of C_D (0.0025). Varying the value of the tuning parameter f_d allowed for a simple approach to account for the influence of benthic environment and depth on C_D in a single variable. A maximum coefficient of drag was assumed to be to be $C_{D_{max}} = 0.010$, consistent with a base coefficient of friction for seagrass used by Backhaus et al. (2008). Final values for the tuning parameters can be found in Table 3.2.

Benthic composition throughout GSV was obtained from results of remote video surveys as conducted and analysed in a habitat change study conducted in 2001 by Tanner (2005). Values for F_b were estimated from the benthic type, with a range of $F_b = 1 \rightarrow 2$ with the lower value representing bare sand and the maximum representing full seagrass meadows. Values of F_b were chosen by estimating the relative roughness of benthic environments to bare sand and seagrass meadows. The full range of benthic types and values adopted can be found in Table 3.1. This is of course a rough approximation, but showed improvement for the tidal model which accounts for benthic type over those which ignore it, implying that accounting for the effect of benthic environment on C_D is important for reproduction of accurate tidal waves.

The extent of the video survey of benthic environments did not encompass IS, BP or shelf waters to the south east of BP, hence coefficient of drag in these regions was was based solely on depth (e.g $F_b = 1$). Benthic types were sampled at approximately 9 km resolution throughout the domain for the Tanner study.

The bottom type distribution for the area covered by the Tanner study is shown in Figure 3.1a, with

Benthic Type	F_b Value
Pinna	1.1
Seagrass Meadows	2
Bare Sand	1
Ascidian	1.05
Bryozoans	1.2
Ascidian/Bryozoan	1.125
Seagrass/Pinna	1.55
Scallops	1.1

Table 3.1: Benthic type quadratic drag multiplier value F_b, estimated by relatively roughness between bare sand ($F_b = 1$) and full seagrass meadows ($F_b = 2$)

Tuning Parameter	Value
$C_{D_{base}}$	0.0022
f_d	0.0004
$C_{D_{max}}$	0.01

Table 3.2: Final values for tuning parameters used to calibrate tidal model.

the resultant C_D determined by Equation 3.7c shown for the same region in Figure 3.1b. Coefficients of drag outside this area were based on depth alone, and are typically quite low (around the typically adopted 0.025) due to the greater depths in those regions. It is also expected that these regions will have little in the way of seagrass meadows due to the vast majority of the area having depth greater than 18 m, which appears to be the limit for seagrasses observed within the surveys (Tanner, 2005).

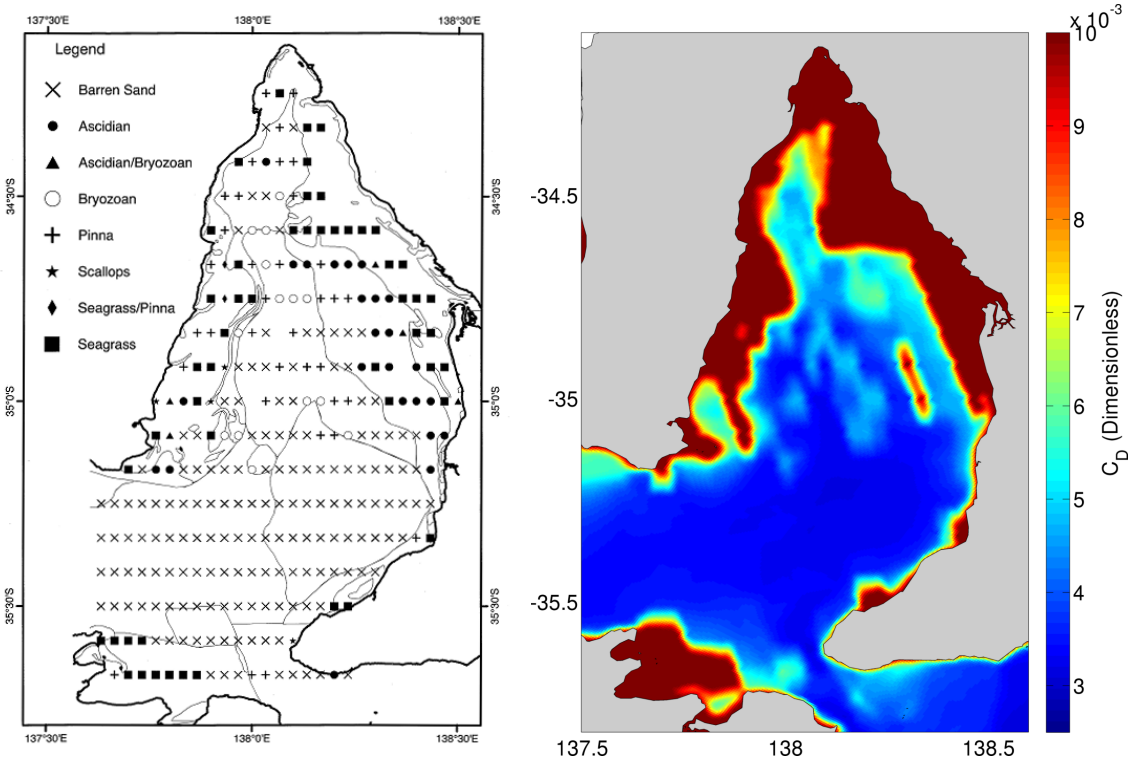

(a) (b)

Figure 3.1: a.) Bottom type distribution sourced from Tanner (2005) and b.) Dimensionless quadratic coefficient of drag (C_D) distribution as determined by Equation 3.7c. C_D is noticeably higher for those regions which are both shallow and also demonstrated to contain seagrass meadows. Areas with greater depth and or benthic types with lower roughness have lower C_D.

3.5 Available Data and Tidal Model Validation (Method)

The tidal models were validated against existing amplitude and phase data for the 9 tidal constituents used for open boundary forcing at 12 locations throughout the model domain shown in Figure 3.2. This data was sourced from the Australian National Tide Tables (ANTT, 2007). The amplitude and phase data has been created by the National Tidal Centre (NTC) through the harmonic analysis of long-term sea level data, which has also been filtered to remove variability due to atmospheric pressure. The raw sea level information from which the ANTT derived the amplitude and phases of tidal constituents at these points was unavailable.

Model grid points closest to the observation sites for ANTT data were selected for comparison. Modeled ROMS phases were adjusted from UTC to local time (-9.5 hours) in order to compare with ANTT data.

The tidal model was tested for accuracy in terms of predictive ability for tidal SSH at the ANTT station locations. This is because it is the SSH elevations that are most important for determining the tidal influence on circulation and dynamics, creating the SSH gradients and hence pressure gradients which drive tidal currents. Accuracy of tidal SSH prediction was measured by determining the correlation (R^2) of the predicted SSH based on the GSVM results with the SSH predictions based on ANTT data. To achieve this, harmonic analysis of SSH results for the tidal GSVM was undertaken to determine the amplitude and phase for each of the ANTT tide gauge locations for the 9 modeled constituents with results shown in Section 3.6.

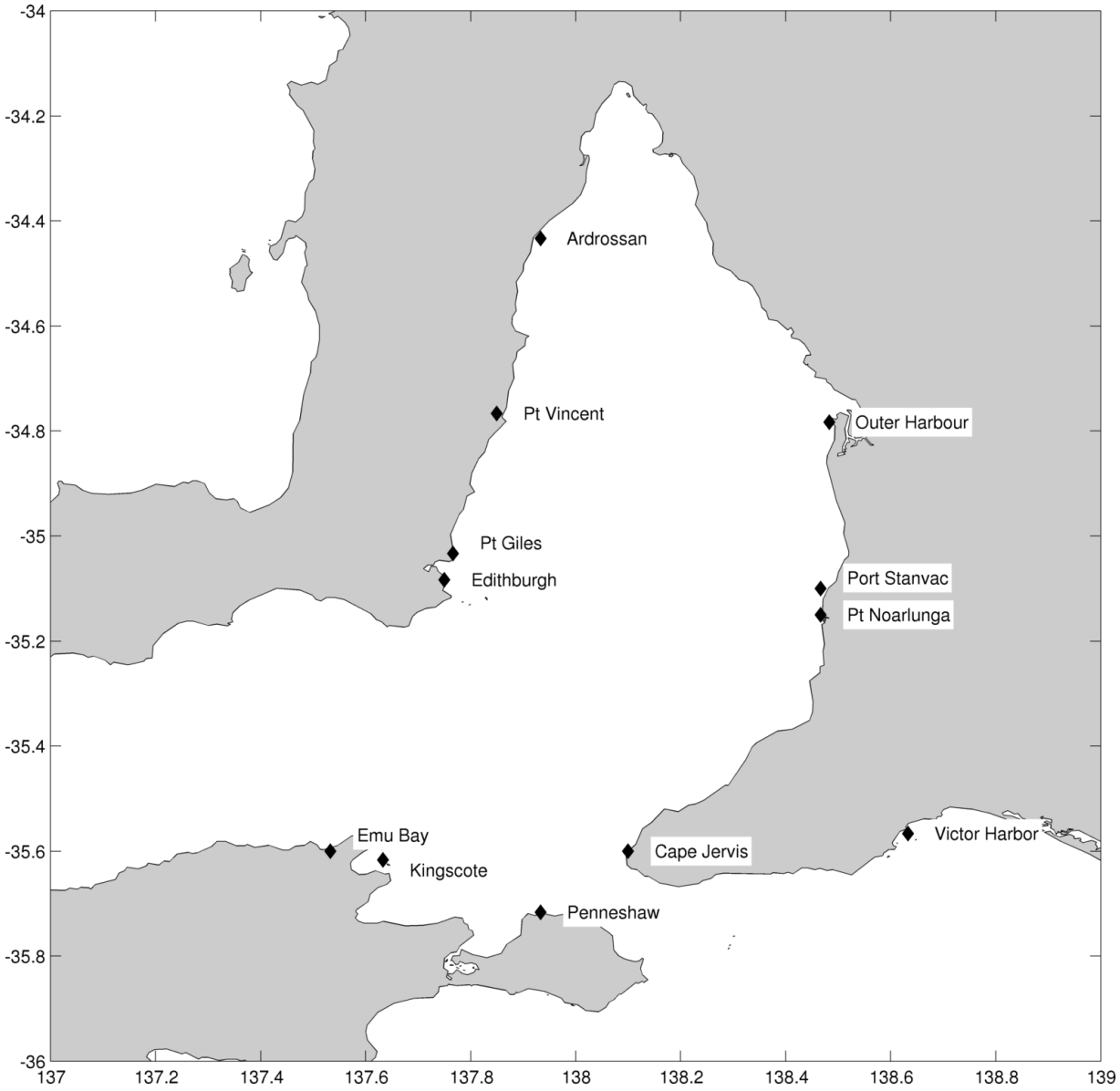

Figure 3.2: Position of ANTT stations used in validation of the tidal GSVM

3.6 Tidal Model Validation (Results)

The final tidal model forced by TPXO at the open boundaries and the estimated quadratic coefficient of drag (Figure 3.1b) returned excellent agreement with the ANTT data at the 12 tested locations throughout GSV as shown in figure 3.2. The predictive ability of the tidal model to replicate sea surface height (η) based on the 9 major tidal constituents at the ANTT tide gauge locations is given by the correlation (R^2) values listed in Table 3.3. The R^2 value can be considered the fraction of variance of observations explained by the model. Hence higher R^2 value indicates a greater accuracy of the model, with $R^2 = 1$ indicating perfect predictive ability of the model. The Root Mean Square Error (RMSE = $\sqrt{\overline{(\eta_{\mathrm{ANTT}} - \eta_{\mathrm{GSVM}})^2}}$ represents the mean error between predictions for the GSVM compared to predictions based on ANTT observations. This gives an indication of the level of error that should be expected when predicting sea levels using the GSVM.

The tidal model performed best at Pt. Stanvac and Outer Harbor, with correlation of 0.99 indicating near perfect reproduction of sea level for the tidal constituents considered. The worst performance within the gulf was found at Ardrossan, with correlation of 0.91. This is assumed to be a result of the complex topography in the area which features a sudden change in depth from the deeper central channel to the shallow coastal waters where ANTT data is collected. Errors within the model topography can result in errors in tidal reproduction. The worst result for the entire domain is in Emu Bay on the north coast of KI, which is again assumed to be the result of complex local topography which is poorly resolved by even the 500 m resolution GSVM.

Location	Sea Level R^2 C_D using eqn **(3.7c)**	σ_{ANTT} (m) ($RMSE_{ROMS}$(m))	Sea Level R^2 for Constant C_D = 0.0025	σ_{ANTT} (m) ($RMSE_{ROMS}$ (m)) for Constant C_D= 0.0025
Ardrossan	0.93	0.39 (0.19)	0.76	0.39 (0.34)
Outer-Harbor	0.99	0.31 (0.06)	0.83	0.31 (0.24)
Pt. Giles	0.99	0.27 (0.06)	0.87	0.27 (0.18)
Pt. Vincent	0.94	0.33 (0.15)	0.76	0.30 (0.29)
Edithburgh	0.98	0.26 (0.07)	0.86	0.26 (0.18)
Emu Bay	0.82	0.16 (0.13)	0.99	0.16 (0.03)
Kingscote	0.97	0.17 (0.06)	0.95	0.17 (0.07)
Pt. Stanvac	0.99	0.27 (0.05)	0.86	0.27 (0.18)
Penneshaw	0.92	0.15 (0.06)	0.75	0.15 (0.14)
Pt. Noarlunga	0.99	0.26 (0.05)	0.82	0.26 (0.20)
Cape Jervis	0.93	0.15 (0.07)	0.77	0.15 (0.13)
Victor Harbor	0.92	0.12 (0.06)	0.89	0.12 (0.07)
Mean	0.95	N/A	0.84	N/A

Table 3.3: Correlation of SSH predictions for tidal GSVM and ANTT data (R^2), Standard Deviation of ANTT SSH predictions (σ_{ANTT})and RMSE of the tidal GSVM SSH ($RMSE_{ROMS}$). Results for tidal GSVM using domain wide constant value of C_D= 0.0025 also shown to indicate relative performance of depth and benthic type dependent model over 'traditional' approach.

The results of the tidal analysis show excellent predictive ability at almost all locations investigated within GSV (Table 3.3). Comparison with a 'traditional' approach using a domain wide C_D with value 0.0025 showed great improvement for the model which accounts for depth and benthic variation in C_D for all locations within the gulf. The only location where the traditional approach was more accurate is Emu Bay on the north shore of KI, where it is suspected the complex topography is not particularly well resolved even by the 500 m resolution grid. GSVM results for Kingscote, a short distance eastward from Emu Bay, indicate that tides are being well predicted for the region in general.

The mean R^2 value including all 12 points investigated is given as 0.95, indicating the model has an excellent over all ability to predict sea surface height based on tidal influences throughout the model domain. An example of the predictive skill of the tidal GSVM for sea surface height at Pt. Stanvac is shown in Figure 3.3.

Typically the ROMS model very slightly overestimates the tidal sea level in relation to the ANTT predicted sea levels (Figure 3.3). Because the model has an excellent predictive ability for tidal sea level variation, it is a fair assumption that the model will also reasonably predict tidal currents. Direct comparisons with current mooring data are not possible due to the inclusion of wind-stress effects in that data.

Maximum simulated tidal velocities over the 90 day model period are shown in Figure 3.4. Tidal velocities were shown to reach in excess of 1 m s^{-1} in BP, indicating a strong mixing ability through that region. It also suggests that under the correct combination of tidal movement and wind-stress that extreme flow velocities may be observed in the region. Maximum tidal velocities through IS reach up to $\sim$ 0.3 m s^{-1} and up to $\sim$ 0.4 m s^{-1} at the heel of Yorke Peninsula where a sea mount is present. At the western open boundary a zone of high velocity is noted around Althorpe Island. For the remainder of the interior of the gulf tidal velocities rarely exceed $\sim$ 0.2 m s^{-1} with the exception of the central northern channel.

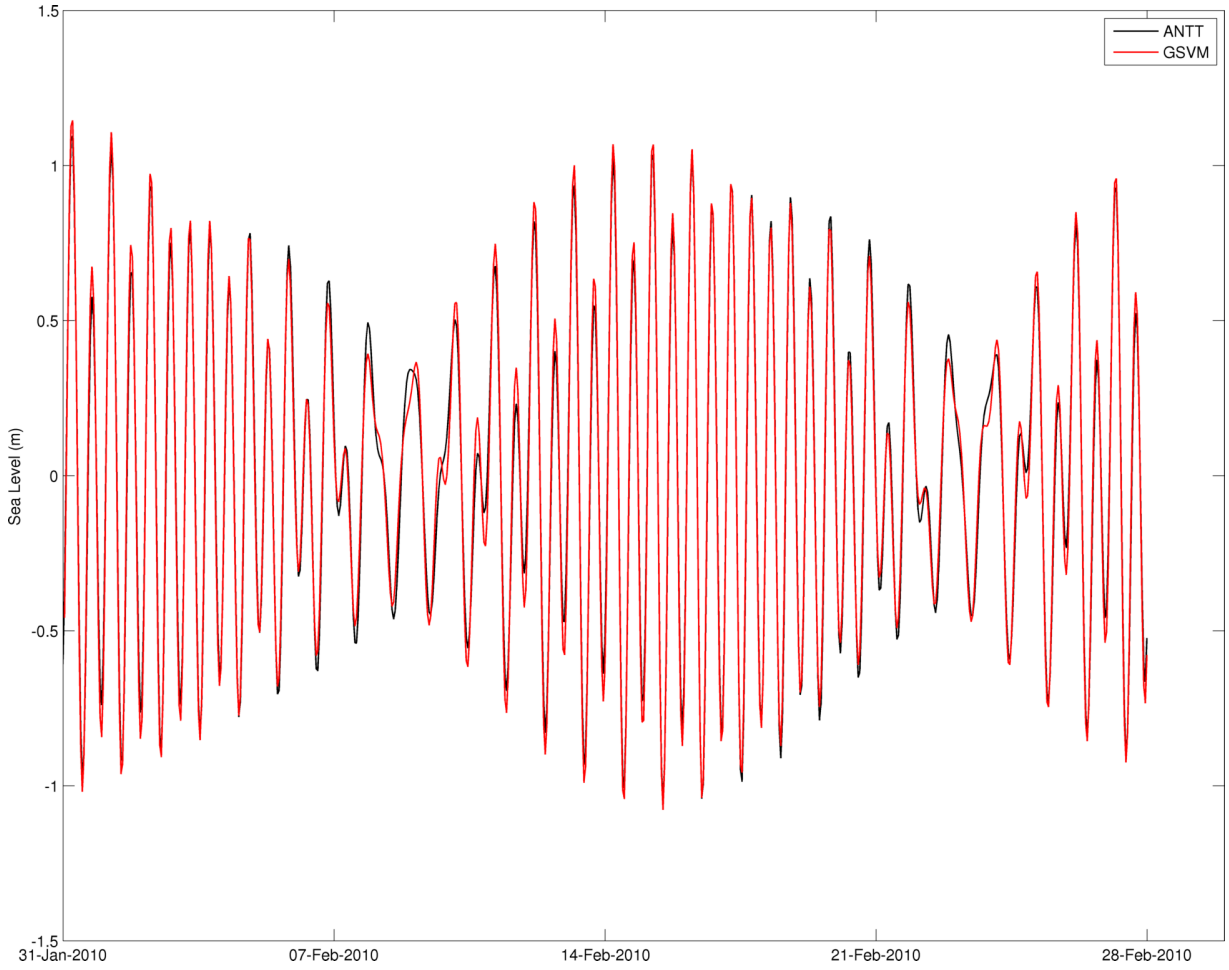

Figure 3.3: Sea level for Pt. Stanvac as predicted by resultant amplitude and phase for 9 considered constituents from tidal GSVM results compared with ANTT amplitude and phases for same location for the period 01-Feb-2010 to 01-March-2010. Pt. Stanvac represents one of the best performing comparison points within the interior of the gulf with correlation of 0.99.

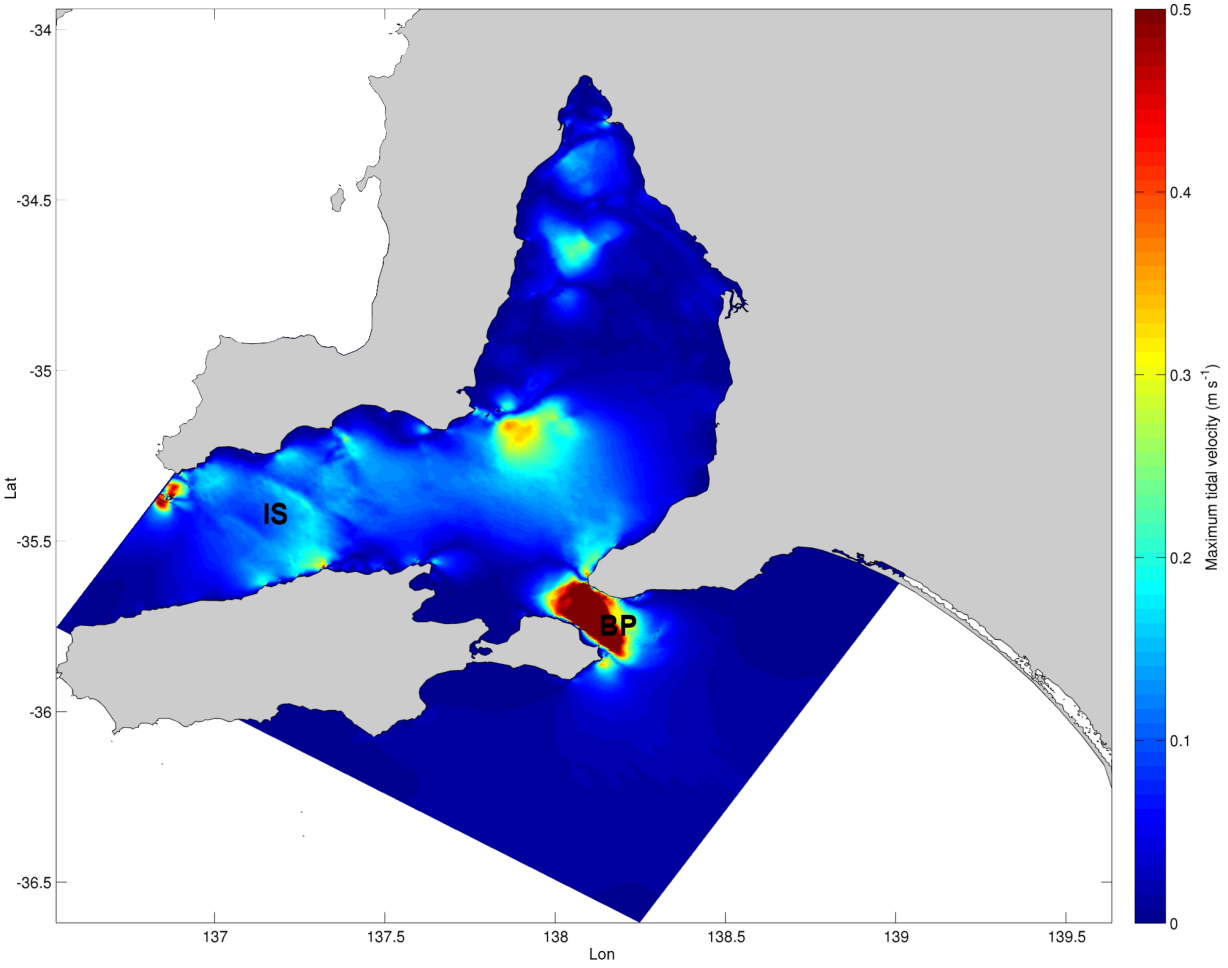

Figure 3.4: Maximum simulated depth integrated tidal velocities for GSVM. Very high tidal induced currents are recorded through BP, with moderate velocities for most of IS and some locations through the central portion of the gulf. Coastal zones, especially on the east, show weak tidally induced current velocities.

Chapter 4

Wind Forcing

4.1 Summary

The importance of local wind-stress on the circulation of GSV is determined through a number of idealised experiments. Current and sea level variation resulting from wind-stress forcing were estimated for the model domain and beyond, using boundary conditions generated by the parent SAROM model under the same wind-stress conditions. Summer winds are typically from the south-east and winter winds from the south-west, hence the cross-gulf axis was oriented SE-NW and the along-gulf axis SW-NE in order to best represent mean seasonal wind directions.

South-easterly cross-gulf winds (summer) result in significant re-circulation within the gulf and limited connectivity between the gulf and straits. Other frequent summer wind regimes (E to NE) resulted in westward flow through BP and similar flow patterns as seen in the SE cross-gulf case, however the gulf-shelf connectivity could be stronger under these winds as the southward central flow was at times able to escape the gulf interior. The presence of Kangaroo Island prevents a typical offshore Ekman flow, resulting in the unique double-gyre formation and re-circulation of gulf waters under typical summer time wind stresses. The Noye (1999) study implies the presence of the summer-time double-gyre system as described here, without explicitly investigating the hydrodynamics, by showing Lagrangian particles released throughout the centre of the gulf eventually settle in the north-western shallows, and remain in circulation in high concentration on the east coast. However this study used particles with biological behaviours, which limits its usefulness in investigating underlying hydrodynamics. Previous studies (Teixeira, 2010) have shown that neighbouring Spencer Gulf exhibits enhanced connectivity with the shelf under similar wind stresses, indicating the presence of KI at the mouth of GSV is a critical factor in response to wind-driven circulation.

South-westerly up-gulf winds (winter) create a gulf-wide clockwise rotation linked to through flow in IS and BP at the mouth. Circulation response under the up-gulf (winter) wind regime resulted in stronger gulf connectivity with IS and BP and hence the shelf when compared with cross-gulf (summer) wind-stresses. Other typical winter wind regimes (SW to N) resulted in eastward flow through BP with similar enhancement to connectivity as the SW up-gulf case. Additional models for wind-stresses from other directions indicated that the wind driven circulation patterns for the entire gulf are heavily influenced by the direction of flow though BP. Stratification in general intensified current magnitudes, but resulted in only minor changes to circulation and connectivity for the gulf with dynamics largely consistent with the

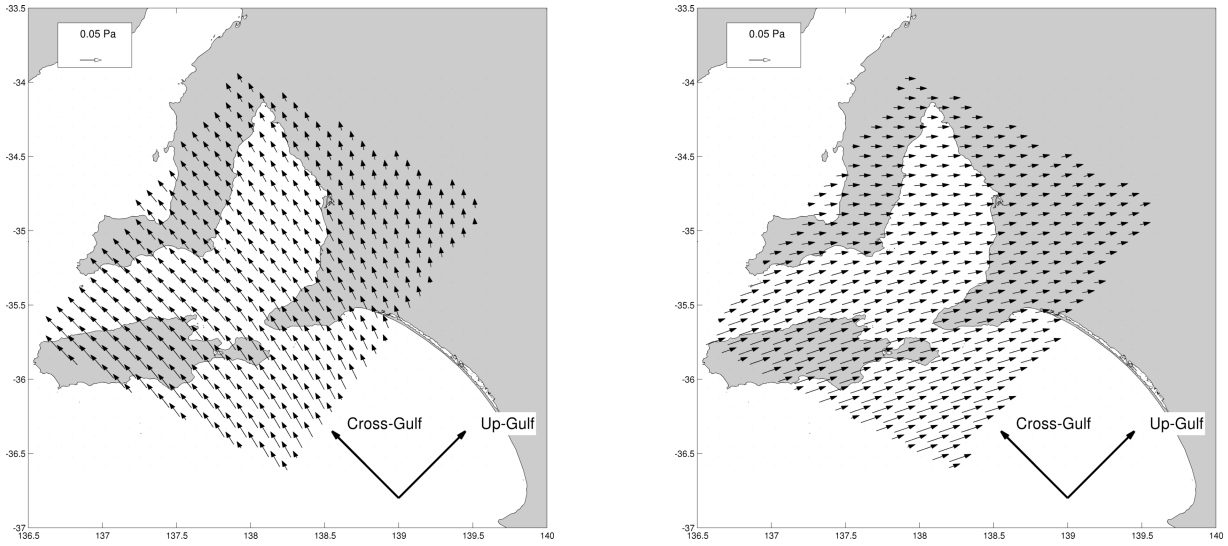

Figure 4.1: Mean seasonal wind-stress for summer (Dec, Jan, Feb 2010-2011) (Left) and; winter (Jun, Jul, Aug 2011) (Right), sourced from ECMWF. Mean seasonal summer and winter wind-stresses align well with the directions chosen to define cross-gulf and up-gulf winds respectively.

baroclinic cases.

The effect of Coastal Trapped Waves (CTWs) on circulation within the gulf was investigated through the application of a CTW paddle on the western boundary of the SAROM model, an estimation of the wind-forced CTW energy energy which is generated backward from the open boundary (Middleton, 2006). Sea level and depth integrated velocity within IS, BP and the gulf interior was investigated. Results suggest that sea level changes due to the passage of CTWs throughout the interior of the gulf are almost uniform and hence little influence on depth-integrated velocity is found, certainly insignificant in comparison to the local wind forcing presented. Velocities due to the passage of CTWs in IS and BP are greater due to their constricted flow paths.

In this chapter: The key features of sea level and depth-integrated velocity fields are identified under typical seasonal summer and winter winds. The dynamics which cause the identified features are investigated, and it is shown that the dynamics of the system under barotropic wind forced conditions are adequately explained by a balance of the Coriolis Force, Pressure Force, Wind-Stress and Bottom-Stress. It is shown that under typical wind-stress conditions for summer (south-easterlies) connectivity between the gulf and straits is reduced due to the formation of a 'double gyre' system within the gulf. Conversely, it is shown that under typical wind-stress conditions for winter (south-westerlies) connectivity between the gulf and straits is enhanced due to the formation of a gulf wide clockwise gyre which draws shelf waters in through the northern coast of IS and expels gulf waters through BP. Finally, Coastal Trapped Waves (CTWs) are shown to have little impact on circulation within the gulf, but may induce notable flows through IS and particularly BP.

4.2 Introduction

It has been suggested that the wind-driven circulation under a south-westerly wind is largely responsible for the flushing of GSV, and may be a more important process in flushing than any density driven circulation

which may occur (Bye, 1976; Bye & Kämpf, 2006). GSV is subject to typical seasonal wind patterns, experiencing predominantly north-westerly and south-westerly winds during winter and south-easterly and occasionally south-westerly winds during summer (BOM, 2012; Gentilli, 1971). As such it is expected that GSV will experience wind driven currents with seasonal variation corresponding to the local wind regimes. Some previous studies have examined the effect of wind-stresses on circulation through GSV, though all to date have been of relatively course resolution and included other limitations that the work here resolves.

Tronson (1974)determined that under a constant SW wind of 10 $m.s^{-1}$ ($\sim$ 0.15 Pa surface stress) a sea level set-up of greater than 20 cm for the upper gulf occurs. The modeled circulation showed the development of a counter-clockwise gyre in the far north of the gulf, along with northward flow along both east and west coasts, with a return southward flow in the deeper central region of the gulf. Results of this modeling show that flows within the gulfs appear quite weak (maximum $\sim$ 6 cm s^{-1}). The Tronson (1974) study also includes the investigation of NW winds of 10 $m.s^{-1}$ and draws the conclusion that the pattern of circulation is reversed when compared to the SW wind-stresses. The study is limited in that it treats the gulf as an isolated system and is of very coarse resolution (6.35 km). Both of these limitations are addressed within this study with the high-resolution GSVM being coupled to the shelf model SAROM, which is forced under the same wind conditions and provides boundary conditions to the GSVM. Additionally, the winds modeled by Tronson are for strong storm conditions, and not typical seasonal circulation, which this study attempts to resolve.

Sharobeam & Sag (1977)conducted a similar experiment, albeit one in which stress magnitude and direction varied in time in order to simulate a passing storm front. In this case light NE winds preceded the stronger SW storm winds with surface wind velocities ranging from 10-15 $m.s^{-1}$ (0.15 - 0.33 Pa surface stress) as the simulated storm front passed. The flow regime which developed was similar to that predicted by Tronson (1974), but missing the anti-clockwise gyre at the head of the gulf. TheSharobeam & Sag (1977) study shared the same limitations as the Tronson (1974) model.

Samarasinghe et al. (2003)created a basic model which used seasonally averaged wind-stress with directional modulation to simulate passing weather band events. The authors found that for a steady south-westerly wind at 5 $m.s^{-1}$ ($\sim$ 0.04 Pa surface stress), which is much more representative of mean wind speeds for the region than the above studies, a similar flow pattern to that predicted by Tronson (1974) emerged (Samarasinghe et al., 2003). The modeling in the Samarasinghe et al. (2003) study was of 3.6 x 3.6 km resolution, a much coarser resolution than the GSVM. The Samarasinghe et al. (2003) study also treated GSV as an isolated system.

The Teixeira (2010) model which focused on Spencer Gulf also included GSV in its domain, however no attempt was made at calibrating for GSV or interpreting results from GSV. The results of the Teixeira (2010) study indicate that local winds can have an effect on short term circulation, but over longer timescales the thermohaline structure of the gulf plays a more dominant role in circulation and flushing. As GSV is quite similar to SG in terms of shape and orientation, it is expected that circulation within GSV will share many traits with SG under the same wind-stress regimes. However, the presence of KI and hence IS and BP complicates the topography of GSV when compared to SG and is expected to have a large impact on the circulatory response to wind-stress.

4.3 Barotropic Experiments

In order to simply identify the effects of wind-stresses on circulation, completely barotropic models were used. In these experiments wind-stresses with typical summer direction (SE) and winter direction (SW) were adopted.

For all barotropic wind-stress experiments a maximum wind-stress value of 0.05 Pa (corresponding to a wind speed of ~ 6 m s^{-1}) was used. This value was chosen based on the mean magnitude of summer and winter wind-stresses as sourced from ECMWF and shown in Figure 4.1.

Wind-stress was modulated using a sine function of periodicity 10 days with maximum positive wind-stress values (0.05 Pa) occurring at 2.5 and 12.5 days in to the simulation and maximum negative values occurring at 7.5 and 17.5 days in to the 20 day simulation. Wind-stress values were spatially constant across the model domain.

To account for effects of wind-generated shelf currents and sea level variation the parent SAROM model was executed under the same wind forcing regimes, and values for two-dimnesional velocity and sea level as generated by the SAROM model were applied at the GSVM open boundaries with nudging time scale of 1 day.

Stratification of the water column was found to have minimal impact on the overall circulation and sea level fields developed under wind-stresses. As such the results are not discussed. Results can be found in Appendix B.

4.3.1 Cross-Gulf South-Easterly (Summer) Wind-Stress

4.3.1.1 Key Features

Sea Level For the cross-gulf (summer) wind-stress case study the results presented are instantaneous values for 12.5 days in to the simulation, representing the model state during the maximum south-easterly wind-stress. The sea level distribution in Figure 4.2 shows a general sea level gradient is formed from the head of the gulf to the mouth. A depression dominates the entire eastern coastline of GSV, while on the western coast the sea level is generally elevated. A trough forms along the central-western portion of the gulf with a corresponding elevated ridge along the central-eastern portion of the gulf.

IS, BP and the shelf exhibit sea level depression (2-3 cm below mean), consistent with the offshore Ekman transport expected for SE winds which are parallel to the coastline of the region. This is the process through which upwelling is forced on the Bonney Coast, an important mechanism for the introduction of nutrient rich water in the coastal waters systems of South Australia (Kämpf et al., 2004; Middleton & Platov, 2003; Schahinger, 1987).

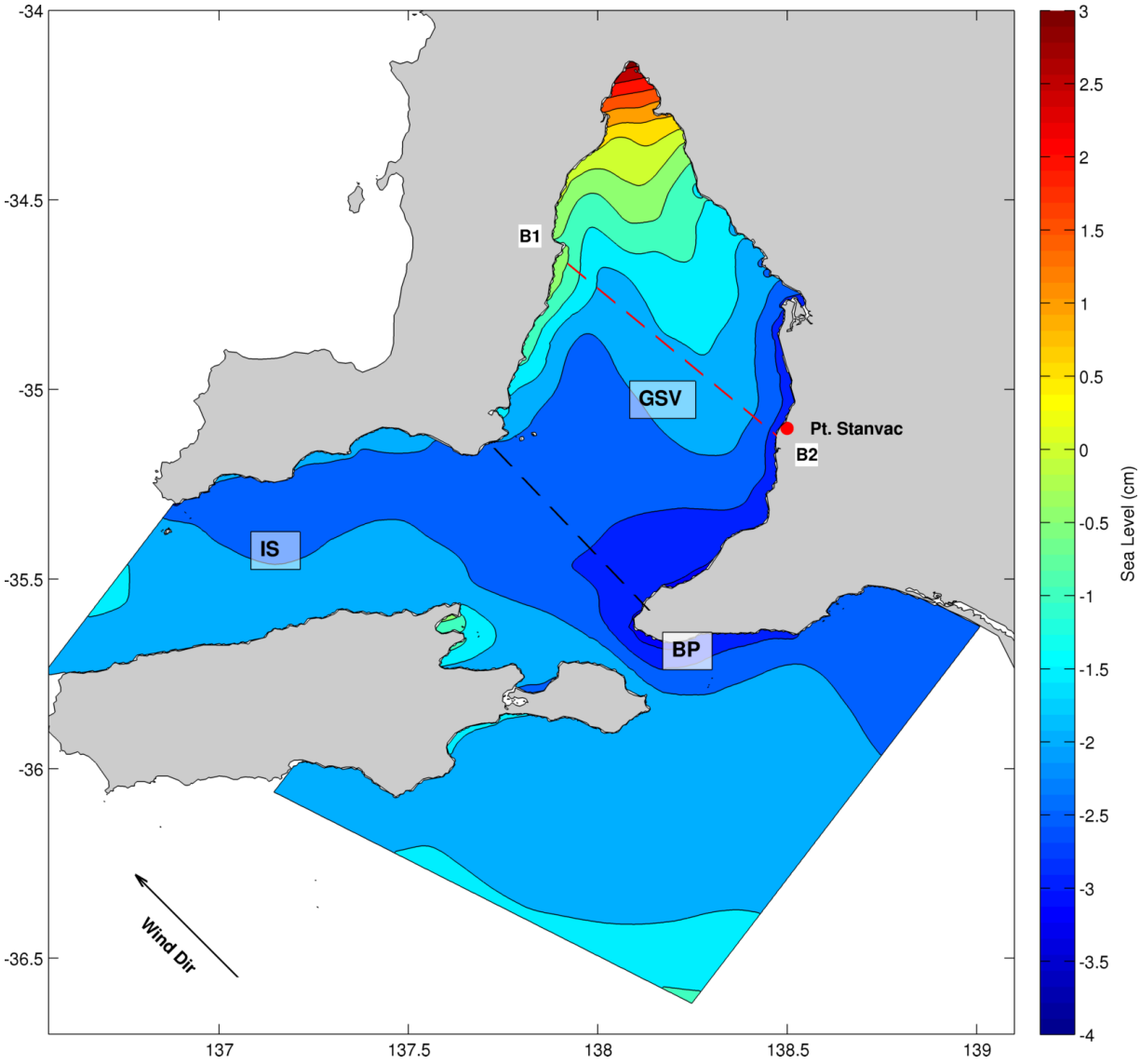

Figure 4.2: Sea level for south-easterly cross-gulf (summer) wind-stress (wind-stress maximum positive = 0.05 Pa). Units cm deviation from mean. Contour interval 0.5 cm. Dashed line B1-B2 indicates the cross section taken to calculate solutions to force balance equations, results shown in Figure 4.4. The cross-gulf south-easterly winds result in a slight sea level set up ($\sim$ 3 cm) on the northern coast of the gulf, but in general a decrease in mean sea level for the majority of the model domain. A north-south trough can be seen offshore the western coast and a corresponding ridge offshore the eastern coast. Sea level is increased on the western coast of the gulf and decreased on the eastern.

Velocity - GSV There are a few major flow features associated with the results for GSV (Figure 4.3) for the south-easterly (summer) wind-stress model. Northward flow on both east and west coasts is modeled, with southward return flow through the centre of the gulf. This is nicknamed the 'double gyre' system. Northward flows on the coasts are quite strong ($\sim$ 10 cm s^{-1}), with return flows through the deeper central gulf slower ($\sim$ 5 cm s^{-1}). Very weak flow is modeled across the mouth M1-M2 (Figure 1.1).

Velocity - IS and BP The major features noted for flow through IS and BP are dominated by a strong westward flow of waters though BP and IS, driven by the SE winds. Flows through BP are very strong ($>$ 10 cm s^{-1}) due to its shallow and narrow nature. Flows in IS are weaker ($\sim$ 4 cm s^{-1}). Waters exiting IS are mostly constrained to the north coast, on the 'toe' of Yorke Peninsula. Flow through BP and IS has very little interaction with gulf waters, with almost no flow across the mouth (M1 - M2, Figure 1.1). To the south of KI there is a weak westward flow.

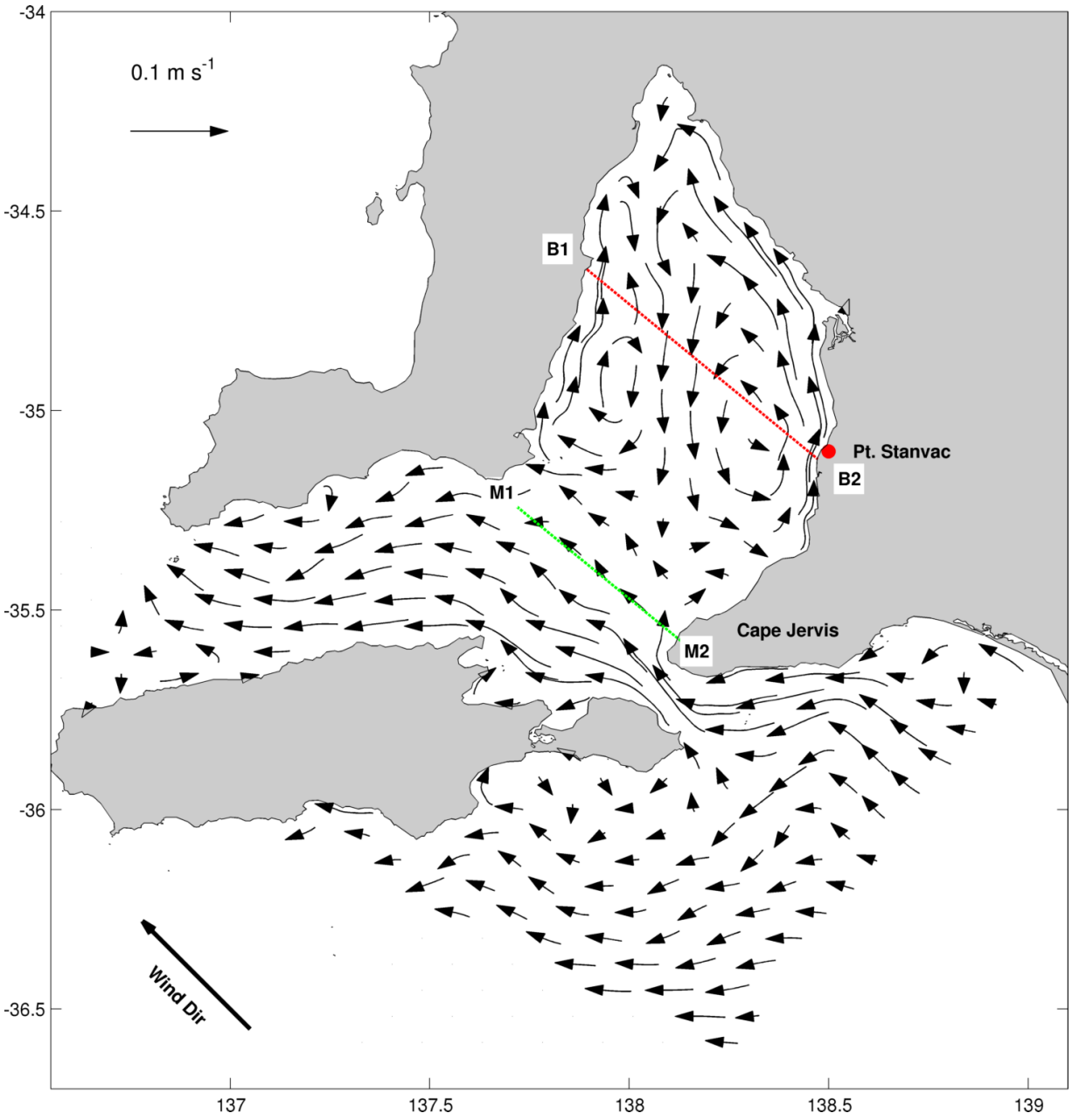

Figure 4.3: Depth-averaged velocity field for south-easterly cross-gulf (summer) wind-stress (wind-stress maximum positive = 0.05 Pa) units cm s^{-1} . Legend arrow indicates flow velocity of 10 cm s^{-1}. Dashed line B1-B2 indicates the cross section taken to calculate solutions to force balance equations, results shown in Figure 4.4. The main features of circulation under the cross-gulf south-easterly winds are the strong westward flow through BP and IS and the formation of a 'double gyre' system within the gulf which re-circulates gulf waters northward on either coast and southward through the deeper central portion. This results in the creation of two mostly separate flow paths; separated by a zone of very weak flow around the mouth of the gulf.

4.3.1.2 Dynamics

The results of the idealised wind experiments can be explained by the momentum balance of Coriolis force, pressure force, bottom-stress and wind-stress:

$$\underbrace{\frac{du}{dt}}_{\mathrm{RC_x}} = \underbrace{+fv}_{\mathrm{CF_x}} - \underbrace{\frac{1}{\rho_0}\frac{dP}{dx}}_{\mathrm{PF_x}} + \underbrace{\frac{\tau_x^w}{\rho_0 h}}_{\mathrm{WS_x}} - \underbrace{\frac{\tau_x^b}{\rho_0 h}}_{\mathrm{BS_x}} \tag{4.1a}$$

$$\underbrace{\frac{dv}{dt}}_{\mathrm{RC_y}} = \underbrace{-fu}_{\mathrm{CF_y}} - \underbrace{\frac{1}{\rho_0}\frac{dP}{dy}}_{\mathrm{PF_y}} + \underbrace{\frac{\tau_y^w}{\rho_0 h}}_{\mathrm{WS_y}} - \underbrace{\frac{\tau_y^b}{\rho_0 h}}_{\mathrm{BS_y}} \tag{4.1b}$$

Where RC is acceleration, CF represents Coriolis Force, WS represents Wind-Stress, PF represents Pressure Force and BS represents Bottom-Stress.

Evaluating model outputs for the terms in Equations 4.1a and 4.1b for the cross-gulf SE (summer) condition along the cross-section B1-B2 are shown in Figure 4.4. Idealised vector representations of the force balances for near shore conditions are shown in Figure 4.5. The acceleration term in Figure 4.4 can be seen to be near zero in both the x and y directions, indicating the system has reached a quasi-steady state. The force balances for the SE wind-stress (summer) conditions are quite spatially variable due to the complexity of the sea level and flow fields developed. Evaluating the components of acceleration allows a greater understanding of the force balances under different wind-stress regimes, and hence the underlying dynamics of wind-induced flows.

- The throughflow in BP and IS is primarily a balance of the CF and PF. Westward flow initially driven by wind-stress entering through BP is deflected to the left due to the CF. As a result, water is piled up on the north coast of KI (see Figure 4.2), resulting in a PF which balances the CF ($PF + CF \backsimeq 0$) and produces the steady westward flow along the north coast of KI shown in Figure 4.3. This process is largely responsible for preventing large scale advective mixing of shelf and gulf waters.

- On the western coast of GSV (nearer B1) in the along-wind x axis a balance is reached between the PF, WS and BS, which is quite strong due to the high depth-integrated velocities seen here (Figure 4.4, upper and Figure 4.5a). In the normal y axis (Figure 4.4, lower and Figure 4.5b), the PF is largely balanced by the CF, as the bottom stress is much weaker in this direction. As B1 is within a local sea level maxima, a strong PF normal to the WS is generated by the offshore sea level trough.

- On the eastern coast (nearer B2) the force balance is almost entirely accounted for by the PF and CF for both the along-wind and normal axes (Figure 4.4). This is due to the positive PF generated by the coastal sea level depression and the corresponding offshore ridge (Figure 4.2). As the WS in this region is relatively weak due to greater depths, the PF generates an onshore flow, which under the influence of the CF is deflected northward, generating the alongshore northward current (Figures 4.5d, 4.5e and 4.5f).

- Through the central portion of the gulf a balance is reached chiefly between the PF and CF in the normal axis. This is due to the SSH configuration, with a general SSH gradient from high within the gulf to low at the mouth, inducing a negative PF which is balanced by the CF. This results in the southward return flow.

Valle-Levinson (2008) showed that for high Ekman number $E_k = \frac{A_z}{fH^2}$ where A_z is vertical diffusivity, f is the coriolis parameter and H is water depth, and high Kelvin number $K_E = \frac{B}{R_i}$ where B is basin width and R_i is internal Rossby radius of deformation, that in the southern hemisphere we should expect to see flow toward the head of the gulf on the coasts and flow toward the mouth in the centre of the gulf. Calculating E_k by estimating A_z from the vertical diffusivity of salt through the process described in equation 7.5 gives $E_k \approx 74$ which is very high, indicating friction dominates over Coriolis effects. Estimating $R_i = \frac{\sqrt{g'h}}{f}$ where $g' = \frac{g\triangle\rho}{\rho}$ is reduced gravity and h is buoyant layer depth gives $R_i \approx 3700m$, giving $K_E \approx 17$ for a gulf of width approximately 63 km. This is also a very high value, and shows that the results presented here are consistent with what is to be expected from the findings of Valle-Levinson (2008).

Models for the easterly and north-easterly wind conditions (see Appendix B) indicate that the central southward current formed under a SE wind can escape the gulf via the central portion of the mouth and result in a discharge of gulf waters via IS. This is important to note as although the SE winds are most prevalent during summer, E and NE winds are not uncommon, hence a complete summer time disconnect of flow between the gulf and shelf due to wind conditions should not be expected. However, these winds are usually not persistent, and therefore unable to form long term paths of connectivity between the shelf and gulf.

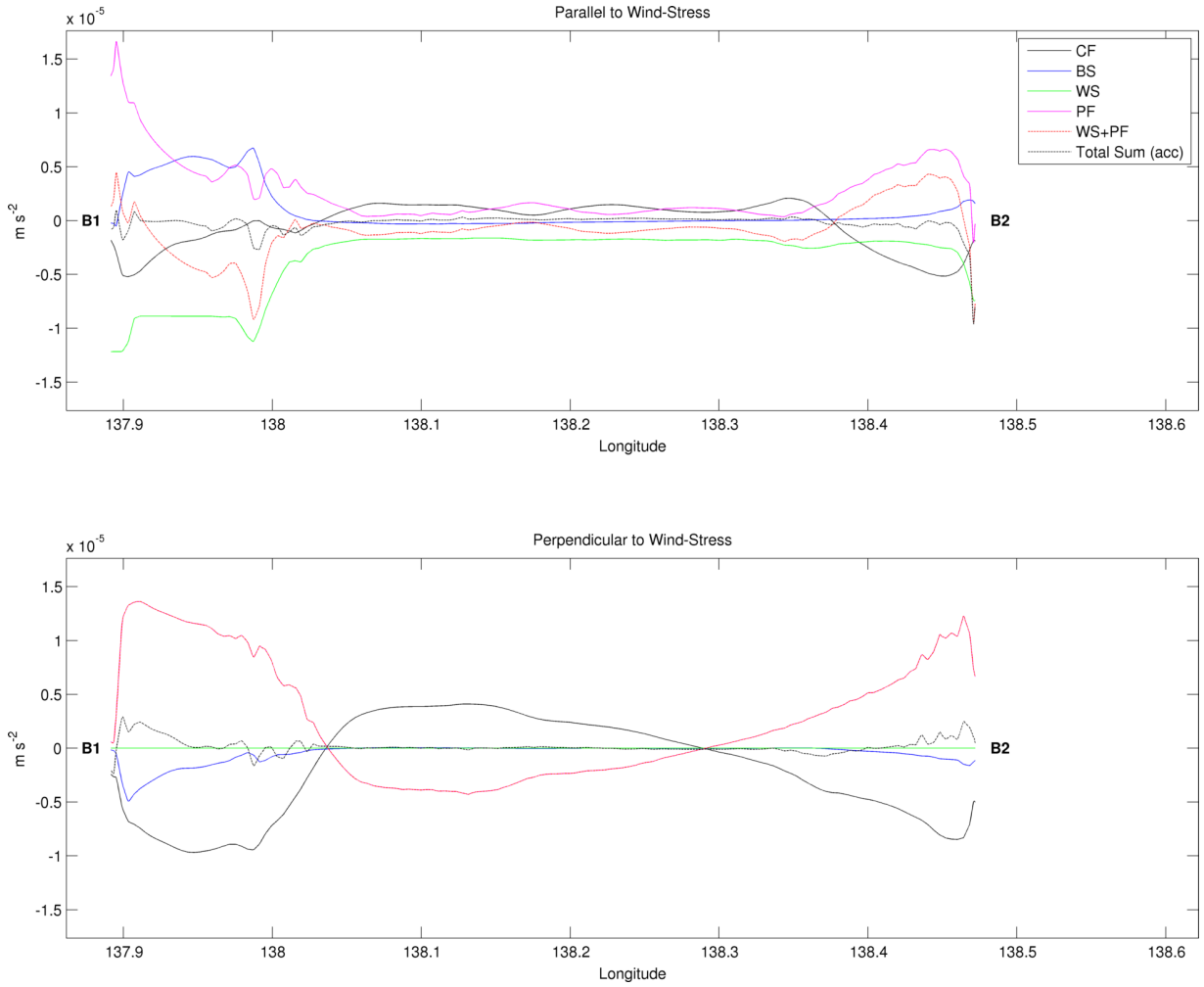

Figure 4.4: Solutions for Equations 4.1a and 4.1b along cross section B1-B2 as defined by Figure 4.3 for SE (summer) winds. Values are calculated and output by the model. The top panel shows results for force balance parallel to the wind-stress, the bottom panel shows results for force balance perpendicular to the wind-stress. Momentum components are Coriolis Force (CF - black line), Bottom Stress (BS - blue line), Wind-Stress (WS - green line) and Pressure Force (PF - magenta line). The combined wind-stress and pressure force (WS+PF - dashed red line) and total sum (representing acceleration - dashed black line) are also shown. The acceleration shows near zero values across the cross section (excepting boundary effects), indicating a quasi-steady state condition.

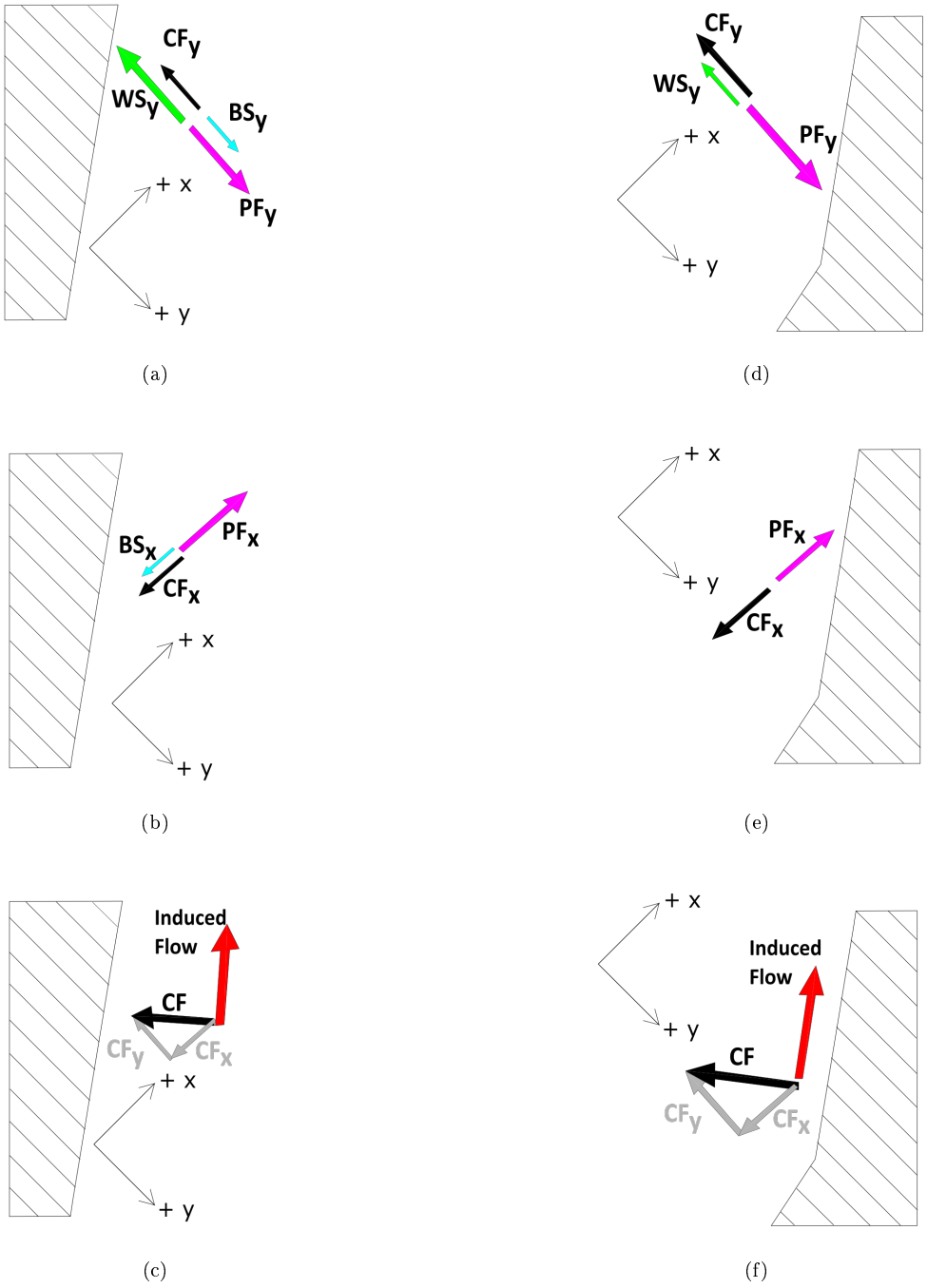

Figure 4.5: Idealised vector dynamical balance for (a, b, c) west coast (near B1) and (d, e, f) east coast (near B2) for SE (summer) wind-stresses. The top row (a and d) shows balances in the $y$direction (parallel to wind-stress), the middle row (b and e) the x direction (perpendicular to wind-stress) and the bottom row (c and f) shows the induced flow created by the necessary force balance for a quasi-steady state condition. For the summer conditions the force balance for each coast is very similar. This is largely due to the SSH conditions which arise, creating positive PF on each coast, counteracted by the WS and CF_y. In the x direction there is again a positive PF on each coast, counteracted by CF_x on each coast (and BS_x on the east coast due to high depth-integrated velocities). The need for the CF to balance the other forces to reach quasi-steady state conditions results in a net CF normal to the shoreline (onshore on the west coast and offshore on the east) and induces northward flow on both coasts. Vectors not to scale.

4.3.2 Up-Gulf SW (Winter) Wind-Stress

4.3.2.1 Key Features

Sea Level The sea level distribution in the up-gulf SW (winter) wind-stress model (Figure 4.6) is dominated by an along-gulf SSH gradient with contours approximately normal to the up-gulf wind-stress. The difference in sea level from mouth to coast is approximately 3-4 cm. The gradient throughout the central portion of the gulf is less strong and manifests as a weak trough. A small area of relatively lower sea level on the central north coast of Kangaroo Island, near Kingscote is also modeled.

In general the sea level is elevated throughout GSV, IS and BP, most notably on the coasts, as a results of waters piling up on the south-east oriented shoreline due to Ekman transport.

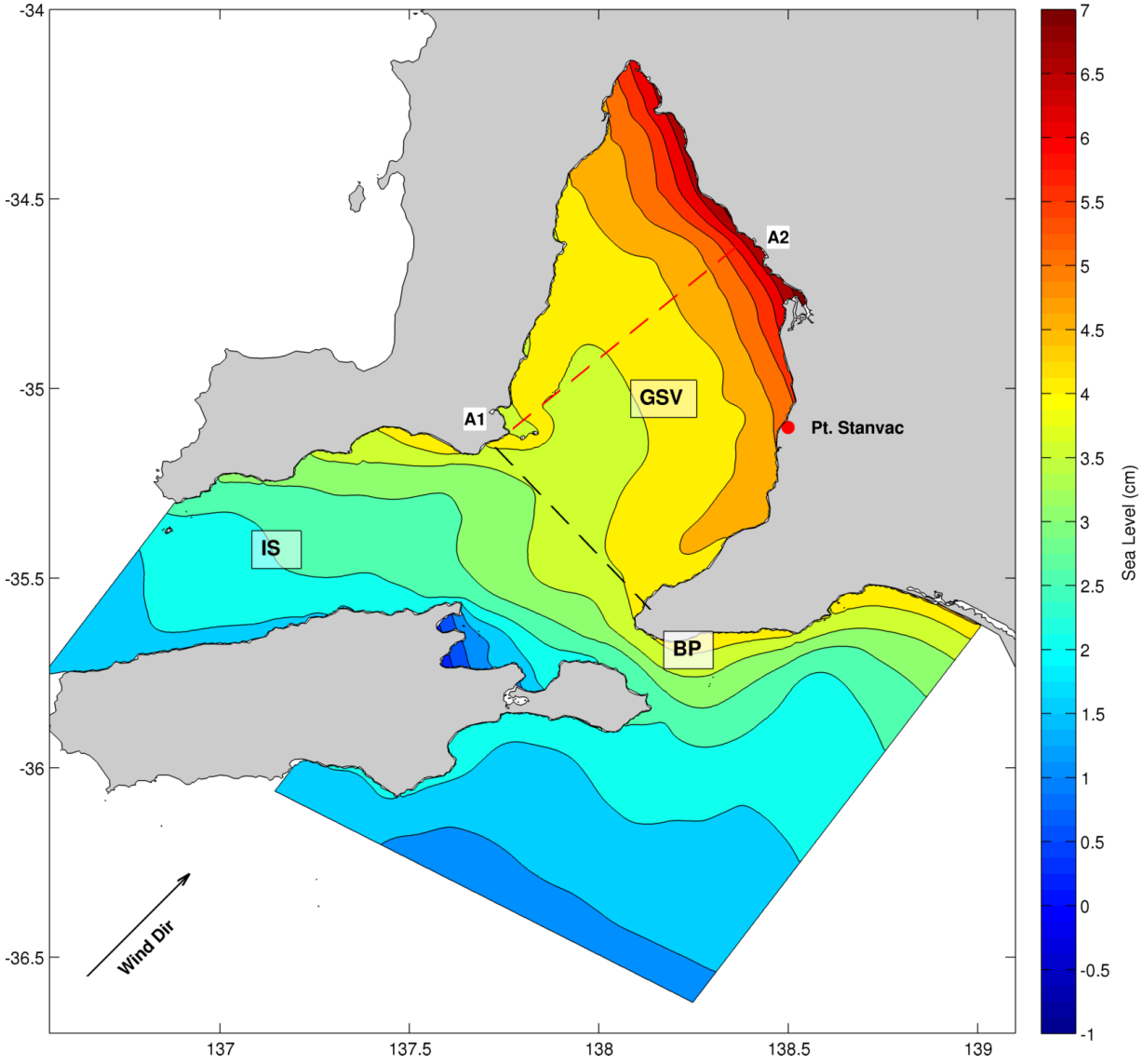

Figure 4.6: Sea level for south-westerly up-gulf (winter) wind-stress (wind-stress maximum positive = 0.05 Pa). Units cm deviation from mean. Contour interval 0.5 cm. Dashed line A1-A2 indicates cross section for the results of the force balance equations 4.1a and 4.1b shown in Figure 4.8. South-westerly wind-stresses result in sea level set up on the north eastern coast of the gulf (up to $\sim$ 8 cm) and increases sea levels throughout the GSVM domain in general.

Velocity - GSV The velocity field associated with the sea-level results is shown in Figure 4.7. The major feature of circulation within GSV resulting from the SW (winter) wind-stress is a gulf wide clockwise circulation. The gulf wide clockwise circulation is formed by northward flow on west coast with maximums of $\sim$ 10 cm s^{-1} and southward flow on the east coast with maximums of $\sim$ 6 cm s^{-1}. The central portion of the gulf shows very weak flow. A small counterclockwise gyre is observed at the head of the gulf. The GSVM shows a counterclockwise gyre with northward coastal flow on the northern coast of Cape Jervis, named the 'Myponga Eddy' by Bye & Kämpf (2006).

Velocity - IS and BP The primary flow path for waters entering IS from the shelf travels eastward along the northern shore of IS and deflects in to the gulf interior. This flow continues as a clockwise gyre spanning nearly the whole gulf interior before exiting the gulf via BP and rejoining the shelf flow. A secondary flow path travels eastward along the southern shore of IS, following the northern coast of KI before exiting the system via BP where it recombines with waters from the primary flow path. On the south coast of KI there is a steady eastward flow.

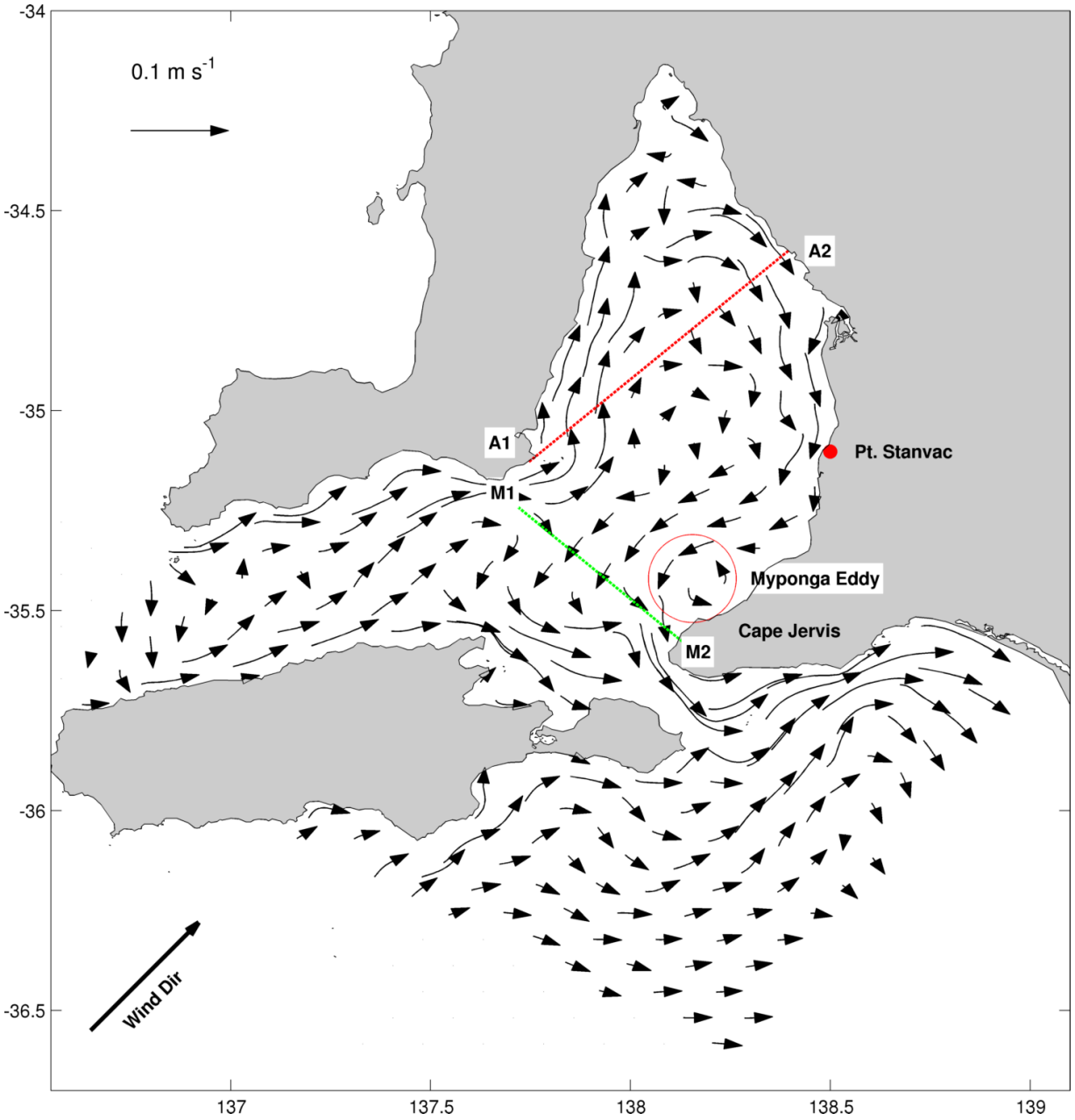

Figure 4.7: Velocity field for south-westerly up-gulf (winter) wind-stress (wind-stress maximum positive = 0.05 Pa). Legend arrow indicates flow velocity of 10 cm s^{-1}. Dashed line A1-A2 indicates cross section for the results of the force balance equations shown in Figure 4.8. The south-westerly wind-stresses induce a general clockwise flow comprising of shelf waters entering through IS, intruding in to the gulf on western coast and circulating gulf waters southward along the eastern coast and out through BP.

4.3.2.2 Dynamics

Analysis of model output for Equations 4.1a and 4.1b for cross-section A1-A2 under SW up-gulf (winter) winds are shown in Figure 4.8. The acceleration term can be seen to be near zero in both the along-wind and normal axes, indicating the system has reached a quasi-steady state. Unlike the summer case, the components of the force balance are largest for the along-wind axis. Vector representation of the dynamical balances are shown in Figure 4.9.

- Dynamical balance on the west coast (closer to A1) is dominated by the Coriolis Force (CF) and Wind-Stress (WS) terms in the wind-stress direction (Figure 4.8, lower and Figure 4.9a). Forces in the normal axis are relatively week, and balance is reached between CF and BS. The net CF is onshore, resulting in alongshore flow toward the head of the gulf.

- On the east coast (closer to A2) the balance is reached between CF, PF and WS (Figure 4.9d). The WS results in SSH increase along the coastline, inducing in an offshore PF. This in turn induces mouth ward alongshore flow. As alongshore flow intensifies, the CF is directed onshore, reinforcing the WS and maintaining the coastal SSH increase to keep the system in a quasi-steady state (Figures 4.9d and 4.9f).

- Along the northern coasts of IS, BP and to the east of BP, strong offshore PFs are generated by the sea level setup, inducing an eastward alongshore flow under the influence of the CF in much the same manner as seen for near A2.

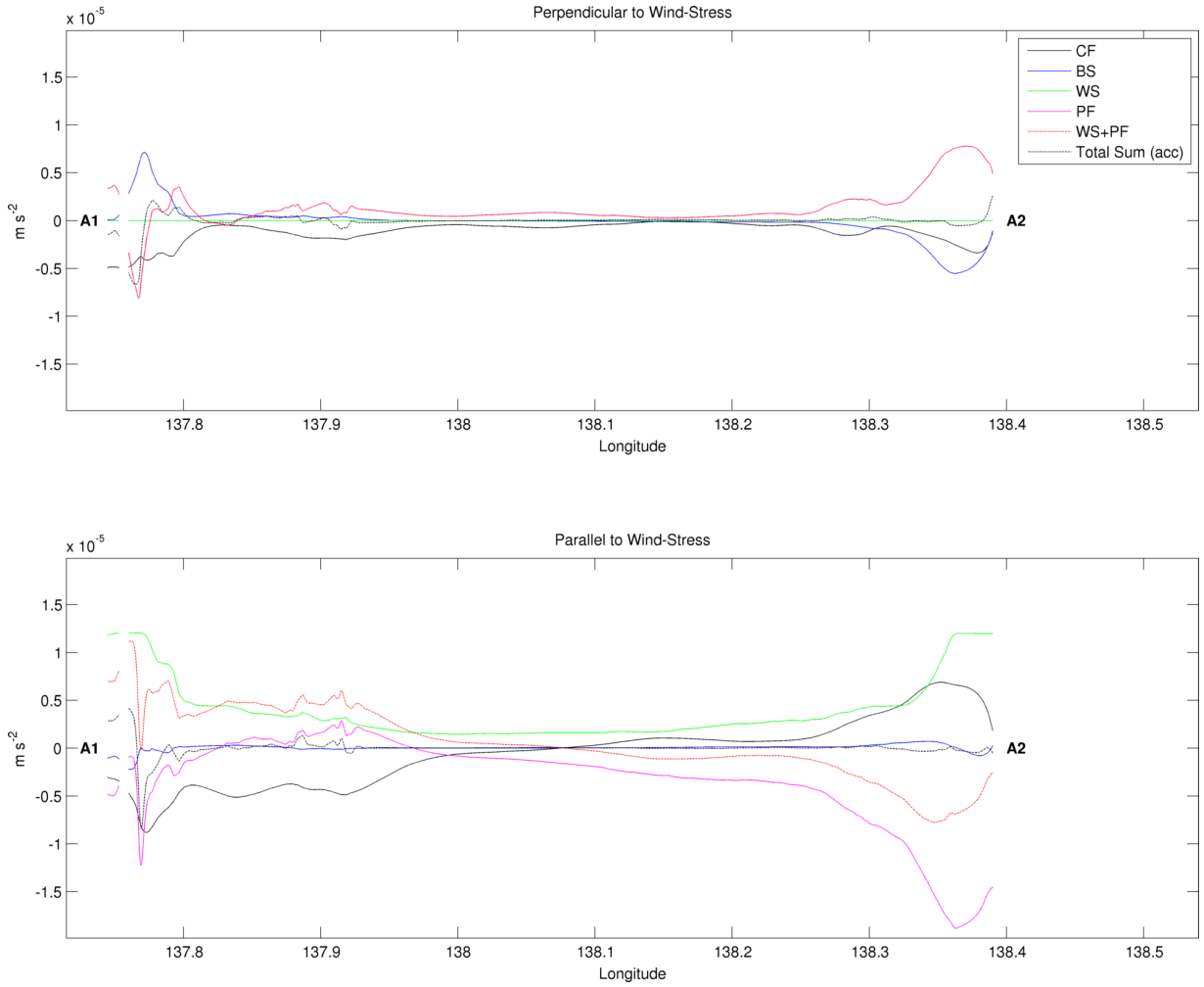

Figure 4.8: Solutions for Equations 4.1a and 4.1b along cross-section A1-A2 as defined in Figure 4.7 for SW (winter) winds. Values are calculated and output by the model. The top panel shows results for force balance perpendicular to the wind-stress, the bottom panel shows results for force balance parallel to wind-stress. Momentum components are Coriolis Force (CF - black line), Bottom Stress (BS - blue line), Wind-Stress (WS - green line) and Pressure Force (PF - magenta line). The combined wind-stress and pressure force (WS+PF - dashed red line) and total sum (representing acceleration - dashed black line) are also shown. The acceleration shows near zero values across the cross section (excepting boundary effects), indicating a quasi-steady state condition.

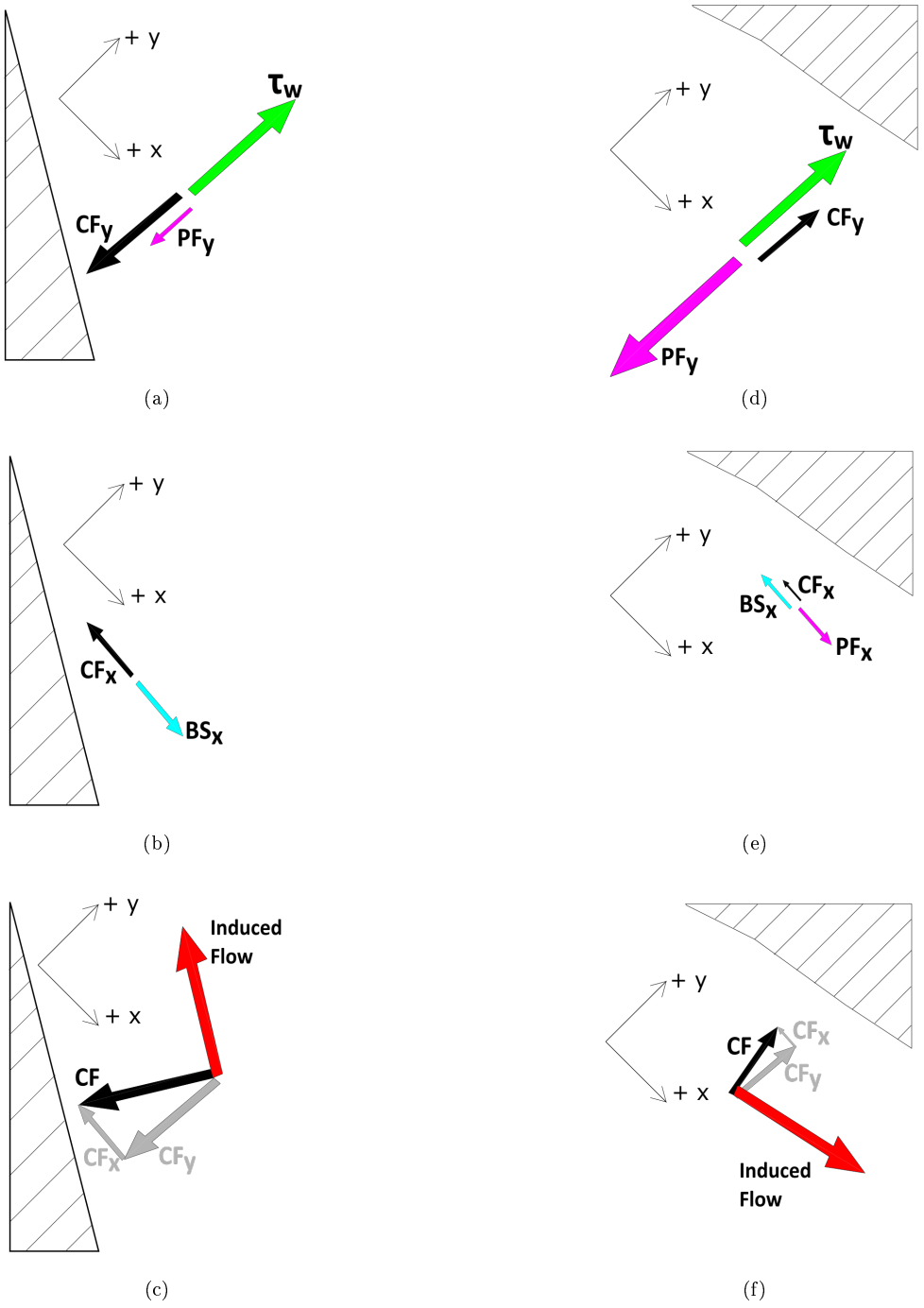

Figure 4.9: Vector representation of dynamical balance for (a, b, c) west coast (near A1) and (d, e, f) east coast (near A2) of GSV under south-westerly (winter) wind-stress conditions. The top row (a and d) shows balances in the y direction (parallel to wind-stress), the middle row (b and e) the x direction (perpendicular to wind-stress) and the bottom row (c and f) shows the induced flow created by the necessary force balance for a quasi-steady state condition. For the west coast the primary balance in the y axis is reached between the WS and CF, with a minor contribution from PF due to the slight sea level depression on the coast in this location. On the east coast the same forces balance, but in this case the PF grows to be stronger than the WS, inducing offshore flow and eventually resulting in CF_y acting against the PF. In the x axis the primary balance is between the BS and CF on the east coast and BS and PF on the west. In both cases the forces become balanced when a flow of sufficient magnitude and direction brings about balance through the associated CF. This results in alongshore flow for both cases, toward the head on the west coast and toward the mouth on the east coast, generating the gulf wide clockwise circulation modeled. Vectors are not to scale.

4.3.3 Net Transport via wind-stress

The difference in connectivity (i.e. the mass exchange of waters) between the gulf and IS/BP for different flow regimes can be estimated by determining the flow in and out of the gulf, defined as the transport across the mouth (e.g. orthogonal to the line M1-M2 as shown in Figure 1.1). Figure 4.10 compares transport (equal to depth-averaged flow velocities multiplied by depth) orthogonal to this line for the different wind-stress regimes indicates the level of connectivity for the gulf.

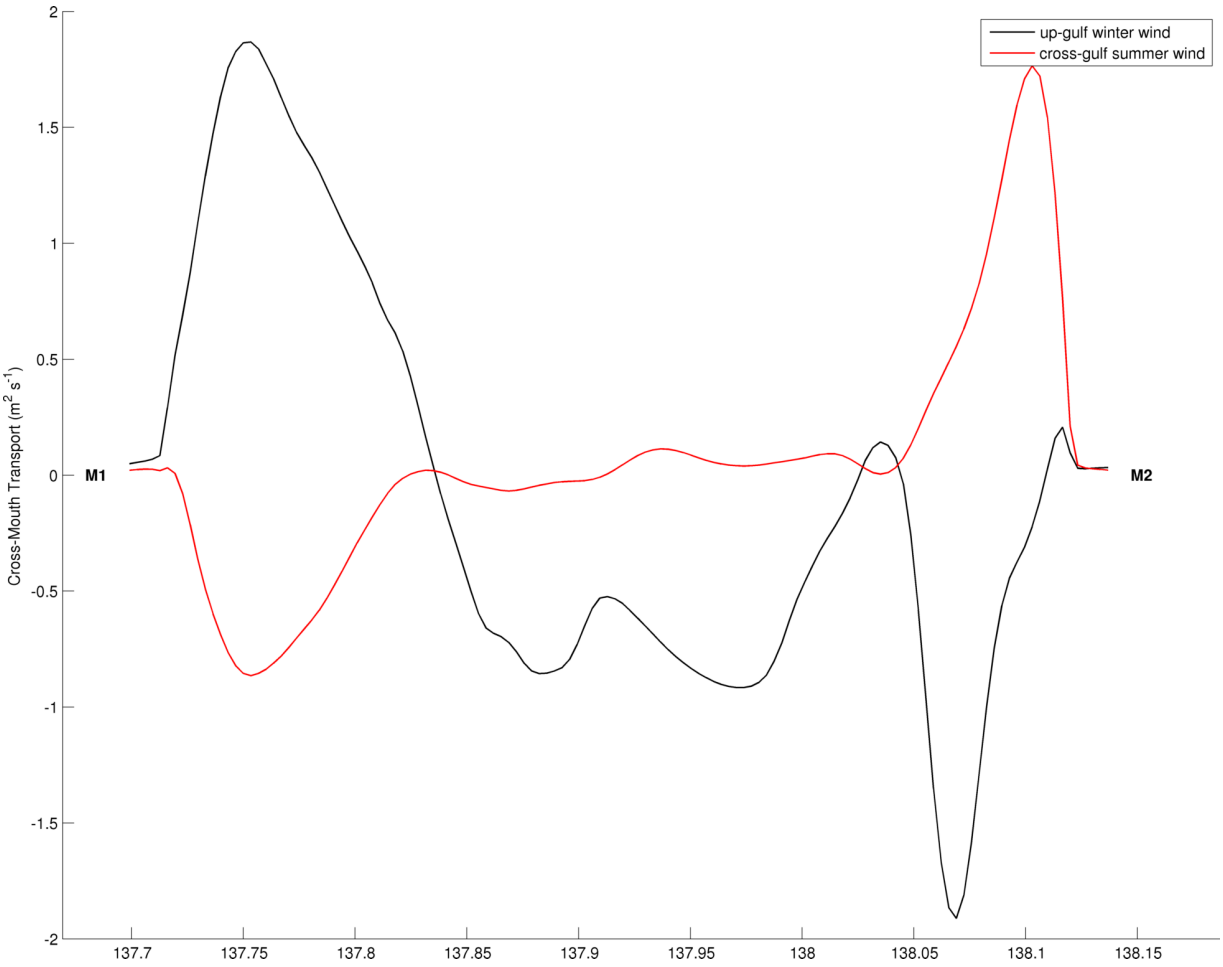

Figure 4.10: Instantaneous values for transport (depth integrated velocity multiplied by depth) (m^2 s^{-1}) at 12.5 days, orthogonal to mouth of gulf (positive in to gulf, negative out from gulf as defined by line M1-M2 in Figure 1.1) for barotropic wind-stress models with up-gulf south-westerly wind (black) and cross-gulf south-easterlies (red). A much greater level of cross-mouth transport is observed for the up-gulf wind model (black line) when compared to the cross-gulf model (red line), indicating enhanced connectivity under SW wind-stresses compared to SE.

As evidenced in Figure 4.10, the level of connectivity is much greater under the up-gulf south-westerly (winter) wind regime than the cross-gulf south-easterly (summer). For the cross-gulf case (summer) there is a small flow in to the gulf on the eastern edge of the mouth at Cape Jervis, with a corresponding outflow at the western edge. Through the middle of the mouth there is a 'dead-zone' where there is effectively no mean transport in or out of the gulf across this line. This is due to the flow at the southern boundary of the double-gyre formation running parallel to the mouth of the gulf. For the up-gulf wind case (winter)

there is a very strong gulf-ward transport on the western edge of the mouth, with moderate outflow through the centre and a strong localised outflow on the eastern edge at Cape Jervis. This demonstrates the strong level of connectivity in the south-westerly wind conditions which incite the clockwise rotation of gulf waters.

4.4 Coastal Trapped Waves

4.4.1 Summary

An understanding of the effect of Coastal Trapped Waves (CTWs) is attained through the use of a first mode CTW paddle model (see below) based on the SAROM grid. The SAROM grid was chosen in order to fully resolve the effect of KI on CTW propagation, which is not possible with the GSVM domain. Model results indicate little depth-integrated circulation within GSV (3-4 cm s^{-1}) due to the passage of the CTWs, with stronger currents modeled for IS (up to 7 cm s^{-1}) and particularly BP (up to 10 cm s^{-1}).

In this section: Previous studies investigating the significance of CTWs on neighbouring Spencer Gulf are examined. A CTW model based on the SAROM grid is developed to investigate the effect of a passing CTW of amplitude 10 cm and periodicity 10 days on sea level and depth-integrated velocity within IS, GSV and BP. Model results indicates that sea level variation within GSV is near uniform for a passing CTW and induces little flow, whereas more significant flows for IS and particularly BP are simulated.

4.4.2 Introduction

Coastal Trapped Waves (CTWs) propagate unidirectionally with the coast on the left (right) in the southern (northern) hemisphere and in the presence of sloped shelf topography. Typically, they are driven by alongshore wind-stress. CTWs on the southern coast of Australia can be of relatively large amplitude, up to 1 m (Krause & Radok, 1977).

IS and BP provide a potential conduit for their meridional propagation in to the gulf. Krause & Radok (1977) argued that CTWs on the southern coast of Australia play a role in the circulation of enclosed bodies such as SG and GSV. Church & Freeland (1987) showed that energy from CTWs preferentially traveled through Bass Strait en-route to the east coast of Australia, suggesting that the topography of GSV could lend itself to funneling energy of CTWs through IS and BP generating CTW induced currents, even though IS is very narrow and shallow when compared to Bass Strait.

A previous three-dimensional model by Teixeira (2010) indicated that the majority of CTW driven flows were diverted to the south of KI, with little energy entering IS. However, the Teixeira model was designed for the analysis of SG and was of a relatively low resolution (5 km). The shallow and narrow nature of IS and BP have the potential to magnify any CTW driven currents. Teixeira (2010) found the CTWs to have only a small effect on the circulation of Spencer Gulf. This was principally due to the wave length of CTWs being several hundred kilometers, meaning that for CTWs passing the mouth of SG the elevation change due to that wave at the west side of the mouth was almost exactly that of the east. The net result then was a uniform slight change in sea level for the whole gulf, and hence little pressure gradient causing circulation. The width of GSV at the mouth is even narrower than SG, so it would stand to reason that the same phenomena would occur there. However, the presence of KI potentially complicates the manner in which the CTW propagates along the shelf in this region.

4.4.3 Methods

Idealised profiles for sea level and depth integrated velocities using a first mode CTW paddle were generated and applied at the western boundary of the SAROM grid (see equation 4.2).

$$\eta = \eta_0 F(x) \sin(\omega t) \tag{4.2}$$

where η is Sea Surface Height (SSH), η_0 is initial SSH, $F(x)$ is the wave form Eigen function of the CTW (Brink & Champan, 1987) with respect to distance from the coast x, ω is the periodicity of the CTW (10 days in this case) and t is time.

No other forcing was applied to the SAROM model. Sea level and depth integrated velocities within the GSVM domain were investigated in order to determine the effect of CTWs on circulation within GSV. The idealised CTW paddle was forced with a period of 10 days, which roughly agrees with typical timescales for CTWs observed on the Southern Australian shelf Krause & Radok (1977). Forcing was ramped up from zero amplitude to amplitude described by equation 4.2 over a period 5 days to prevent shock and instability to the system.

4.4.4 Results

The results show that, for the majority of GSV, the sea level is elevated and mostly uniform during the passage of the peak of CTWs and depressed and mostly uniform during the passage of CTW troughs (see Figure 4.11 and Appendix B, Figure B.13), with small sea level gradients observed within IS and BP. The animation shown in Figure 4.11 clearly indicates that the currents induced by the CTW are relatively weak through IS and BP, with much greater effect on currents following approximately the path of the 100 m isobath around the SW tip of KI. A small amount of energy enters IS, causing a weak eastward flow ahead of the CTW peak. Part of this flow is deflected along the western coast of GSV by the Coriolis force, which induces an extremely weak clockwise circulation within the gulf. This flow has maximum speeds of ~ 4 cm s^{-1} on the western coast, and rapidly diminishes to below 1 cm s^{-1} for all other regions of the gulf. The narrow flow path of BP causes flow speeds to peak at to over 10 cm s^{-1} in this region. Following the peak of the CTW passing GSV the flow reverses, again with stronger flows within BP and IS, with very weak (~ 3 cm s^{-1}) depth integrated flows on the western coast of GSV.

While CTWs are shown to have very little effect on circulation within GSV, induced flow through IS and particularly BP could be important in the removal of gulf waters or introduction of shelf waters when combined with circulation resulting from other processes, such as local winds. The majority of energy of the CTWs bypass GSV to the south of KI, following the 100 m isobath.

Figure 4.11: Sea surface height for the SAROM domain with depth integrated velocity for GSV inset. SSH and depth integarted velocity as modelled on the SAROM grid with forcing from a 10 day periodic CTW with amplitude of 10 cm. Units SSH (main): cm, depth integrated velocity (inset): m s^{-1}. Legend arrow indicates flow velocity of 10 cm s^{-1}. Depth integrated currents within the gulf due to passing CTWs are very weak, with stronger flows through IS and particularly BP due to their narrow flow paths. Maximum velocities within GSV occur as the peak of CTW approaches(e.g. hour = 580). Animation Location: Electronic Appendix/CTW inset movie.avi

Chapter 5

Geostrophically Adjusted Thermohaline Circulation

5.1 Summary

Geostrophically adjusted models are developed to represent idealised mean summer and winter conditions. As the temperature and salinity fields for the gulf are not well known, the circulation driven by the thermohaline structure is also not known. The temperature and salinity fields adopted for geostrophic modeling were taken from the quasi-realistic GSVM (Chapter 6) in the absence of a suitable data set or well validated thermohaline model. Differences in depth-integrated density fields resultant from temperature and salinity profiles lead to changes in sea level, with denser (lighter) waters sitting lower (higher) than surrounding waters, generating pressure gradients and hence geostrophic flow (Middleton & Platov, 2003). As temperature and salinity fields are taken from the quasi-realistic GSVM, they include influences from all forcing fields such as winds, and not just thermohaline fluxes. Therefore, results shown here depict mean geostrophic currents to be expected for quasi-realistic conditions. As results for the geostrophically adjusted models are representative of the mean thermohaline structures of the gulf, stronger thermohaline currents may well occur in reality.

Models were run for a period of 4 days with fixed temperature and salinity fields (derived from quasi-realistic model results), after which they reached a quasi-steady state condition wherein pressure-gradient forces reach a balance with Coriolis and bottom friction forces (geostrophy). No forcing is applied at either the surface or boundaries for the geostrophically adjusted models. Results indicate the typical thermohaline circulation to be expected under seasonal conditions. The result of geostrophic balance is the formation of currents parallel to isobars rotating about centres of low or high pressure (clockwise about low, anti-clockwise about high for the southern hemisphere) of magnitude proportional to the pressure gradient.

In this chapter: Idealised geostrophically balanced models are developed based on the thermohaline structure derived from the fully forced quasi-realistic GSVM (Chapter 6). Depth-integrated density fields are shown to differ for summer and winter, with summer showing very weak and disorganised density gradients from the head of the gulf to shelf and winter results much stronger and well defined. Geostrophically adjusted sea level shows the gulf is dominated by a low in the south-eastern portion for

both summer and winter, whereas the sea level in IS is high for summer and low for winter. For both summer and winter weak clockwise circulation within the gulf is generated in geostrophically adjusted models.

For summer model results indicate the gulf circulation is partially isolated from the shelf circulation, whereas for the winter model a shelf waters flow in to the gulf via the north coast of IS and gulf waters flow out via the south coast of IS. Geostrophic flows are shown to transport salty waters from the head of the gulf to the deep central basin year-round.

For both summer and winter the geostrophic flows are weaker than those observed for the idealised wind models and indicate that thermohaline circulation is likely less influential than wind-stress in total circulation and flushing of the gulf.

5.2 Introduction

Thermohaline circulation is driven by density gradients within a water body, chiefly influenced by surface heat and freshwater fluxes. Density-driven flows have been observed in smaller semi-enclosed bodies, including SG (Horsburgh & Hill, 2003; Kämpf et al., 2009; Teixeira, 2010), where they have been demonstrated to play a critical role in the circulation and flushing of those bodies. Though maximum density driven flows are typically in the order of only a few cm s^{-1}, they can play an important role in net transport as they often act over prolonged periods of time.

The temperature and salinity fields were obtained from high-resolution results of the quasi-realistic GSVM averaged over 3 months, 1st December to 1st March for summer and 1st May to 1st August for winter. The chosen winter period is not the calendar winter and was selected due to tendency for density driven outflow from SG to begin occurring around this time (Teixeira, 2010).

5.3 Summer Conditions

5.3.1 Thermohaline Structure

Figure 5.1 clearly shows that for the summer months the waters within GSV are much warmer than the neighbouring shelf. This is especially true for upper GSV and the northern shore of IS, where average temperatures approach 24 degrees. There appears to be a front around 35 degrees south separating the very warm upper GSV waters from the lower. However, the lower GSV waters including IS and BP are still significantly warmer than shelf waters at approximately 20 ^{o}C compared with 16 ^{o}C on the shelf.

A quick note on salinity units; these are presented as Practical Salinity Units (PSU) and are dimensionless, thus appear as only a number. The average salinity field shows extremely salty water in the upper eastern reaches of GSV due to year round excess of evaporation over precipitation, with mean value around $\sim$ 38. This very salty water is mostly confined to the upper reaches of GSV, with no values of salinity south of Adelaide exceeding 37. A slightly fresher plume ($\sim$ 36.5) of wind forced water intrudes on the western coast. Fresher shelf water of $\sim$ 35.5 can be seen intruding on the southern side of BP and spreading westward across the northern coast of KI. This plume does not appear to interact with the interior of GSV in any significant manner.

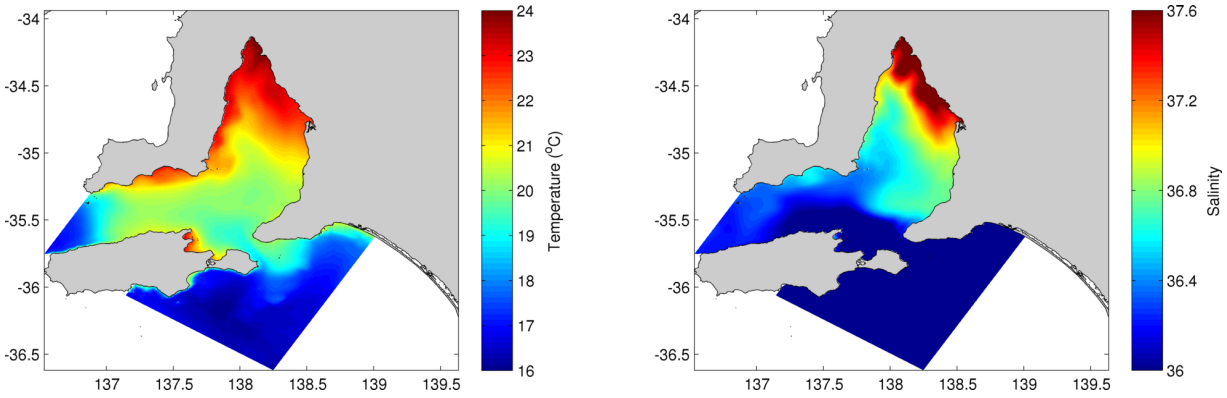

Figure 5.1: Three-monthly mean bottom temperature and salinity values for summer geostrophically adjusted model. three-dimnesional temperature and salinity fields are generated from the mean values of results from quasi-realistic GSVM for the period 1st December 2010 to 1st March 2011. GSV exhibits both much warmer and saltier waters than the neighbouring shelf.

5.3.2 Depth-Integrated Density Distribution

As mentioned earlier, and demonstrated by Middleton & Platov (2003), the density field of the system, in the absence of other forcing fields, will determine the sea level and hence pressure gradients which result in geostrophic flows. Figure 5.2 shows the depth-integrated density anomaly (e.g. $\sigma - 1000$) for the system under the assumed temperature and salinity fields for summer where σ is the density in kg m^{-3} and 1000 kg m^{-3} is a reference density . The gulf exhibits a region of slightly denser water on the east coast, with relatively less dense waters through eastern IS, BP and on the shelf. Isopycnals within GSV are oriented north-south with a density differential from east to west of approximately 0.6 kg m^{-3}. From the gulf interior to the western boundary in IS there is essentially a zero gradient, and from gulf to shelf via BP a gradient of only $\sim$ 0.2 kg m^{-3}. Inspecting the vertical structure for mean summer temperature, salinity and density anomaly (Appendix C, Figures C.1 and C.2) indicates that the system is well mixed in the vertical over seasonal timescales and depth-integrated values are a useful proxy to describe the circulation.

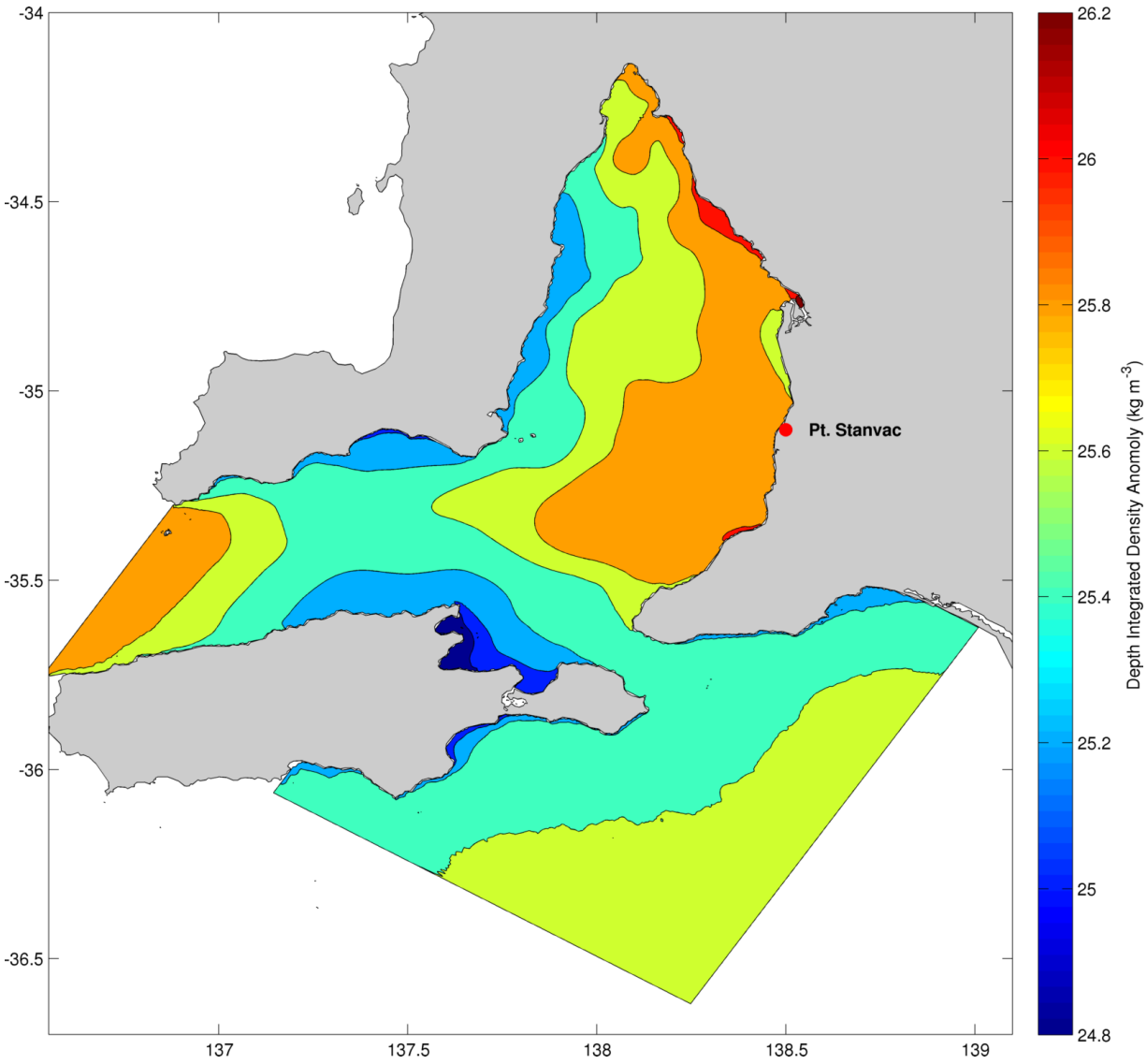

Figure 5.2: Three-monthly mean depth-integrated density anomaly for the mean summer conditions. Contours at 0.2 kg m^{-3} intervals.

5.3.3 Sea Level

The magnitude of sea level variations (Figure 5.3) are quite small, with a range of less than 2 cm. However, there is a clear zone of depressed sea level within the south eastern reaches of GSV. Conversely, the western shore of GSV has a raised sea level. This is consistent with the density field and follows expectations that lighter (denser) waters sit higher (lower). There is also a minor local depression at the head of GSV, but it is weaker than the main south-eastern depression. On the north coast of KI through the central portions of IS there is a sea level elevation.

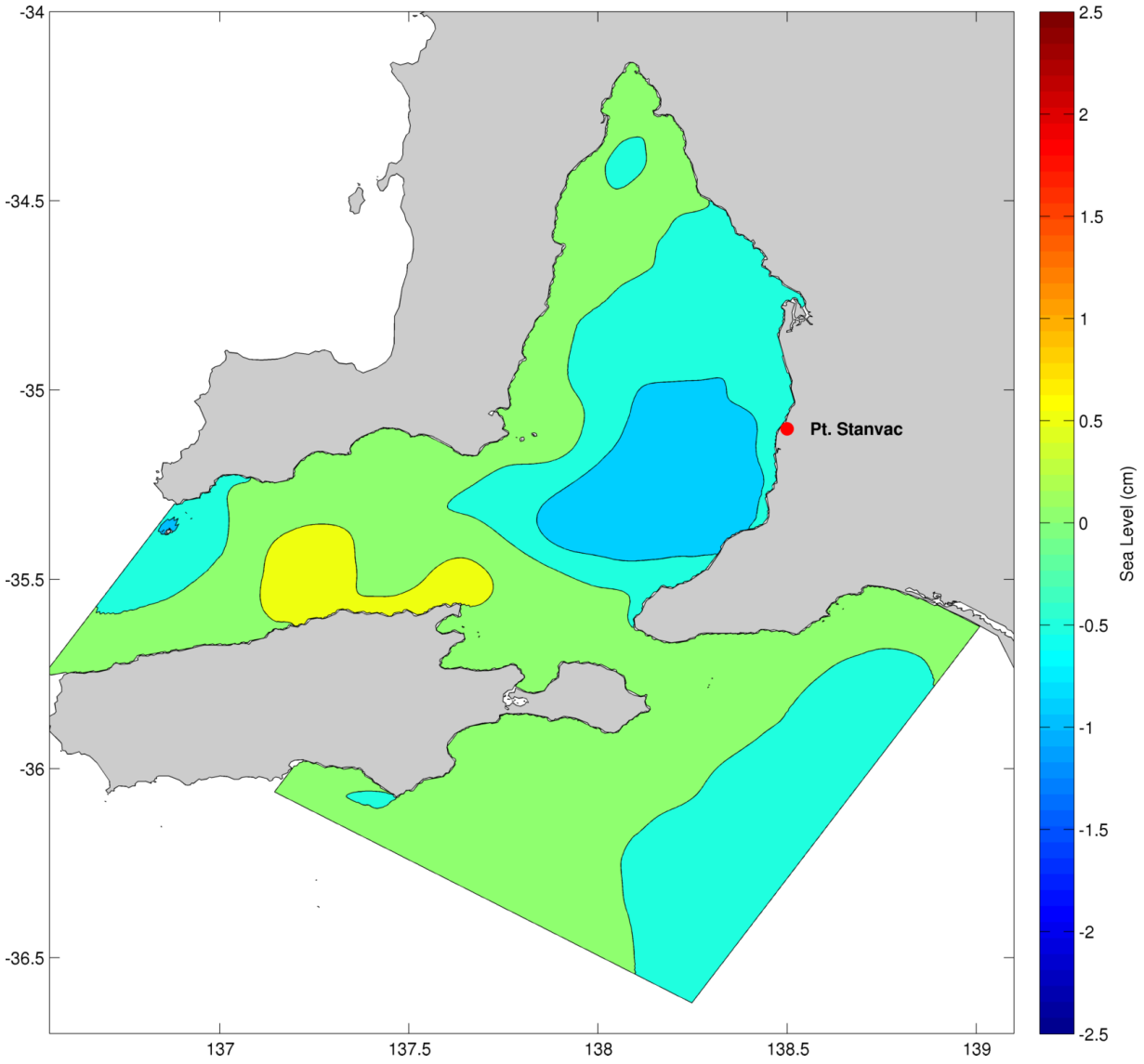

Figure 5.3: Three-monthly mean geostrophically adjusted sea level (cm) for typical summer thermohaline structure. Contours at 0.5 cm intervals. The main feature is the sea level depression over the deep central basin near the mouth of the gulf.

5.3.4 Depth-Integrated Velocity

The quasi steady-state flow field shown in Figure 5.4 indicates the circulation patterns that develop for the given thermohaline structure. The main feature in terms of GSV circulation is the large clockwise gyre, which results from the depression in sea level the south-east region caused by the greater density within this region. In IS there are two smaller counter-clockwise gyres formed about the sea level elevations on the north coast of KI. These gyres, in conjunction with the clockwise circulation within the gulf, result in the restriction in connectivity of flows between the gulf and shelf via IS. The effect of this restriction of connectivity through re-circulation can be seen in a passive Lagrangian float animation provided in the electronic appendix (Electronic Appendix/LTRANS animations/Geostrophic Summer.avi).

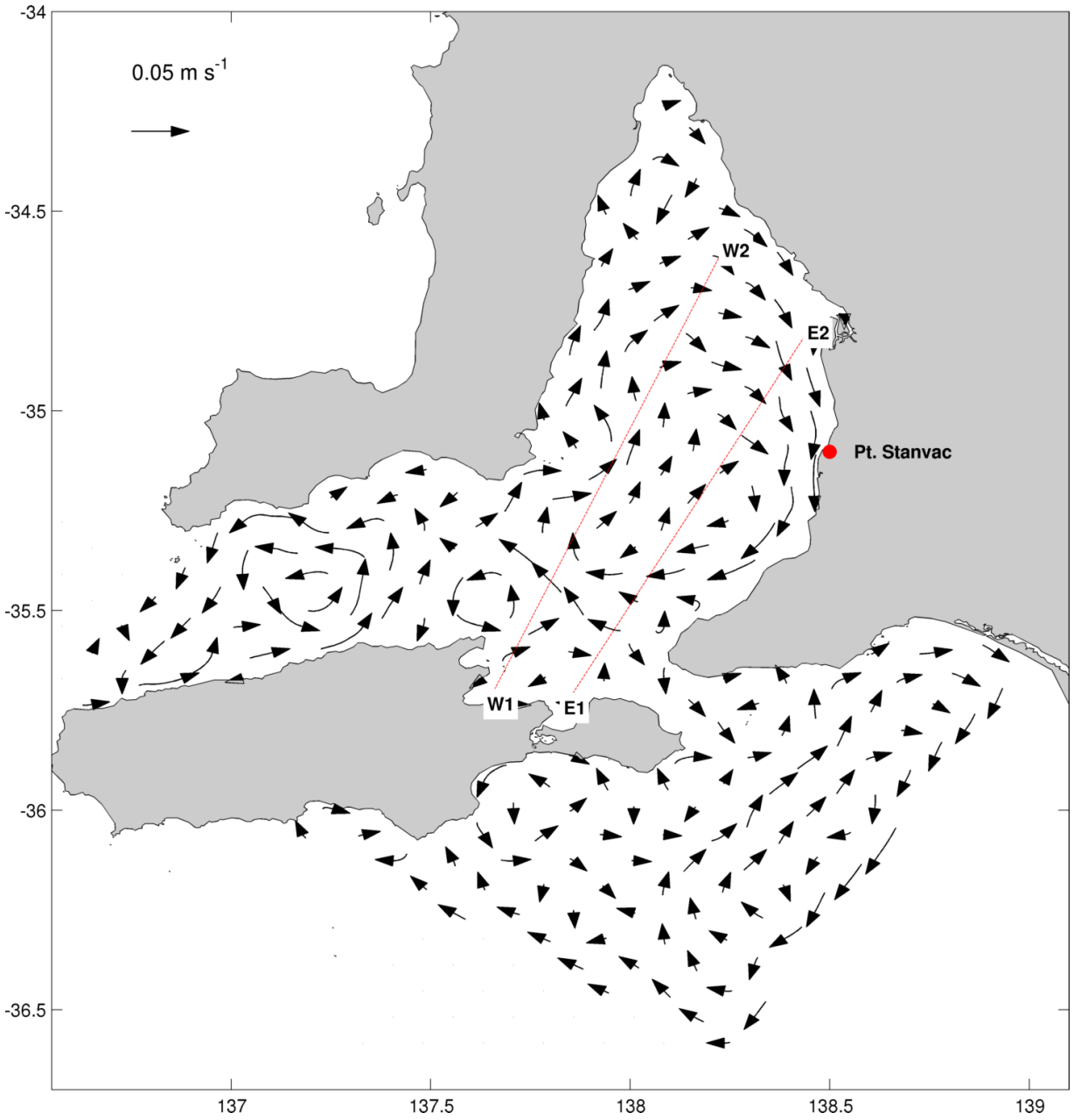

Figure 5.4: Three-monthly mean geostrophically adjusted depth-averaged velocity field for summer months. Legend arrow indicates flow velocity of 5 cm s^{-1}. Dashed lines show cross sections taken for analysis of temperature, salinity and density anomaly cross sections, figures can be found in Appendix C. Cross sections names are W for west and E for east. The main feature of circulation is the clockwise flow around the sea level depression centred over the deep central basin. This circulation is mostly isolated from flows within IS and BP.

5.4 Winter Conditions

5.4.1 Thermohaline Structure

The thermohaline structure of the gulf is significantly different during winter when compared with summer (Figure 5.5). Most strikingly, mean bottom temperatures of the gulf drop to below 15 degrees for large swathes of coastal regions, especially in the upper gulf due to atmospheric cooling. Meanwhile, mean shelf temperatures remain around the 16 degree level, having little change from the summer conditions.

The distribution of salinity has also changed significantly, with a very strong plume of salty water with mean value exceeding 37 occupying the central/eastern portion of GSV all the way to Cape Jervis (Figure 5.5). A strong divide between this plume and an intruding finger of fresher ($\sim$ 36) water can be seen through the lower central portion of GSV. There is evidence of the SG outflow on the western boundary of the model domain. In this location there is a rapid drop in depth from approximately 45 m within IS to 100 m on the north-western tip of KI. Due to the dense nature of SG outflow, this water is constrained to follow the deeper isobaths and little appears to make its way into IS or GSV.

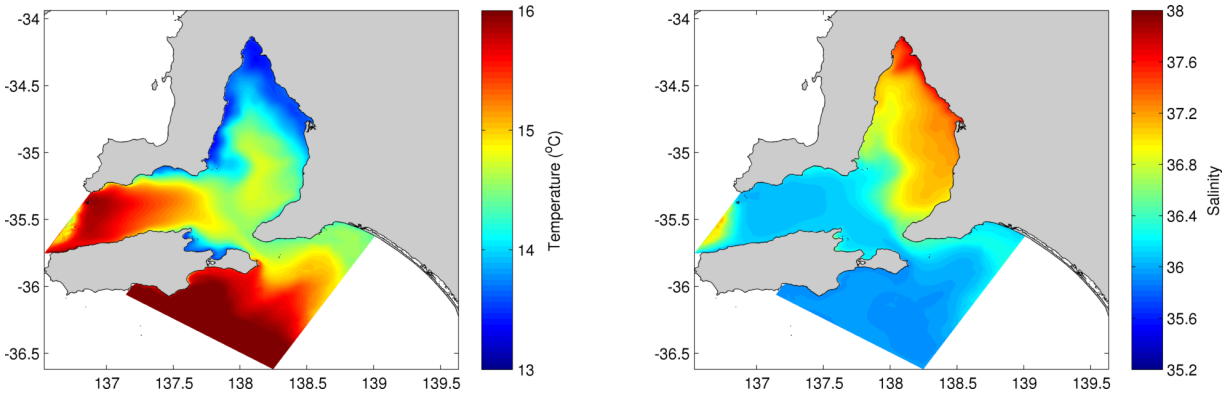

Figure 5.5: Three-monthly mean bottom temperature and salinity values for winter geostrophically adjusted model. Note the different temperature color bar values compared to summer figure, altered to better illustrate the narrower temperature distribution for winter. Salinity colorbar values are consistent with summer figure to allow for direct comparison.

5.4.2 Depth-Integrated Density

The density anomaly field (Figure 5.6) indicates a clear density gradient from the head of the gulf to the shelf through IS and BP, with differential of approximately 2 kg m^{-3} for both flow paths. The orientation of isopycnals is also different for the winter case, being mostly parallel to the mouth of the gulf. As with the summer case, inspection of the vertical structure for mean winter temperature, salinity and density anomaly (Appendix C, Figures C.3 and C.4) indicates that the system is well mixed in the vertical over seasonal timescales and depth-integrated values are a useful proxy to describe the circulation.

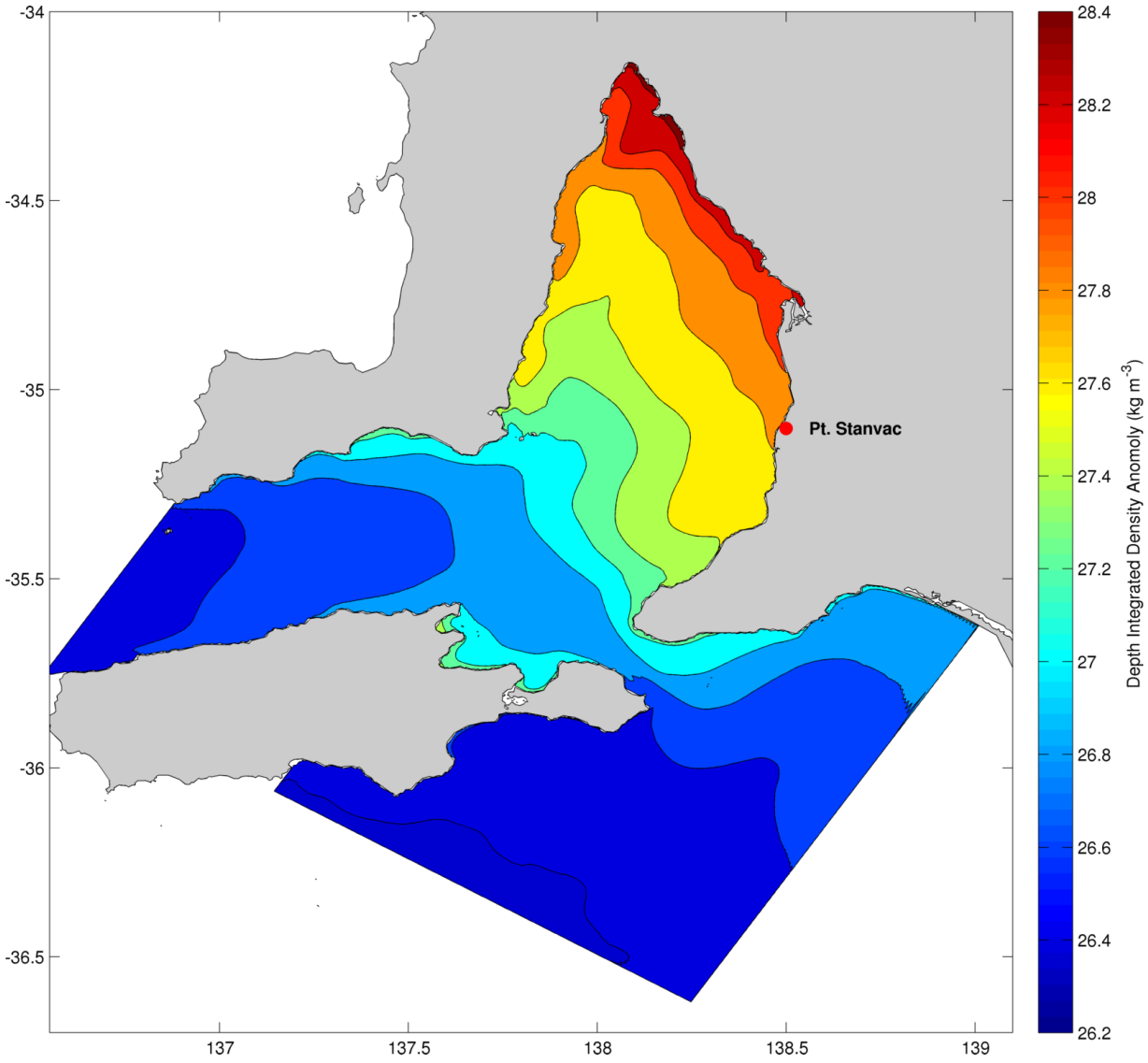

Figure 5.6: Three-monthly mean depth-integrated density anomaly for mean winter conditions. Contours at 0.2 kg m^{-3} intervals. A well defined density gradient from the head of the gulf to the shelf is shown, indicating density driven flows from head to mouth are likely to occur.

5.4.3 Sea Level

The sea level for the averaged winter conditions (Figure 5.7) shows a depression throughout much of GSV proper. The depression within the gulf largely follows the distribution of the high salinity plume shown in Figure 5.5. The centre of the depression is slightly further north than what is observed for the summer case. To the east of BP the sea level shows a gradient from the coast to shelf. Within IS there is a finger of relatively elevated sea level, with a region of lower sea level off the north coast of KI and central to IS.

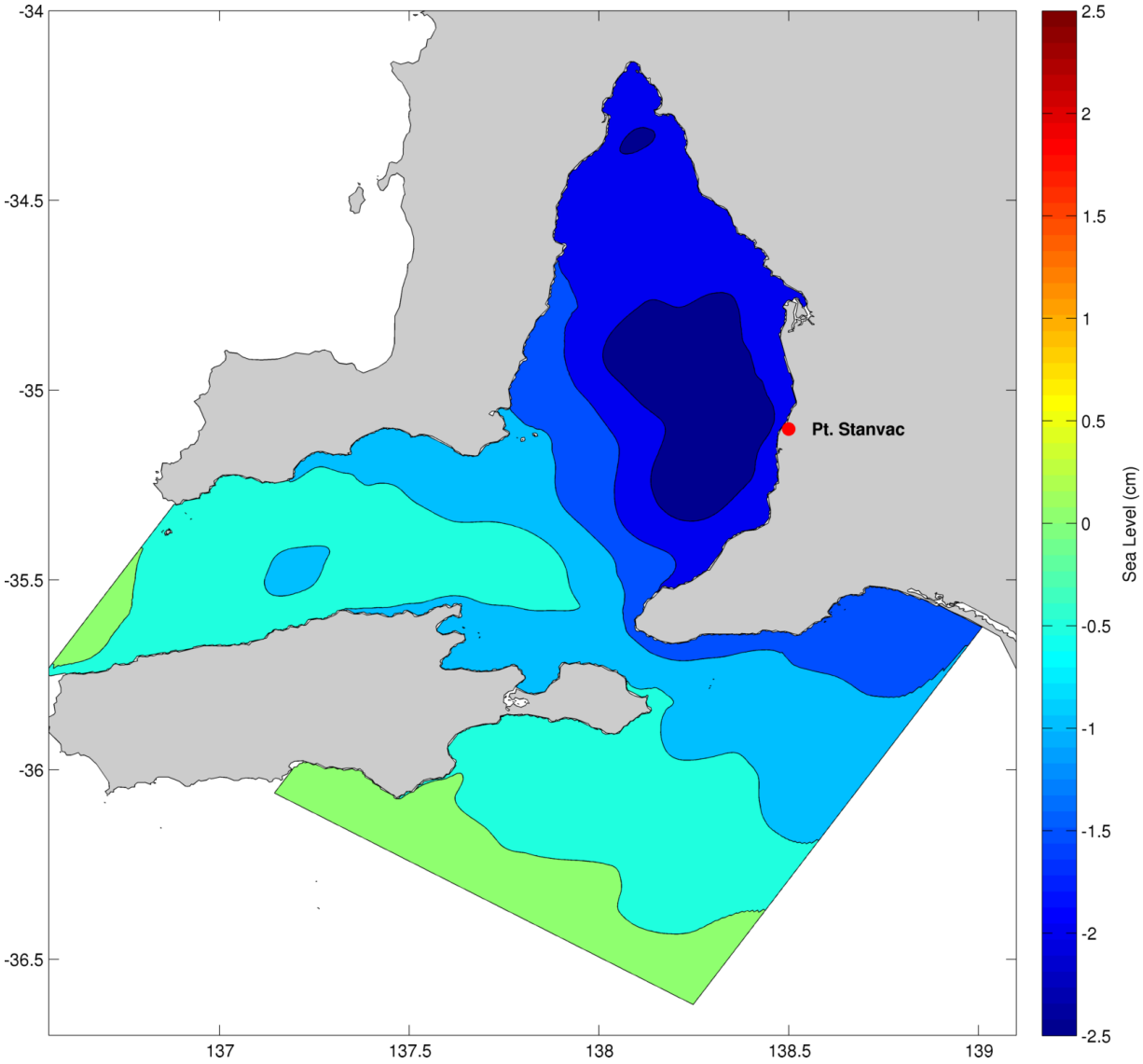

Figure 5.7: Three-monthly mean geostrophically adjusted sea level (cm) for typical winter thermohaline structure. Contours at 0.5 cm intervals. The main feature is the gulf-wide sea level depression when compared to IS and shelf, strongest in the central-eastern portion.

5.4.4 Depth-Integrated Velocity

As with the summer case, the interior of the gulf is dominated by a clockwise gyre formed about the sea level depression (Figure 5.8). Currents are generally stronger for the winter case due to the stronger

pressure gradient. A counter-clockwise circulation to the south of and central to the mouth (M1-M2) is formed by the relative sea level elevation on the north coast of KI. In combination with the southern edge of the gulf wide clockwise gyre, this counter-clockwise circulation provides an exit pathway for gulf waters. This method of exchange for shelf and gulf waters can be more clearly seen in the passive Lagrangian float animation provided in the electronic appendix (Electronic Appendix/LTRANS animations/Geostrophic Winter.avi).

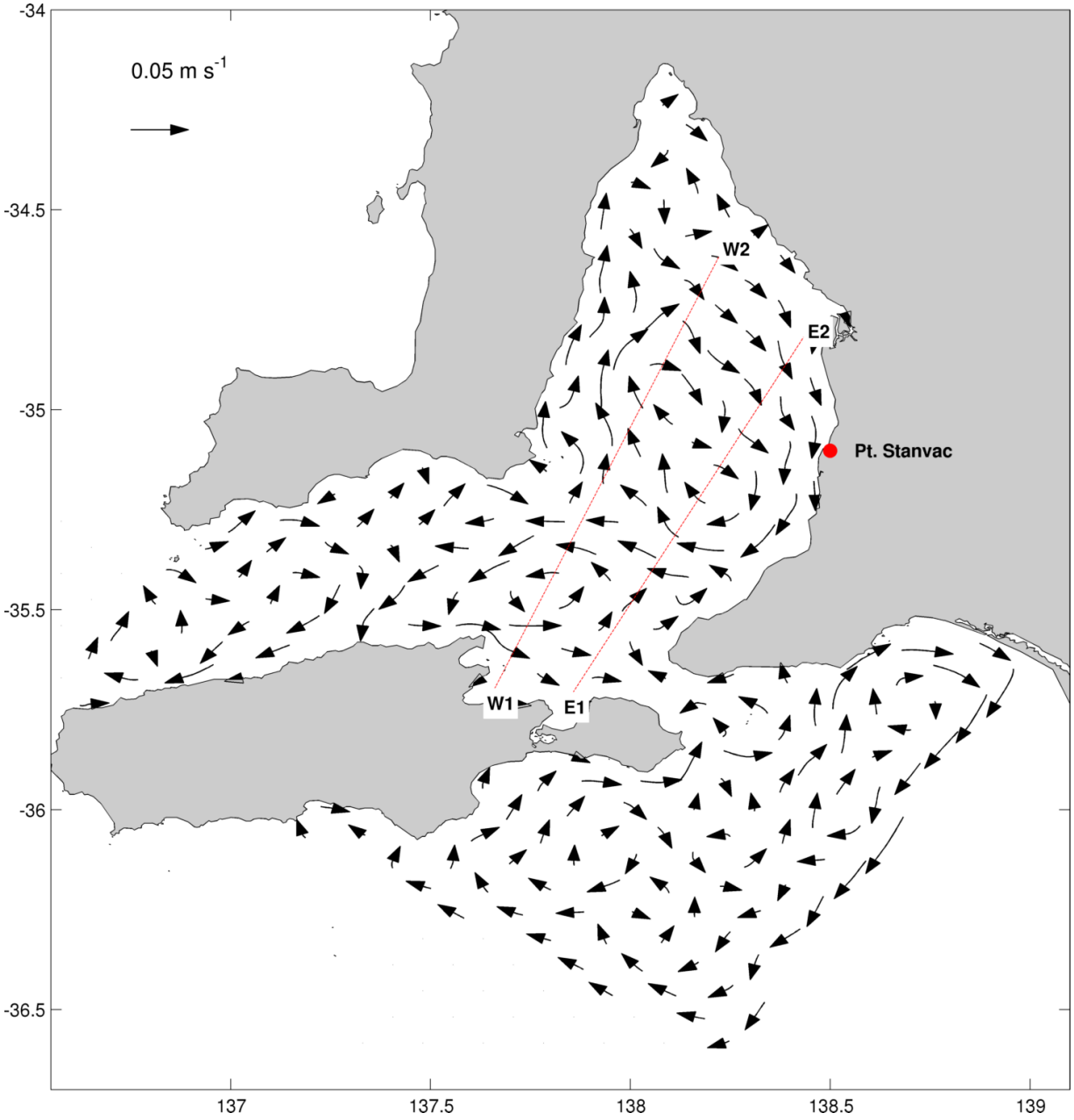

Figure 5.8: Three-monthly mean geostrophically adjusted depth-integrated velocity field for winter time. Legend arrow indicates flow velocity of 5 cm s^{-1}. Dashed lines show cross sections used to depict temperature, salinity and density anomaly cross sections, figures can be found in Appendix C. The circulation is dominated by relatively strong clockwise circulation throughout the entire gulf interior, which shows a partial discharge of gulf waters through the central portion of the mouth and an intrusion of waters along the northern coast of IS around the heel of Yorke Peninsula.

5.5 The Effect of Thermohaline Circulation on Connectivity

The above experiments indicate that, for both summer and winter mean temperature and salinity fields, a sea level distribution is created which induces gulf-wide clockwise circulation within GSV. For the summer case the sea level distribution creates flow fields within IS and BP which act to keep the gulf wide circulation largely isolated. The density gradient from head to mouth is very weak and does not allow for a mode to break through the flow restriction across the mouth. For the winter case the sea level distribution within IS and BP, combined with the large pressure gradient from head to shelf, results in a mode of partial discharge for westward flowing southern edge of the gulf wide gyre, forming a shelfward flow along the northern coast of KI. In effect, the thermohaline circulation modeled here acts to enhance the connectivity seen for the idealised winter wind modeling, and also to further the restriction in connectivity seen for the idealised summer wind modeling. The mode of flow restriction for the summer conditions is different for the geostrophically adjusted model though, with the formation of the single gulf wide gyre as opposed to the 'double gyre' system modeled for the idealised winds.

Chapter 6

The GSV Model: Methods, Validation and Physical Drivers

6.1 Summary

A quasi-realistic GSV Model (GSVM) is developed and forced using meteorology surface fluxes provided by the European Centres for Medium range Weather Forecasting (ECMWF), tides from the TPXO model and boundary conditions from SAROM results. The model adopts the same bottom friction as applied in Section 3.4.2. The model is validated against observations for 2010 and 2011 obtained at Pt. Stanvac on the eastern coast of GSV. Validation against observations for sea level and currents generally show very good agreement between model and data. Validation for temperature and particularly salinity are less robust, due in part to difficulties with forcing fluxes and issues with the reliability of salinity data.

Model results suggest circulation of the GSV system is largely driven by wind-stress, with thermohaline circulation playing a minor role. Circulation patterns under full atmospheric forcing showed similarities with idealised wind-stress models for similar wind regimes. This result is in contrast to existing works (Samarasinghe et al., 2003; Kämpf et al., 2009) which suggest that density driven outflows are a dominant factor in the Gulf-shelf connectivity.

In this chapter: The configuration of the fully forced quasi-realistic Gulf St. Vincent Model (GSVM) including the boundary conditions and forcing fields is explained. Animations of daily mean bottom temperature, bottom salt, depth-integrated velocity, sea level and surface fluxes are made, showing the seasonal and weather band responses of the GSVM to the full 'quasi-realistic' suite of forcing. Methods and results for validation against sea level, current, temperature and salinity observations are shown, with the GSVM producing very good predictive skill for currents and sea level. Generally good predictive skill for temperature is found and less reliable reproduction of salinity observations;

Circulatory responses of the GSVM are shown to share several characteristics with the idealised models, and physical drivers of circulation are examined with the aid of the daily averaged animation of key GSVM results.

Addtionally, the relative importance of local forcing compared to advective processes is investigated using a simple idealised model. Results indicate the relative influence of local heat fluxes on temperature is spatially variable. Salinity is found to be highly dependent upon advection throughout the entire domain.

6.2 Introduction

A quasi-realistic model is developed in order to better understand the dynamics of GSV under realistic conditions. The model is not intended to be a perfect reproduction of the conditions within GSV during 2010-2011, since the ECMWF meteorology available for forcing the model are not free of error. Instead, the model is intended to accurately reproduce the major features of circulation that are to be expected under a certain set of forcing conditions.

The model is validated against a data set of temperature, salinity, sea level and residual currents at Pt. Stanvac, in addition to seasonal sea level data sets for Port Giles and Outer-Harbor. With the exception of the salinity comparisons, which were problematic, the GSVM results show good agreement with observations.

6.3 Model Configuration

6.3.1 Initial Conditions

The GSVM was initialised with conditions interpolated from results of the SAROM parent model. These conditions included three-dimensional temperature, salinity and velocity fields. As with the idealised tidal model, tidal forcing was ramped over a period of 3 days to avoid introducing shock and instability to the system. All other forcing fields were initialised with no ramping at the first time step of the model.

6.3.2 Implementation of Boundary Forcing

Larger scale shelf and global circulation, in addition to thermohaline conditions, are accounted for within the GSVM 'child' model by forcing the boundaries with results from the larger coarse-resolution SAROM regional model (the 'parent model'). Key parameters which were used were salinity, temperature, three-dimensional momentum and free surface level. Tidal forcing was applied in the same manner as the idealised tidal model (Chapter 3) through the implementation of TPXO 8.1 for the 9 most dominant tidal constituents. Boundary conditions used for the GSVM can be seen in Table 6.1.

	Western	Southern	Eastern
Tracers (S and T)	RadNud	RadNud	RadNud
Two-Dimensional Momentum	Shchepetkin	Shchepetkin	Shchepetkin
Three-Dimensional Momentum	RadNud	RadNud	RadNud
Free Surface	Chapman	Chapman	Chapman

Table 6.1: Open boundary conditions for child model

Under the RadNud (radiation/nudging) boundary condition the tracers of temperature and salinity are permitted to radiate across the boundary whilst also being nudged to the external values supplied by the parent model. This is also true for the three-dimnesional momentum, allowing net currents from the SAROM model at all 15 vertical layers to be accounted for in the GSVM. Inflow nudging uses a 1 day timescale, meaning cells at the boundary are nudged at a rate such that they will converge on the boundary condition values after 1 day when water is flowing in to the model domain. Outflow nudging uses a 120 day timescale, meaning boundary condition values are nudged to outflow values at a rate that they will converge on boundary cell values after 120 days when water is flowing out of the model domain.

This allows internal GSV processes to occur whilst ensuring that changes in passive tracers due to local forcing do not overwrite the boundary conditions as imposed by the parent model. The strong inflow nudging to boundary conditions was required due to the need to accurately capture short term weather band variability, particularly in regards to sea level and velocity.

The Shchepetkin (2D momentum) boundary conditions adopted are essentially an adaptation of a Flather boundary condition to a staggered grid, in which deviations in internal barotropic velocity from the external value radiate out at the speed of external gravity waves. For more detail see Mason et al. (2010). The Chapman (free surface) boundary condition is the corresponding approach to the free surface, whereby the free surface at the boundary changes at the same rate as the speed of gravity waves (Chapman, 1985; Hedström, 2010).

6.3.3 Local Forcing Surface Fluxes

Atmospheric forcing was applied via net surface fluxes within the ROMS models. The local forcing for the GSVM is sourced from the 0.125 degree resolution ECMWF global model (www.ecmwf.int). This model was chosen due to its relatively high resolution and availability of continuous information for the desired modeling period of the 2010-2011 calendar years.

6.3.3.1 Wind-Stress Data

Wind-stress data was determined using the 10 m u and v wind speed sourced from ECMWF. In the absence of a wave model the surface stress as a result of winds were determined via a simple empirical formula:

$$\tau_u = |u_{10}|\, \rho_a C_{D_a} u_{10} \tag{6.1a}$$

$$\tau_v = |u_{10}|\, \rho_a C_{D_a} v_{10} \tag{6.1b}$$

where τ_u and τ_v are the u and v components of surface stress in Pa, $|u_{10}| = \sqrt{u_{10}^2 + v_{10}^2}$ is the wind speed in m s^{-1} at 10 m above the sea surface, u_{10} and v_{10} are the u and v components of the 10 m wind, ρ_a is the density of air and C_{D_a} is a dimensionless coefficient of drag which is estimated following the technique shown in Large & Pond (1981). In the absence of a coupled atmospheric model which would calculate the effect of SST on air temperature, the air density is taken as a constant 1.225 kg m^{-3} (Mustafa, 2005). Applying equations (6.1a) and (6.1b) to the 10 m wind speed sourced from ECMWF gives mean stress of 0.0595 Pa and standard deviation 0.067 Pa for the whole domain over the modelled period.

6.3.3.2 Thermal Flux

Shortwave Radiation

The primary source of incoming heat to the ocean is via short wave solar radiation. This of course varies through both space and time, with seasonal variability at lower latitudes. The incoming shortwave radiation heat flux is given as:

$$Q_I = Q_{I_0}\,(1 - \alpha_s)\,(1 - 0.7\eta_c) \tag{6.2}$$

where Q_I is the incoming shortwave radiation heat flux in W m^{-2}, Q_{I_O} is the net incoming shortwave radiation above cloud level, α_s is surface albedo (fraction of light reflected) and n_c is the fraction of sky covered by cloud. ROMS has the ability to distribute short wave radiation absorption throughout the water column dependent upon Jerlov water type which is largely determined by turbidity, see Figure 6.1. As GSV is mostly dark coastal water of moderate wave activity, a Jerlov water type of 9, or "Dark coastal water" was selected. Under this regime the majority of incoming shortwave radiation is absorbed in the surface layer, with little penetration to greater depths.

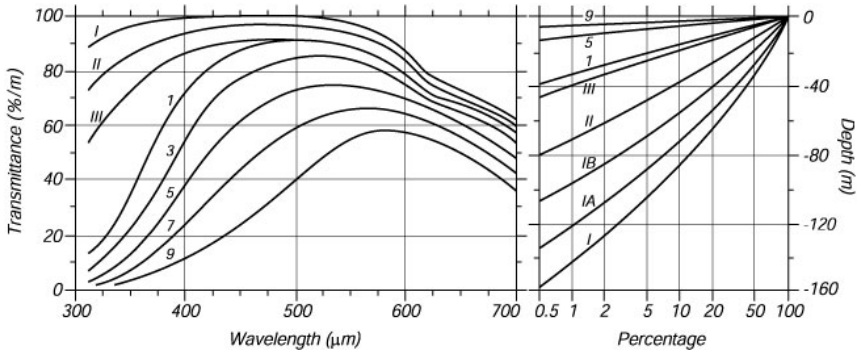

Figure 6.1: Downward shortwave radiation transmission by Jerlov water types. Reproduced from Stewart (2006). The left panel indicates the transmittance of light of different wave lengths through 1 m of sea water. The right panel indicates the total amount of sunlight to reach given depths for different Jerlov water types. Type 9, or dark coastal water, is absorbed entirely within the first ~5 m.

Latent Heat Flux

Latent heat flux is the transfer of energy due to the evaporation and condensation of water, i.e. a function of the freshwater flux. As ROMS does not consider precipitation as a positive incoming freshwater flux directly (instead treating evaporation as a positive downwards salt flux), latent heat flux can only be the product of evaporation and not precipitation, hence is negative at all times, and is expressed as

$$Q_L = L_v \left(\frac{c_E u \left(q_s - q_a \right)}{\rho_a} \right) \tag{6.3}$$

where Q_L is the latent heat flux, L_v is the latent heat of vaporisation of water (2.5×10^6 J kg^{-1}), c_E is a dimensionless coefficient known as the Dalton number ($10^3 c_E = 1.5$), u is the wind speed in m s^{-1}, q_s is the specific humidity at sea level, q_a is specific humidity of the air at the standard level (10 m), and ρ_a is the density of air taken as a constant 1.225 kg m^{-3}.

Sensible Heat Flux

Sensible heat flux is the transfer of energy via conduction and convection, and hence is heavily reliant upon wind speed. As sensible heat flux is directly proportional to the temperature difference between the air-sea interface ($Ts - Ta$) it can be both positive or negative dependent on atmospheric temperature and SST. The sensible heat flux is given as

$$Qs = \frac{c_H u \left(T_s - T_a \right)}{\rho_a c_p} \tag{6.4}$$

where Q_S is the sensible heat flux in W m^{-2}, c_H is a dimensionless coefficient known as the Stanton number which is smaller for stable conditions and larger for unstable ($0.83 < 10^3 c_H < 1.10$), u is wind speed in m s^{-1}, T_s is sea surface temperature in degrees K, T_a is the air temperature in degrees K, c_p is the specific heat capacity of the air ($\sim$ 1000 J kg^{-1} K^{-1}) and ρ_a is the density of air taken as a constant 1.225 kg m^{-3}

Long-Wave Radiation

Long wave radiation, or black body radiation, is the heat which leaves the system via infra-red radiation. Having absorbed incoming short wave solar radiation, the oceanic body warms up and then begins to emit long wave radiation, much the same as any massive body with thermal energy. This is considered a negative flux in ROMS, as energy is leaving the system. The key determinant in outgoing longwave radiation is the SST. The outgoing long wave radiation is given by

$$Q_B = 0.985\sigma T_s^4 \left(0.39 - 0.05 e_a^{1/2}\right)\left(1 - 0.6 n_c^2\right) \tag{6.5}$$

where Q_B is the outgoing long wave radiation, T_s is the sea surface temperature, e_a is the vapor pressure of water at the standard height and n_c is the fraction of sky covered by cloud. The water vapor pressure term accounts for back radiation from the atmosphere, while the 0.985 modifier accounts for deviation from standard black body radiation that the ocean has been observed to exhibit (Gill, 1982).

Net Heat Flux

The net heat flux (Q), which is a value applied directly to the model, is the sum of the above heat fluxes. Figure 6.2 shows the individual components of the heat flux for a single point within the GSVM at Pt. Stanvac for the 2011 calendar year, and the sum Q. Shortwave radiation is the dominant component and shows a clear seasonal pattern, with short term variation attributed mostly to cloud cover. Long-wave radiation is also lower when shortwave radiation is reduced, in part due to lower SST but also due to the greater back radiation resultant from cloud cover and humidity.

Latent heat flux is also highly seasonal, with much larger losses of heat during summer when evaporation is greater than winter. Sensible heat flux has the least impact, and also experiences the least seasonal variability, due to air and sea surface temperatures at this location fluctuating with the same seasonality. As the ECMWF results are produced by an atmospheric model, there are limitations in the accuracy of the provided values, especially in the impact of cloud cover. This is due to the notoriously difficult problem of modeling the formation of clouds (Cess et al., 1990; Colman, 2003; Houghton et al., 2001; Stephens, 2005), and the relatively high impact that cloud cover has on both incoming shortwave radiation and outgoing longwave radiation. As a result, there is inherently a moderate level of error in the heat fluxes presented from ECMWF.



Figure 6.2: The 4 separate components of heat flux and total net heat flux applied to model for Pt. Stanvac for 2011. Units W m^{-2}. The sensible heat flux has the least impact on net heat flux and is mostly negative throughout the year, indicating a loss of heat from the ocean to the atmosphere through conduction and convection at the surface. The latent heat flux is negative throughout the year as it represents heat lost through evaporation, which is naturally more prevalent during the summer months. Shortwave solar radiation is always positive and the single largest contributor to net heat flux and is strongest during the summer months. Outgoing longwave radiation is negative year round as it is a loss from the system. There is little seasonal variation as the SST in ^{o}K does not vary drastically and is the most influential variable in longwave radiation emmited. The net heat flux is a combination of all other fluxes. Sourced from ECMWF.

6.3.3.3 Salt Flux

Salt flux forcing for the model is determined from the freshwater flux (evaporation minus precipitation) multiplied by the salinity of the water column at the surface layer. Therefore positive values of salt flux are the accumulation of salt through net evaporation and negative values are the reduction in salinity due to net precipitation. As evaporation for GSV is greater than precipitation on a seasonal timescale, the net salt flux is almost always positive. Figure 6.3 shows the balance of daily mean precipitation and evaporation for Pt. Stanvac during 2011. As Pt. Stanvac is in the mid latitudes of the gulf it provides a good mean estimate for the model domain. Evaporation rates can be much higher for the head of the gulf however, leading to the extreme salinities observed there. The salt flux is typically positive year round, with short duration precipitation events occasionally interrupting this. Salt fluxes are difficult to estimate reliably, as they are dependent upon precipitation and evaporation, both of which can be sensitive to a multitude of atmospheric parameters.



Figure 6.3: Daily mean evaporation, precipitation and resultant salt flux for Pt. Stanvac for 2011. Units mm day^{-1}, sourced from ECMWF

6.4 Model Calibration

6.4.1 Bottom Friction Coefficients

The bottom friction coefficients dependent upon depth and bottom type distribution as described in Section 3.4.2 were used for the GSVM.

6.4.2 Heat Flux Calibration - SST Nudging

Heat flux calibrations were found to be necessary as implementing the ECMWF forcing data set without adjustment resulted in extreme water temperatures compared to that observed within the gulf. Other available data sets for heat fluxes were found to be incomplete spatially or temporally and hence unsuitable for forcing the model. The solution was to calibrate the ECMWF heat fluxes using observations in Sea Surface Temperature (SST).

The nudging to observed SST is manipulated through the variable dQdSST as per Equation 6.6 and described in Barnier et al. (1995). ROMS allows dQdSST to be spatially and temporally variable, but a lack information for heat flux errors and temperature observations means that level of dQdSST customisation would be pointless. As such a value for dQdSST is set as spatially and temporally constant. NOAA fisheries Climate Sciences Strategy (NCSS) SST values were used for nudging the ECMWF net heat fluxes. The method for applying the NCSS SST nudging is described in Appendix D.

The heat flux (Q) is nudged at each grid cell within the model via the linear equation:

$$Q_{\mathrm{New}} = Q_{\mathrm{Old}} + \mathrm{dQdSST} \times (\mathrm{SST}_{\mathrm{model}} - \mathrm{SST}_{\mathrm{nudge}}) \tag{6.6}$$

where Q_{New} is the adjusted heat flux, Q_{Old} is the original supplied heat flux from the ECMWF derived forcing file, dQdSST is the heat flux adjustment in W m^{-2} per degree K, $\mathrm{SST}_{\mathrm{model}}$ is the SST as determined by the model and $\mathrm{SST}_{\mathrm{nudge}}$ is the SST as prescribed by the nudging data set. Therefore the term $\mathrm{dQdSST} \times (\mathrm{SST}_{\mathrm{model}} - \mathrm{SST}_{\mathrm{nudge}})$ denotes a heat flux adjustment in W m^{-2} proportional to the difference between the modeled SST and the prescribed nudging SST. A value for dQdSST must be selected such that short term weatherband variability in SST is allowable whilst minimising long term accumulation of errors which can lead to the model diverging from reality. As the nudging SST data set uses monthly means, the nudging processes smoothes out diurnal and weatherband variability to a degree, with greater values of dQdSST leading to greater levels of smoothing.

A brief sensitivity study for 3 different guesses bof dQdSST was conducted to determine the most appropriate value for use within the GSVM, with dQdSST for case A = - 20 W m^{-2} K^{-1}, B = - 60 W m^{-2} K^{-1} and C = - 500 W m^{-2} K^{-1} . Important to note is that the SST for the nudging data set does not necessarily match perfectly with the observations. This is important as the model while being nudged to that data set is not 'aware' of other observations, so the error may be larger for the observations than what is applied for Equation 6.6. As can be seen in Figure 6.4 the 'relaxed' case A shows excellent model responsiveness to weatherband frequency events. However there is a large discrepancy in SST at this grid cell during late Summer and Autumn where the model diverges from the observations, suggesting the model is not cooling rapidly enough during this period. For case B, the same issue is present but far less pronounced while still replicating the weatherband frequency temperature changes well. For case C (not shown) the cooling issue is almost non-existent, but due to the strength of the nudging the model has very little room to move and respond to short term heat flux events, essentially locking the SST to the nudging

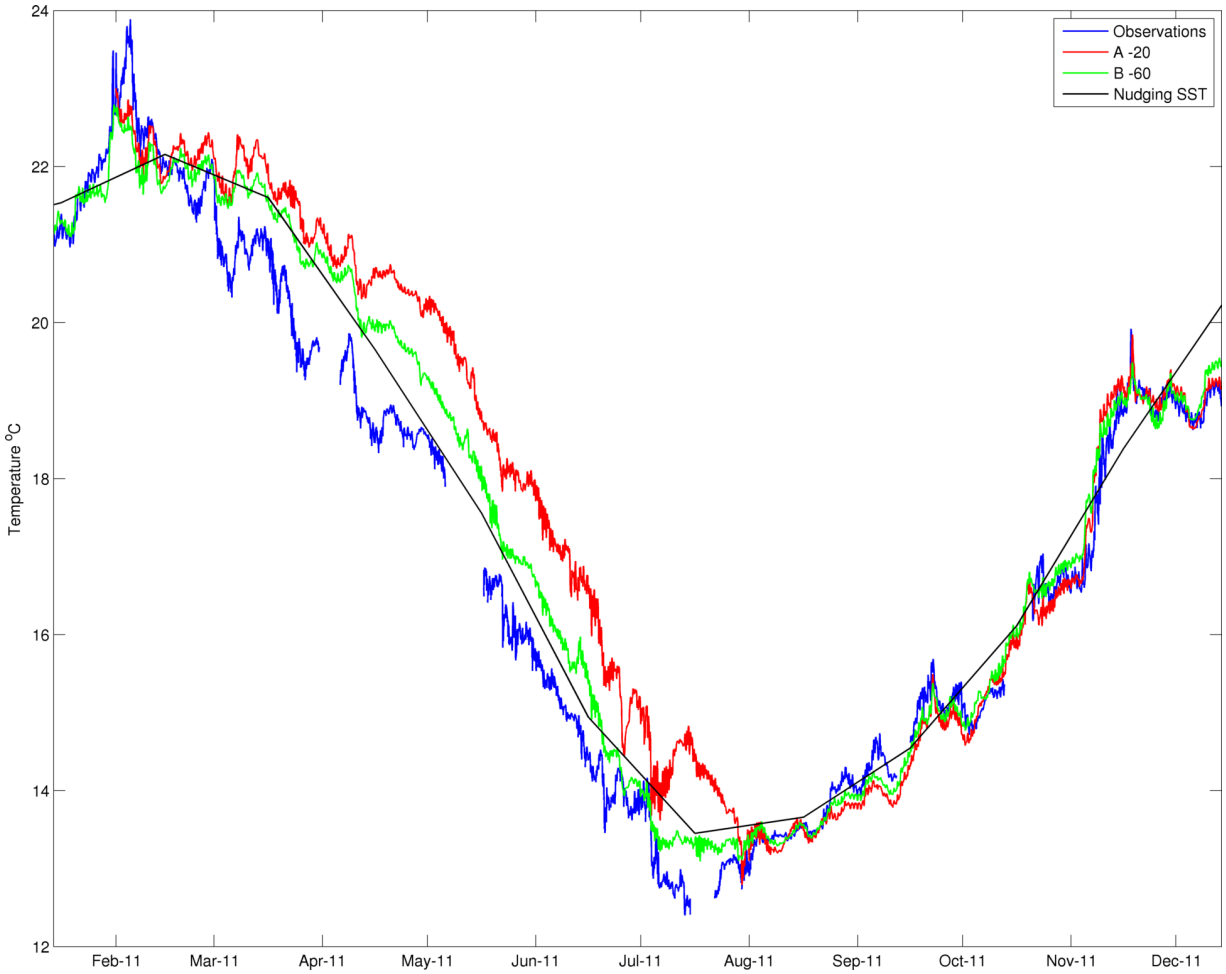

Figure 6.4: Temperature results for GSVM at 18m depth at Pt. Stanvac under different adopted dQdSST values compared with observations at 18m depth (shown in blue). Gaps in observations indicate periods when intrumentation was not deployed. Case A (red line) shows temperature results for a dQdSST value of -20 W m^{-2} and case B (green line) for a value of -60 W m^{-2}. Case C (-500 W m^{-2}) is not shown, as the nudging is so strong to essentially lock the modelled SST to the nudging data set. The black line indicates the monthly mean SST values adopted for nudging.

data set. As such the 'medium' case B was chosen due to its ability to respond to short-term events whilst maintaining long-term trends. This also agrees well with the findings of Barnier et al. (1995), who found a value of -50 W m^{-2} K^{-1} for dQdSST to strike the best balance.

6.5 Model Validation and Physical Drivers

The GSVM was validated for residual currents, sea level, temperature and salinity using long-term observations from the Pt. Stanvac region. In all fields except salinity the GSVM results compare favourably with observations. Salinity observations were difficult for use in validation possibly due to biofouling of instruments. An animation of model results is used as a tool to interpret model results and observations, and help identify the physical drivers of changes in SSH, velocity, temperature and salinity. The animation also provides greater gulf-wide context for events observed at Pt. Stanvac.

6.5.1 Daily Mean Animation: Introduction

Note: If reading this thesis as an electronic copy, the animation is embedded within the PDF file and can be controlled with the built in player. An update to Flash Player may be required, and can be downloaded at the following link: `https://get.adobe.com/flashplayer/`

Otherwise if reading a hard copy, please open the provided electronic appendix and find the relevant file.

The daily mean animation is a good starting point for understanding the response of GSV under local quasi-realistic forcing and corresponding boundary conditions from the parent SAROM model. The reader is encouraged to view the animation in its entirety before reading further, and then again when specific events are discussed below. The animation shows daily averaged bottom salinity (top left) and temperature (top right), depth-integrated velocity (middle left) and sea level (middle right) as well as domain averaged heat, salt and wind-stress fluxes (bottom). The mean domain wide wind direction is given by the vector on the depth-integrated velocity panel. Examining the animation allows for better understanding of gulf-wide processes which are tied to events which can be identified in the observations for Pt. Stanvac. As long-term observations are only available for a single point within the model domain, the animation provides greater context for circulation and thermohaline climate to the point data at Pt. Stanvac. In this section a few events which typify the important processes within the gulf are identified in the animation and discussed.

Figure 6.5: Animation displaying the daily mean bottom salt (top left), bottom temperature (top right), speed and current direction (middle left), sea level (middle right) and domain averaged heat flux, salt flux and wind-stress (bottom 3 panels). Animation Location: Electronic Appendix/Daily Mean Animation.avi

27th February 2010: At this time the circulation is under the influence of a strong summer (0.2 Pa) SE wind-stress. The response of GSV circulation is the formation of a 'double gyre' as expected from the idealised model results (Chapter 4, Figure 4.3), with a notable difference from the idealised result in that the southward central flow is able to escape the GSV interior under the strong SE wind-stress. The other features remain mostly consistent with the idealised results, with northward flow on both the east and west coasts, and the southward central return flow. Very strong westward flow is seen on the shelf, which enters through BP and continues through IS. The result of this is the formation of a strong salinity front forming along the mouth of the gulf, with the fresher shelf waters along the north coast of KI being very distinct from the much saltier gulf waters along the mouth and northern shore of IS. The salinity is also lower for both the east and west coasts of GSV, reflecting the fresher water being brought northward by the double gyre system, with waters at the head of the gulf being much saltier than the mouth. The central southward flow is much saltier than the coastal waters, advecting the hyper-saline head waters to the mouth. This is due to the relatively high density, causing the saltier waters to flow to the deeper central channel. A temperature front is also formed along the mouth, with shelf waters being both fresher and cooler than gulf waters. The central southward flow is also warmer than the coastal waters, advecting the hotter head waters towards the mouth. The Sea Surface Height (SSH) is lowered throughout the entire domain, particularly within GSV and IS. This is also consistent with expectations from the idealised model (Chapter 4, Figure 4.2). At the western end of IS the bottom temperature and salinity is much lower than waters to the east. This is due to the rapid increase in depth here, and the flow pattern which indicates shelf waters follow the isobath around the SW tip of KI resulting in northward flow of cooler and fresher waters.

18th August 2010: The system in now under the influence of a very strong (0.2 Pa) winter SW wind-stress event, inducing a general gulf-wide clockwise circulation which exhibits many similarities with the idealised model results (Chapter 4, Figure 4.7). The main difference is the northward flow is displaced further off the west coast due to the formation of a series of gyres along that coast resulting from the variable nature of winds prior to this time. The southward flow on the eastern coast is present, as is the very strong westward through-flow in IS and BP. The salinity distribution shows a clear finger of relatively fresher waters intruding in to the gulf on the western coast and a plume of saltier gulf waters being transported southward along the eastern coast. The salinity of waters entering the system via IS is higher than that of the shelf waters to the south of KI. This is due to the effect of the ejection of the highly saline Spencer Gulf Eddies (named SPEDDIES by Teixeira (2010)) from SG to the west of IS which, under the effect of the strong SW winds and corresponding eastward shelf flows, are partially forced in to IS. To the east of BP evidence of the salty GSV waters being ejected from the system via BP is noticeable, with coastal waters to the east noticeably saltier than for the shelf waters to the south. Bottom temperature also shows evidence of the relatively cool GSV waters being expelled from the system to the east of BP. SSH for the entire domain is elevated, which is also consistent with expectations from the idealised model (Chapter 4, Figure 4.6).

4th September 2010: This event shows another strong (0.1 Pa) winter SW wind. Even though the wind-stress and through-flow in IS is weaker than the previously identified event, the southward coastal flow in the east is actually much stronger, and the general circulation of the system matches the idealised case (Figure 4.7) much better, with a very defined gulf-wide clockwise circulation present. After a series of strong SW and NW wind events in the preceding months, the salinity of the system is now generally

reduced due to the resultant flushing of the gulf, with on only a few pockets of hyper saline waters remaining along the east coast. This salinity distribution also explains some of the difficulty experienced with validation of salinity (see Section 6.5.5) due to the high spatial variability. Though difficult to see, those pockets of hyper-saline waters also have lower temperature than surrounding waters.

28th November 2010: Now under a summer SE wind-stress again, the system exhibits a near perfect double gyre flow field. This is somewhat a transitional period, with salinity and temperature both beginning to increase once again after their winter time minimums due to atmospheric fluxes. The salinity front which is typically present for summer is beginning to form, and over the next few days (28th November to 2nd December) while SE winds persist the front becomes much stronger. The effect of the double gyre on salinity and temperature is also present, with higher salinity and temperature at the head of the gulf, with the southward central plume also exhibiting higher salinity and temperature than the east and west coastal northward flows.

10th March 2011: Here the system exhibits its maximum salinity state, with extremely high salinity at the head of the gulf due to maximum summer net evaporation and a lack of wind driven advective flushing. A clear plume bringing salty waters from the head southward through the centre of the gulf is also visible. The temperature for the entire gulf is high. A salinity and temperature front is shown through IS and BP, clearly demonstrating a separation of gulf and intruding shelf waters.

10th May 2011: Under the influence of a relatively strong (0.15 Pa) SSW wind-stress, the system is now in a transitional state between typical summer and winter states. A gulf-wide clockwise circulation is present, and while the gulf is still highly saline in comparison to the shelf waters, the highly saline southward flowing plume has migrated to the east coast. Temperature for coastal regions has begun to decrease and only the deeper central regions of the gulf are showing as warmer than the shelf waters.

6.5.2 Validation - Filtered Currents: Tides Removed

Current velocities were recorded at Pt. Stanvac (Figure 6.6) for the period spanning July 2010 to December 2011 (with some gaps in data when instrumentation was not deployed or suffered failure) as a part of the desalination plant monitoring. This data was used to validate the GSVM's ability to reproduce seasonal (low-pass, 30 day) and weatherband (band-pass, 3-30 days) currents. High-pass (0 - 3 days) filtered results (not shown) are dominated by the tidal cycle discussed earlier (Chapter 3).

Currents were filtered using a running boxcar average with the form $sin(x)/x$ over 30 days to find the seasonal currents. High-pass currents were filtered by running a 3 day running boxcar average with the same form. Weatherband currents were determined by removing both the high-pass and seasonal averaged currents from the original unfiltered data.

The low frequency currents investigated were expressed in terms of along-isobath and cross-isobath velocity, defined as the major and minor axis respectively. This is because low frequency currents tend to follow isobaths, which around Pt. Stanvac are rotated approximately 19 degrees clockwise from true north (Figure 6.6). Minor axis velocities (not shown) are typically an order of magnitude weaker than the major axis velocities.

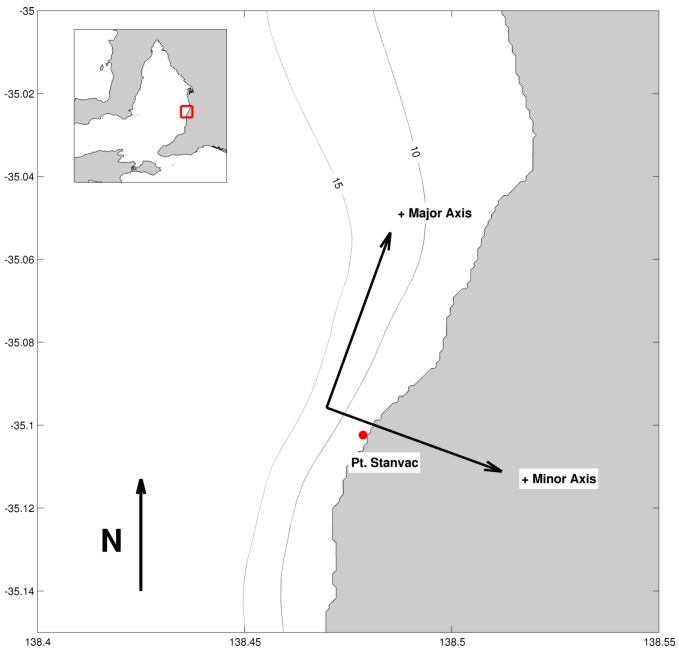

Figure 6.6: Major and minor current axis orientation for Pt. Stanvac model and observation comparisons. 10 and 15m model isobaths shown. Inset shows location of main figure within domain.

Weatherband Band-pass filtered depth-integrated current velocities for the major axis and the corresponding weatherband filtered wind-stresses are shown for model results (red) and observations (blue) in Figure 6.7. The results show very good agreement between the model and observations, indicating that the circulatory response of the model to weatherband frequency events is well resolved at this location. The observed filtered currents appear to behave as expected in response to wind-stresses based on the results of the idealised modeling (Chapter 4). Three individual events were selected for more detailed analysis, and highlighted in Figure 6.7 as the shaded areas. Mean sea level pressure maps (BOM) for these events are presented in Figure 6.8, explaining the weather systems which led to the adopted wind-stresses. Events are also identified in the daily mean animation (Figure 6.5, Electronic Appendix/Daily Mean Animation.avi) and discussed in order to bring greater context to the point data for Pt. Stanvac.

1: 13th - 27th August 2010: A relatively strong southward flow event is shown in the GSVM results and observations at Pt. Stanvac (Figure 6.7 upper). This event coincides with a period of W and SW winds (up-gulf) caused by a deep low directly south of GSV (Figure 6.8a), which are expected to induce clockwise circulation within the gulf (Chapter 4, Figure 4.7). This is consistent with the observations and model results for depth-integrated velocity for this period. The animation for this period indicates that under the strong SW wind-stresses the expected gulf-wide clockwise circulation is present. Additionally, the animation shows the anti-clockwise Myponga Eddy to be intensified for the 19th-22nd, deflecting the southward gulf discharge further offshore to the centre of the mouth. The good correlation of observations and GSVM results indicates that the Myponga Eddy is also well resolved, as poor representation of that feature would otherwise incorrectly influence flows at Pt. Stanvac.

2: 15th - 31st October 2010: GSVM, observations and the animation show a strong northward flow event followed by a weak southward flow event (Figure 6.7 upper). The northward event is forced by southerly winds (15th Oct) formed by the combination a low to the east of GSV and a high to the south-west (Figure 6.8b), which switch to a northerly wind over a period of a few days (19th - 20th Oct) as the high moves eastward over GSV and force the weak southward flow. The animation for this period indicates that under the strong S wind-stress a velocity field similar to the 'double gyre' system is formed. In this case however, the northward eastern coastal flow is partially fed by shelf waters entering through BP, and the central southward flow is able to partially escape GSV through a strong westward flow via IS (15th - 17th), indicating an alternative method for flushing the Myponga Eddy region of the gulf.

3: 25th November - 2nd December 2010: Observations and GSVM results show a northward flow event, though the GSVM appears to overestimate the magnitude (Figure 6.7 upper). In this case the overestimation is likely caused by an error in the ECMWF forcing, which indicates very strong SE winds (Figure 6.7 lower). However, the mean sea level pressure maps (Figure 6.8c) for this period suggest that the winds would not be so strong. The flow pattern however is again consistent with expectations from the idealised wind models, which indicate that under a SE wind-stress regime the 'double gyre' circulation pattern will emerge and result in northward flow in the Pt. Stanvac region (Chapter 4, Figure 4.3). The animation supports this, showing that as SE wind-stresses intensify on the 27th the double-gyre system becomes apparent and is fully formed for the 28th - 30th. As the wind-stresses weaken and change direction on the 1st and 2nd of December, the double gyre system decays.

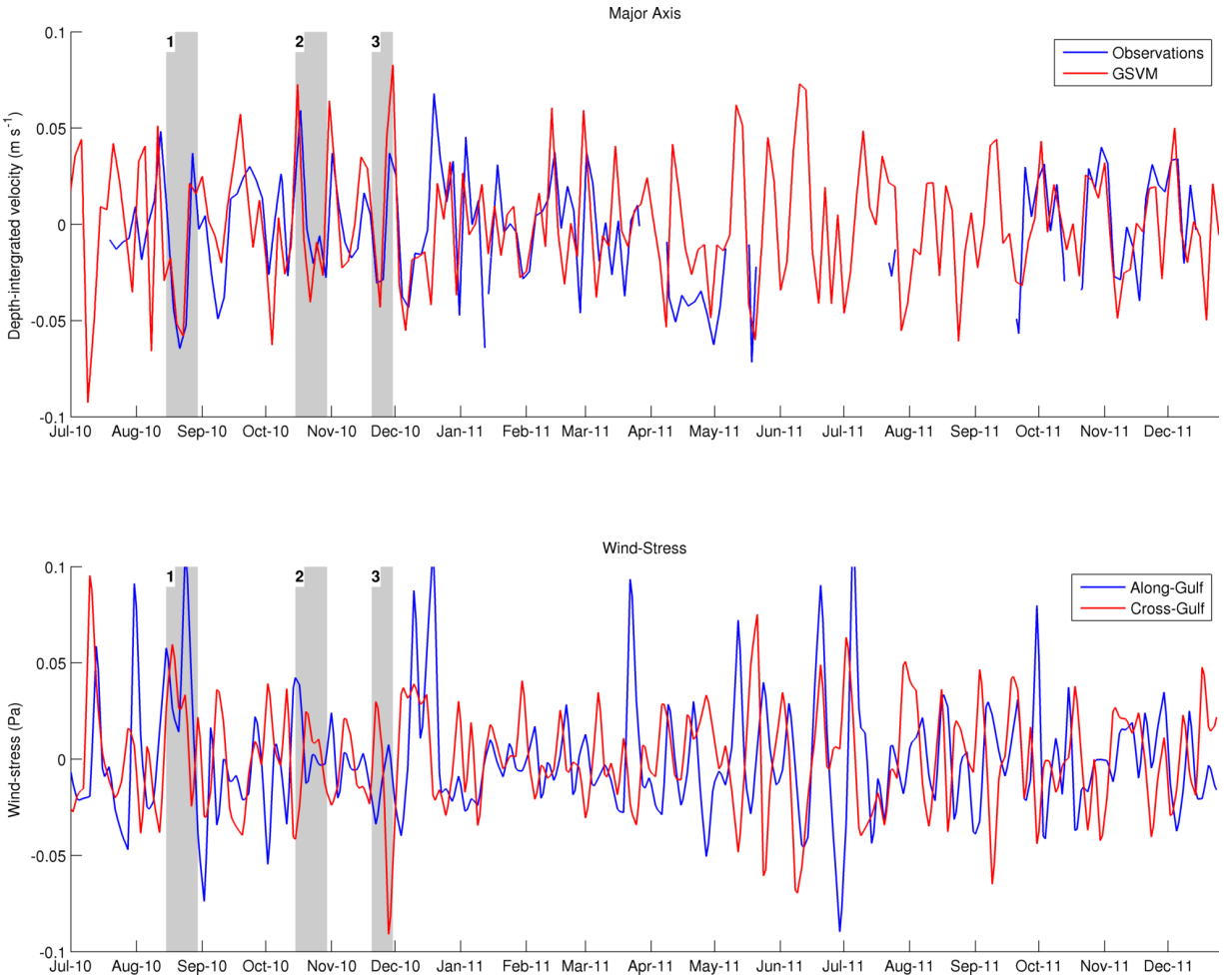

Figure 6.7: Upper: Time series comparison for weatherband pass filtered depth-integrated velocity of GSVM (red) and observatiuons (blue) on major axis (alongshore, 19 degrees from true north, following isobaths). Gaps in observations occur when instrumentation was not deployed or suffered error. Lower: Corresponding along-gulf (blue) and cross-gulf (red) wind-stresses. Along-gulf stress is positive for SW winds (negative for NE) and cross-gulf positive for NW winds (negative for SE). Shaded and numbered areas highlight events chosen for further investigation.

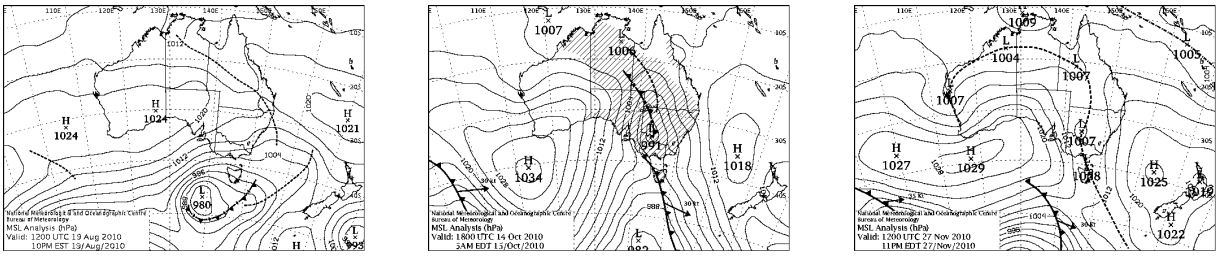

(a) (b) (c)

Figure 6.8: Mean Sea Level Pressure (MSLP) maps for (a) 19th August 2010 showing pressure gradients inducing SW winds, (b) 14th October 2010 showing pressure gradients inducing S winds and (c) 27th November 2010 showing pressure gradients inducing SE winds for GSV. Sourced from Bureau of Meteorology.

Low-pass (seasonal) Low-pass filtered depth-integrated velocities for Pt. Stanvac indicate a general seasonal trend in which as expected there are northward flows during the summer months and southward during the winter months (Figure 6.9 upper). This trend is present for both the observations and GSVM results. This is consistent with the expectations from the idealised wind models (Chapter 4) and mean seasonal SE summer and SW winter wind-stresses (Figure 4.1). Indeed, as expected from the results of the idealised models (Chapter 4, Figures 4.3 and 4.7), the seasonal directionality of depth-integrated velocities at Pt. Stanvac is closely tied to the mean up-gulf and cross-gulf wind-stresses. Negative cross-shore wind-stresses (SE wind) during the summer months are dominant with weak along-gulf winds (Figure 6.9 lower) and lead to positive (northward) alongshore flow (Figure 6.9 upper) as a result of the typical double gyre formation. For the winter months the cross-gulf wind-stresses are weaker and the along-gulf winds are dominated by SW winds (Figure 6.9 lower), inducing the clockwise circulation within the gulf which results in the corresponding southward (negative) alongshore depth-integrated velocity at Pt. Stanvac (Figure 6.9 upper).



Figure 6.9: Upper: Monthly mean alongshore current velocities for the GSVM (red) and observations at Pt. Stanvac (blue). Gaps in the observations correspond to periods when instrumentation was not deployed for a long enough period to determine monthly means. Lower: Monthly mean along-gulf (blue) and cross-gulf (red) wind-stresses for Pt. Stanvac. Positive along-gulf wind-stresses are SW winds (negative NE) and positive cross-gulf winds are NW winds (negative SE). A clear seasonal pattern is evident in both the GSVM results and observations wherein the mean depth-integrated velocities during the winter months are negative (toward the mouth) and positive during the summer months (toward the head). There is a clear correlation between SE wind-stresses (summer months) and positive (northward) mean depth-integrated currents. As winds become dominated by W and SW during the cooler months, the depth-integrated velocity tends to negative (toward the mouth) flows.

6.5.3 Sea Surface Height at Pt. Stanvac

Barometrically adjusted Sea Surface Height (SSH) comparisons are made between GSVM results and data observed at Pt. Stanvac, Pt. Giles and Outer Harbour, whereby the effects of atmospheric pressure are filtered from observations for accurate comparison with model results. Weatherband (3-30 days) and seasonal (30 day) filtered SSH data are compared with GSVM results in order to validate model performance. As with the residual current comparisons, the high-pass filtered (0-3 days) SSH (not shown) is dominated by the tidal signal and no meaningful comparison for the model results and observations can be made for the impact of non-tidal forcing fields. SSH filtering is performed the same way as described above in the analysis of currents.

Weatherband The weatherband (band-pass, 3-30 days) filtered results shown (Figure 6.10 upper) show good agreement between the GSVM results and observations for SSH recorded by a high frequency pressure gauge at Pt. Stanvac during the 2010 calendar year. Weatherband SSH comparisons are only available for 2010, as high temporal resolution SSH observations are not available for 2011.

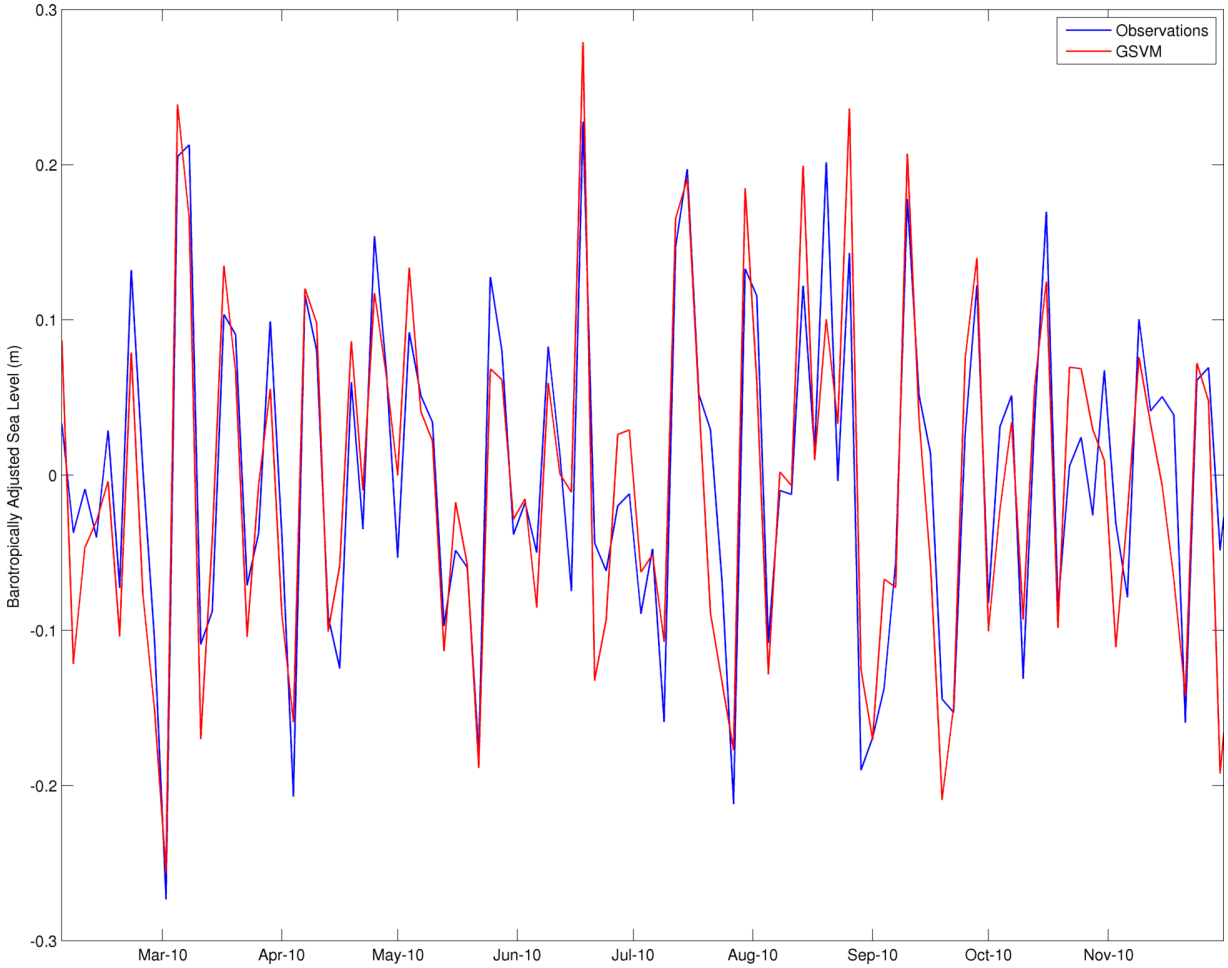

Figure 6.10: Time series comparison for barometrically adjusted sea level (m) in the band pass (weather band frequency) at Pt. Stanvac for GSVM (red line) and observations (blue line).

Seasonal Long term monthly mean GSVM results are compared with SSH records from the Australian Baseline Sea Level Monitoring Project (ABSLMP) (BOM) at Pt. Stanvac and the Permanent Service for Mean Sea Level (PSMSL) at Pt. Giles and Outer-Harbour (Figure 6.11) and indicate good agreement. Unfortunately, the SL gauge at Pt. Stanvac for the ABSLMP was removed at the end of 2010, hence comparisons with the GSVM for this location are only available for 2010. The seasonal pattern is well reproduced, with sea level depressions at Pt. Stanvac, Pt. Giles and Outer-Harbour during the summer months under the influence of dominant SE winds indicated by both the model and observations, whilst sea level elevations for the winter months under the influence of dominant SW winds are also seen in both the data and GSVM results. Though there are minor differences from the west (Pt. Giles) to east (Pt. Stanvac), the seasonal patterns are more or less the same. This is due to the gulf wide decrease in SSH for summer and increase for winter as expected from the idealised wind models (see Figures 4.2 and 4.6).

Comparisons for Pt. Giles and Outer-Harbour SSH show the model compares favourably for the 2010-2011 period, with the exception of January 2011 when there appears to have been an event which led to a sea level increase throughout the gulf which was missed by the GSVM.

Mean SSH on the seasonal scale appears to be dominated by wind-stresses, and thermohaline structure has little impact. The results of the geostrophically adjusted models (Chapter 5) indicate that SSH is expected to be below mean for both summer (Figure 5.3) and winter (Figure 5.7) for most locations throughout the interior of GSV, with winter SSH predicted to be lower than summer. However the opposite has been shown to be true in both the GSVM results and observations for the three locations considered, which span a large proportion of the gulf. This indicates that thermohaline influences are being overpowered by wind-stresses, which cause SSH elevations during winter and depressions during summer.

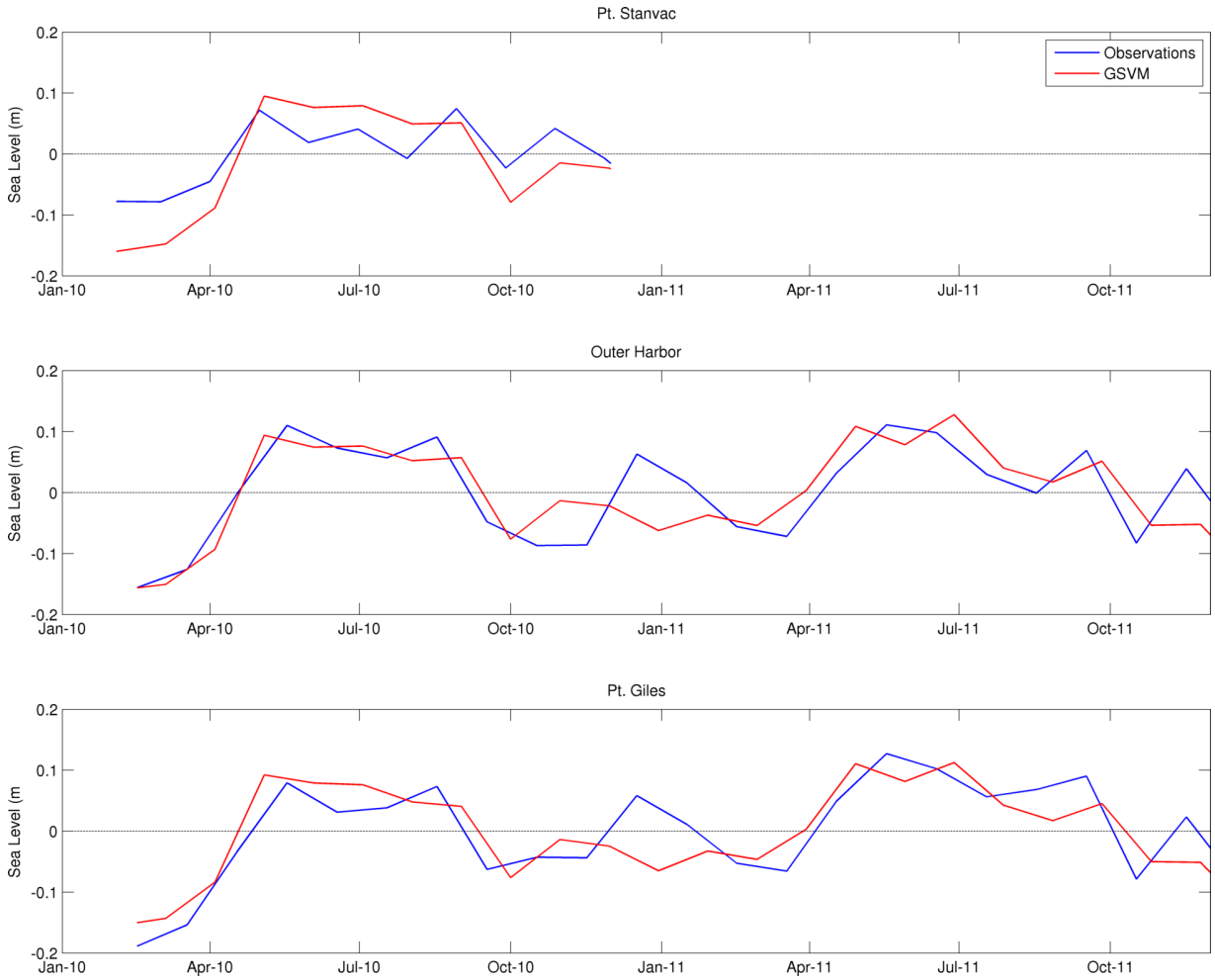

Figure 6.11: Seasonal sea level 2010-2011 time series comparison for Pt. Stanvac, Outer-Harbor and Pt. Giles, observations (blue line) and GSVM (red line). Observations for Pt. Stanvac sourced from ABSLMP, Pt. Giles and Outer-Harbor from PSMSL. Pt. Stanvac results only available to the end of 2010.

6.5.4 Temperature

Temperature comparisons for 2011 are made between the GSVM and observations recorded off the coast of Pt. Stanvac taken at a depth of approximately 18 m. An idealised one dimensional heat flux model is employed to discern the effects of local forcing and advective changes in temperature. Observations in the weatherband are compared with GSVM results and the idealised model, which indicate good performance of the GSVM and poor performance of the idealised model for Pt. Stanvac. Year long predictions from the idealised model are made for 4 locations within GSV and compared with GSVM results, indicating the importance of advection on resolving temperature is spatially variable.

6.5.4.1 Weatherband

Weatherband temperature results of the GSVM are compared with observations at Pt. Stanvac (Figure 6.12), with the splines of the monthly mean values removed to isolate the weatherband (3-30 day) changes in temperature from seasonal changes. The results of this comparison indicate the GSVM reproduces

temperature changes at this location quite well for the weatherband, with the best agreement in the latter half of the year. In the earlier months the model tends to underestimate the extremes of variability. This is likely due to the 10 year climatology SST data set used for nudging, which suggests the early months of 2011 are unusually cool (see Figure 6.4). This results in nudging which reduces the extremes in heat flux and therefore short term temperature fluctuations.

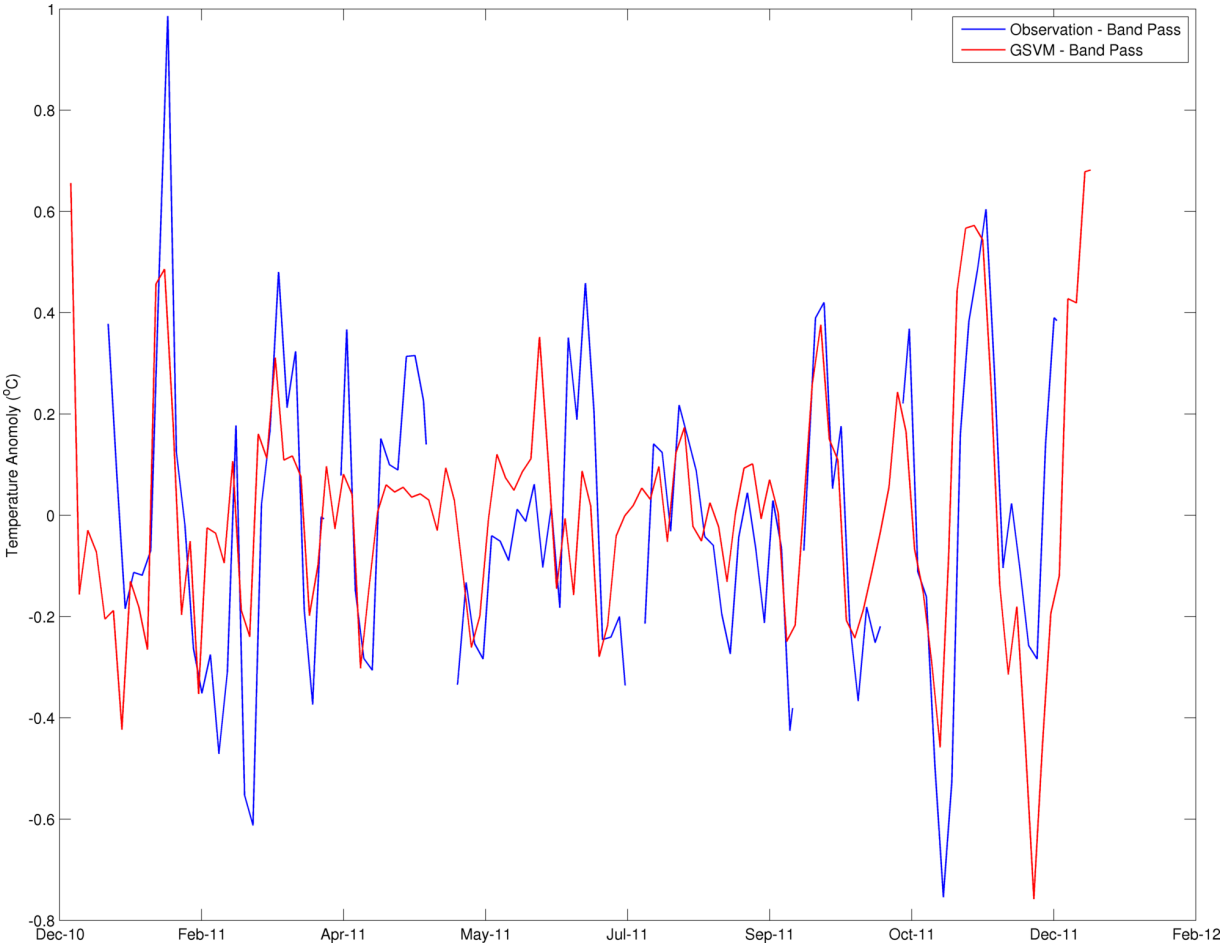

Figure 6.12: Band pass filtered temperature anomaly (raw temperatures minus spline interpolation values, with means removed) for temperature observations from Pt. Stanvac (blue) and GSVM (red) results. Gaps in observation plot indicate periods when instrumentation was not deployed. Weather band variability is generally well resolved by the GSVM, especially in the latter half of the year.

6.5.4.2 Long Term

The Idealised Heat Flux Model In order to better understand the relative impact on long term temperature of local heat fluxes compared with advection, an idealised thermal flux model was developed and the results compared with the GSVM results and observations. Close agreement between the idealised model results and GSVM/observations suggests that changes in temperature are largely due to local forcing, whereas divergence indicates advection is important for accurately resolving temperature changes. If the GSVM results better match the observations than the idealised model, the GSVM must therefore be resolving additional processes leading to temperature change which are necessary to accurately simulate

realistic conditions.

The idealised model was based around a volume of water with the same cross sectional area as the grid cells within the GSVM domain (e.g $A = 250{,}000$ m^2) and depth equal to the comparison point from the model domain (16 m for Pt. Stanvac). Advective and diffusive processes are assumed to be zero, hence the only pathway for thermal flux is through the surface. The volume is considered as a single perfectly mixed layer, e.g. all fluxes at the surface are instantly and evenly distributed throughout the volume. The idealised volume is shown in Figure 6.13 where Q_S is the surface neat heat flux, d is the depth in meters and $Q_{x,y}$ and Q_z are lateral and bottom fluxes respectively, both equal to zero.

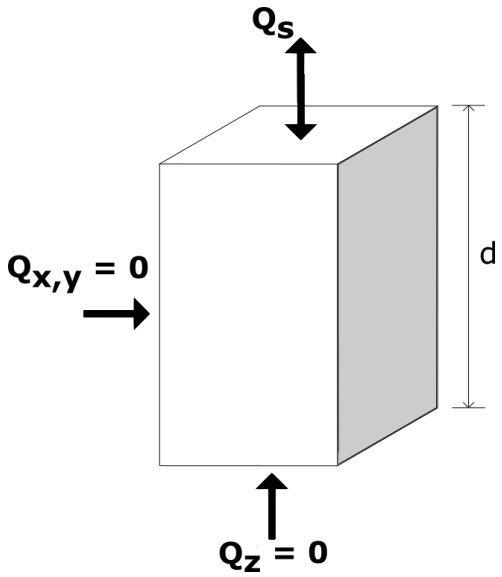

Figure 6.13: Idealised model configuration

In order to create an accurate comparison with the GSVM and observations, the idealised model depth and surface fluxes must be the same as those applied to the GSVM. As such, the heat flux applied to the idealised model is exactly the same as that applied to the relevant grid cell in the GSVM, including the same correction for $dQdSST$ as applied to the GSVM (see Equation 6.6).

Taking equation (2c) from Barnier et al. (1995) and assuming that change in temperature is instantaneous throughout the entire body, and the insitu potential temperature is equal to the actual temperature (e.g. $\theta = T$):

$$\frac{dT}{dt} = \frac{Q_{NET}}{\rho_0 . C_{p_W} . \Delta z}$$

where dT is the change in temperature, $\rho_0 = \rho\,(p, T, S)$ is the density of the considered volume, $C_{p_W} = C_{p_W}\,(p_{\text{ref}}, T, S)$ is the specific heat of the considered volume, Δz is the depth of the considered volume, Q_{NET} is the surface heat flux in W m^{-2} equal to Q_{New} as determined by equation 6.6 and dt is the time step between predicted temperature values. For simplicity of calculation in the idealised case, the pressure is assumed to be 1 atmosphere (101 kPa) for calculations of density and the reference pressure p_{ref} is equal to zero for specific heat calculations.

Other sources of temperature flux such as chemical potential and dissipation of kinetic energy have previously been demonstrated as negligible (Bacon & Fofonoff, 1996) and have hence been ignored in calculating thermal response to surface forcing. Calculating the volume averaged temperature of the

theoretical volume is thereby given by the formula:

$$\bar{T} = \bar{T}_0 + dT \tag{6.7}$$

where $\bar{T}$ is the volume averaged temerature and $\bar{T}_0$ is the volume averaged temperature for the previous time step, assumed to be equal to the potential temperature of the volume. Time stepping on the same interval as the GSVM results (1 hour) gives a time series of the predicted temperature for the idealised volume which is directly comparable to the GSVM results and observations. Comparisons are made for the 2011 calendar year, and the initial temperature for the idealised model is equal to the GSVM temperature for the first timestep.

Comparing the Idealised Model and GSVM Analysis using the idealised model at four points within the GSVM domain was undertaken to discern the relative importance of local heat fluxes and advective temperature changes in resolving the temperature of those points. For comparison, GSVM results are also presented in Figure 6.14.

The idealised model shows excellent agreement with the GSVM temperatures for Pt. Wakefield, which is near the very head of the gulf. This suggests that local forcing is the key determinant in thermal response of waters around Pt. Wakefield. This might be expected since advection in this constrained and shallow region is likely small and heating and cooling fluxes large. This is in contrast to Pt. Stanvac, where the idealised model predicts warmer waters than those of the GSVM results nearly year round by approximately 2.5 degrees. This is likely due to the year round advection which during the summer brings relatively cool water north from the mouth, and during winter the clockwise gyre which draws cooler gulf waters from the head and western coast to the eastern. Observations at Pt. Stanvac are also included, and show good agreement with the GSVM results. The idealised model has poor predictive skill, rapidly diverging from the observations. This indicates that advection is an important process in determining temperature at this point.

The influence of the seasonal circulation is also evident in the results for Edithburgh, which lies on the western coast of GSV near the mouth of the gulf. For that location there is a slight divergence between the GSVM results and idealised model during the summer of approximately 1 degree, indicating that advection plays a small role in regulating the temperature around this location during summer. Greater divergence of around 2.5 degrees is seen during winter, when comparatively warm shelf waters are being drawn in to the gulf. The intrusion and mixing of these shelf waters keeps the temperature higher for this location than would otherwise be possible if the sole influence were local heat fluxes. This is again supportive of the arguments regarding seasonal circulation and connectivity, which indicate a weak northward flow of cooler water during the summer months and a stronger northward flow of relatively warmer water during the winter months.

A large divergence between the GSVM and idealised model is noted for Emu Bay, on the northern coast of KI. In this case the idealised model shows wildly varying seasonal temperatures, with maxima around 31 degrees and minima around 9.5 degrees. However, the GSVM results show a much narrower temperature range, between 15 and 22 degrees. This is consistent with the results of the seasonal variability in flow through IS and BP, which are predicted by the GSVM to bring in shelf waters throughout the entire year. This would therefore reduce the summer maxima by advecting and mixing comparatively cooler shelf waters, and also increase the winter minima by advecting and mixing relatively warmer shelf waters. Large advective events can also clearly be seen in the GSVM results for Emu Bay, demonstrated by sudden

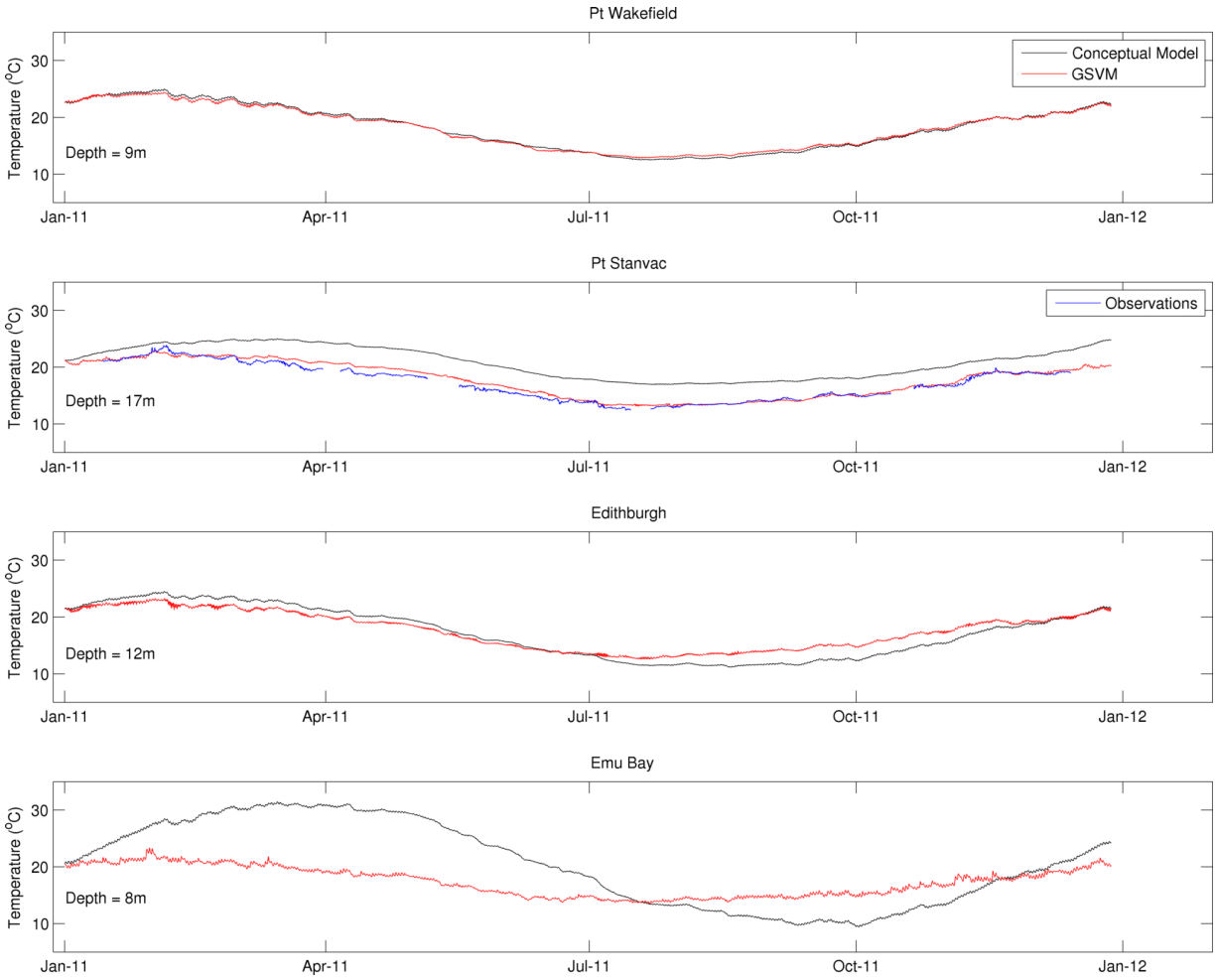

Figure 6.14: GSVM depth averaged temperature vs. idealised model predicted depth averaged temperature for several locations throughout GSV. Locations ordered top to bottom from northern most to southern most point. For Pt. Stanvac the observations are also shown, and indicate that the GSVM far more accurately reproduces temperatures for this location when compared to the idealised model. In general the idealised model more closely matches the GSVM the further toward the head of the gulf of the location.

changes in temperature (e.g. February and November) which do not appear in the idealised model (and hence not related to local heat fluxes).

It is important to note that the patterns observed for the idealised model can vary depending on the selected starting date, and hence initial temperature. This not withstanding, the results give an excellent indication of the importance of advection on the thermal balance for the areas investigated.

6.5.5 Salinity

For a period from May 2010 to December 2011 SA Water collected data from a series of Conductivity, Temperature and Depth (CTD) instrument casts and long-term continuous fixed location SeaBird deployments in conjunction with the desalination plant monitoring project. All CTD casts were performed within a 10 km radius of the desalination plant outfall, while the fixed position logger was placed on the Pt. Stanvac jetty, a few hundred meters from the desalination plant outfall. This data set

is the source of the only long-term salinity records available for GSV.

As shown in Figure 6.15, there is often quite poor agreement between the CTD casts and the fixed position long-term salinity logger, even for those casts which were undertaken within 2 km of the outfall. This is most likely due to two main reasons. The first is that the salinity sensors used appear to have a quite high level of inherent error. In January 2011 another 4 loggers were deployed within the same region (not shown), and though they replicated the same pattern in variability as shown by the continuous logger, there was a constant error of ~ 0.5 between the highest and lowest logging time-series.

The second is that the area around Pt. Stanvac appears to be quite dynamic and displays a large spatial variability in salinity as discussed earlier. This is possibly because it is near the northern most point of a semi-persistent gyre, the Myponga Eddy (Bye & Kämpf, 2006), which causes fresher pulses of water to be drawn northward from the mouth of the gulf under the right wind conditions. As a result, salinities can vary largely in the space of only a few kilometers. For example, during February 2011 the observations and CTD records indicate large variability. Watching the animation during this period shows a plume of salty water traveling south near Pt. Stanvac. This plume moves in response to local wind forcing, resulting in salinities on the coast at Pt. Stanvac which can vary rapidly in both space and time.

The salinity validation for the GSVM is not as robust as with the temperature, sea surface height and residual currents. However, the general seasonal pattern appears to be consistent between the model and the continuous observations, with salinity at Pt. Stanvac appearing to peak during June/July and reaching a minimum around late spring or early summer.

6.5.5.1 Idealised Salt Model

An idealised model using the same approach as the thermal flux model was developed for salinity fluxes. Due to the year round excess of evaporation over precipitation, the salinity of the idealised model which ignores advection will naturally increase with time with no mechanism for reduction. The results of the salinity idealised models (not shown) reinforce the notion that the gulf is completely dependent upon advection to remove the accumulated salt within the system, showing a near continual increase in salinity for all modeled locations. Simply put, precipitation is so outweighed by evaporation in the region that the only realistic method for removal of accumulating salt is the advection of hyper saline water to the shelf, and the advection of fresher water in to the system.

Considering this result for Pt. Wakefield for example shows that while predicting temperature for the area can be achieved through the use of a simple idealised model which completely ignores advection, attempting to do so for salinity would give disastrous results, as the salinity balance is entirely reliant upon advection.

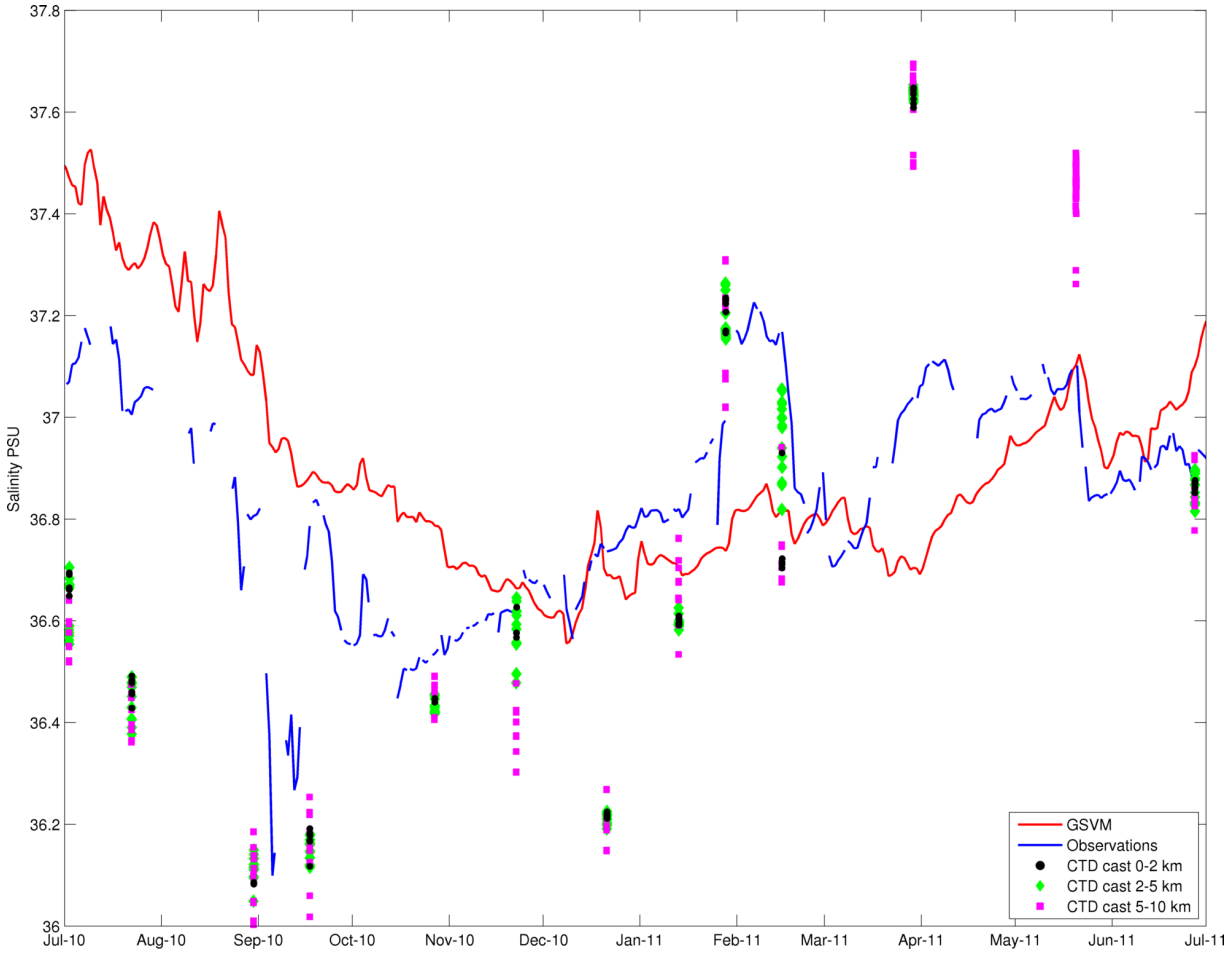

Figure 6.15: Daily mean salinity for GSVM and SA Water desalination plant investigation observations. Concurrent CTD casts are also shown where available. Data for casts is limited to those taken within a 10km range of the outfall and within a depth limit of 13-18m as to be comparable with the continuous observations and model results.

Chapter 7

Connectivity and Flushing of GSV

7.1 Summary

The shelf-gulf connectivity, or exchange, of GSV is investigated using the results of the quasi-realistic GSVM discussed above (Chapter 6), especially in regards to seasonal variability. Clear seasonal variability is expected based on the seasonal circulation outlined in previous chapters. Mean seasonal depth integrated velocity fields, local flushing timescales, long-term salt balances and passive Lagrangian floats are all employed in order to determine seasonal variability in connectivity and its key drivers.

Results of flushing timescales and passive float tracking indicate clear seasonal variation in gulf-shelf connectivity, with summer showing restricted connectivity and winter showing enhanced connectivity. Comparison between float tracking studies using mean seasonal velocity fields and studies using mean velocity fields averaged over a 1.5 day period show the importance of weatherband frequency wind-stress events in connectivity and flushing. The inclusion of those short term events results in much greater connecitivy over the same time period when compared to seasonal means.

In this chapter: Mean seasonal circulation for both summer and winter are found to be as expected based on the idealised models (results above), i.e. reduced connectivity between the shelf and gulf during summer and enhanced connectivity during winter. A volume averaged salt balance for the interior of GSV shows an accumulation of salt within the system while under the influence of typical summer wind regimes and only begins to decrease when winter westerly wind systems begin to dominate, further illustrating the role of local winds in flushing.

Localised seasonal flushing timescales at the 500 m regional scale of the GSVM grid are calculated and indicate that for summer these small regions are more slowly flushed than for winter, while IS and BP experience little seasonal variation;

Passive Lagrangian float tracer models are run for fixed mean seasonal velocity fields and support the theory that the level of connectivity between the gulf and shelf is much lower for summer than winter. Additional passive Lagrangian float tracer models are run for 1.5 daily mean velocity fields over the summer and winter periods, reiterating the previous finding and also illustrating that connectivity/flushing events are largely driven by winds with strong westerly component.

7.2 Seasonal Depth-Integrated Velocities

The mean depth-integrated velocity fields for the GSVM are investigated for the summer months and winter months with focus on flushing and connectivity of GSV. Results share similarities with the idealised models presented in Chapters 4 and 5, with generally less organised structures. Summer results indicate a restriction in gulf-shelf connectivity and winter results indicate enhanced gulf-shelf connectivity.

7.2.1 Mean Depth-Integrated Summer Velocities

The GSVM shows a restriction in connectivity between GSV and the shelf via IS and BP during the Summer months. The mean circulation over the summer period (Figure 7.1) is dominated by a few key features. Westward shelf flow enters through BP and mostly exits the system via IS without interacting with GSV waters, illustrating the reduced summer time connectivity.

A modified double-gyre system, dominated by the western gyre, is present. This appears to be a combination of the idealised wind (Figure 4.3) and geostrophically adjusted (Figure 5.4) flow fields. The northward coastal flow on the west coast is broken in to a series of eddies, most likely due to weatherband variability in wind stress. Here a slight extension of the southern most point of the central southward flow can be seen, taking it beyond the mouth and allowing a small discharge of gulf waters to northern coast of IS. This is also evident in the mean salinity (Figure 5.1), which indicates a small level of mixing of salty gulf waters with fresher shelf waters occurring at the western end of the mouth.

The apparent temperature and salinity front which forms across the mouth near BP (Figure 5.1) is the result of cooler and fresher waters being advectived in to the system by SE wind-stresses, and hence is a symptom of those flows as opposed to a feature which determines circulation.

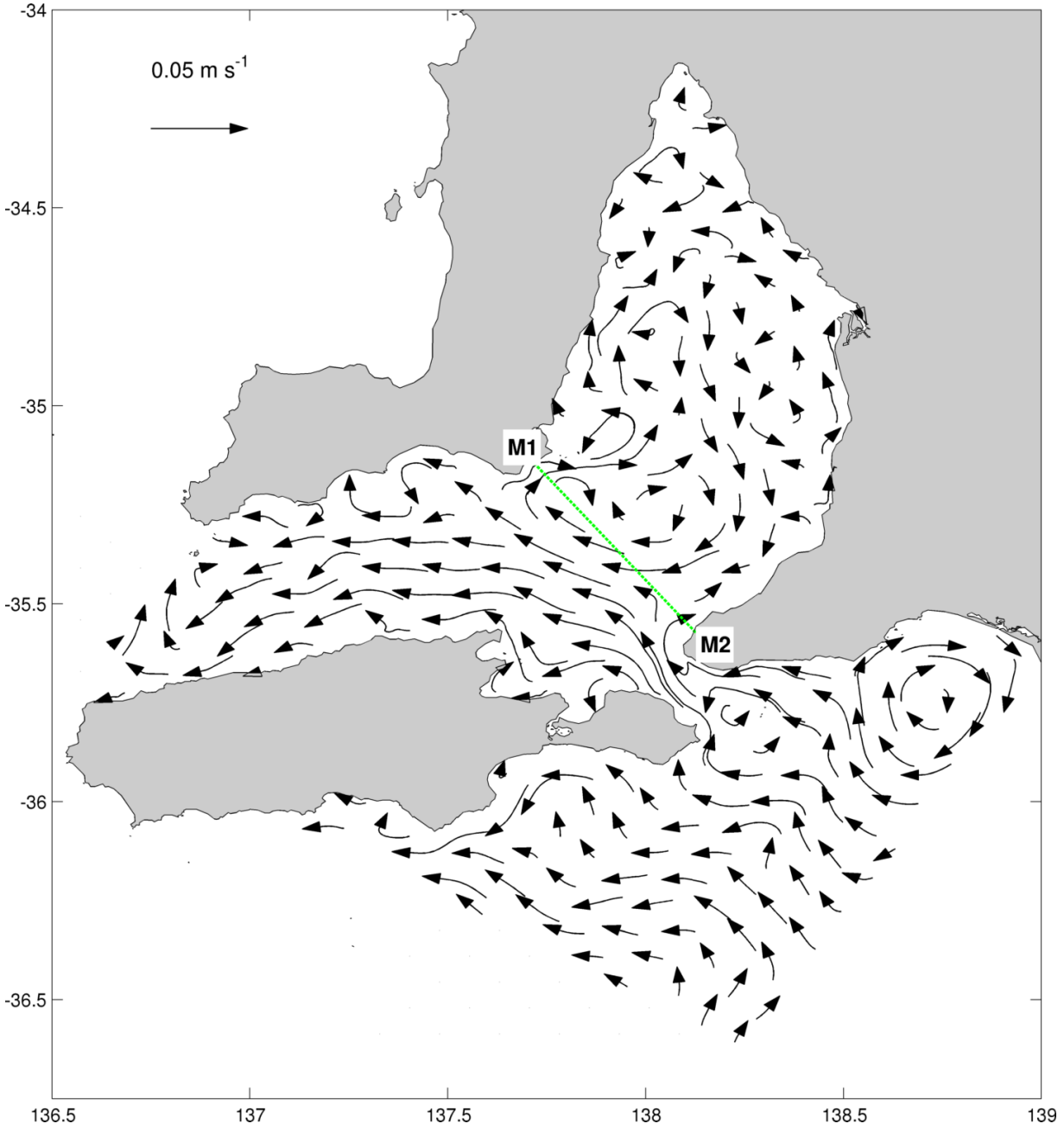

Figure 7.1: Mean summer time depth-integrated velocity field, averaged from 1st December 2010 to 1st March 2011. Legend arrow indicates velocity of 5 cm s^{-1}. The gulf shows very little connectivity with IS and BP and therefore the shelf, with gulf waters being recirculated via a modified double gyre system which is dominated by the western gyre. Flows through BP show little interaction with gulf waters, largely exiting the system via IS. The line M1 - M2 indicates the mouth of the gulf.

7.2.2 Mean Depth-Integrated Winter Velocities

The mean winter depth-integrated velocities indicate a much greater degree of gulf-shelf connectivity than seen for the mean summer circulation, with a general gulf-wide clockwise circulation forming. The mean winter circulation (Figure 7.2) shows some dominant flow features. Most obvious is a very strong eastward flow through IS and BP. Southward flow on the western open boundary, roughly following the 100 m isobath, indicates the pathway for out flowing dense SG waters.

A general gulf-wide clockwise circulation within GSV similar to the idealised model (Figure 4.7) is present, with a series of eddies traveling northward on the west coast bringing in fresh water via IS and a steady southward flow on the east coast expelling GSV waters. Finally, a very strong eastward flow on the shelf to the south of KI and east of BP is modeled.

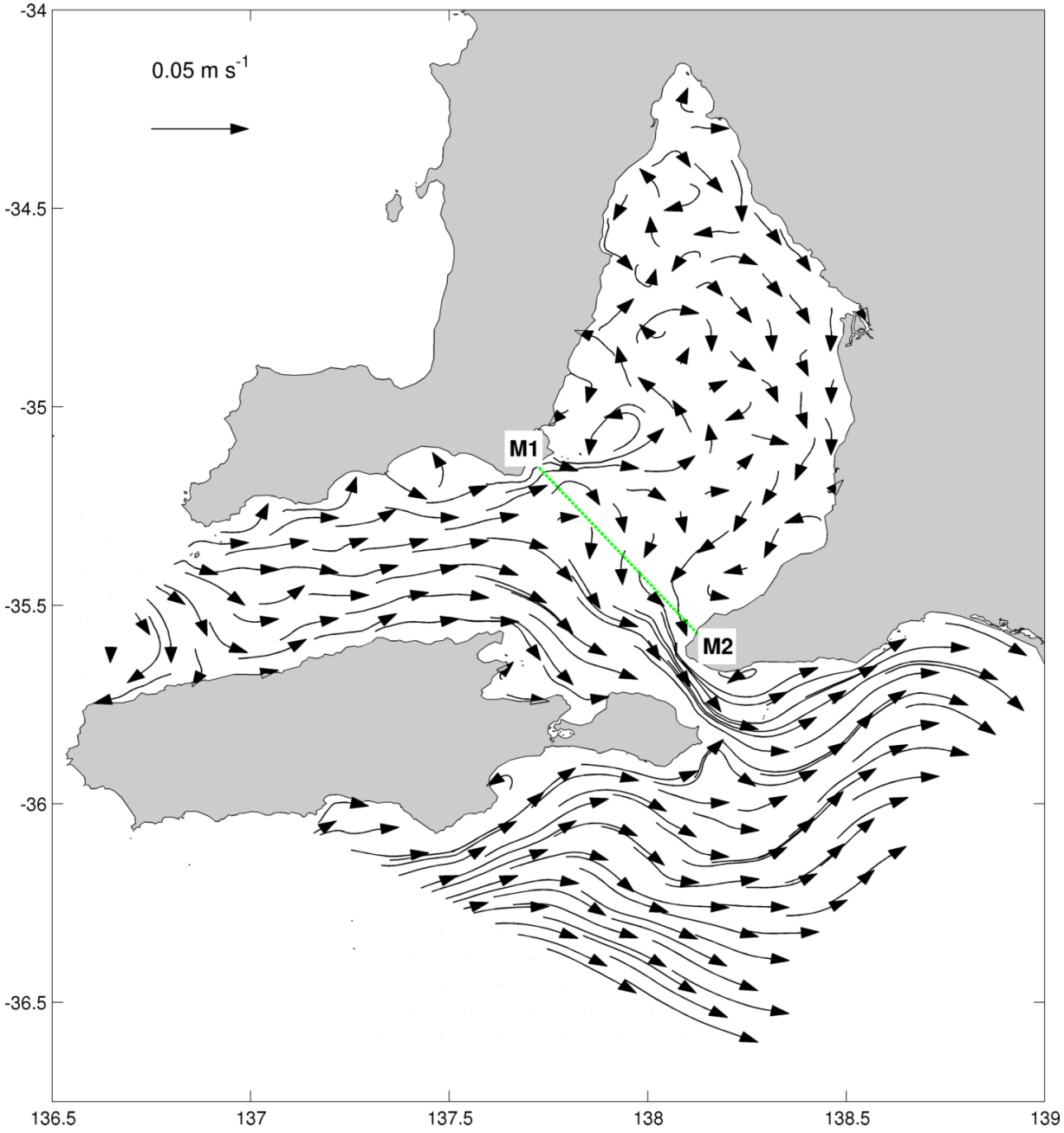

Figure 7.2: Mean winter time depth integrated velocity field, averaged from 1st May 2011 to 1st Aug 2011. Legend arrow indicates velocity of 5 cm s^{-1}. The gulf shows enhanced connectivity with the shelf with shelf waters entering the gulf on the western side via IS. A series of eddies transports this water to the head of the gulf, where it then flows southward along the east coast of GSV before rejoining through-flow in IS and exiting the system via BP. The line M1 - M2 indicates the mouth of the gulf.

7.3 Flushing Gulf St. Vincent: Small Local Scale

Flushing timescale (T^*) in this section is an estimation of the period of time required for a passive tracer to leave an area of interest by means of advection and turbulent diffusion. Here the flushing of GSV is examined at the spatial scale W, which is in the order of a model grid cell (~500 m) and representative of an isolated point source of pollutant such as sewage outfall, stormwater runoff or fish farming net.

Middleton et al. (2014) demonstrate that estimates of flushing timescales can be determined using three key parameters of the fluid motion; the vector mean speed (U), r.m.s tidal amplitude (U_K) and the associated mean shear dispersion diffusivity (K_S). As each of these are readily attainable from the hydrodynamic model results, estimations for flushing times within the model domain are easily obtained. From the Middleton et al. (2014) study:

$$T^* = \frac{T_d p}{1+p} \tag{7.1}$$

$$p = \frac{T_a}{T_d} \tag{7.2}$$

$$U = \left(\langle u\rangle^2 + \langle v\rangle^2\right)^{\frac{1}{2}} \tag{7.3}$$

$$\langle T_a\rangle = \frac{W}{U} \ , \quad \langle T_d\rangle = \frac{W^2}{2\langle K_S\rangle} \tag{7.4}$$

$$\langle K_S\rangle = \frac{\frac{1}{2}\gamma\left(hU_K\right)^2}{378\langle K_V\rangle} \ , \quad U_K = \left(9\left\langle u^2\right\rangle + 9\left\langle v^2\right\rangle\right)^{\frac{1}{2}} \tag{7.5}$$

$$\gamma = \frac{240}{\pi^4}\left(\left(\frac{T_T}{T_v}\right)^2 \sum_{n=1}^{\infty}(2n-1)^{-2}\left\{\left[\frac{\pi}{2}(2n-1)^2\left(\frac{T_T}{T_v}\right)\right]^2 + 1\right\}^{-1}\right) \ , \quad T_v = \frac{h^2}{K_V} \tag{7.6}$$

where T^* is the total flushing timescale, T_a is the advective component of flushing timescale which represents the time taken for a 'cell' of width W to be flushed by the mean current speed U, T_d is the diffusive component which represnts the time taken for a spot to diffuse over a distance W, W is the scale of pollutant input source which is the model cell width (~ 500 m) or greater, U is the mean advective velocity, K_S is a constant value for vertical diffusivity, estimated from the time averaged vertical diffusivity of salt K_V in the model results, γ is dispersion efficiency derived from equation 4.55 in Fischer et al. (1979) (equation 4.55 in Fischer et al. (1979) contains a typographical error in which $\left(\frac{T_T}{T_v}\right)^2$ should be $\left(\frac{T_T}{T_v}\right)$, as noted by Middleton et al. (2014)) , T_T is the tidal period, T_v is the vertical mixing timescale, h is depth and U_K is r.m.s tidal amplitude determined from mean depth integrated velocities u and v as determined by the GSVM. The notation $\langle\rangle$ indicates a time averaged value.

Approximate flushing timescales can therefore be calculated for different periods by averaging values from the GSVM for U, u, v and K_V over the desired period. Middleton et al. (2014) determined seasonal flushing timescales by averaging model results over 3 month periods, which is also applicable in this case for demonstrating the seasonal variability in circulation and connectivity within GSV. It is important to note that these flushing timescales are estimates of local connectivity (e.g. cell to cell), and not gulf-shelf connectivity.

Comparing the summer (Figure 7.3) and winter (Figure 7.4) total flushing timescales (T^*) shows that

for the winter time the regions within the gulf proper are flushed faster than during summer. This is especially true for the upper eastern coastal reaches. Curiously, the eastern coastline south of Adelaide experiences longer total flushing timescales during winter when compared with the summer. This is likely due to the fact that mean circulation in this region is a weak northward current for both seasons, but stronger during the summer (see Figures 7.1 and 7.2). The western coastline of GSV experiences little change from summer to winter, due to the near constant presence of northward traveling eddies year round. Flushing timescales are slightly lower during winter, when these northward flows are generally stronger. IS and BP experience very little seasonal variation in flushing timescales due to their high r.m.s tidal amplitudes and the year-round advective wind-driven currents.

On the north coast of KI there is little seasonal variation, with the exception of the American River region which forms the bay towards the eastern end of the island, which experiences longer flushing timescales during winter when compared to summer. This is because the area is on the leeward side of the dominant winter NW-SW winds, yet fully exposed to summer easterlies. To the south of KI and over to Encounter Bay the summer flushing timescales are significantly longer than those during winter. This is largely due to the more prominent easterly summer winds, which are not only weaker in general than winter westerlies, but also result in the formation of meandering eddies. This is in comparison to the strong eastward currents which form during winter due to the dominant winds with westerly component.

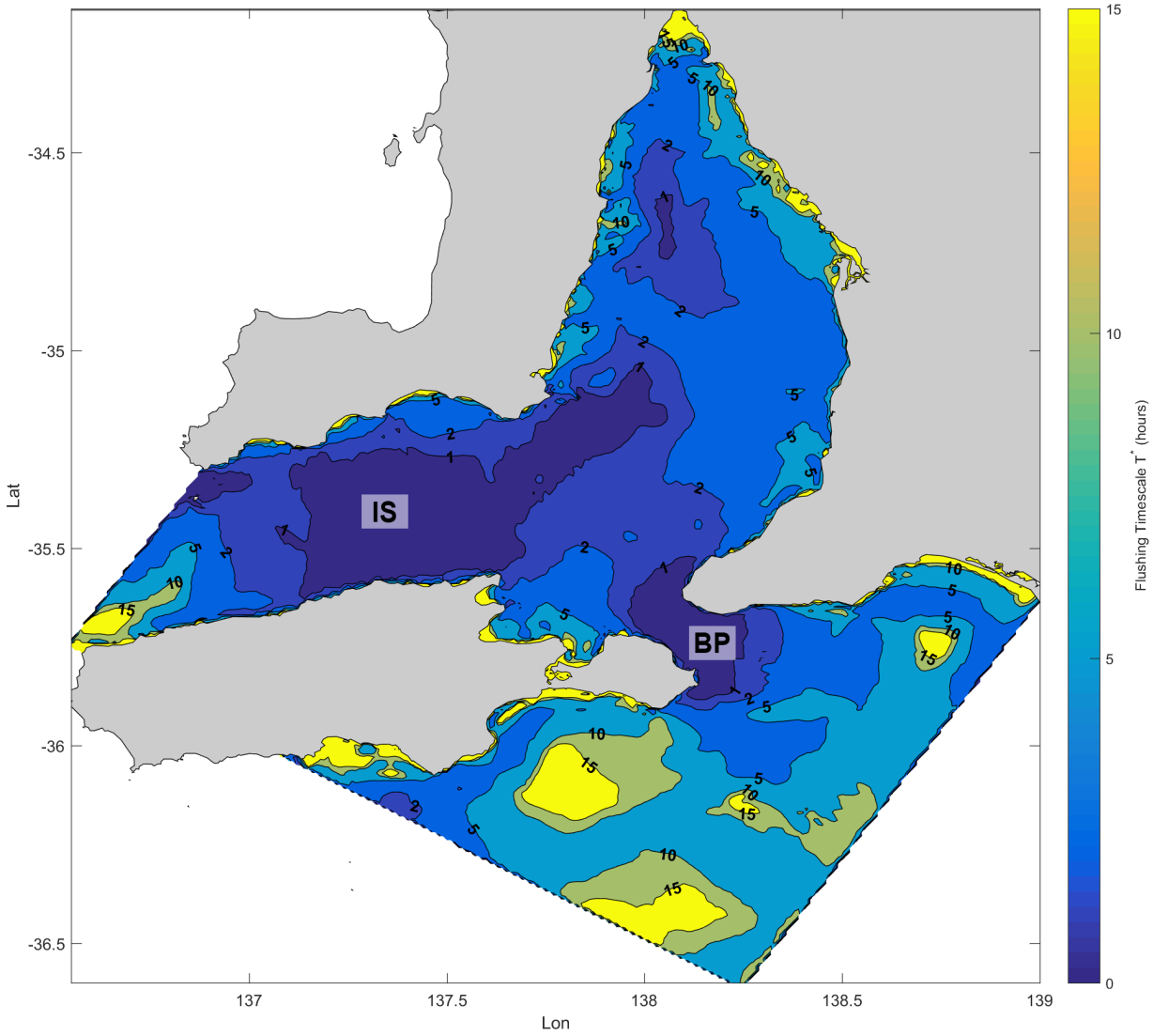

Figure 7.3: Estimated flushing timescales (T^*) for Summer. Units in hours. The majority of the gulf proper experiences flushing times of 2 to 5 hours, with areas in the north-east coastal zones of 10+ hours. BP experiences very low ($<$ 1 hour) flushing times due to the high tidal r.m.s amplitudes, while IS experiences flushing times less than 2 hours for the most part, with the northern coast of IS slightly higher. Total flushing timescale (T^*) to the south of KI and around the Victor Harbor coast is generally high ($\sim$5 - 10 hours). Contour values are [1, 2, 5, 10, 15] hours.

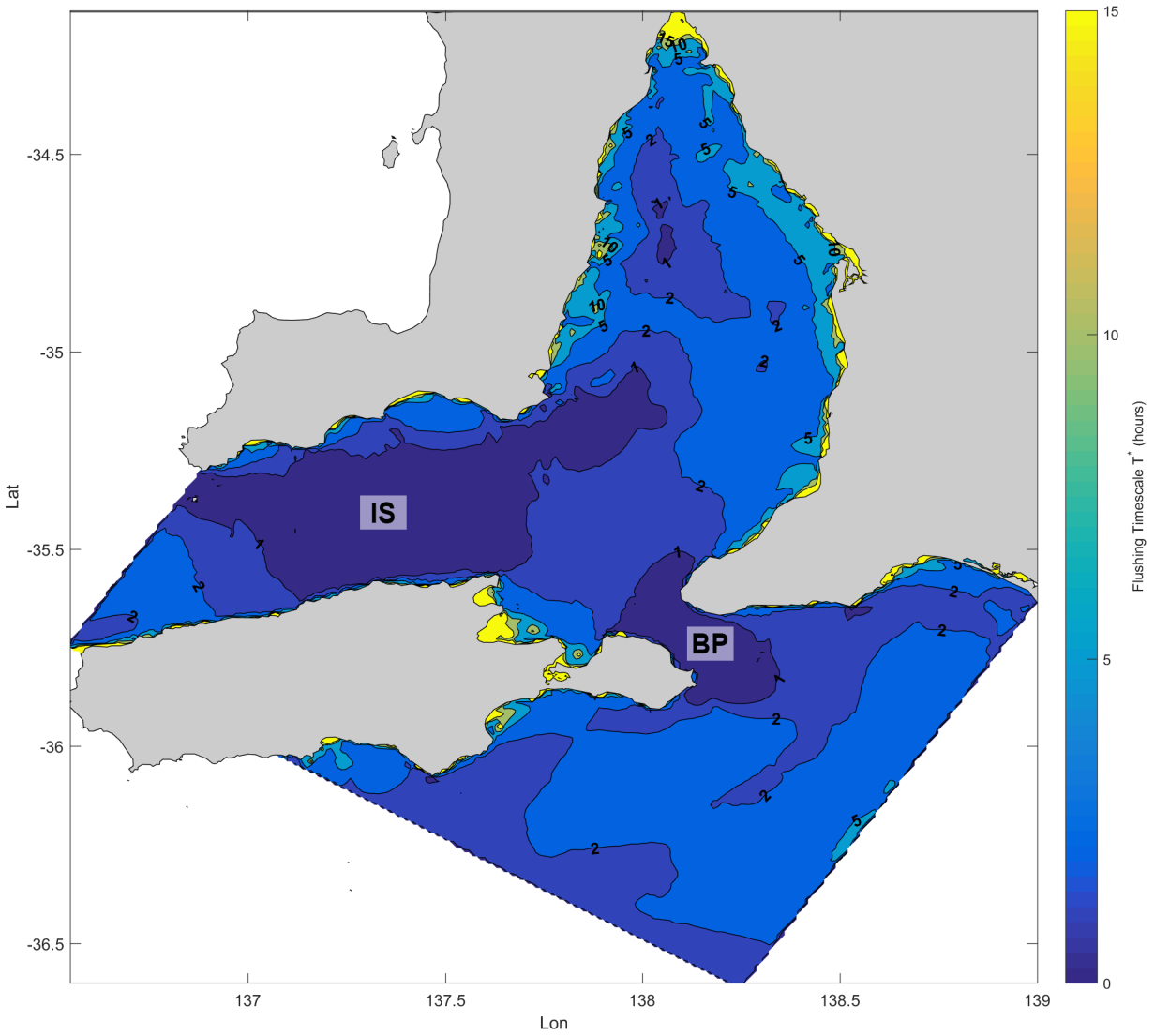

Figure 7.4: Estimated flushing timescales (T^*) for Winter. Units in hours. The majority of the gulf proper exhibits flushing timescales of $\sim$ 2 hours or less, with the eastern coast showing flushing timescales of 5+ hours, especially the Adelaide metro coastline with $T^* >$ 10 hours. T^* to the south of KI and around the Victor Harbor coast is quite low ($\sim$2 hours), especially in comparison to the summer results. Contour values are [1, 2, 5, 10, 15] hours.

7.4 Flushing of GSV: Large Scale

7.4.1 Mechanism

The gulf is found to be primarily flushed through the ejection of pulses of old and salty gulf waters under the influence of wind-stresses with westerly component. As the idealised models show, for all seasonal wind and thermohaline structures flow is induced which brings salty waters from the head of the gulf to the deeper central portion near the mouth. The central basin therefore acts a "holding cell" where these old salty waters remain until conditions become favourable for their removal (e.g. correct wind-stresses).

Figure 7.5 shows the ejection of one such salty pulse over a period of a few days. For the first panel (4th December 2010) the wind-stresses have previously been of easterly component, hence the formation of a relatively strong salinity and density front along the mouth of the gulf . Over the next few days the winds change to a SW and increase in strength, inducing the clockwise flow which pushes a pulse of salty gulf water out of the system via BP.

Another example of this process can clearly be seen in the animation (28th November - 1st January 2011) during a transitional period in which there are both SE and SW winds. Initially under the influence of SE winds, the salinity front across the mouth builds and the old salty waters are trapped in the holding cell. As the winds change to N and then SW, a gulf wide clockwise circulation is induced, and this water is pushed in to the strong eastward IS/BP throughflow and ejected via BP. This is in contrast to SG, where the discharge of salty gulf waters is clearly largely driven by a density gradient from head to mouth (Teixeira, 2010).

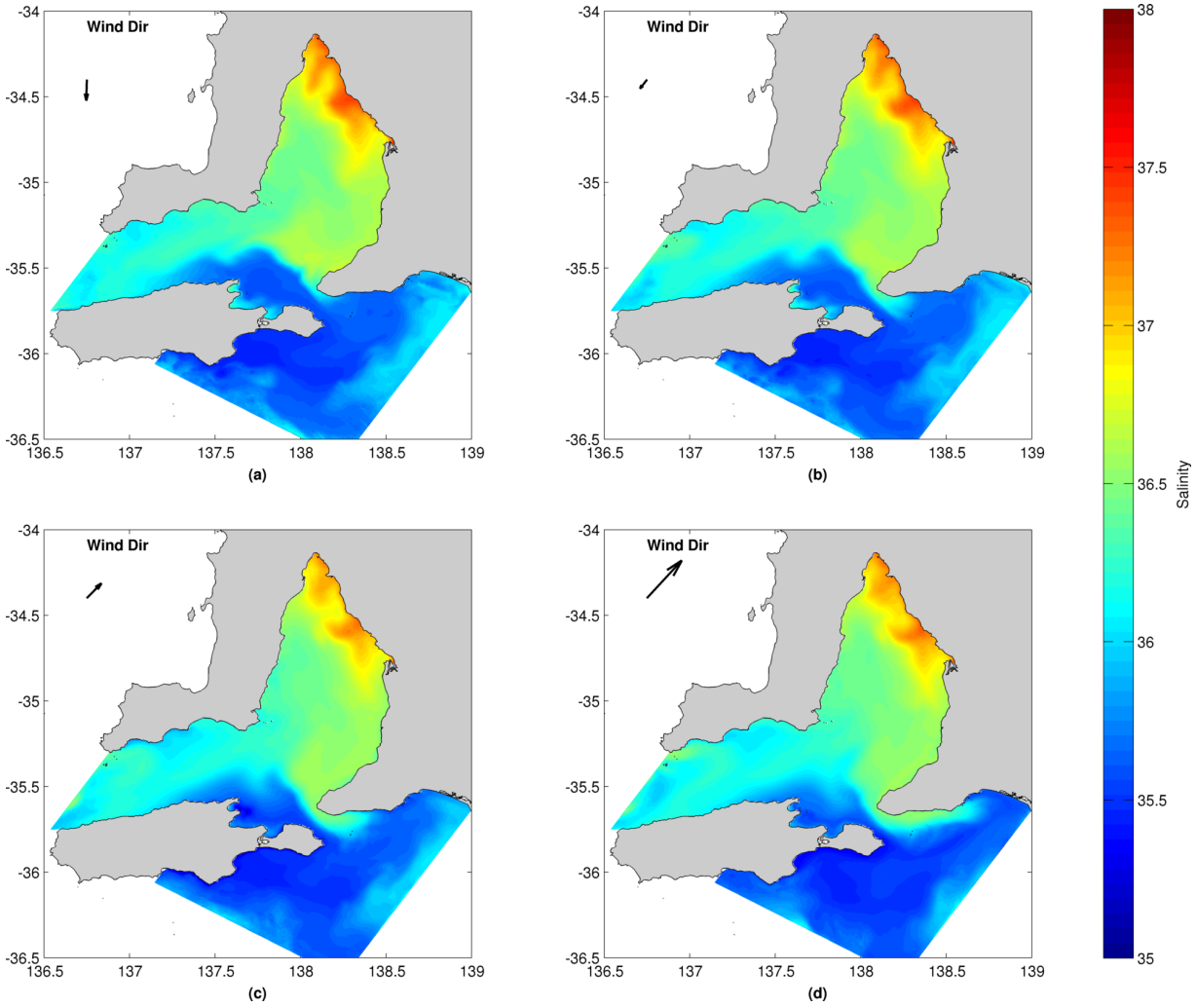

Figure 7.5: Bottom salinity for (a) 4th December, (b) 6th December, (c) 8th December and (d) 10th December 2010. Under the influence of favourable winds, a pulse of salty gulf water is ejected from the system via BP. Wind vectors are scaled to indicate magnitude of stress.

7.4.2 Long Term Salinity Balance

A simple volume averaged salt balance is determined for the interior of the gulf (Figure 7.6) for the 2011 calendar year, where the gulf is defined by the line M1-M2 shown in Figure 7.2, and the relationship between salinity and wind-stress is explored. A clear annual cycle is seen, with gulf waters increasing in salinity during summer and autumn and decreasing rapidly during winter. Salinity remains largely constant for spring. Annually there appears to be little or no net change in volume averaged salinity.

Summer winds with easterly component (especially south easterlies) result in the formation of the double gyre system, which holds waters in the gulf and subjects them to high levels of evaporation. As such, when these winds are dominant (summer), salinity increases. Conversely, winter winds with westerly component induce gulf wide clockwise circulation and the flushing of the gulf. As such, even though evaporation dominates precipitation year round, salinity decreases under these wind regimes as fresher shelf water is introduced.

Rapid decreases in volume averaged salinity can be directly tied to high magnitude wind-stress events with westerly component. Seasonal trends in volume averaged salinty are more heavily defined by wind-stresses rather than precipitation.

These findings agree well with the animation, which shows that under the influence of strong winds with westerly component large pulses of salty water are removed from the system.

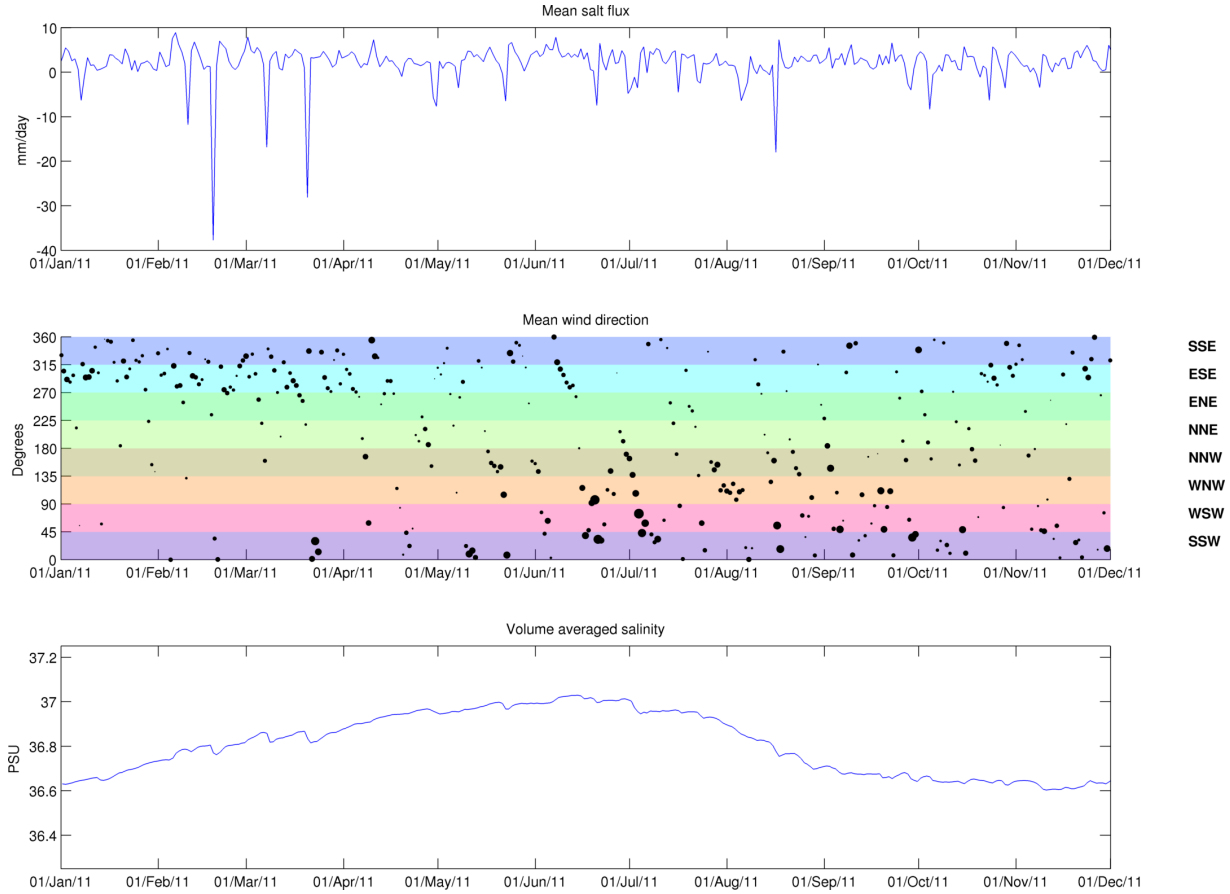

Figure 7.6: Upper: Daily averaged surface salt flux (mm/day) for 2011. Centre: Daily mean wind direction for 2011, point size scaled from zero to maximum (~ 0.25 Pa) wind-stress value. Left axis is degrees from true north and right axis indicates the wind direction. Shaded areas are defined to more easily identify the wind direction for a specific event. Lower: Daily volume averaged salinity for all waters within gulf (as defined by line M1-M2 in Figure 1.1). The seasonal pattern in volume averaged salinity has a strong correlation with the mean wind direction, showing increasing salinity for periods dominated by SE winds (summer) and decreasing salinity for periods dominated by winds with W component (winter). Salinity noticeably decreases in the short term for large precipitation events (negative salt flux) such as those in late February and early and mid March. However, long term decrease in salinity during the winter months does not correlate with substantial precipitation, but rather the domination of high wind-stress events with westerly and south-westerly direction.

7.5 Lagrangian Float Tracer Studies

Better understanding of the connectivity of GSV was obtained using passive Lagrangian float tracking models based on the GSVM results. These studies were conducted using the Lagrangian TRANSport model (LTRANS), an offline particle tracking software package which utilises the results of ROMS models to predict particle trajectories based on flow velocities, including a 4th order Runge-Kutta scheme for particle advection and a random displacement model for vertical turbulent particle motion (Schlag & North, 2012).

All LTRANS models were initialised with 10,000 passive particles randomly spatially distributed through the 2 zones shown in Figure 7.7. Particles were seeded at 2.5m below the surface. Zone 1 is considered the gulf interior and Zone 2 is the majority of the domain, including the gulf (Zone 1), IS, BP and shelf to south and east of BP. The demarcation of Zone 1 along the M1-M2 line (see Figure 7.2) was selected based on the results of preceding chapters, which indicate the formation of a zone of restricted connectivity between the tip of Cape Jervis and the heel of Yorke Peninsula during summer. Therefore by tracking the trajectories of particles which start within the gulf and those that start outside GSV a greater understanding of the connectivity of the two can be obtained. The random seeding was performed only once, and all LTRANS model runs used the same distribution for initial position. The particles were allocated to the zones such that each zone has the same number of particles per unit area. Initial positions were restricted to model cells with depth greater than 5 m in order to avoid coastal entrapment. Particles which reach the open boundary of the model are trapped there and considered to have completely exited the system and may not re-enter.

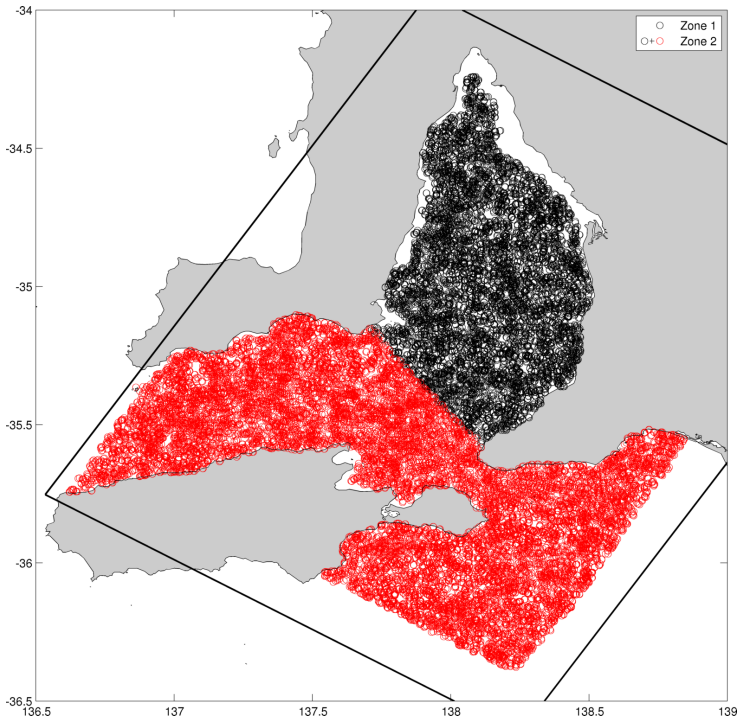

Figure 7.7: Initial positions for the 10,000 Lagrangian floats used in LTRANS models. Zone 1 is the interior the gulf as defined by the line M1-M2 (Figure 1.1) with particles seeded in this zone shown as black. Zone 2 is the majority of the model domain, including the interior of the gulf (Zone 1). Particles which are seeded within Zone 2 but outside Zone 1 are shown in red. Model domain is outlined.

Results of the LTRANS models indicate strong support for the previous arguments in relation to reduced summer connectivity and enhanced winter connectivity. The results of the LTRANS models also support the earlier assertions that circulation and flushing within GSV and the straits are largely driven by wind-stresses, in particular large flushing events are associated with strong wind-stresses with westerly component.

7.5.1 Seasonal Mean Depth-Integrated Velocity

Float studies were undertaken using seasonal depth-integrated velocity fields (as seen in Figures 7.1 and 7.2) in order to determine the typical flow paths and connectivity for particles for seasonal flows. The location of particles which are seeded within Zone 1 (black particles) is tracked against time to determine if the are still within the gulf (Zone 1), within the domain (Zone 2) or removed from the system. A greater percentage of particles remaining within Zone 1 indicates poorer levels of connectivity between GSV and IS/BP and a greater percentage of particles within Zone 2 indicates poorer gulf-shelf connectivity. As Zone 2 also includes Zone 1, the percentage of particles remaining in Zone 2 can never be lower than Zone 1.

7.5.1.1 Mean Summer Depth-Integrated Flow: 1st December 2010 - 1st March 2011

Taking the mean depth-integrated flow for the 2010-2011 summer, a particle tracking simulation was run in order to determine the 'typical' connectivity between the interior of the gulf and the shelf via the straits for the summer months. Figure 7.9 indicates the percentage of particles with initial position within Zone 1 which remain in Zone 1 (black line) and Zone 2 (red line) against time in days. The simulation shows weak outlfow of GSV waters through the central portion of the mouth and weak inflow of shelf waters to GSV on the eastern and western edges of the mouth.

Limited connectivity between GSV and IS/BP is shown, with $\sim 82\%$ of gulf particles remaining within the gulf after 90 days simulation time (see Figure 7.9) and extremely limited gulf-shelf connectivity, with $\sim 97\%$ of gulf particles remaining within the system after 90 days. Many of the particles re-enter the gulf via the western inflow and a clear front through central IS where there is very little interaction of gulf and shelf waters can be seen.

Many of these features are visilble in Figure 7.10, which shows a snapshot taken after 60 days simulation.

Figure 7.8: Animation displaying the paths and distribution of Lagrangian particles under a fixed, depth-integrated and seaonsally averaged flow field for summer time. Animation Location: Electronic Appendix/LTRANS animations/Seasonal Fixed Summer.avi

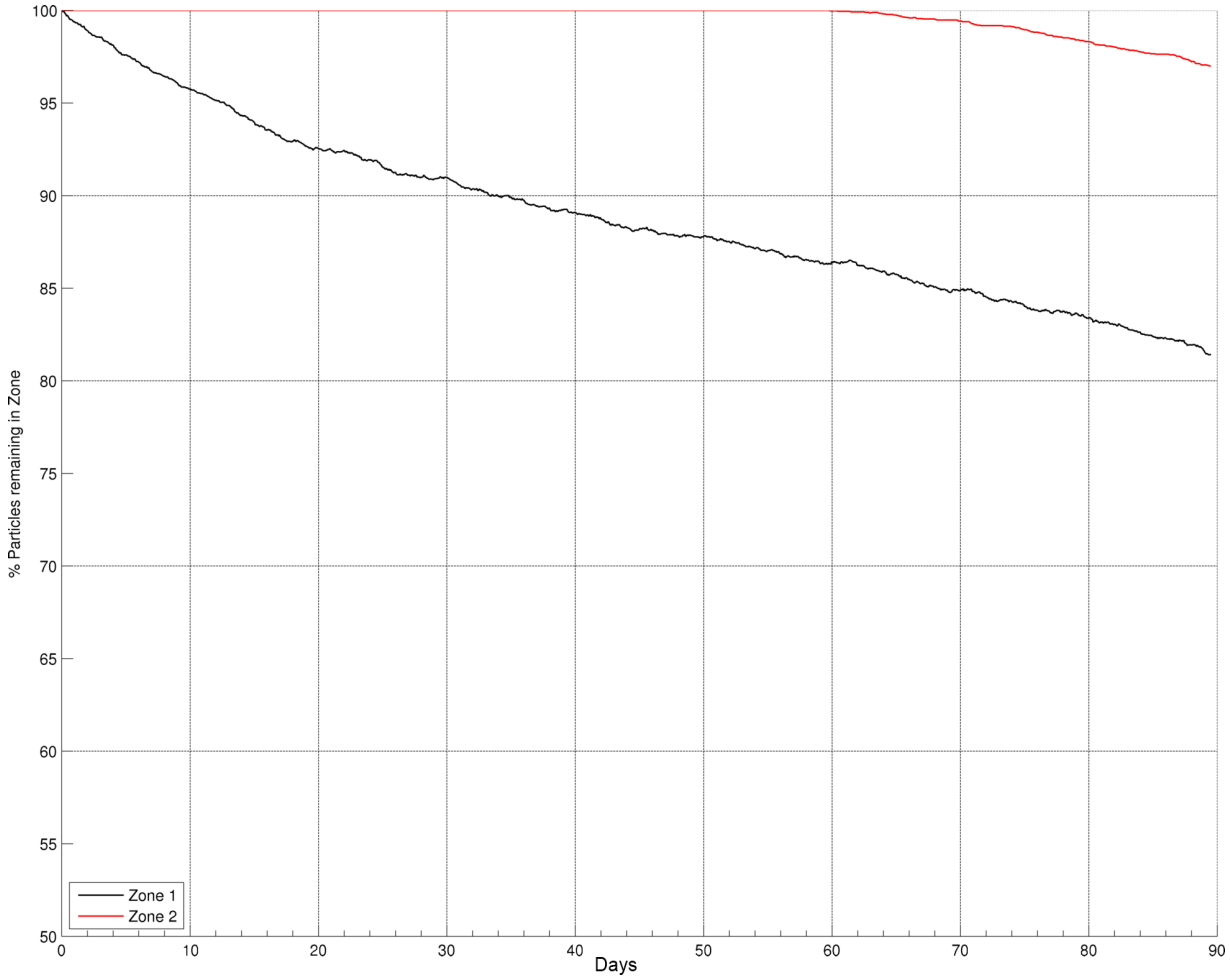

Figure 7.9: Percentage of particles with initial position within the gulf (Zone 1) remaining in Zone 1 (black line) and Zone 2 (red line) vs time in days for the fixed mean depth-integrated velocity field for summer. Slow decline in percentage for particles remaining in Zone 1 (black line) indicates weak connectivity between GSV and IS/BP. Extremely slow decline for Zone 2 (red line) indicates extremely weak gulf-shelf connectivity.

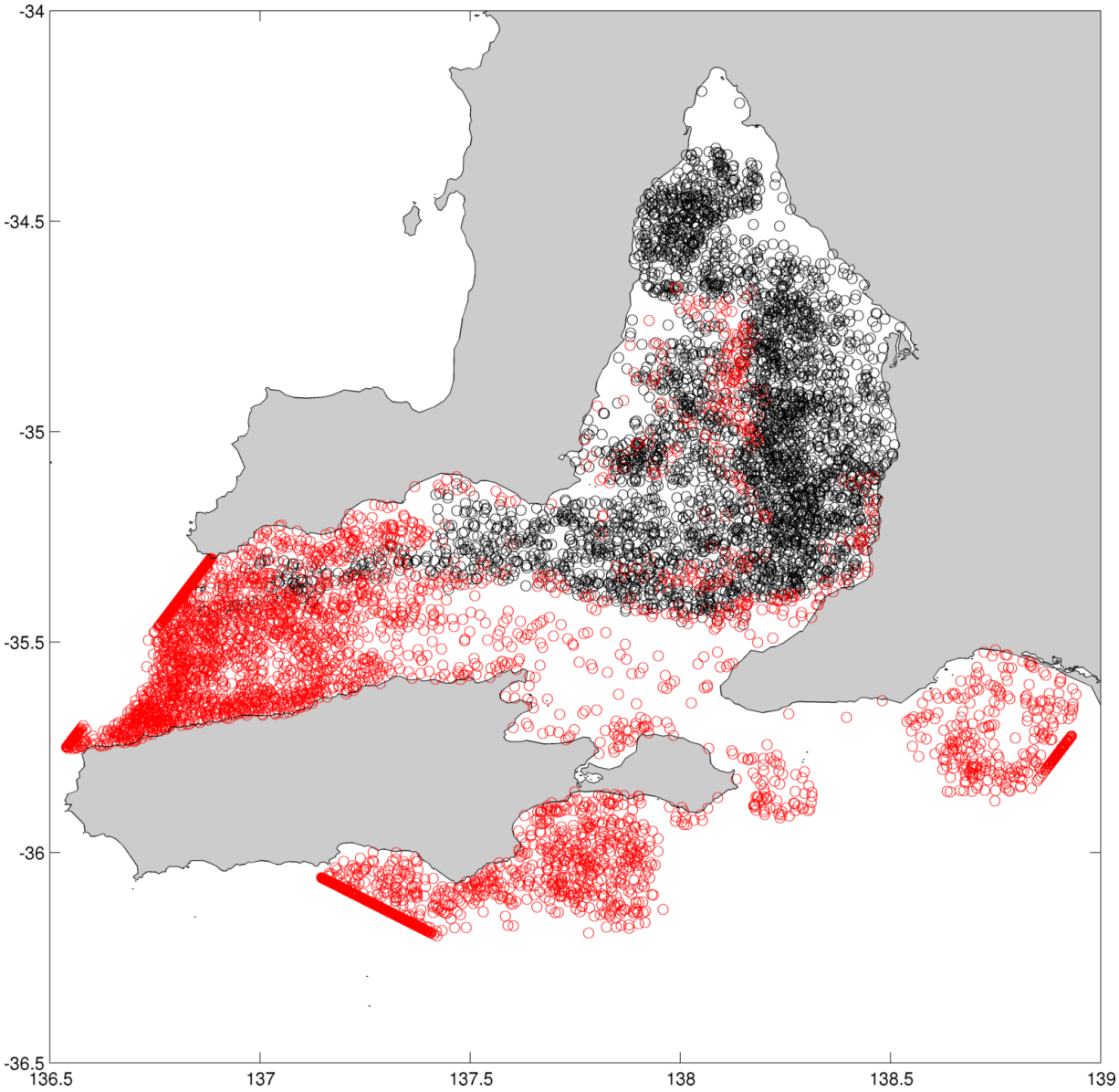

Figure 7.10: Particle distribution for summer using fixed mean depth-integrated velocity (see Figure 7.1) after 60 days of simulation time. A clear front is visible roughly across the mouth of the gulf, keeping intruding shelf waters and gulf waters separate. A weak outflow of gulf particles can be seen in the upper portion of IS. A small number of 'strait' particles can be seen to have made their way in to GSV proper. A high concentration of particles on the open boundary shows particles which have left the domain and become 'stuck' such that they do not re-enter the model.

7.5.1.2 Mean Depth-Integrated Flow: 1st June - 1st September

Taking the mean depth-integrated flow for winter 2011, a particle tracking simulation was run in order to determine the 'typical' connectivity between the interior of the gulf and the shelf via the straits for the winter months. Figure 7.12 shows the percentage of particles with initial position within the gulf (Zone 1) still remaining within Zone 1 (black line) and Zone 2 (red line). The animation shows clear gulf-wide clockwise circulation with an inflow of shelf waters around the heel of Yorke Peninsula and discharge of gulf waters waters on eastern side of mouth and out to shelf via BP.

In contrast to the mean summer flows, there is a clear and steady decline in the concentration of particles for both Zone 1 and Zone 2, indicating that particles which exit the gulf interior will not find their way back in, but rather be discharged to the shelf via BP. A snapshot taken after 60 days simulation (Figure 7.13) shows these features.

7.5.1.3 Summer vs. Winter Results

Gulf - IS/BP connectivity (black line, Figures 7.9 and 7.12) is higher for winter than summer, with ∼82% of gulf particles remaining within the gulf after 90 days simulation for summer and ∼67% for winter. Similarly, gulf - shelf connectivity (red line, Figures 7.9 and 7.12) is much higher for winter than summer, with ∼97% of gulf particles remaining in the system after 90 days simulation for summer and ∼73% for winter. Gulf - shelf connectivity occurs at much greater rate for winter, with first particles beginning to exit the system after 13 days for winter compared with 60 days for summer.

Figure 7.11: Animation displaying the paths and distribution of Lagrangian particles under a fixed, depth-integrated and seaonsally averaged flow field for winter time. Animation Location: Electronic Appendix/LTRANS animations/Seasonal Fixed Winter.avi

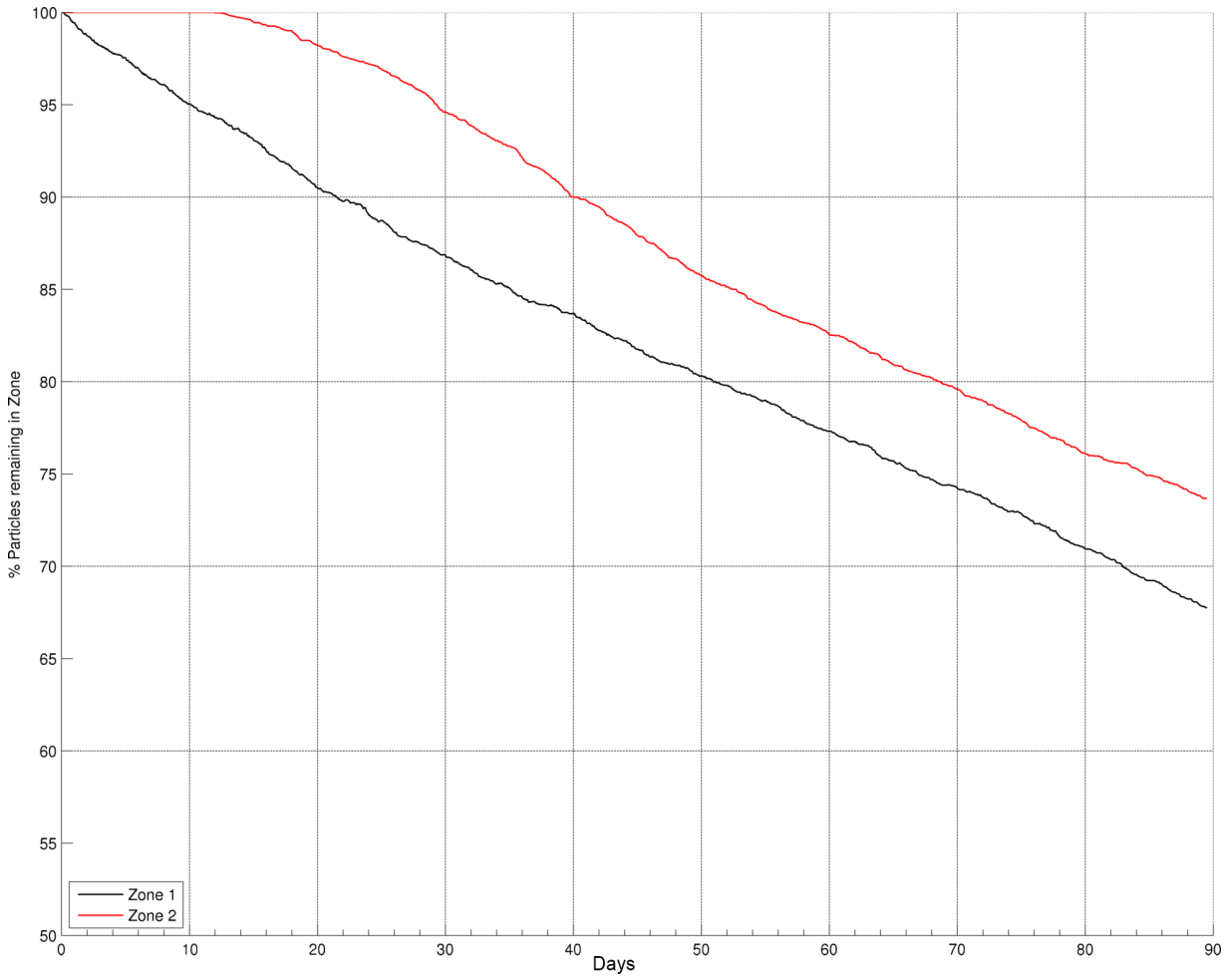

Figure 7.12: Percentage of particles with initial position within the gulf (Zone 1) remaining in Zone 1 (black line) and Zone 2 (red line) vs time in days for fixed winter mean depth-integrated velocity field (see Figure 7.2). Steep decline in percentage for Zone 1 (black line) indicates strong connectivity for GSV and IS/BP. Matching decline for Zone 2 (red line) suggests strong gulf-shelf connectivity.

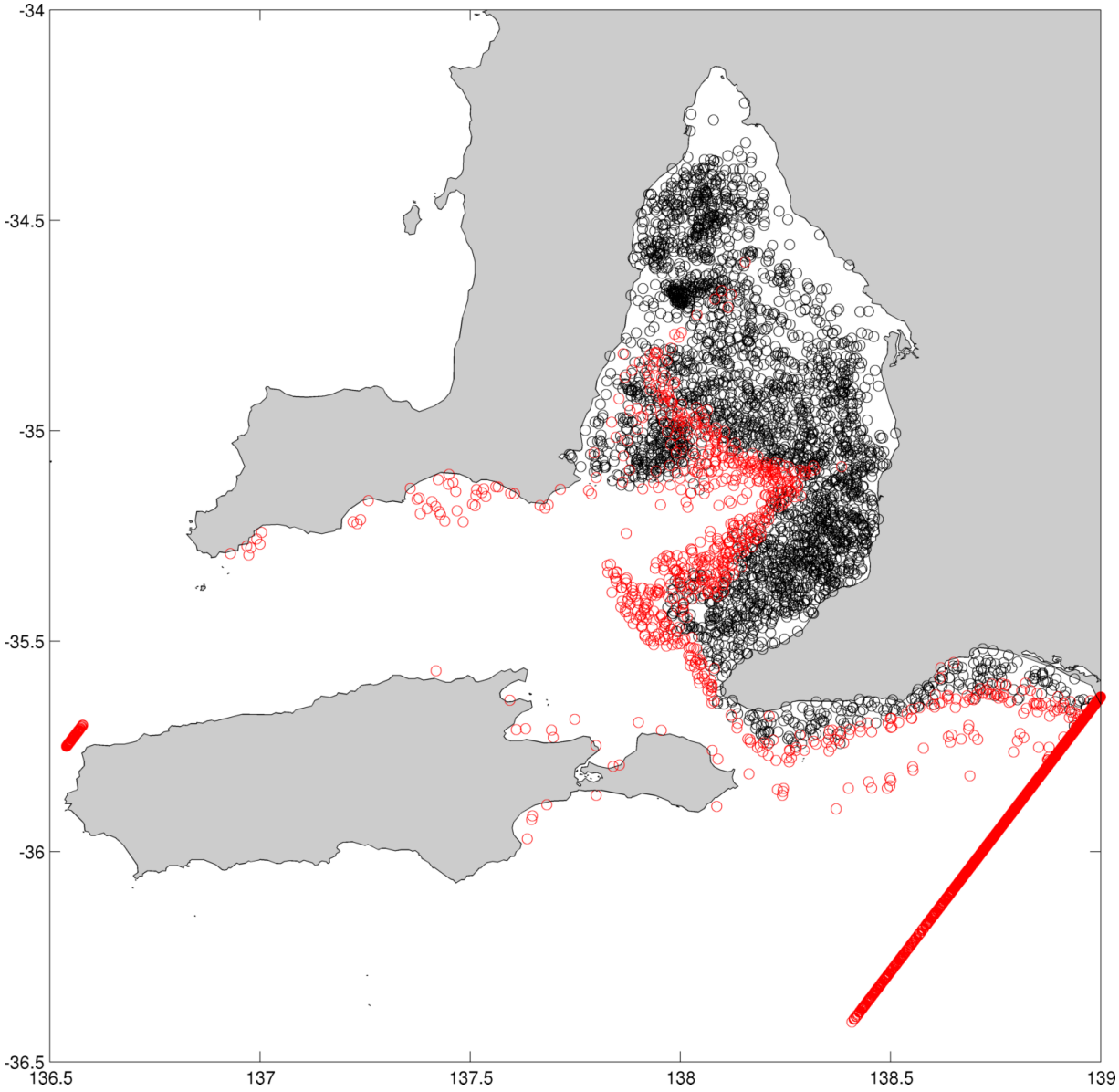

Figure 7.13: Particle distribution for winter using fixed mean depth-integrated velocity (see Figure 7.2) after 60 days of simulation time. Very few particles remain within IS and the southern coast of BP, indicating the strong intrusion and throughflow of shelf waters. A high concentration of particles on the open boundary (especially on the eastern boundary) shows particles which have left the domain and become 'stuck' such that they do not re-enter the model.

7.5.2 Quasi-Realistic 1.5 Daily Mean Velocity Fields

Results of the quasi-realistic GSVM for mean three dimensional velocity fields averaged over 1.5 days were used to drive particle circulation throughout the domain. Using 1.5 daily means filtered out the tidal signal, leaving only weatherband and seasonal frequency flow events. Animations were created from the LTRANS model results and can be found in the electronic appendix (Electronic Appendix/LTRANS animations). As the periods modeled here are the same as used for the seasonal fixed velocity fields in the preceding section, comparisons between the summer and winter weather band results and the seasonal mean flows indicate the importance and effect of individual weather band events have on particle distribution and gulf-shelf connectivity.

The results clearly show that individual weather events, such as passing low pressure fronts and the associated SW winds, have a large impact on flushing particles from the gulf (for example see early July Figure 7.17). The results for 1.5 daily mean currents show significant increase in gulf-shelf connectivity over the seasonal mean velocity fields for both summer and winter (see Figure 7.9, 7.12, 7.15 and 7.17).

This also implies changes in wind speed and direction resultant from climate change have the potential to alter the timing and level of gulf-shelf connectivity. A recent review of 19 climate models (McInnes et al., 2011) preditced mean 10 m wind speeds over GSV for 2081-2100 increase by 5-10 $m.s^{-1}$ over the December-January-February period, and decrease by 0-5 $m.s^{-1}$ for the June-July-August period. This would suggest a reduction in winter time gulf-shelf connectivity, whilst not necessarily increasing summer time connectivity due to the isolating influence of the double-gyre formation.

7.5.2.1 Summer time Particle Distribution

The results of the summer 1.5 daily mean velocity LTRANS model (Figure 7.15) indicate that while approximately 34% of particles released within Zone 1 escape the interior of the gulf after 3 months, only approximately 13% of particles starting within the gulf escape the domain entirely. This suggests that there is limited connectivity between the gulf and IS/BP, but very limited connectivity between the gulf and the shelf.

Significant flushing events occur in early and mid December, driven by winds with strong westerly component. A noteable flushing event of the gulf interior in early January under winds with easterly component also occurs. However, this is not reflected in Zone 2, as these particles re-enter the gulf via the western inflow.

Tellingly, no other major flushing events for the remainder of the period, which is heavily dominated by weak winds with easterly component. The dissimilarity in reduction of particles for Zone 1 and Zone 2 suggests events which may induce gulf - IS/BP connectivity do not act to flush the entire system during summer.

The percentage of particles remaining for Zone 1 and Zone 2 (66% and 87% respectively) is much less for the summer 1.5 daily mean results when compared to the mean summer seasonal velocity (82% and 97% respectively). This discrepancy is largely due to the greater level of eddies and cross-mouth currents which result from the weather band variability in flows (see Animation), which are not present in the fixed seasonal mean velocity field models.

Figure 7.14: Animation displaying the paths and distribution of Lagrangian particles under a depth-integrated one and-a-half day mean flow field for summer time. Animation Location: Electronic Appendix/LTRANS animations/1.5 Daily Mean Summer.avi

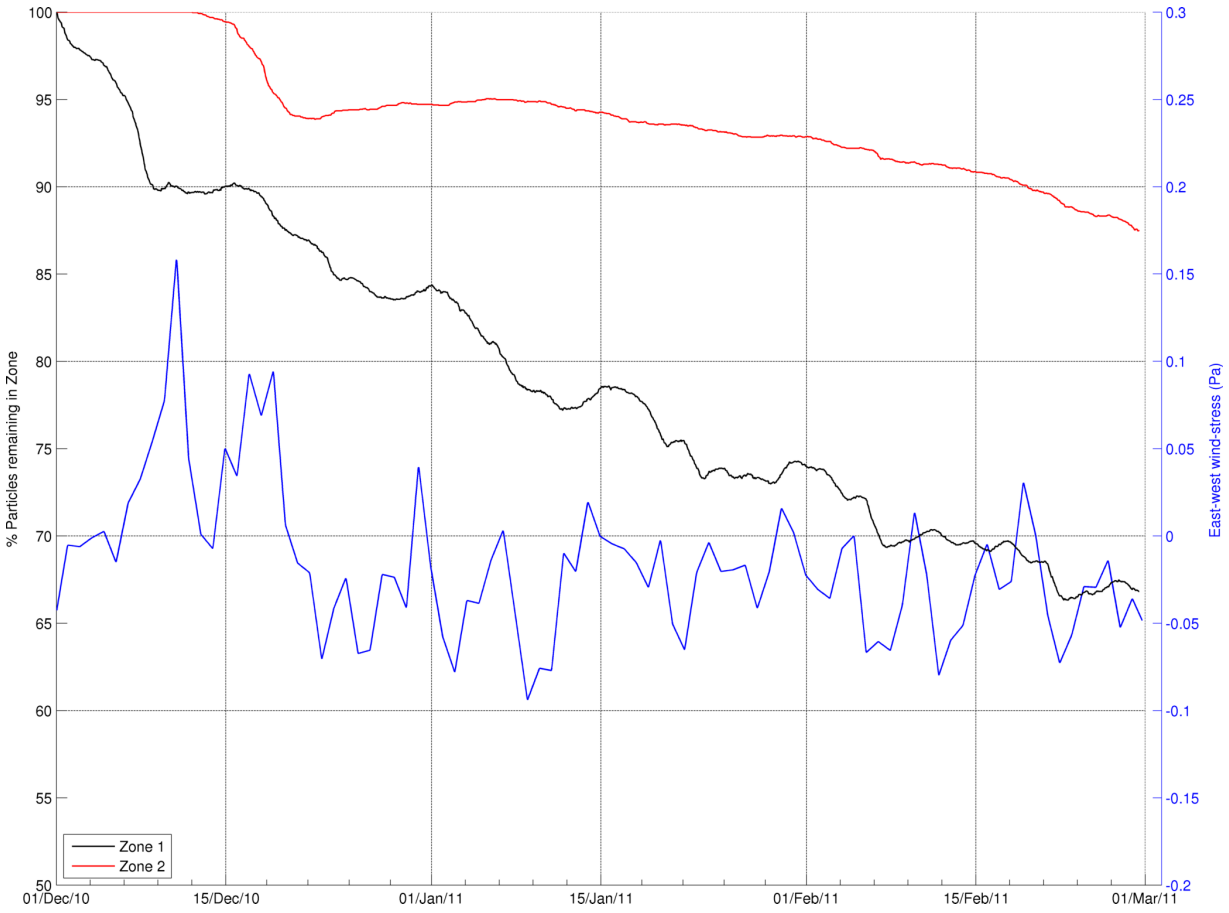

Figure 7.15: Left Axis: Percentage of those particles released within Zone 1 still remaining in: the interior of gulf (Zone 1 - black line) and total model domain (Zone 2 - red line) versus time for summer months. Right Axis: Weatherband filtered wind-stress (Pa) in the east-west direction (blue line). Positive values for wind-stress correspond to westerly winds (positive stress towards the east).

7.5.2.2 Winter time Particle Distribution

Figure 7.17 shows the percentage of particles with initial position within the gulf (Zone 1) which remain within the gulf and the domain as a whole (Zone 2) against the date for the winter period. In contrast to the summer months, there is a steady decline in the number of particles released within the interior of the gulf which remain within both Zone 1 and Zone 2.

Zone 1 and Zone 2 experience defined periods of rapid decline in particle concentration, which correlate for both zones and correspond to strong westerly wind events (e.g. 16th - 19th June and 1st - 5th July). The correlation between flushing of Zone 1 and Zone 2 suggests that westerly wind events which flush the interior of GSV also act to flush the entire system. Periods of little or no reduction in particle concentration correspond to easterly winds (e.g. 9th - 12th August).

Only $\sim$ 50% of particles remain in Zone 1 after 90 days simulation for the winter case, compared with $\sim$ 66% for summer, and $\sim$ 60% remain in Zone 2 for the winter case compared with nearly 90% for summer. This indicates the greatly enhance connectivity for winter compared to summer. The percentage of particles remaining for Zone 1 and Zone 2 (50% and 60% respectively) is much less for the 1.5 daily mean winter results when compared to the mean winter seasonal velocity (66% and 74% respectively),

Figure 7.16: Animation displaying the paths and distribution of Lagrangian particles under a depth-integrated one and-a-half day mean flow field for winter time. Animation Location: Electronic Appendix/LTRANS animations/1.5 Daily Mean Winter.avi

highlighting the importance in high-intensity and short duration events in the flushing of the system.

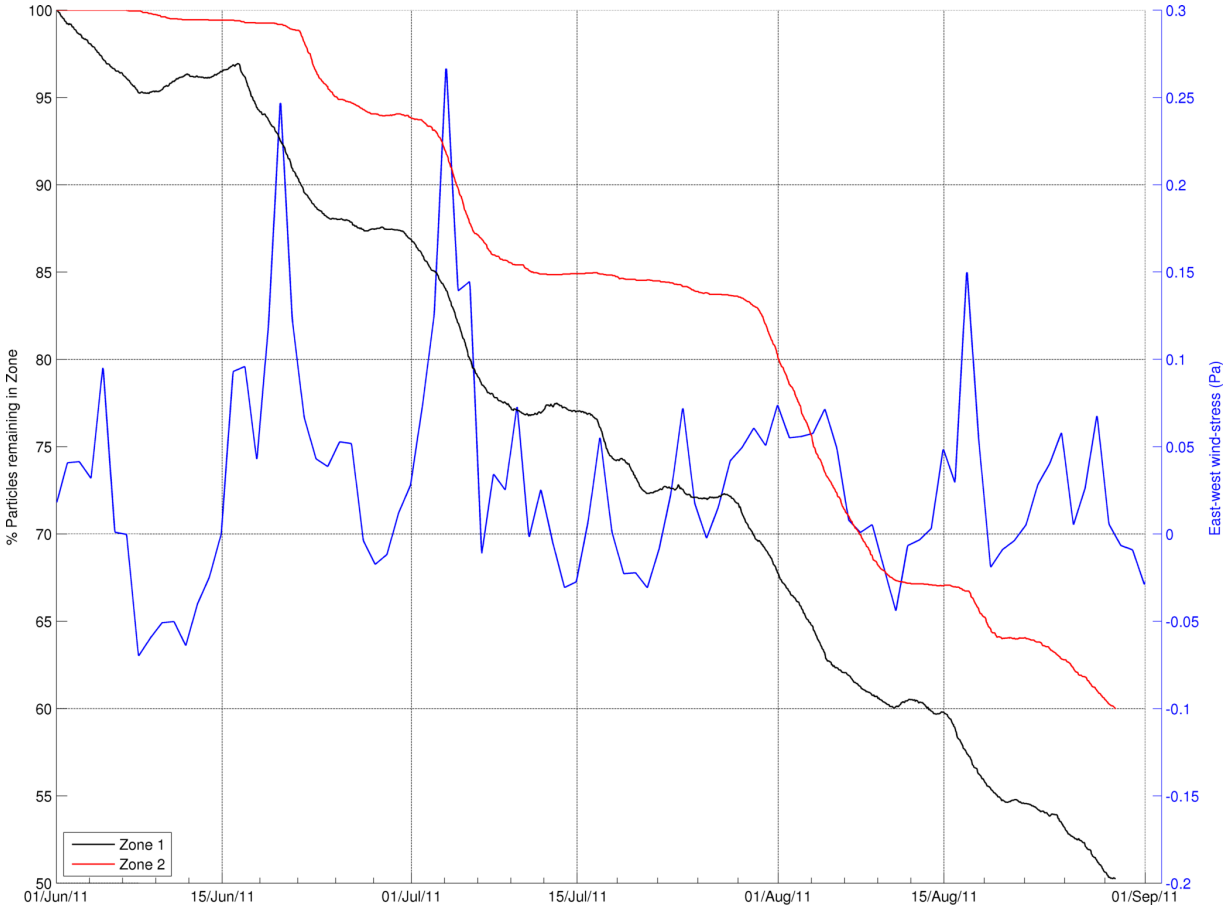

Figure 7.17: Left Axis: Percentage of those particles released within Zone 1 still remaining in: the interior of gulf (Zone 1 - black line) and total model domain (Zone 2 - red line) versus time for winter months. Right Axis: Weatherband filtered wind-stress (Pa) in the east-west direction. Positive values for correspond to westerly winds (positive stress towards the east). Strong correlation between winds with westerly component and flushing events for both Zones 1 and 2 is seen.

Chapter 8

Conclusions and Recommendations for Future Work

New understanding of the hydrodynamics of GSV has been attained through the use of a number of three-dimensional numerical models. The importance of individual processes such as tides, winds and thermohaline circulation were all investigated by using idealised models which study them in isolation. A quasi-realistic model for the 2010-2011 calendar years was run, the results of which were interrogated using the greater understanding gained through the idealised models to elucidate the truly important processes and their role in the hydrodynamics of GSV. Particular attention was paid to the role of these processes in creating or preventing connectivity of the gulf interior to the shelf via IS and BP.

The hydrodynamics of the quasi-realistic model were further probed through the calculation of flushing timescales, the creation of passive Lagrangian float experiments and the creation of idealised models to help identify the importance of local forcing compared with advection for several locations throughout the gulf.

8.1 Key Findings

8.1.1 Tidal Circulation

A critical part of accurately reproducing the hydrodynamics of a highly tidal coastal environment, the calibration of coefficient of drag, responded extremely well to dependence upon depth and the presence of seagrass meadows. This method of estimating coefficient of drag has not previously been used for GSV, and model results showed extremely favourable reproduction in sea level predictions when compared with a traditional uniform coefficient of drag distribution. This also suggests that variation in the distribution of seagrass meadows could have implications for the tidal propagation and general greater circulation of the gulf, in addition to the well known disastrous implications for marine life (Fox et al., 2005; Bryars et al., 2008).

The approach used within the tidal model used in this thesis was rather blunt. Further studies could use optimised sensitivity studies which alter bottom friction in order to reduce errors in tidal phase, amplitude and predicted sea level. The results of this optimisation could then be compared with benthic type distribution in order to gauge the true importance of bottom type on coefficient of drag.

This finding could also be important in other shallow gulfs with large seagrass meadows, especially in regards to changing seagrass distributions due to anthropogenic influences and climate change.

8.1.2 Wind-stresses: The Dominant Force in Subtidal Circulation of GSV

Results of the modeling within this thesis show that wind forcing plays a much greater role in circulation and flushing than what has been found for SG, which was long considered a larger scale version of GSV. The modeling indicates that the response of circulation throughout the gulf, IS and BP is extremely sensitive to the east-west component of wind-stresses, with easterly winds generally reducing connectivity of the gulf and westerlies enhancing connectivity. The apparent temperature and salinity front which forms near the mouth of the gulf during summer is not so much a primary cause of reduced connectivity, but rather a symptom of the circulation pattern formed by the prevailing south-easterly summer winds which drive less saline and relatively cool water in to the system through BP. In this way GSV is quite distinct from SG, whose temperature front formation is the primary cause of the disconnect between SG and the shelf during summer. Conversely, the prevailing south-westerly and north-westerly winds during winter enhance connectivity between the shelf and gulf by driving a clockwise circulation throughout the gulf.

Critical to all wind driven flows are the pathways of Investigator Strait and Backstairs Passage, formed by the presence of KI. Because these passageways constrict flows, they generally force all flows through the area to conform to a single direction. This is especially true for BP, which is so narrow it only really allows flow in a single direction at a time. The system is therefore at the mercy of the prevailing direction of flow through BP and IS, with westward flow being constrained to the north coast of KI due to the Coriolis force and eastward flows able to enter the gulf around the heel of Yorke Peninsula, again due to the Coriolis force. So under easterly winds inducing westward flow, the gulf interior is largely isolated from the through flow of BP and IS. This is potentially an important finding for other partially obstructed or enclosed gulfs, whos circulation could be heavily influenced by wind-stresses and the changes in hydrodynamics caused by the gulf-shelf obstruction.

8.1.3 The Temperature Front: A False Flag

The results of modeling within this thesis showed that the temperature front which appears to form each summer through the central portion of IS and across the western boundary may not play as large a role as previously thought in dictating connectivity of the gulf. Instead, it is a symptom of the wind driven circulation, which is the primary determinant in connectivity between the gulf and shelf. Thermohaline climate was shown to play a small role in the circulation of the gulf by adjusting the circulation through the enhancement of pressure gradients when density gradients were strong. However, these density gradients are rarely strong during the summer months, hence circulation is almost entirely reliant upon wind-stresses.

During winter these density gradients are stronger, however unlike SG where strong density gradients cause a 'breaking of the dam' type effect, in GSV they merely act to enhance the clockwise circulation largely driven by winds with westerly component. The density gradients are not strong enough in isolation to cause outflow from the gulf if the wind-stresses are unfavourable. This is again largely due to BP, which under westerly winds provides a path of escape for gulf waters, but under easterly winds creates the formation of a strong westward flow, isolating dense gulf waters which become trapped in the deep central basin until favourable wind conditions reemerge.

8.2 Limitations and Future Work

As with all numerical modeling projects, some concessions were made for the models within this thesis due to time restraints and data limitations. These present not only limitations on the work undertaken within this thesis, but also as avenues for future research and discovery.

8.2.1 Flood Modeling

The first of the modeling limitations is the lack of flood modeling. The result of this is the prescription of a minimum depth in order to prevent model instability, which obviously requires intentionally misrepresenting the near-shore topography. This is especially true for the far northern reaches of GSV, which are typically very shallow and tidal. This limitation was chosen due to the extremely computationally expensive nature of flood modeling, which would increase model run times for a single year simulation from a few days to several weeks. In the future when more computational power is made available, incorporating flood modeling will tell us how much effect, if any, tidal flooding has on both the near-shore environment and the circulation of the gulf as a whole.

8.2.2 Domain Extents

The placement of the western boundary for the GSVM is currently within a area of high complexity. Due to the high resolution nature of the GSVM, and the resultant lengthy model run times, the domain had to be constrained in this area. Given more time or more powerful computers to run the models, it would have been preferable to include SG in the domain in order to gain better understanding of the connectivity of the two gulfs. Increasing the extents of the model to also incorporate SG and choosing open boundaries further south of KI would allow greater understanding of how SG and flows around the south coast of KI impact on the circulation of GSV itself.

8.2.3 Additional Connectivity and Flushing Studies

Using the fully forced quasi-realistic model at a much higher temporal resolution (~1hr) to include the tidal influence would allow the calculation of flushing timescales, residence, water age and e-folding times as accurately as possible. This is however extremely computationally expensive, hence the exclusion from this study. Additional Langrangian float studies could be undertaken to explore the inter-gulf connectivity of separate zones of the gulf, as well as their gulf-shelf connectivity.

8.2.4 Further Data Collection and Model Validation

The data limitations in terms of model validation were perhaps the most constrictive. This is due to the high cost and effort involved in data collection for oceanographic purposes. As a result, little long term data was available within the model domain, with the vast majority being available for a single point at Pt. Stanvac. It would be advantageous to gather data simultaneously from multiple points within the model domain in order to have much better spatial coverage for validation data in order to ensure the system wide circulation and conditions are well resolved. As a only a single point of long-term data was available, a measure of doubt is cast over the model. Simultaneous collection of data for several locations throughout the gulf would give far better confidence in the model, or shed light upon those areas where it needs improvement.

Appendix A

Additional Tidal Modeling Results

The results for sea level predictions over a period of one month for all considered tidal gauge locations are presented and compared with sea level predictions based on the ANTT tide gauge observations. Predictions for both the GSVM and ANTT are based on the 9 tidal constituents used in modeling (M_2, S_2,K_2, N_2, K_1, O_1, Q_1, P_1 and M_4).

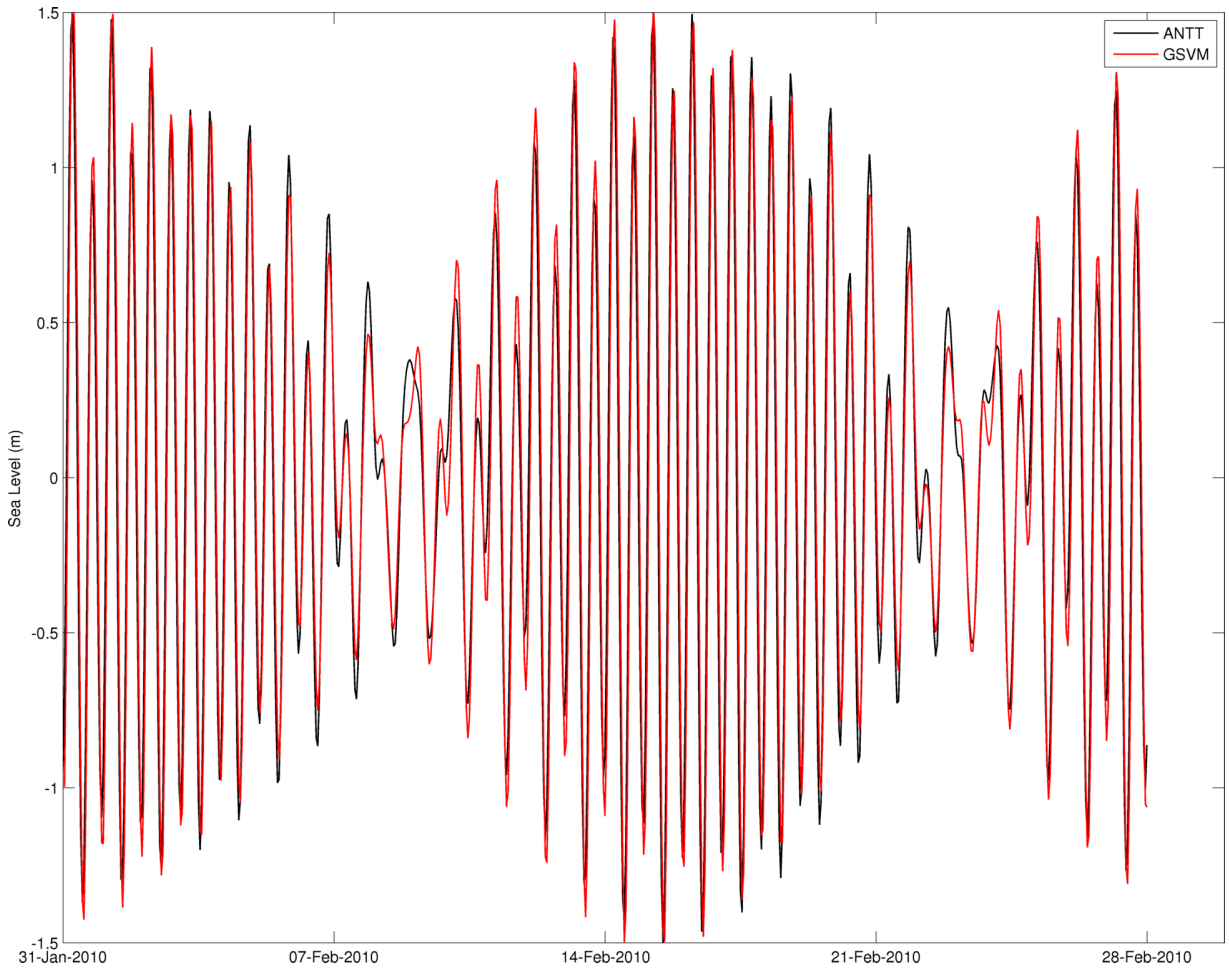

Figure A.1: Sea level predictions for GSVM tidal model versus ANTT predictions for Ardrossan

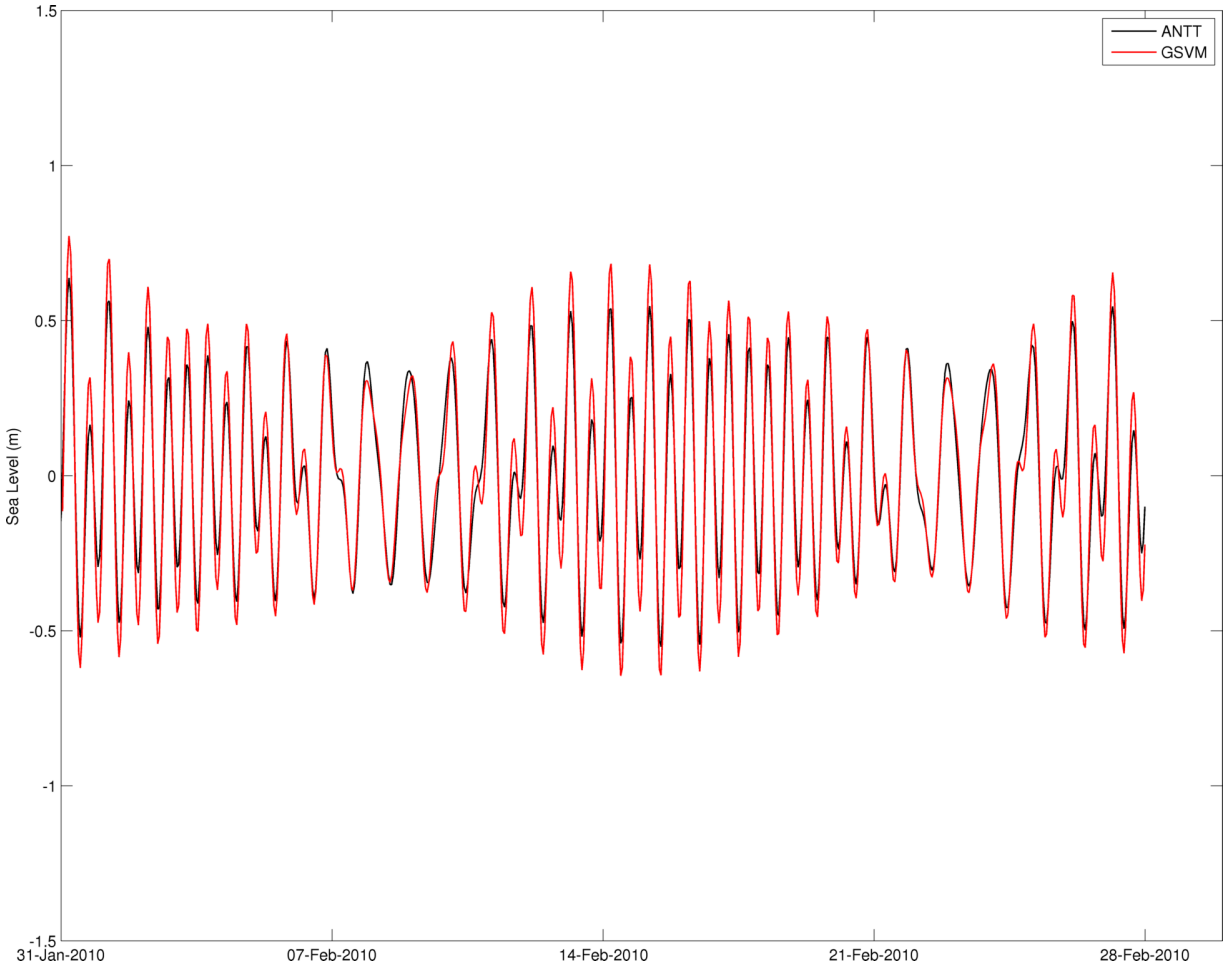

Figure A.2: Sea level predictions for GSVM tidal model versus ANTT predictions for Cape Jervis

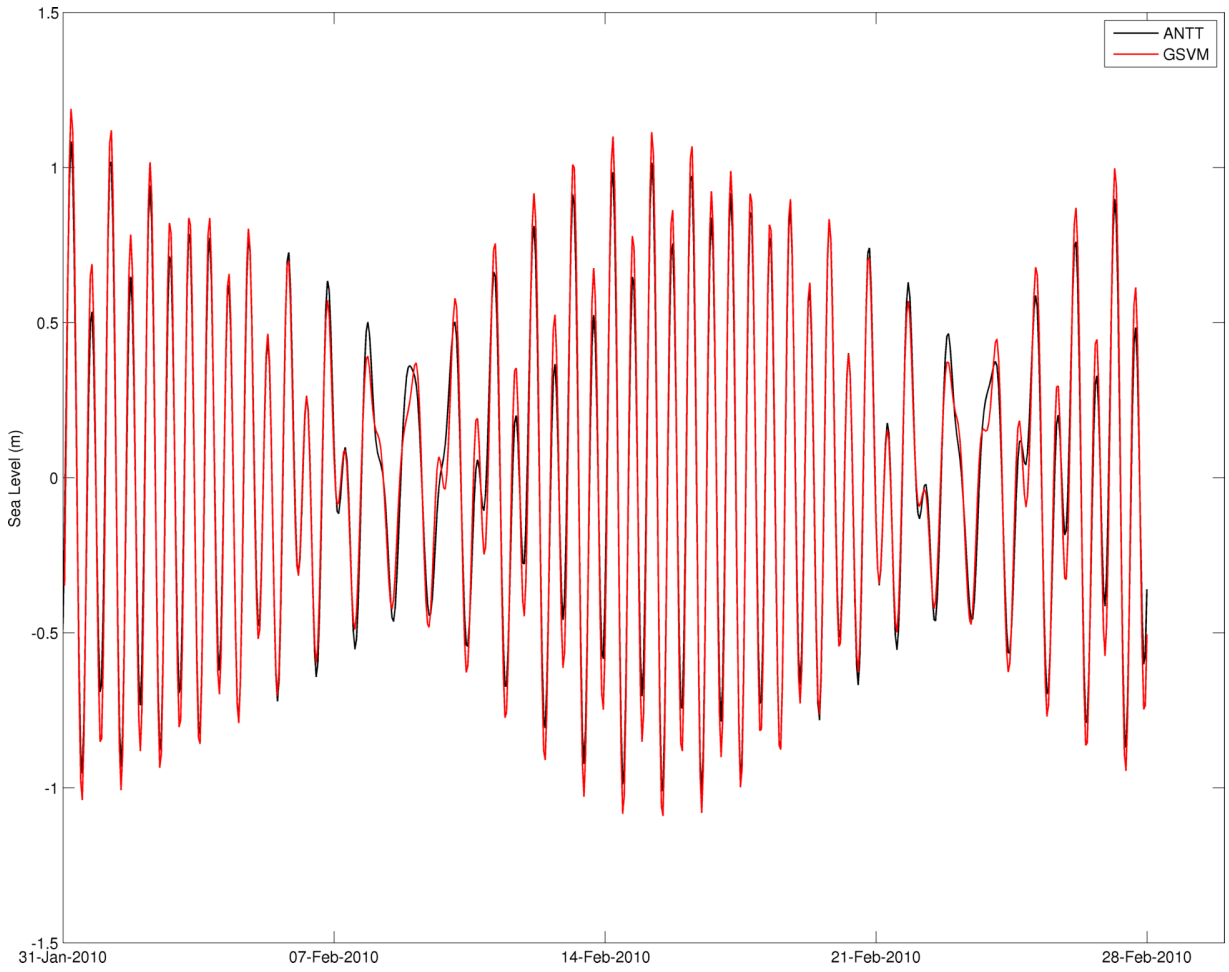

Figure A.3: Sea level predictions for GSVM tidal model versus ANTT predictions for Edithburgh

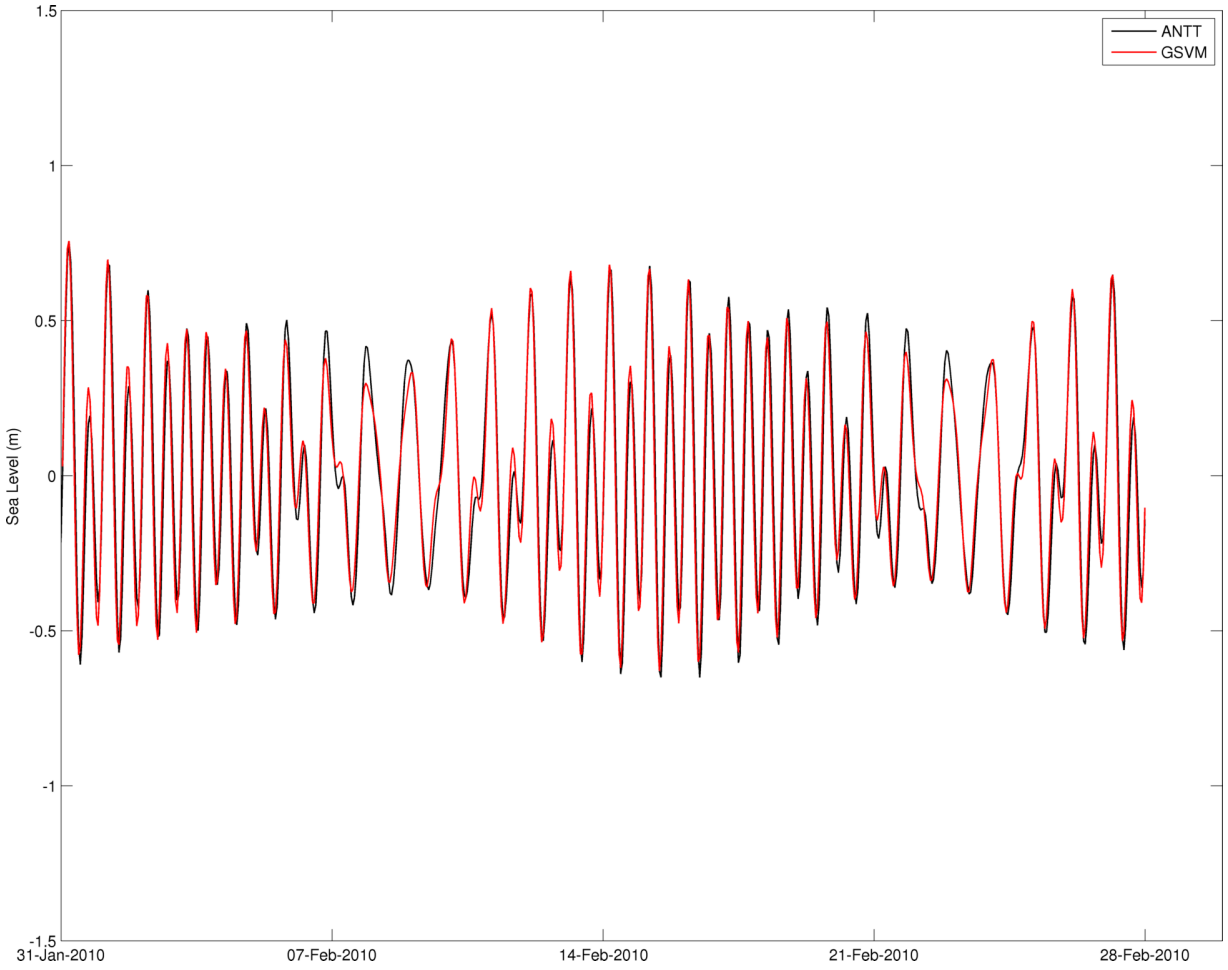

Figure A.4: Sea level predictions for GSVM tidal model versus ANTT predictions for Kingscote

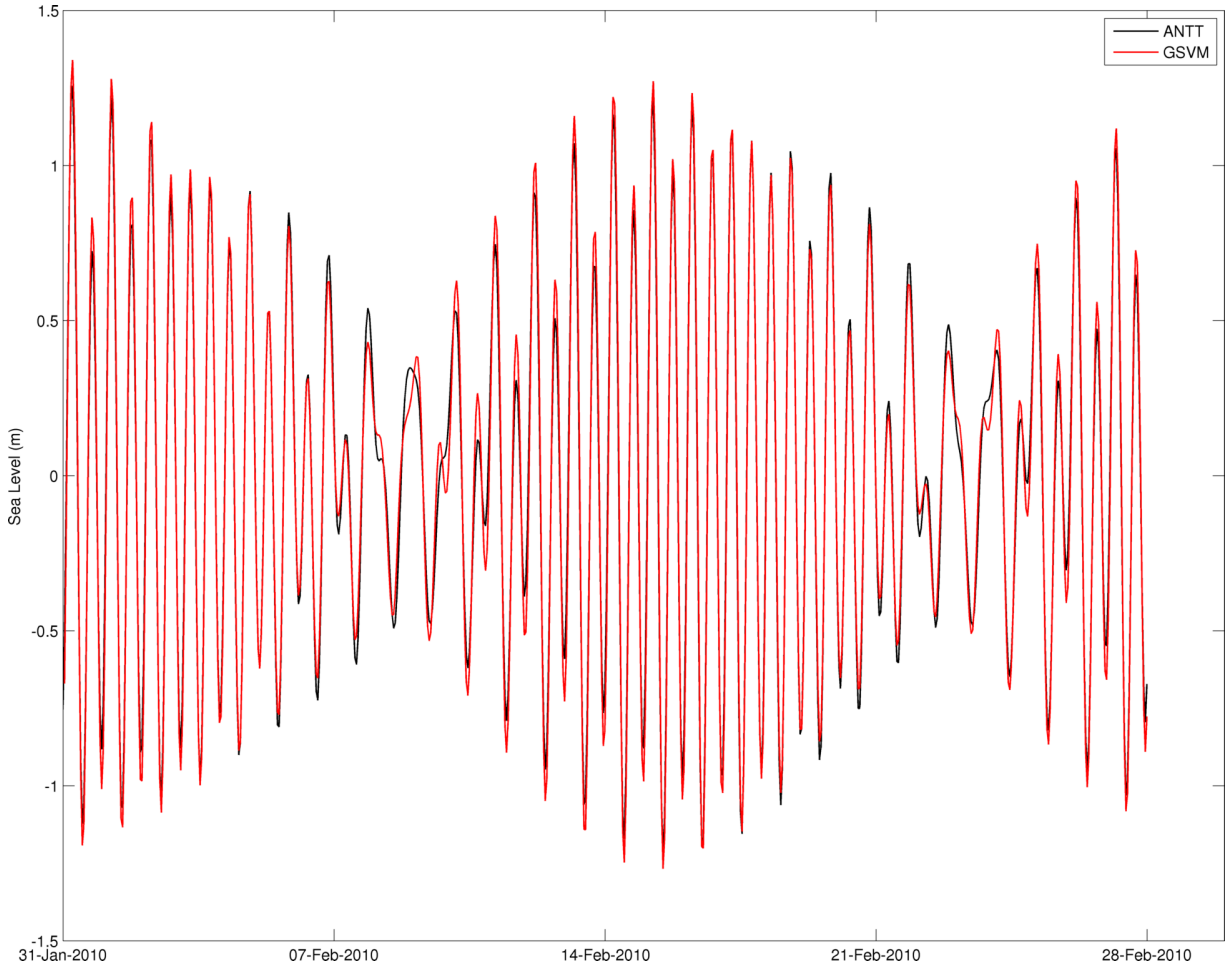

Figure A.5: Sea level predictions for GSVM tidal model versus ANTT predictions for Outer Harbour

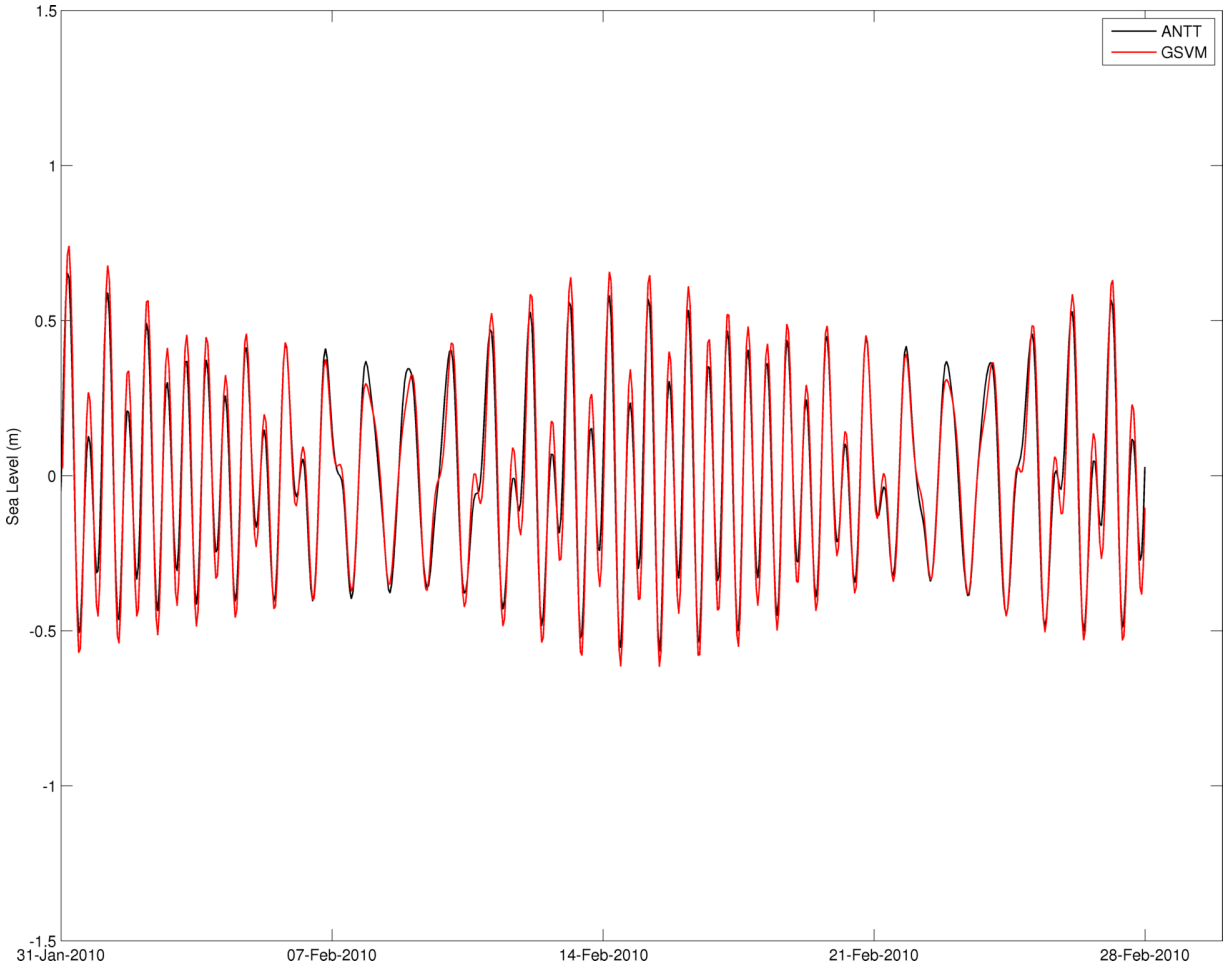

Figure A.6: Sea level predictions for GSVM tidal model versus ANTT predictions for Peneshaw

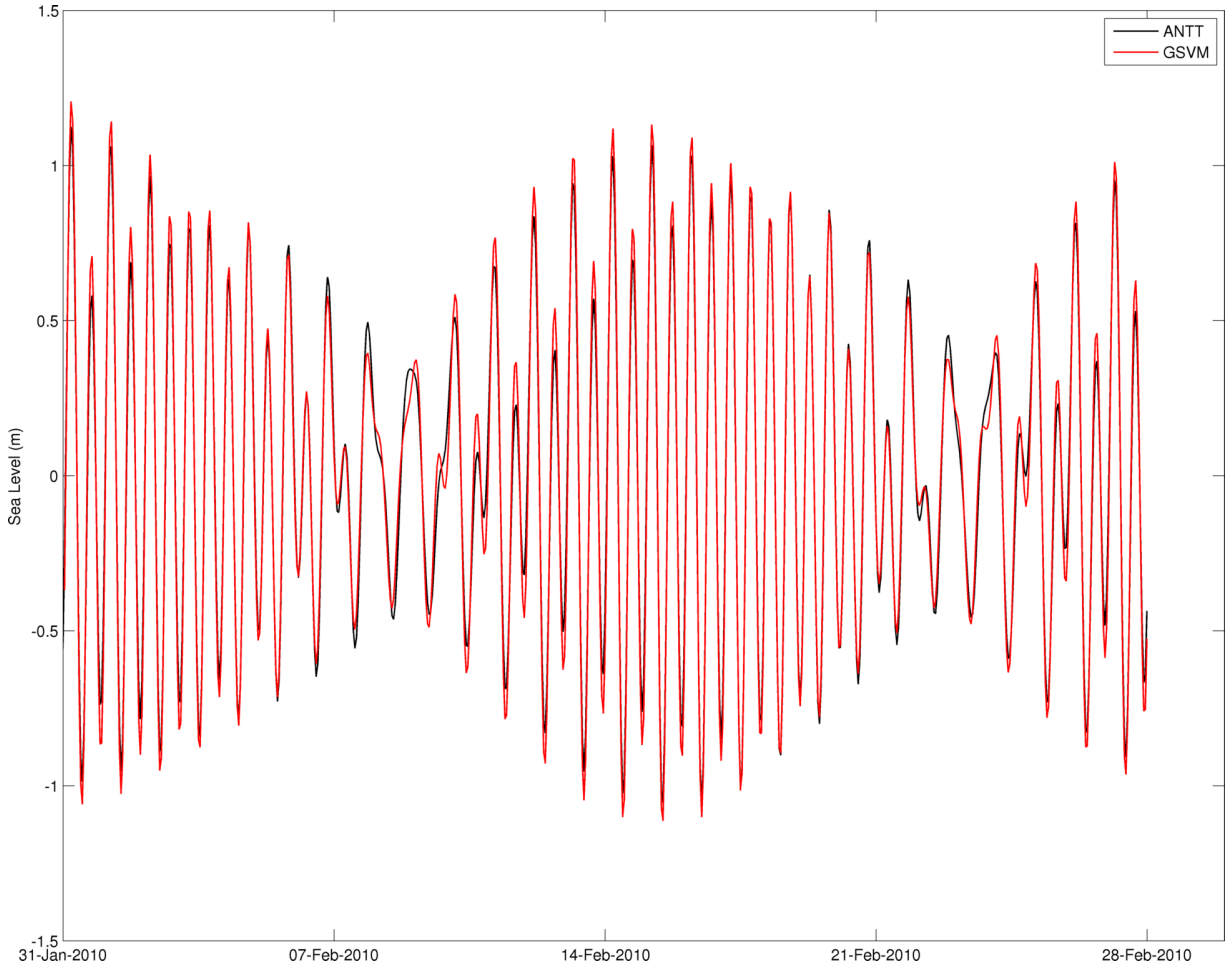

Figure A.7: Sea level predictions for GSVM tidal model versus ANTT predictions for Port Giles

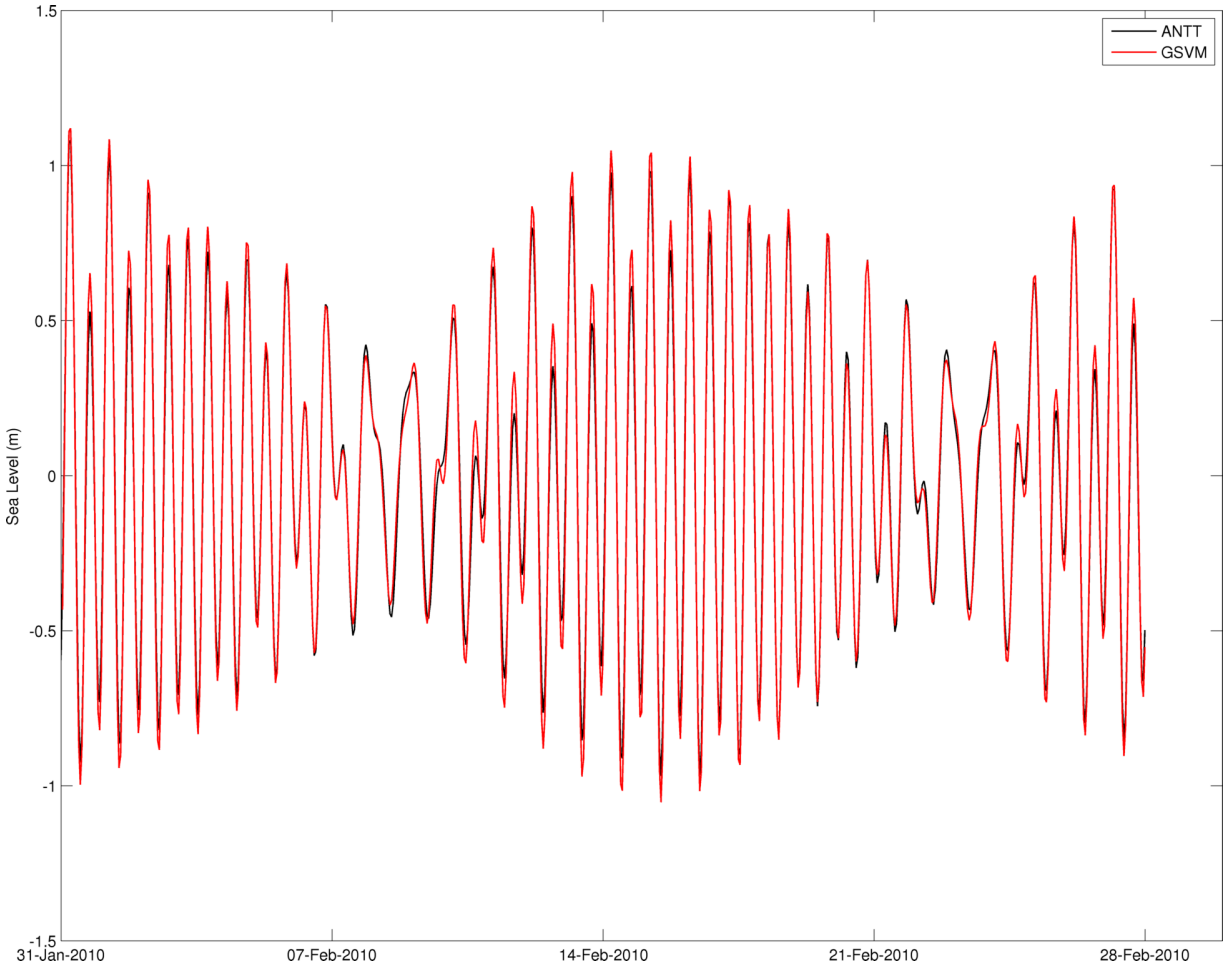

Figure A.8: Sea level predictions for GSVM tidal model versus ANTT predictions for Port Noarlunga

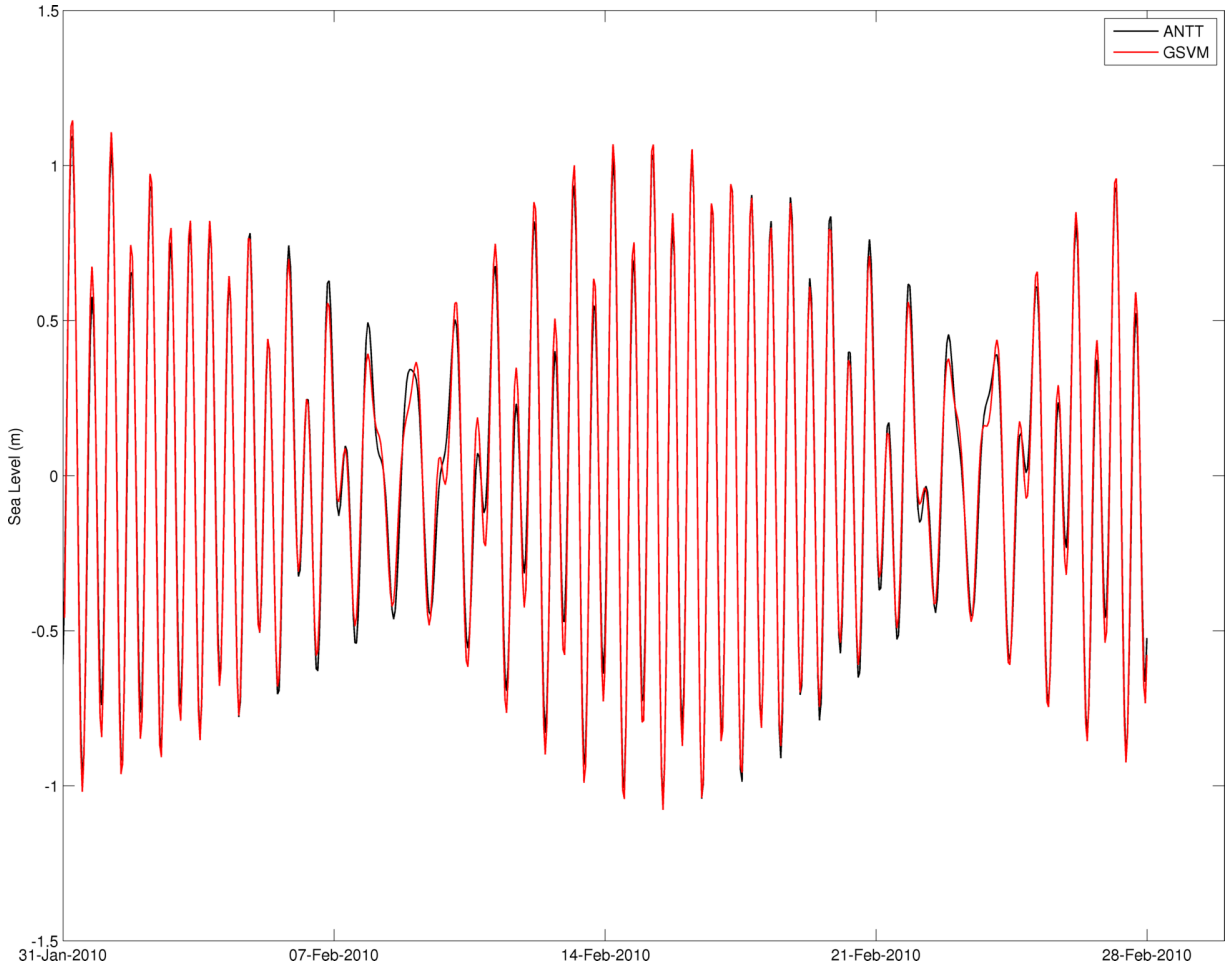

Figure A.9: Sea level predictions for GSVM tidal model versus ANTT predictions for Pt. Stanvac

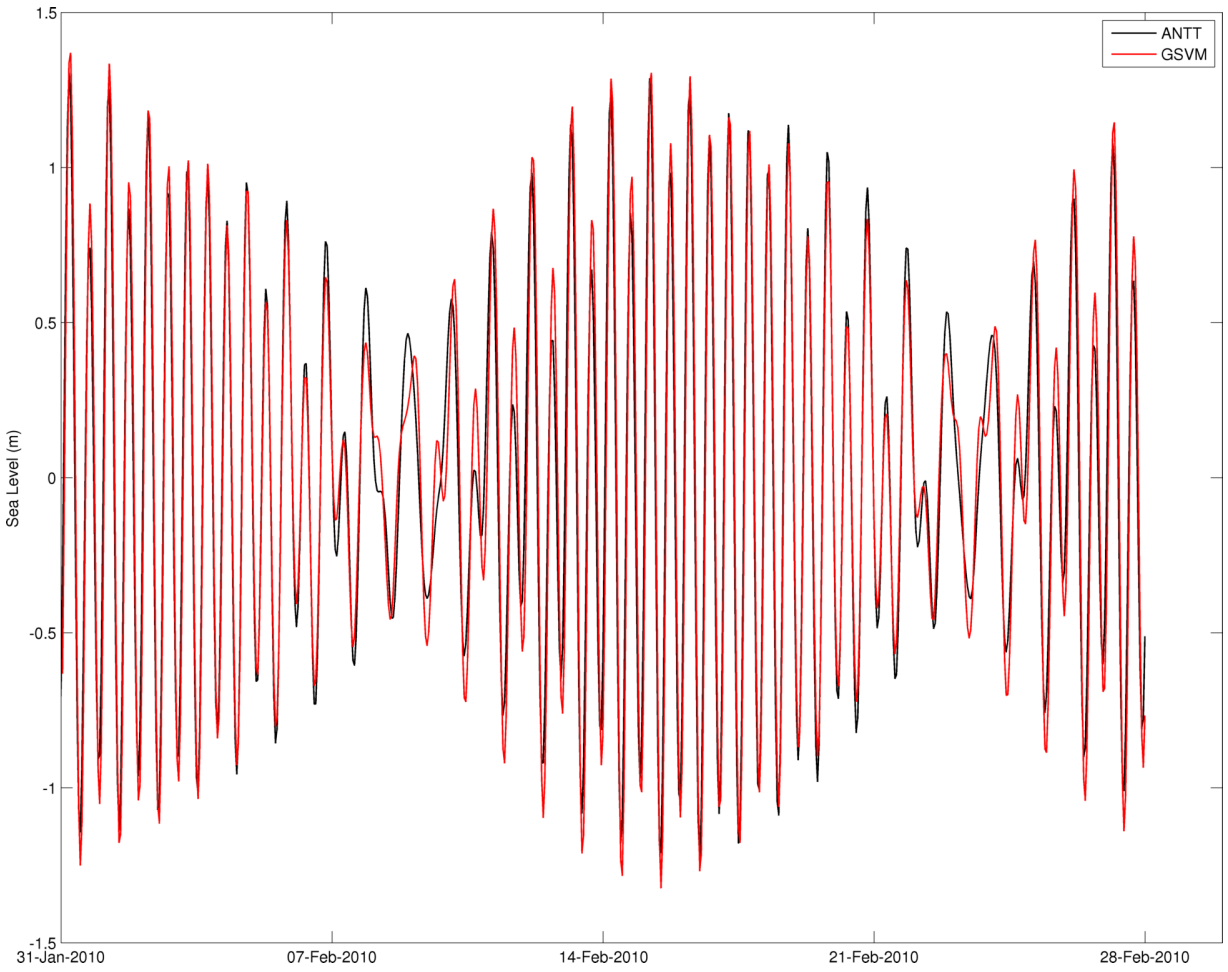

Figure A.10: Sea level predictions for GSVM tidal model versus ANTT predictions for Port Vincent

Appendix B

Additional Wind Modeling Results

B.1 Additional Barotropic Experiments

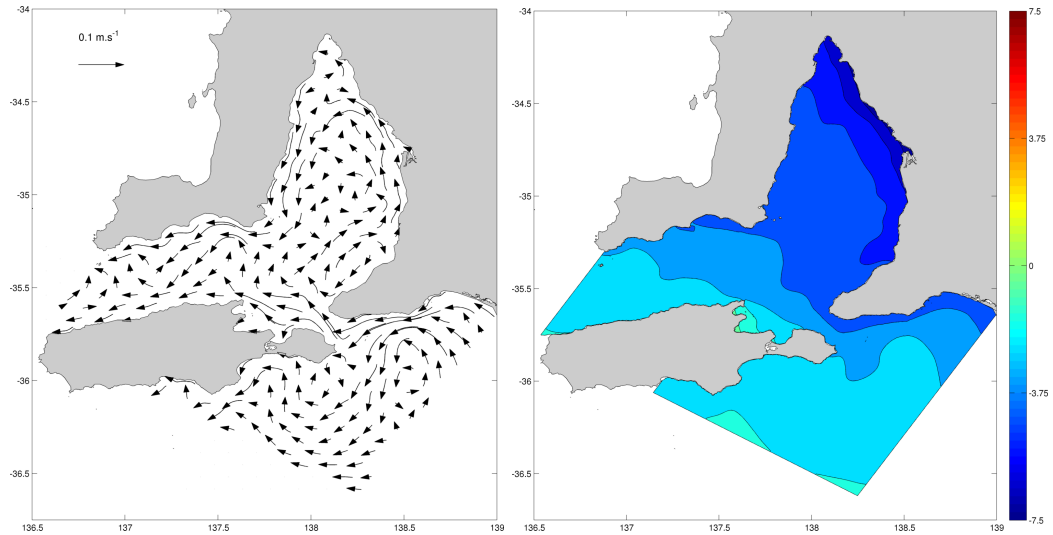

(a) (b)

Figure B.1: Velocity field (a) and sea level (b) for idealised barotropic wind model under NE wind with 0.05 Pa stress. Results indicate a counterclockwise gulf-wide gyre with enhanced connectivity compared to SE flow patterns. The Myponga Eddy is strengthened, leading to recirculation of waters in this region.

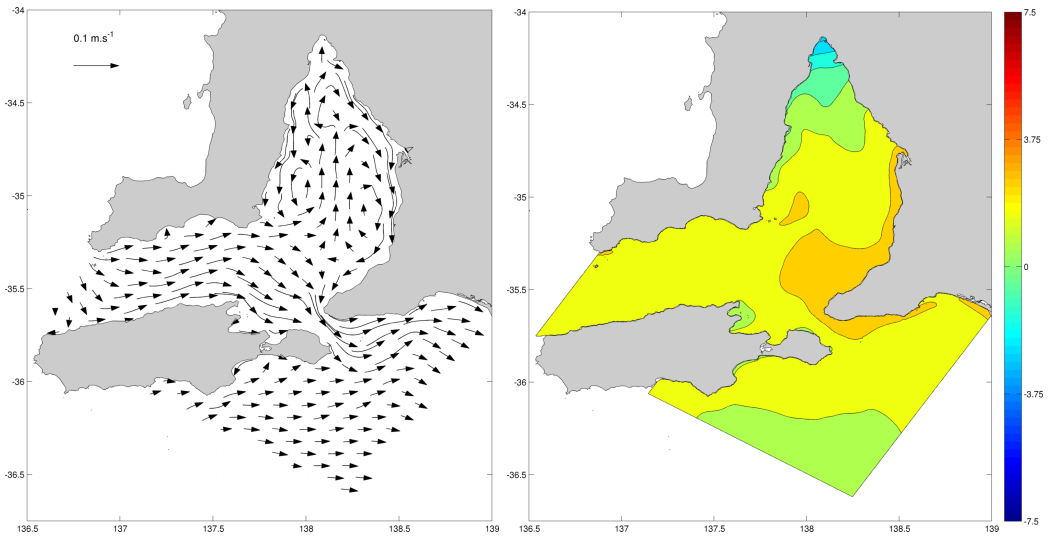

(a) (b)

Figure B.2: Velocity field (a) and sea level (b) for idealised barotropic wind model under NW wind with 0.05 Pa stress. Results indicate a 'reverse double-gyre' system, in which a northward flow is formed in the central portion of the gulf, fed by shelf waters entering via IS. Waters on the west coast show significant recirculation, whilst on the east coast a strong discharge from the gulf via BP is shown.

B.2 Baroclinic Experiments

Wind-stress experiments were repeated with baroclinic conditions represented by the stratification profile shown in Figure B.3, indicating the presence of denser waters beneath a fresher and warmer mixed surface layer. A stratification was adopted with a transition occurring between 5 and 15 meters depth, as the depth of the gulf is in general very shallow.

Baroclinic models were initialised with the stratification profile applied uniformly across the model domain and circulation patterns were developed with the same wind forcing stresses as in the barotropic cases. Boundary conditions for sea level and two-dimnesional momentum were once again imposed by results of the SAROM model under the same wind-stress conditions. Due to the low run times of the models, no temperature or salinity values were imposed at the open boundaries, instead radiation conditions were applied to the tracers.

Differences between the barotropic and baroclinic cases were investigated by examining the differences between sea level and velocity fields for the same timestep within each model. As the barotropic and baroclinic models are run under the same wind-stress and boundary condition regimes, any differences are attributed to the presences of stratification and the density variations this creates.

The inclusion of stratification in the wind forced models generally resulted in the amplification of circulation patterns seen in the barotropic cases. Some minor differences in circulation and connectivity were observed, but the over-arching major patterns remained consistent with what was observed under the barotropic cases.

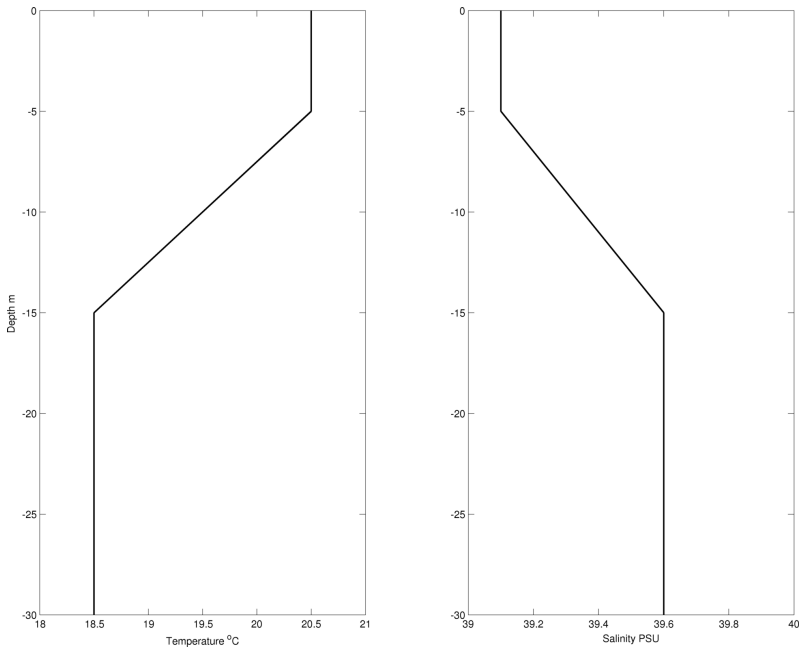

Figure B.3: Water column profiles for temperature and salinity used in baroclinic wind-stress model initialisation

B.2.1 Up-Gulf Wind-Stress

For the up-gulf wind-stress under barotropic conditions the resulting circulation acts to enhance connectivity between GSV and the shelf via the intrusion of shelf waters via the north coast of IS. This is important, as the south-westerly winds are most likely to occur during the cooler months when stratification is expected to be strongest.

When stratification is introduced the central southward flow velocity is increased marginally due to the enhanced pressure gradient force resultant from the density differential, which results in a slightly stronger northward inflow on the western coast of GSV (see Figure B.5).

Westward flow through IS is increased under the baroclinic case, as is the westward flow exiting the system via BP. This is slightly encouraged by the stronger central outflow from GSV. A slight intensification of the Myponga Eddy on the north shore of Cape Jervis is observed when compared to the baroclinic case.

Comparing the barotropic (Figure 4.7) and baroclinic (Figure B.5) cases it can be seen that the over arching circulation structure is mostly unchanged. The sea level state (shown in Figure B.4) shows a stronger sea level gradient under the stratified case than the barotropic, which explains the strengthened central southward flow. The general configuration matches that of the barotropic case, with water piling up in the north-east of the gulf. A region of relatively lower sea level develops around the tip of Cape Jervis, which is likely the cause of the intensification of the Myponga Eddy when compared to the barotropic case..

Comparing the solutions to the force balance equations for the baroclinic case (Figure B.6) with those of the barotropic case the same basic structure is observed. The key differences are in the strengthening of the pressure force in some regions due to the density differentials introduced by the stratification of the water column. These increases in pressure force are counter acted by increases in the Coriolis force,

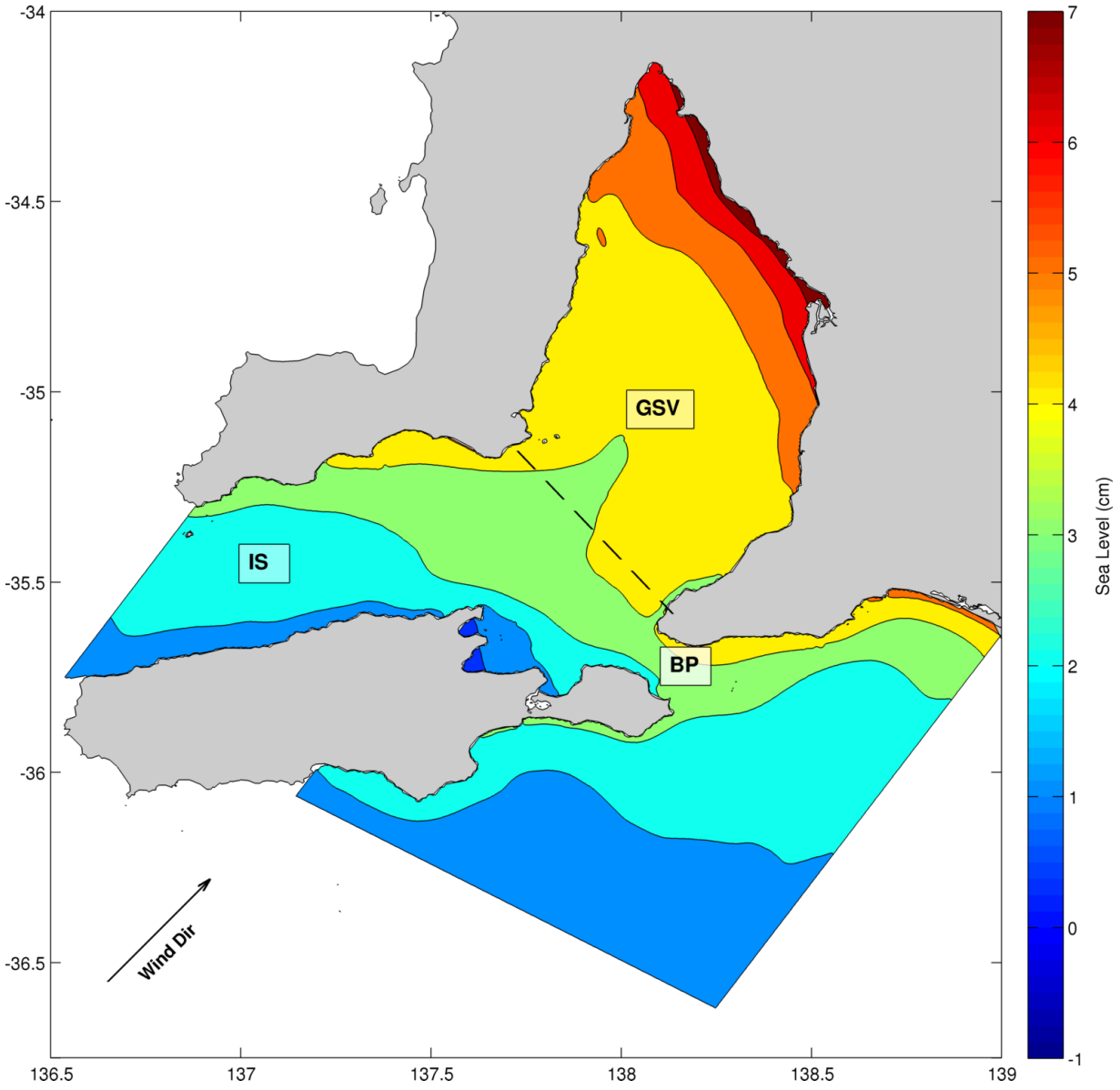

Figure B.4: Sea level for south-westerly along-gulf wind-stress (wind-stress maximum positive = 0.05Pa) and stratified water column. Units cm deviation from mean. Contour interval 1.5 cm. With the introduction of stratification the sea level set up on the north eastern coast is stronger when compared to barotropic case.

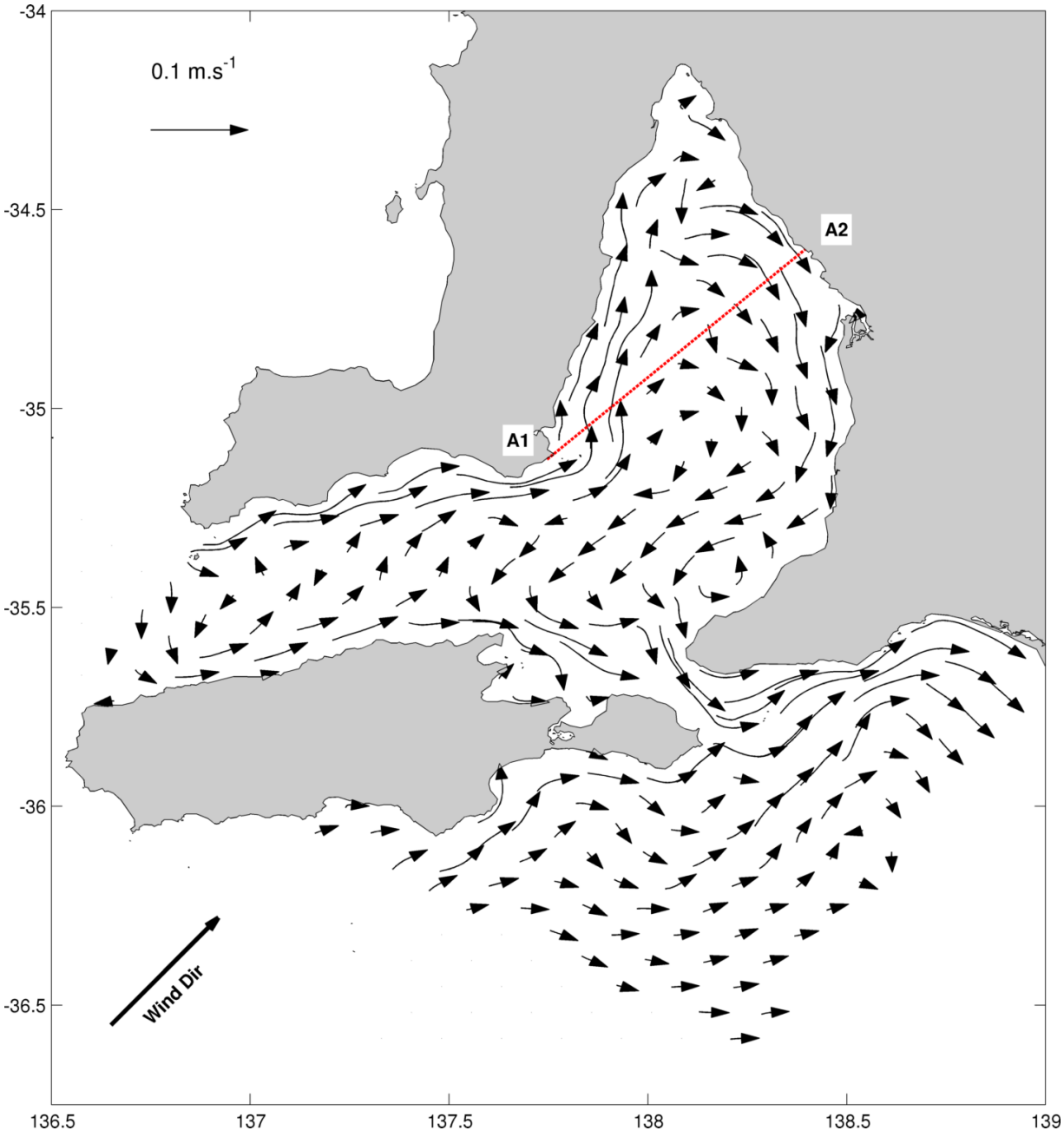

Figure B.5: Flow velocity for south-westerly wind at maximum strength (0.05 Pa) and stratified water column. Legend arrow indicates flow velocity of 10 cm s^{-1}. The circulation pattern for the baroclinic case shares the same structure as the barotropic case, however exhibits an increase in intensity.

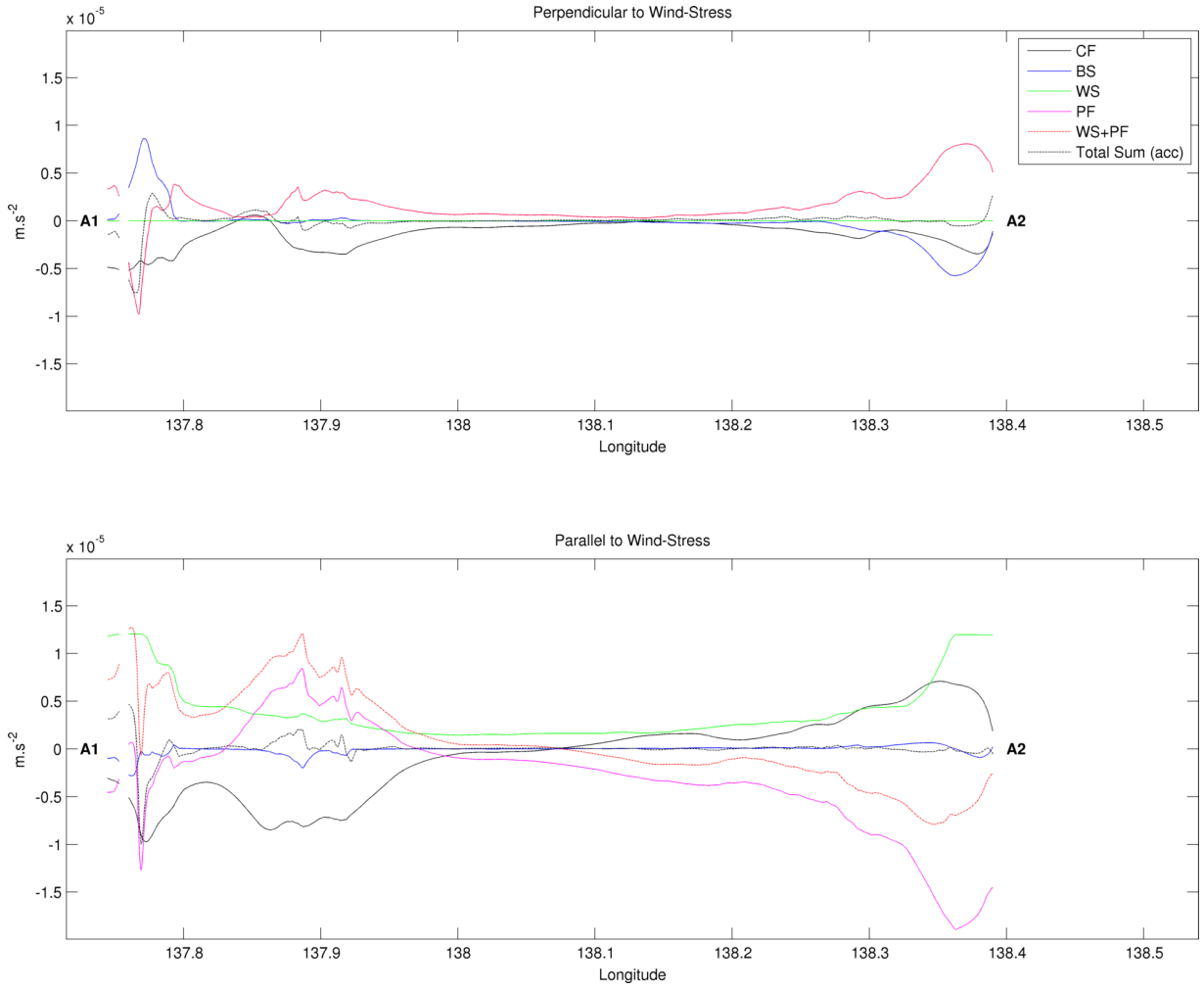

Figure B.6: Solutions for Equations 4.1a and 4.1b along cross section as defined by line A1-A2 in Figure B.5 for SW winds and baroclinic conditions. The top panel shows results for force balance perpendicular to the wind-stress, the bottom panel shows results for force balance perpendicular to the wind-stress. Momentum components are Coriolis Force (CF), Bottom Stress (BS), Wind-Stress (WS) and Pressure Force (PF).

which results from the increased flow velocities induced by the greater pressure forces.

B.2.2 Cross-Gulf Wind-Stress

The baroclinic south-easterly wind model shares its main features with the barotropic case. The key difference in terms of sea level (shown in Figure B.7) is the deepening of the depression along the mouth of the gulf, especially in the region of the deep central basin. The slight increase in sea level at the head of the gulf however remains consistent with the barotropic model, indicating an increase in sea level and hence pressure gradient from head to mouth. There is also a magnification of the depression along the entire shelf, with the sea level approximately 3 cm below mean all the way to the southern boundary of the model domain. This is also reflected through BP and IS, both of which experience lower sea level under the baroclinic case than the barotropic.

The effect of stratification can also be seen in the flow field generated in the baroclinic case (Figure B.8). Though the general pattern remains consistent, an amplification in both the northward flow on the eastern coast of GSV and the southward central flow is evident. A slight amplification is also noted on the western coast, though to a lesser extent as what is seen through the centre and in the east. This amplification of current speeds results in the southern extent of the double gyre system being driven further south, impeding somewhat on the westward flow through BP and IS. However the presence of the deep central basin in this region means that the pressure gradient begins to act against the southward flow as it approaches KI, as do the south-easterly winds. The result is that the current is turned about within the basin and re-enters the gulf, driven by the wind-stresses. This in effect keeps the double-gyre as a mostly closed loop, with the southward intrusion merely confining the westward flow closer to the north coast of KI and in turn increasing its flow velocities.

As for the up-gulf baroclinic model, the introduction in of stratification to the cross-gulf model acts to increase the pressure force through density differentials, which is countered by an increased Coriolis force. This is particularly noticeable for the cross-gulf model in the mid portion of the gulf, where the central southward flow is a more dominant feature for the baroclinic case compared to barotropic (Figure B.8 and Figure B.9).

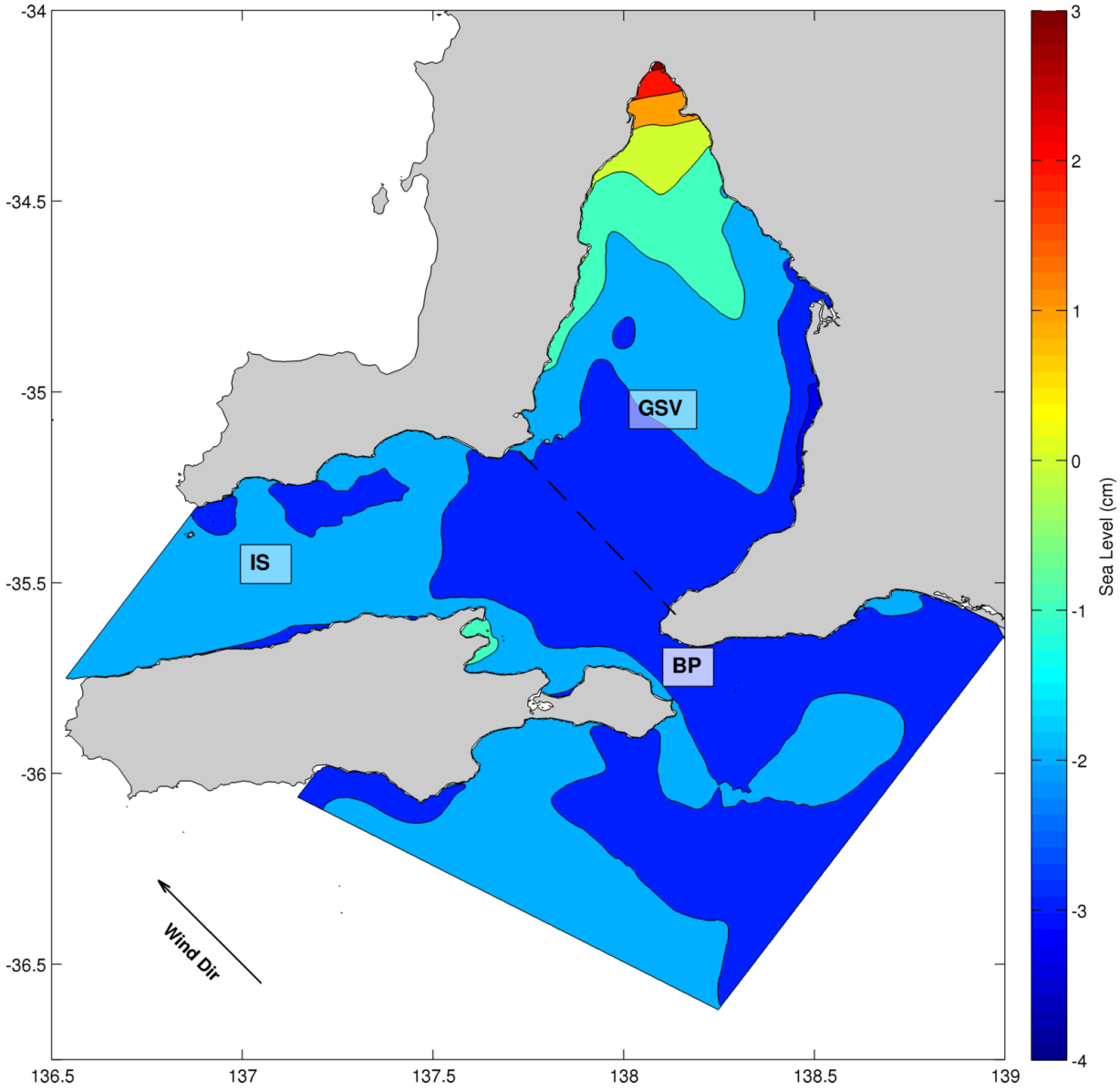

Figure B.7: Sea level for south-easterly cross-gulf wind-stress (wind-stress maximum positive = 0.05Pa) and stratified water column. Units cm deviation from mean. Contour interval 1.5 cm. The sea level under the south-easterly baroclinic case shares the same basic structure as the barotropic.

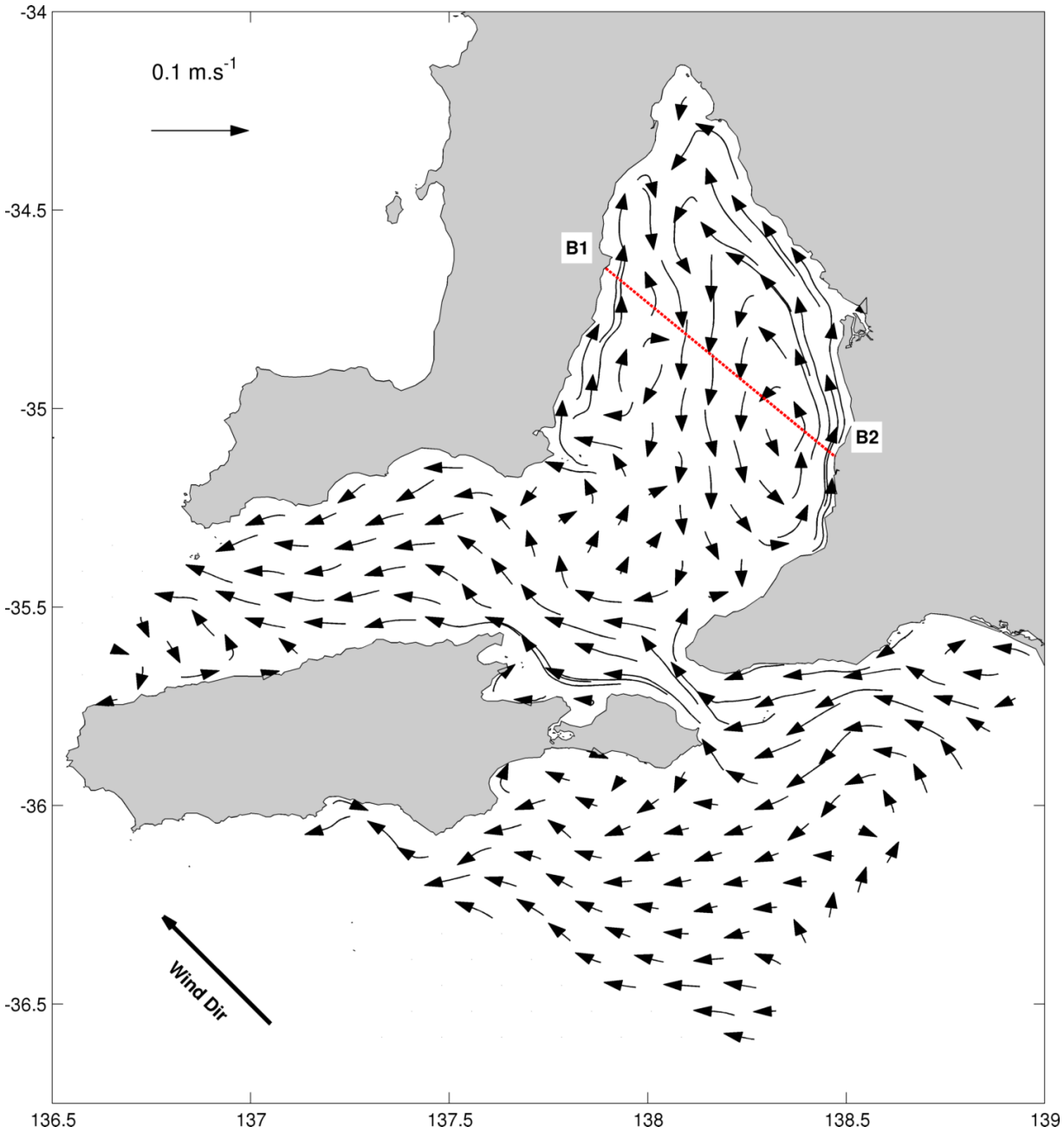

Figure B.8: Cross-gulf flow field under maximum SE wind-stress for baroclinic case. Legend arrow indicates flow velocity of 10 cm s^{-1}. The baroclinic depth integrated velocity for the south-easterly case shares the same basic pattern as the barotropic with the most notable difference being the intensification of the southward central flow, and its extension further south toward KI.

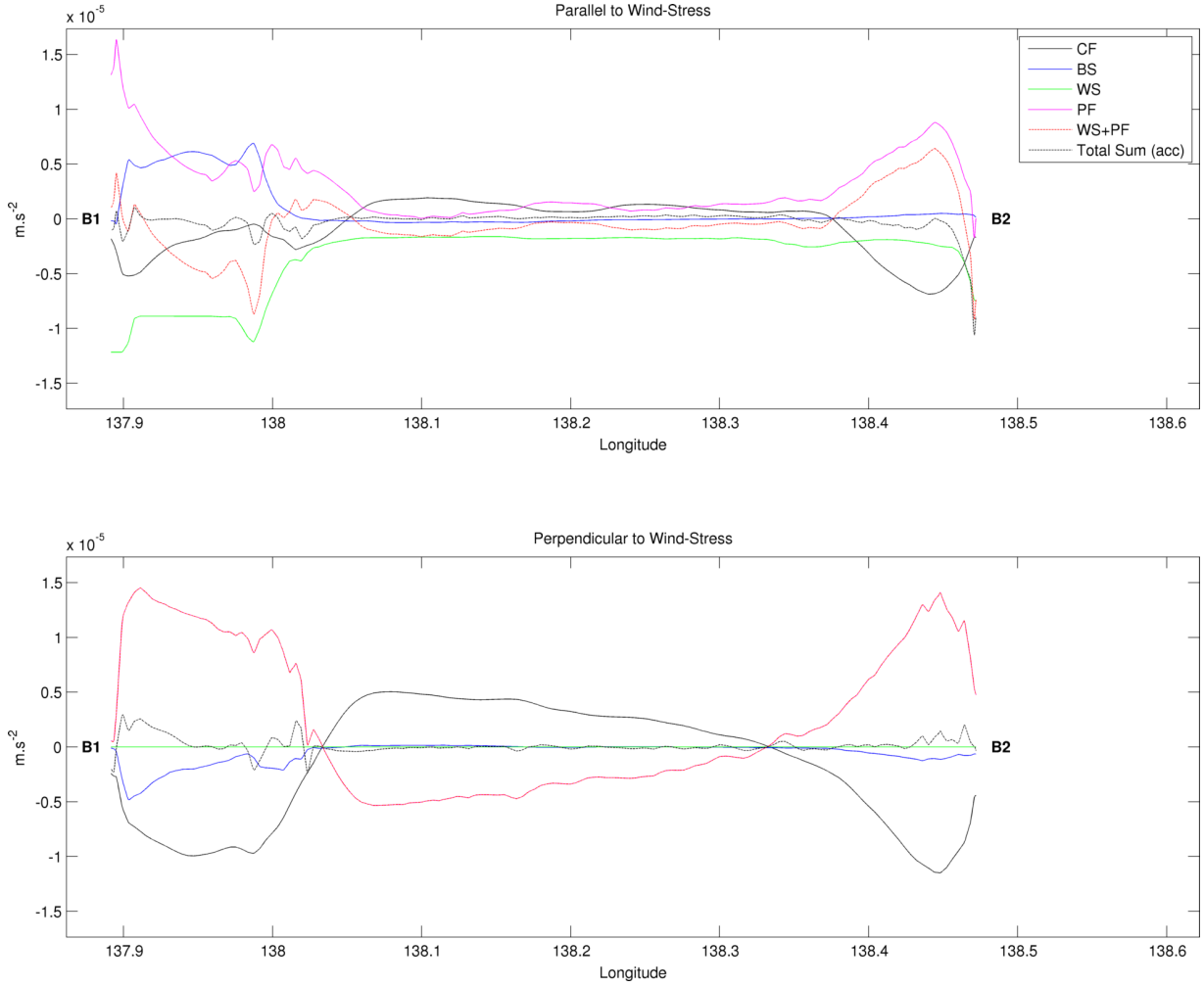

Figure B.9: Solutions for Equations 4.1a and 4.1b along cross section as defined by line B1-B2 in Figure B.8 for SW winds and baroclinic conditions. The top panel shows results for force balance perpendicular to the wind-stress, the bottom panel shows results for force balance perpendicular to the wind-stress. Momentum components are Coriolis Force (CF), Bottom Stress (BS), Wind-Stress (WS) and Pressure Force (PF).

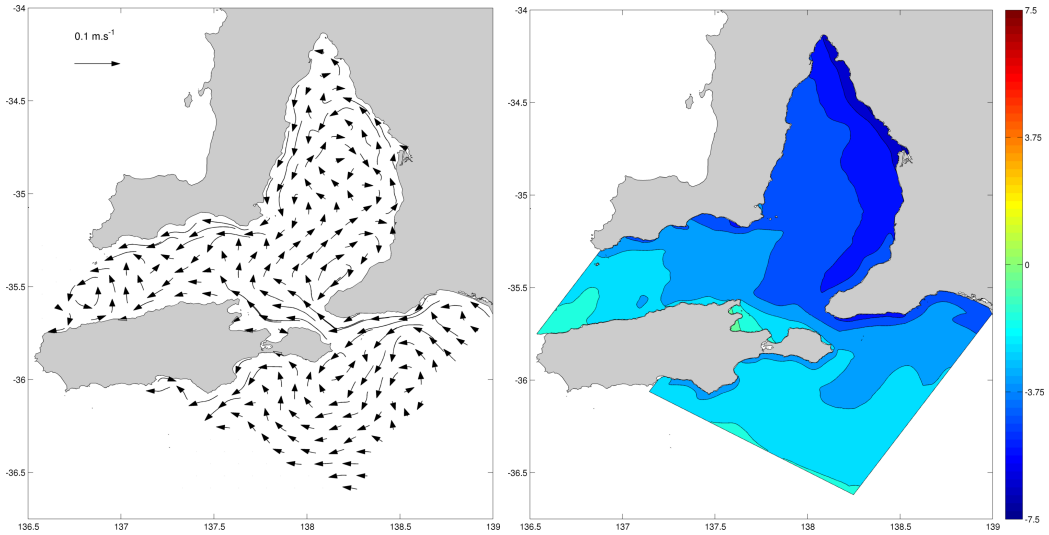

(a) (b)

Figure B.10: Velocity field (a) and sea level (b) for idealised baroclinic wind model under NE wind with 0.05 Pa stress

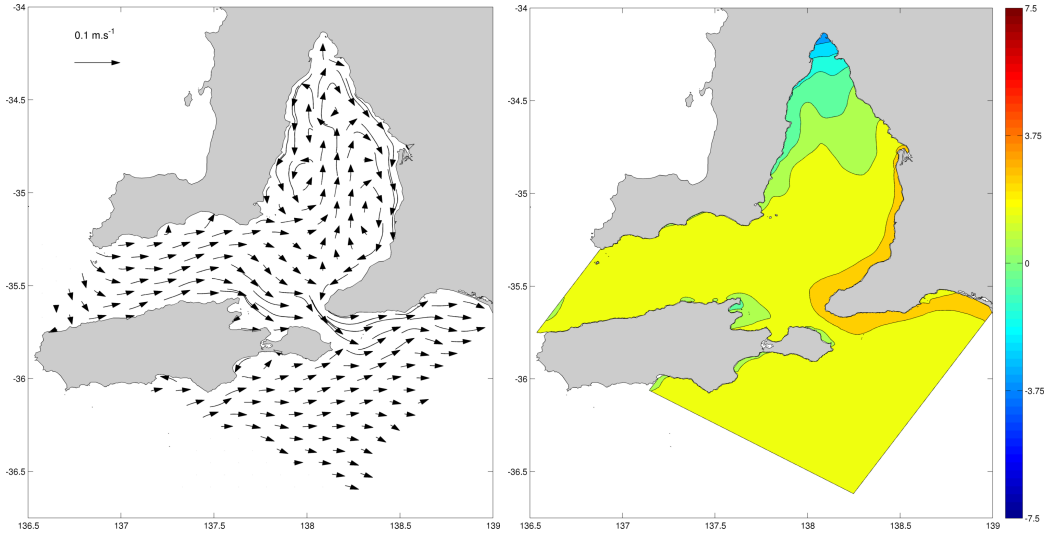

(a) (b)

Figure B.11: Velocity field (a) and sea level (b) for idealised baroclinic wind model under NW wind with 0.05 Pa stress

B.2.3 Net Transport

Figure B.12 shows the impact on transport across the mouth of the introduction of stratification to the wind-stress models. The general form of transport across the mouth of the gulf for the up-gulf case follows that of the barotropic case, with amplified magnitude. Inflow on the western side of the mouth is concentrated closer to the coast and greatly amplified over the barotropic case, while outflow on the eastern side is weaker than the barotropic case. Outflow through the central portion is magnified, due to the density driven flows arising from the stratification imposed on the system, which encourage greater transport through the central deeper portions.

The flow pattern of the cross-gulf case is impacted more than the up-gulf with the introduction of stratification. First appearances would suggest a much enhanced level of connectivity with inflows through the central portion and additional outflows on the eastern side, immediately next to a much stronger inflow around Cape Jervis. Inspection of the flow field (Figure B.8) indicates that the southern boundary of the double gyre system has moved further south. This is due to the stronger southward currents in the central portion of the gulf which are now enhanced by pressure gradients caused by the stratification. Due to the topography of the gulf however, this southward density driven flow is arrested upon entering the deep central basin of GSV, and the wind-stress then becomes dominant again, redirecting flow back in to the gulf to keep the western clockwise gyre a mostly closed system. Though the protrusion of this gyre further south than what was seen in the barotropic case is likely to enhance the mixing of gulf and shelf waters to some degree through the interaction with the strong westward currents through IS, there is no clear advective path of shelf waters in to the gulf.

It is also important to note that density gradients are expected to be much weaker during the summer months when the south-easterly cross-gulf winds are most prevalent. Therefore the flow pattern in Figure B.8 is likely a 'worst case scenario', indicating the southern limit that the double gyre system is able to reach under these wind-stress conditions.

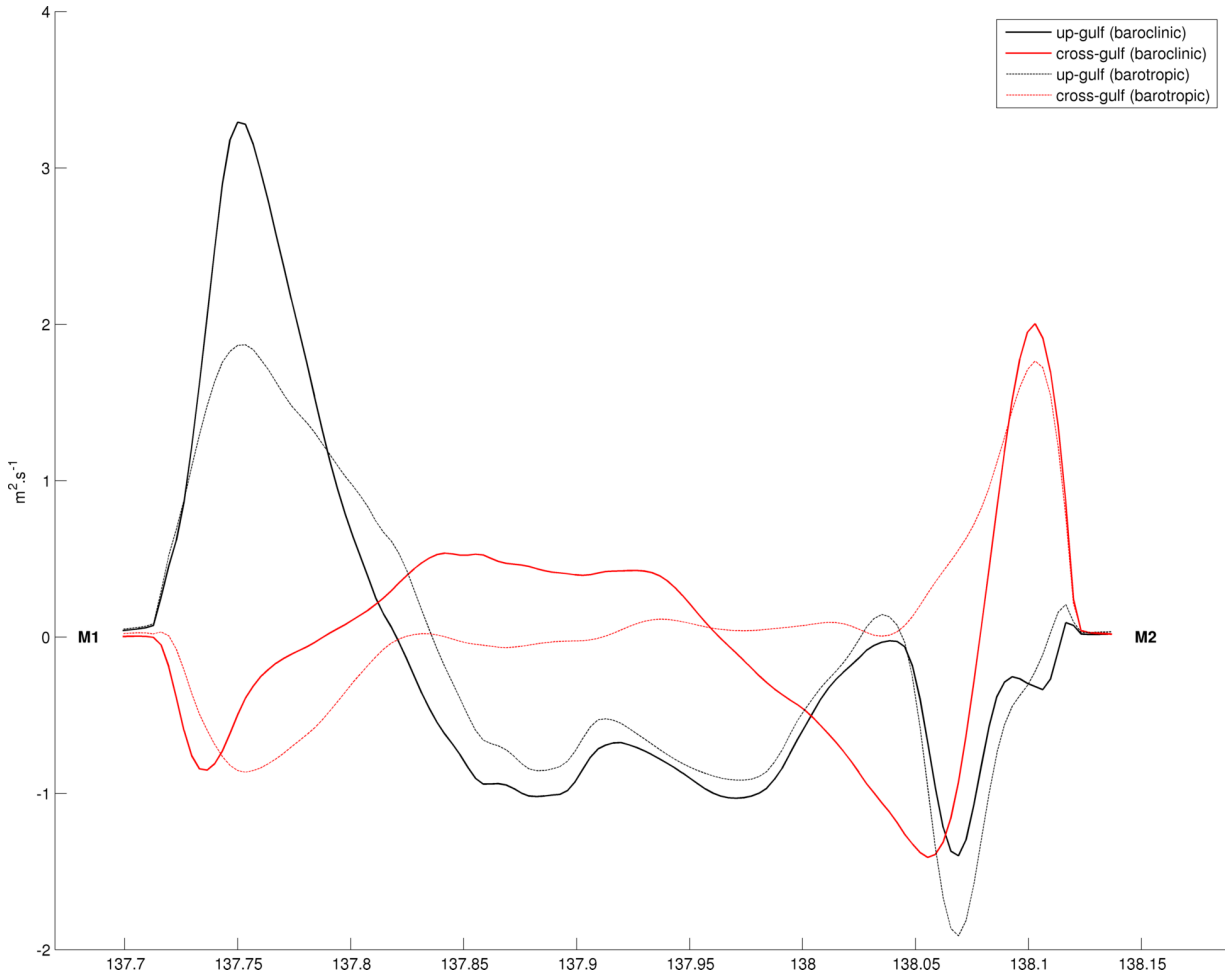

Figure B.12: Transport ($m^2.s^{-1}$) orthogonal to mouth of gulf (positive in to gulf, negative out from gulf as defined in Figure 1.1) for baroclinic wind-stress models. Up-gulf south-westerly models are shown in black and cross-gulf south-easterlies in red. Barotropic model results (dashed lines) are shown for comparison. The introduction of stratification appears to increase the intensity of cross-mouth transport for both up-gulf and cross-gulf wind-stress models.

B.3 Coastal Trapped Waves

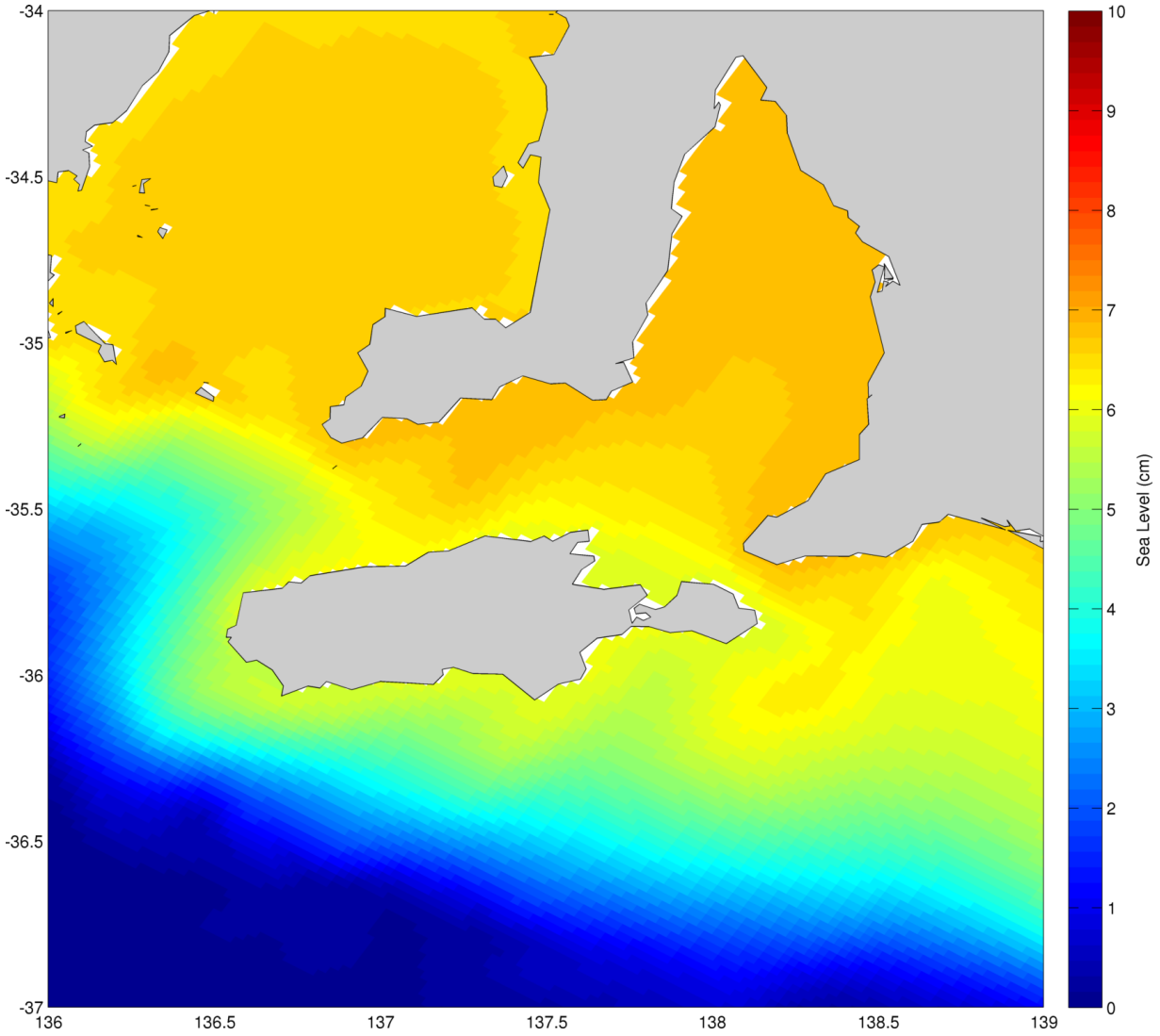

Figure B.13: Sea level (cm) results for a 10 day periodic CTW with amplitude of 10cm when sea level is maximum and positive within the gulf. Units: cm. Sea level increase within the gulf due to passing CTWs is mostly constant, with small variation shown within IS and BP.

Appendix C

Additional Geostrophic Modeling Results

C.1 Mean Summer Cross Sections

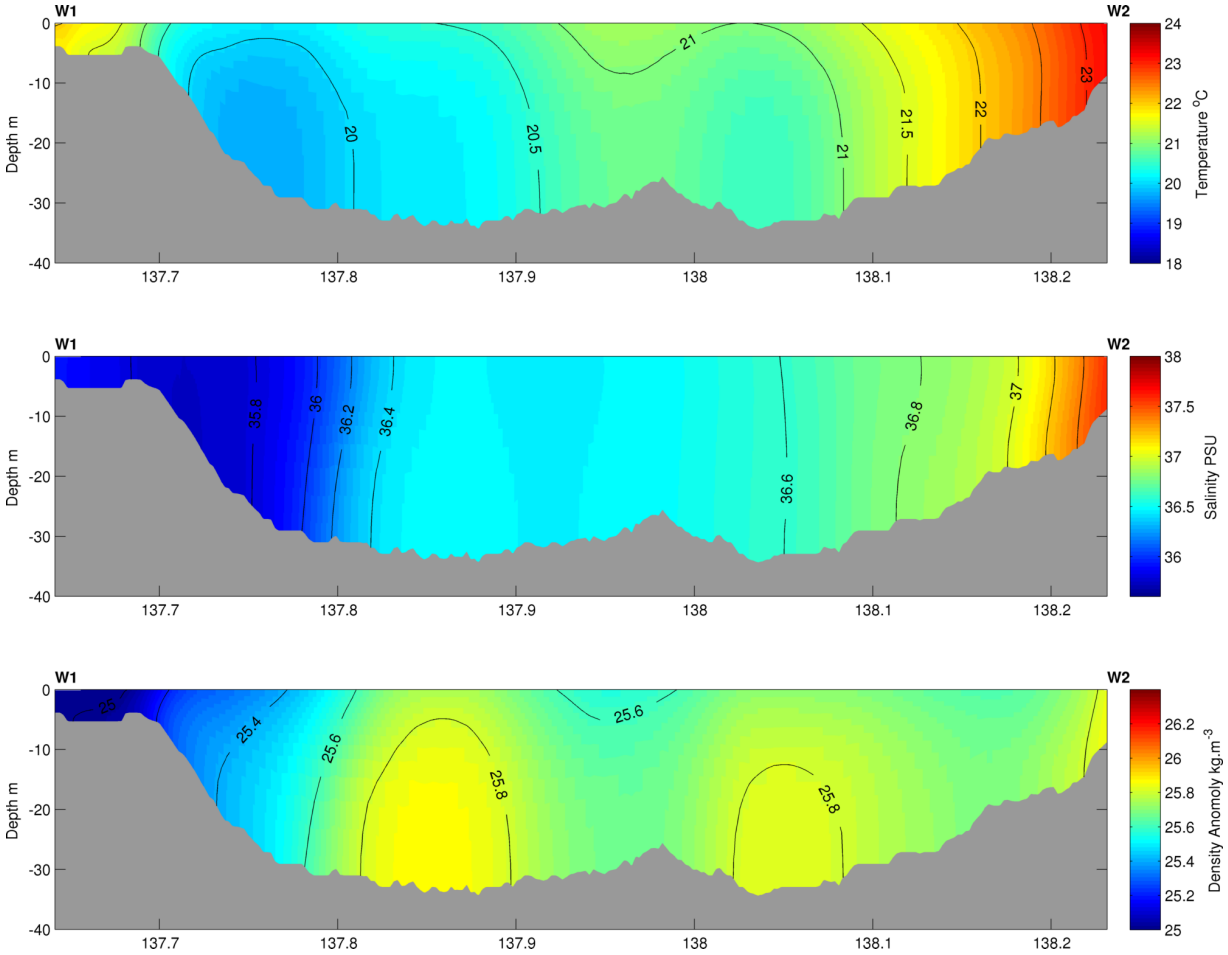

Figure C.1: Cross sections for mean seasonal summer temperature, salinity and density for section W1-W2 as marked in Figure 5.4. The temperature and salinity distribution throughout the gulf and straits results in a very weak density gradient for the western cross-section, with two bodies of almost equal density sitting within the gulf basin and in the strait.

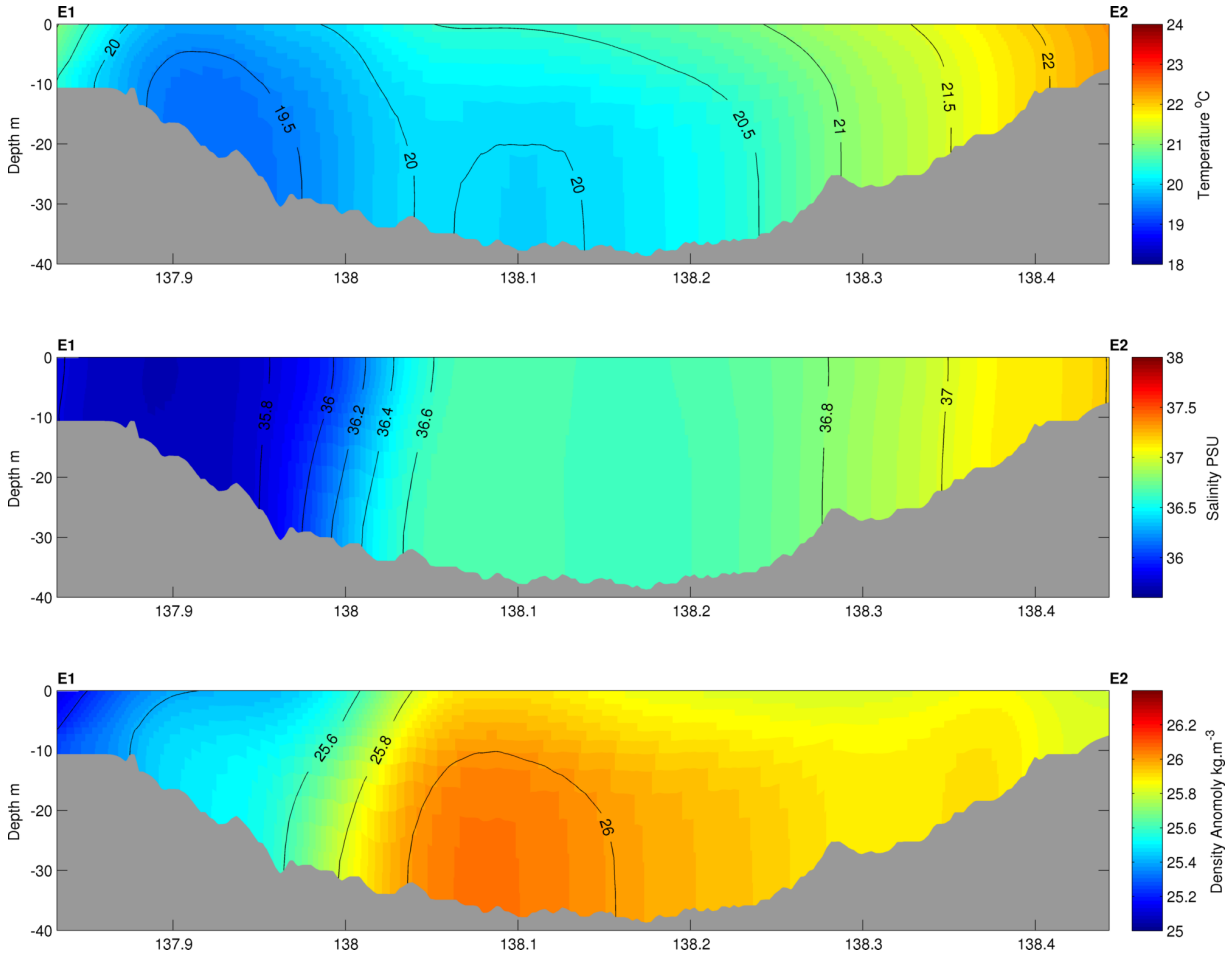

Figure C.2: Cross sections for mean seasonal summer temperature, salinity and density for section E1-E2 as marked in Figure 5.4. The eastern cross-section shows stronger temperature and salinity gradients due to the intrusion of cooler and fresher shelf waters through BP under the influence of SE wind-stresses. This results in a stronger density gradient than is seen in the west, but the denser water is centered over the deep basin within GSV and hence no pressure gradient resulting in flow out of the gulf is created.

C.2 Mean Winter Cross Sections

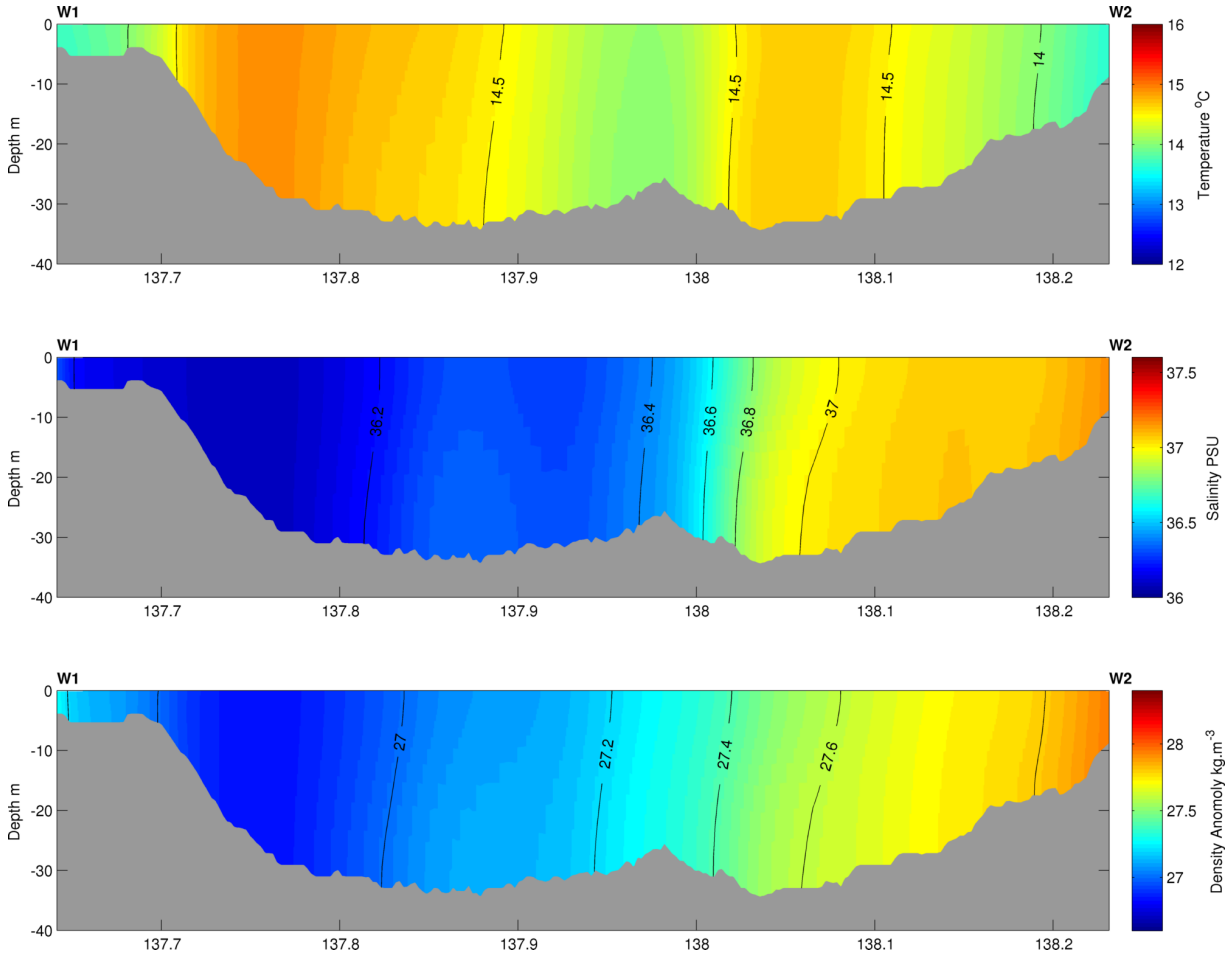

Figure C.3: Cross sections for mean seasonal winter temperature (°C, intervals 0.5), salinity (intervals 0.2) and density (kg m^{-3}, intervals 0.2) for section W1-W2 as marked in Figure 5.4. Temperature for the west cross-section varies very little while salinity shows a strong gradient towards the head. As temperature is relatively constant, the density field closely follows that of salinity, with strong positive gradient towards the head.

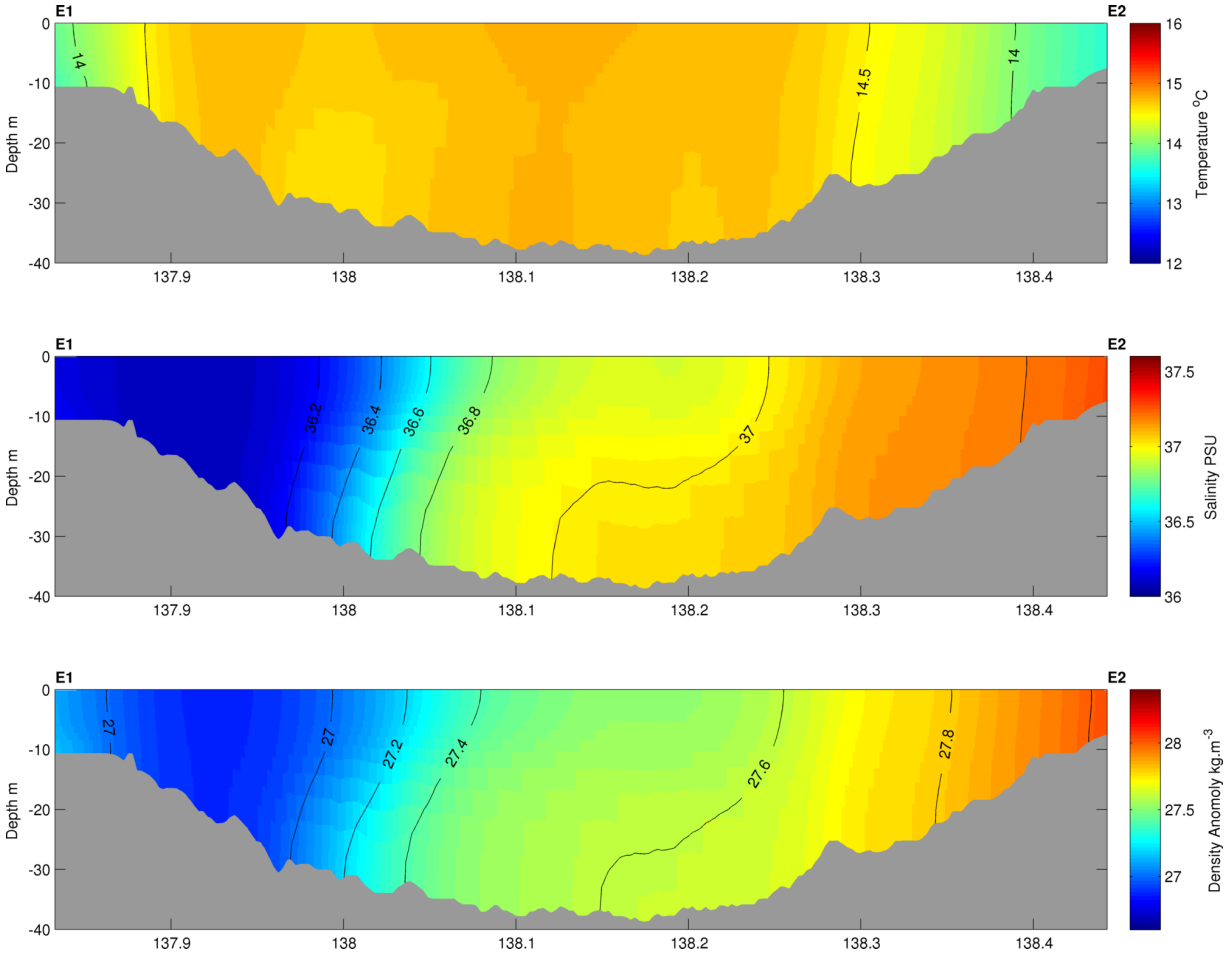

Figure C.4: Cross sections for mean seasonal winter temperature (°C, intervals 0.5), salinity (intervals 0.2) and density (kg m^{-3}, intervals 0.2) for section E1-E2 as marked in Figure 5.4. The eastern cross-section also shows very little variation in temperature and strong positive salinity gradient towards the head. However, the salinity front is both strong and closer to the mouth for the eastern cross-section compared to the western. This is also mirrored in the density field, which also shows evidence of a denser plume of water travelling from the head of the gulf to the deeper basin in the south-east.

Appendix D

Additional GSVM Calibration Information

The monthly averaged NCSS SST values were nudged toward the 10 year average climatology from NCSS in order to remove any outliers which could potentially corrupt the signal. By doing this the inter-annual variability was maintained whilst eliminating the risk of outliers polluting the SST signal. Monthly averaged data allowed the model to determine weather band frequency variability via the directly forced heat fluxes whilst ensuring the model did not stray too far from observations. The effect of this nudging can be seen in Figure D.1, which shows the best example of an undesirable outlier in the SST data (September 2010) and how the nudging reduces the effect of this. The nudging to the 10 year climatological monthly mean SST values is achieved through a simple linear equation;

$$SST_{nud} = SST_{10} + 0.4 * (SST_{monthly} - SST_{10}) \tag{D.1}$$

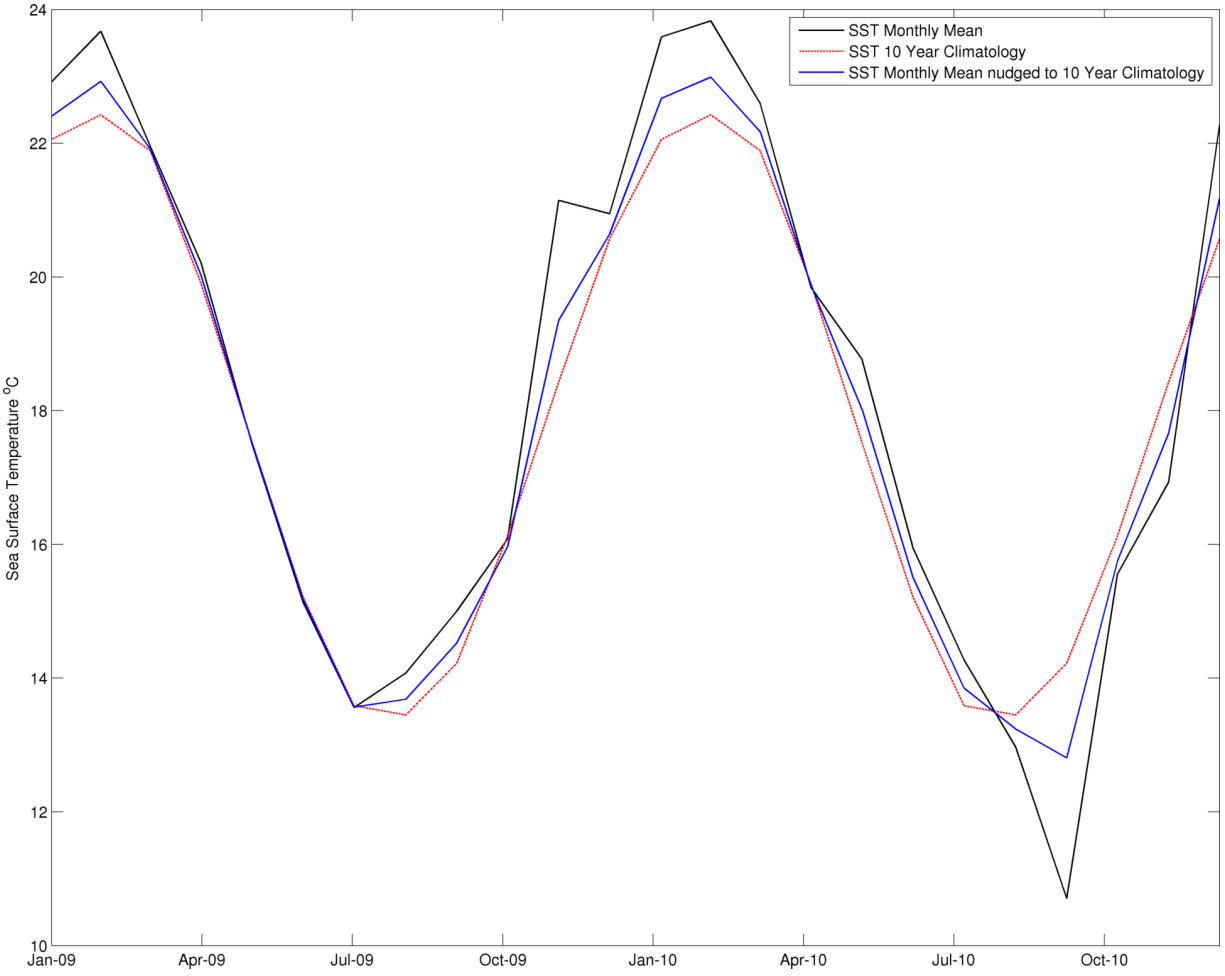

Figure D.1: Comparison of monthly mean SST values for Pt. Stanvac from NCSS data set (black line), 10 year climatology of monthly mean SST values from NCSS data set (red line) and monthly mean SST values nudged toward 10 year climatology values (blue line) which were used for SST nudging within the quasi-realistic models.

Appendix E

Index of Electronic Appendix/DVD

The contents of the electronic appendix are explained by folder name (heading, bold) and file name where appropriate.

Animations

This folder and its sub folders contain animations.

Quasi-Realistic

This folder contains all animations pertaining to the qausi-realistic model as described in Chapter 6.

Daily Mean Animation.avi

This file is the 5 panel animation showing the daily mean bottom salinity, bottom temperature, depth integrated velocity and sea level in addition to domain averaged forcing salt, heat and wind-stress fluxes as referenced in Chapter 7.

LTRANS animations

This folder contains animations showing the results of the Lagrangian float tracer studies, which were all based on the results of quasi-realistic modeling.

Seasonal Fixed Summer.avi This animation shows the float tracer results for the model which is based on the mean depth-integrated velocities over the Dec 2010, Jan 2011 and Feb 2011 period, as discussed in section 7.5.1.1.

Seasonal Fixed Winter.avi This animation shows the float tracer results for the model which is based on the mean depth-integrated velocities over the Jun, Jul and Aug 2011 period, as discussed in section 7.5.1.2.

1.5 Daily Mean Summer.avi This animation shows the float tracer results for the model which is based on the 1.5 daily averaged depth-integrated velocities over the Dec 2010, Jan 2011 and Feb 2011 period, as discussed in section 7.5.2.1.

1.5 Daily Mean Winter.avi This animation shows the float tracer results for the model which is based on the 1.5 daily averaged depth-integrated velocities over the Jun, Jul and Aug 2011 period, as discussed in section 7.5.2.2.

Bibliography

Arakawa, A, Lamb, V 1977 'Computational design of the basic dynamical processes of the UCLA general circulation model', Methods of Computational Physics, vol. 17, pp. 173-265.

Babu, M, Vethamony, P and Desa, E 2005 'Modeling tide-driven currents and residual eddies in the Gulf of Kachchh and their seasonal variability: A marine environmental planning perspective', Ecological Modeling, vol. 184, pp. 299–312.

Backhaus, J, Verduin, J 2008 'Simulating the interaction of seagrasses with their ambient flow', Estuarine, Coastal and Shelf Science, vol. 80, pp. 563-572.

Bacon, S and Fofonoff, N 1996 'Ocean Heat Flux Calculation', Journal of Atmospheric and Ocean Technology, vol. 13, pp. 1327-1329

Bao, X, Gao, G and Yan, J 2000 'Three dimensional simulation of tide and tidal current characteristics in the East China Sea', Oceanologica ACTA, vol. 24, pp. 135-149

Barnier, B, Siefridt, L and Marchesiello, P 1995 'Thermal forcing for a global ocean circulation model using a three-year climatology of ECMWF analyses', Jounral of Marine Systems, vol. 6, pp. 363-380

Blaas, M, Dong, C, Marschesiello, P, McWilliams, J and Stolzenbach, K 2007 'Sediment-transport modeling on Southern Californian shelves: A ROMS case study', Continental Shelf Research, vol. 27, pp. 832-853

Bureau of Meteorology 2012, Wind Roses for Selected Locations in Australia, Bureau of Meteorology, viewed 23/01/2015, www.bom.gov.au/climate/averages/wind/selection_map.shtml

, A 2001, 'High-Resolution Modeling of the Thermohaline and Wind-Driven Circulation', in Siedler, G, Church, J and Gould, J (eds), Ocean Circulation and Climate, Academic Press, Massachusetts, pp. 59-75

Bowers, D and Lennon, G 1990 'Tidal progression in a near-resonant system—A case study from South Australia', Estuarine, Coastal and Shelf Science, vol. 30, no. 1, pp. 17-34.

Bowers, D, Rippeth, D and Simpson, J 1991 'Tidal friction in a sea with two equal semidiurnal tidal constituents', Continental Shelf Research, vol. 11, no. 2, pp. 203-209.

Brink, K and Chapman, D 1987 'Programs for Computing Properties of Coastal-Trapped Waves and Wind-Driven Motions Over the Continental Shelf and Slope' Technical Report, Woods Hole Oceanographic Institution, Woods Hole, Massachusetts

Bryars, S, Wear, R and Collings, G 2008 'Seagrasses of Gulf St. Vincent and Investigator Strait', Chapter 11 in *Natural History of Gulf* St. *Vincent*, Royal Society of South Australia, pp. 132-147.

Bye, J 1976 'Physical Oceanography of Gulf St. Vincent and Investigator Strait' In. *Natural History of the Adelaide Region*. South Australia: Royal Society of South Australia

Bye, J and , K 2006 'Physical Oceanography' in: Natural History of Gulf St. Vincent, Royal Society of South Australia, pp. 56-70

Capet, X, McWilliams, J, Molemaker, M and Shchepetkin, A 2007 'Meososcale to Submesoscale Transition in the California Current System. Part II: Frontal Processes', Jounral of Physical Oceanography, vol. 38, pp. 44-64

Cess, R., Potter, G, Blanchet, J, Boer, G, Del Genio, A, Déqué, M, Dymnikov, V, Galin, V, Gates, W, Ghan, S, Kiehl, J, Lacis, A, Le Truet, H, Li, Z, Liang, Z, McAvaney, B, Meleshko, V, Mitchell, J, Morcrette, J, Randall, D, Rikus, L, Roeckner, E, Royer, J, Schlese, U, Sheinin, D, Slingo, A, Sokolov, A, Taylor, K, Washington, W, Wetherald, R, Yagai, I and Zhangem, M 1990, Intercomparison and interpretation of cloud-climate feedback processes in nineteen atmospheric general circulation models, Journal of Geophysical Research, vol. 95, pp. 16,601–16,615.

Chapman, R 1892 'On the dodging tides of South Australia', Australian Association of Advanced Science, vol. 4, pp. 261

Chapman, D 1985 'Numerical treatment of cross-shelf open boundaries in a barotropic coastal ocean model', Journal of Physical Oceanography, vol. 15, pp. 1060–1075.

Cheng, R, Casulli, V and Gartner J 1993 'Tidal, Residual, Intertidal Mudflat (TRIM) Model and its Applications to San Francisco Bay, California', Esturine, Coastal and Shelf Science, vol. 36, pp. 235-280.

Church, J and Freeland, H 1987 'The Energy Source for the Coastal-Trapped Waves in the Australian Coastal Experiment Region', Journal of Physical Oceanography, vol. 17, pp. 289-300.

Chunyan, L, Valle-Levinson, A, Atkinson, L, Wong, K and Lwiza, K 2004 Estimation of drag coefficient in James River Estuary using tidal velocity data from a vessel-towed ADCP, Jounral of Geophysical Research, vol. 109, C03034

Colman, R 2003, A comparison of climate feedbacks in general circula- tion models, Climate Dynamics, vol. 20, pp. 865–873.

Davies, A and Lawrence, J 1995 'Modeling the Effect of Wave-Current Interaction on the Three-Dimensional Wind-Driven Circulation of the Eastern Irish Sea', Journal of Physical Oceanography, vol. 25, pp. 29-45

Easton, A 1978 'A Reappraisal of the Tides in Spencer Gulf, South Australia', Journal of Marine and Freshwater Research, vol. 29, pp. 467-477

Egbert, G, Bennett, A, Foreman, M 1994 'TOPEX/POSEIDON Tides Estimated Using a Global Inverse Model', Journal of Geophysical Research, vol. 99, pp. 24821-24852

Egbert, G and Erofeeva, S 2002 'Efficient Inverse Modeling of Barotropic Ocean Tides', Journal of Atmospheric and Oceanic Technology, vol. 19, pp. 183-204

Fennel, K, Wilkin, J, Levin, J, Moisan, J, O'Reilly, J, and Haidvogel, D 2006 'Nitrogen cycling in the Middle Atlantic Bight: Results from a three-dimensional model and implications for the North Atlantic nitrogen budget', Global Biogeochemical Cycles, vol. 20, no. 3.

Fischer, B, List, E, Koh, R, Imberger, J and Brooks, N 1979 'Mixing in Inland and Coastal Waters', Academic Press Inc, San Diego, California

Fox, D, Batley, G, Blackburn, D, Bone, Y, Bryars, S, Cheshire, A, Collings, G, Ellis, D, Fairweather, P, Fallowfield, H, Harris, G, Henderson, B, Kämpf, J, Nayar, S, Pattiaratchi, C, Petrusevics, P, Towsend, M, Westphalen, G and Wilkinson, J 2005 The Adelaide Coastal Waters Study: Final Report, Canberra. CSIRO ISBN 1 921125 20 9

Gentilli, J Ed. 1971 'Climates of Australia and New Zealand' World Survey of Climatology Volume 13, Elsevier Publishing Company, Amsterdam, The Netherlands

Gill, A and Clarke A 1974 'Wind-induced upwelling, coastal currents and sea-level changes', Deep Sea Research and Oceanographic Abstracts, vol. 21, pp. 325-345.

Gill, A (Ed) 1982 'Atmoshpere-Ocean Dynamics', Academic Press, San Diego, California USA

Gils, J and Erftemeijer 2016 'Adelaide Receiving Environment Model - Phase 2 Inception Report', DELTARES

Guo, X and Valle-Levinson, A 2008 'Wind effects on the lateral structure of density-driven circulation in Chesapeake Bay', Continental Shelf Research, vol. 28, pp. 2450-2471.

Hedström, K 2010 'Technical Manual for a Coupled Sea-Ice/Ocean Circulation Model (Version 3)', U.S. Department of the Interior Minerals Management Service, Anchorage, Alaska

Hinckley, S, Napp, J, Hermann, A and Parada, C 2009 'Simulation of physically mediated variability in prey resources of larval fish: a three-dimensional NPZ model' Fisheries Oceanography, vol. 18, pp. 201-223

Horsburgh, K and Hill, A 2003 'A Three-Dimensional Model of Density-Driven Circulation in the Irish Sea' Journal of Physical Oceanography, vol. 33, pp. 343-365.

Houghton, J, Ding, Y, Griggs, D, Noguer, M, van der Linden, P, Dai, X, Maskell,K and Johnson, C (Eds.) 2001, Climate Change 2001: The Scientific Basis, pp. 49, Cambridge Univ. Press, New York.

Jones, R and Pattiaratchi, C 2005 Nearshore Currents and Surf Zone Dispersion on Adelaide Metropolitan Beaches [online]. In: Townsend, M and Walker, D (Eds). Coasts and Ports 2005 : Coastal Living - Living Coast; Australasian Conference; Proceedings. Barton, A.C.T.: Institution of Engineers, Australia, pp. 625-630

Kara, A, Wallcraft, A, Metzger, J and Hurlburt, H 2007 'Wind Stress Drag Coefficient over the Global Ocean' Journal of Climate - Notes and Correspondence, vol. 20, pp. 5856-5864

Kämpf, J, Doubell, M, Giffin, D, Matthews, R and Ward, T 2004 'Evidence of a large seasonal coastal upwelling system along the southern shelf of Australia' Geophysical Research Letters, vol. 31, L09310

Kämpf, J 2006 In-situ Field Measurements for Adelaide Coastal Waters Study - Final Technical Report. ACWS Technical Report No. 7, School of Chemistry, Physics and Earth Sciences, Flinders University, Adelaide.

Kaempf, J and Bye, J 2008 Physical oceanography. Kaempf, J, Brokensha, C and Bolton, T 2009 'Hindcasts of the fate of desalination brine in large inverse estuaries: Spencer Gulf and Gulf St. Vincent, South Australia', Desalination and Water Treatment, vol. 2, pp. 325-333.

Kämpf, J, Brokensha, C and Bolton, T 2009 'Hindcasts of the fate of desalination brine in large inverse estuaries: Spencer Gulf and Gulf St. Vincent, South Australia' Desalination and Water Treatment, vol. 2, issue 2, pp. 325 - 333

Kantha, L H and Clayson C 1994 'Numerical models of oceans and oceanic processes' In: International Geophysics Series, vol 66 Academic Press, San Diego USA

Koch, E and Gust, G 1999 'Water flow in tide- and wave-dominated beds of the seagrass *Thalassia testudinum*', Marine Ecology Progress Series, vol. 184, pp. 63-72

Krause, G and Radok, R 1977 'Long Waves on the Southern Ocean. Waves on Water of Variable Depth', Lecture Notes in Physics, vol. 64, pp. 221

Kumar, N and Feddersen, F 2015 'Midshelf to Surfzone Coupled ROMS–SWAN Model Data Comparison of Waves, Currents, and Temperature: Diagnosis of Subtidal Forcings and Response', Journal of Physical Oceanography, vol. 45, pp. 1464-1490

Large, W and Pond, S 1981 'Open Ocean Momentum Flux Measurements in Moderate to Strong Winds' Journal of Physical Oceanography, vol. 11, pp. 324-336

Li, M, Zhong, L, and Boicourt, W 2005 'Simulations of Chesapeake Bay estuary: Sensitivity to turbulence mixing parameterizations and comparison with observations' Journal of Geophysical Research, vol. 110, issue C12,

Lim, H, Chun, I, Kim, C, Park, K, Shim, J and Yoon, J 2013 'High-Resolution Operational Coastal Modeling System for the Prediction of Hydrodynamics in Korea Using a Wave-Current Coupled Model', Journal of Coastal Research, Special Issue no. 6, pp. 314-319

Liu, Y, MacReady, P, Hickey, B, Dever, E, Kosro, P and Banas, N 2009 'Evaluation of coastal ocean circulation model for the Columbia River plume in summer 2004' Journal of Geophysical Research, vol. 114, C00B04

Lu, X. and Zhang, J. 2006 'Numerical study on spatially varying bottom friction coefficient of a 2D tidal model with adjoint method' Continental Shelf Research, Vol. 26, pp. 1905-1923

Luhar, M and Nepf, H 2013 'From the blade scale to the reach scale: A characterization of aquatic vegetative drag', Advances in Water Resources, vol. 51, pp. 305-316

MacReady, P and Geyer, W 2001 'Estuarine salt flux through an isohaline surface' Journal of Geophysical Research, vol. 106, pp. 11,629-11,637

Manabe, S and Stouffer, R 1999 'The role of thermohaline circulation in climate', Tellus, vol. 51, pp. 91-109.

Marchesiello, P, McWilliams, J and Shchpetekin, A 2001 'Open boundary conditions for long-term integration of regional oceanic models', Ocean modeling, vol. 3, pp. 1-20

Mason, E, Molemaker, J, Shchepetkin, A, Colas, F, McWilliams, J 2010 'Procedures for offline grid nesting in regional ocean models', Ocean Modeling, vol. 35, pp. 1-15

Matthews, R 2009 'A Three-Dimensional Oceanographic Model of Gulf St. Vincent, South Australia: Flushing Times and Mechanisms.' PhD Thesis, Flinders University.

McInnes, K, Erwin, T and Bathols, J 2011 'Global Climate Model projected changes in 10 m wind speed and direction due to anthropogenic climate change', Atmospheric Science Letters, vol. 12, pp. 325-333

Middleton, J 2006 'The coastal-trapped wave paddle and open boundary conditions', Ocean Modelling, vol. 12, issues 1-2, pp. 224-236

Middleton, J and Guennadi, P 2003 'The mean summertime circulation along Australia's southern shelves: A numerical study', Journal of Physical Oceanography, vol. 33, pp. 2270-2287

Middleton, J and Platov, G 2005 'Hydrodynamic model of the Great Australian Bight' in Ward, T, Goldsworthy, S and Page, B (eds.), Trophodynamics of the GAB: Assessing the need for an ecological allocation in the SA Pilchard fishery, pp. 51-99.

Middleton, J, Doubell, M, James, C, Luick, J and van Ruth, P 2013 PIRSA Initiative II: carrying capacity of Spencer Gulf: hydrodynamic and biogeochemical measurement modeling and performance monitoring. Final Report for the Fisheries Research and Development Corporation, South Australian Research and Development Institute (Aquatic Sciences), Adelaide. SARDI Publication No. F2013/000311-1. SARDI Research Report Series No. 705, pp. 97

Middleton, J, Luick, J and James, C 2014 'Carrying capacity for finfish aquaculture, Part II – Rapid assessment using hydrodynamic and semi-analytic solutions', Aquacultural Engineering, vol. 62, pp. 66-78.

Middleton et al 2016 'Great Australian Bight Research Program: Final Milestone Report 1.1', *South Australian Research and Development Institute*

Mofjeld, O 1988 'Depth Dependence of Bottom Stress and Quadratic Drag Coefficient for Barotropic Pressure-Driven Currents', Jounral of Physical Oceanography, vol. 18, pp. 1658-1669

Mustafa, C 2005 'The international Standard Atmosphere (ISA)', Anadolu University, 26470 Eskisehir, Turkey. pp. 1 - 7

Mysak, L 1980 'Topographically Trapped Waves', Annual Review of Fluid Mechanics, vol. 12, pp. 45-76.

Nepf, H and Ghisalberti, M 2009 Shallow Flows Over a Permeable Medium: The Hydrodynamics of Submerged Aquatic Canopies, Transport in Porous Media, vol. 78, pp. 309-326.

Noye, B and Grzechnik, M 1995 'Tides and Current of Gulf St. Vincent, South Australia', In Aung, T [ed] Proceedings of the Ocean and Atmosphere Pacific Internation Conference, pp. 253-258

Noye, J & National Tidal Facility 1999, 'Modelling coastal sea processes: Ocean and Atmosphere Pacific: OAP 95', World Scientific Publishing, Singapore.

Nunes, R, Lennon, G and Bowers, D 1990 'Physical behaviour of a large, negative or inverse estuary' Continental Shelf Research, vol. 10, pp. 277-304

Oake, P, Sakov, P, Cahill, M, Dunn, J, Fielder, R, Griffin, D, Mansbridge, J, Ridgway, K and Schiller, A 2013 'Towards a dynamically balanced eddy-resolving ocean reanalysis: BRAN3' Ocean modeling, vol. 67, pp. 52-70

Oke, P, Griffin D, Schiller, A, Matear J, Fielder, R, Mansbridge, J, Lenton, A, Cahill, M, Chamberlain A and Ridgway K 2012 'Evaluation of a near-global eddy-resolving ocean model' Geoscientific Model Development Discussions, vol. 5, pp. 4305-4354

Parker, K, Royer, T and Deriso, R 1995 High-latitude climate forcing and tidal mixing by the 18.6-yr lunar nodal cycle and low-frequency recruitment trends in Pacific Halibut (Hippoglossus stenolepis), In Beamish, R [ed.] Climate chnage and northern fish populations, Canadian special publication of fisheries and aquatic sciences, pp. 447-459

Pattiaratchi, C and Jones, R 2005 Physical oceanographic studies of Adelaide coastal waters using high resolution modeling, in-situ observations and satellite techniques, Adelaide Coastal Waters Study: Technical Report No. 8 prepared for the Adelaide Coastal Waters Study Steering Committee. Centre for Water Research, University of Western Australia

Penven, P, Debreu, L, Marschesiello, P and McWilliams, J 2006 'Evaluation and application of the ROMS 1-way embedding procedure to the central california upwelling system', Ocean Modelling, vol. 12, pp. 157-187

Petrusevics, P 1993 'SST Fronts in Inverse Estuaries, South Australia – Indicators of Reduced Gulf-Shelf Exchange', Australian Journal of Marine and Freshwater Research, vol. 44, pp. 305-323

Platov, G and Middleton, J 2000 'A barotropic model of tides along Australia's southern shelves', Tech. Rep. AMR00/22, School of Mathematics, University of New South Wales

Roed, L and Cooper, C 1986 'Open boundary conditions in numerical ocean models', In: O'Brien (Ed.), Advanced Physical Oceanographic Numerical Modeling, NATO ASI Series C, vol. 186, pp. 411-436

Rong, Z, Hetland, R, Zhang, W and Zhang, X 2014 'Current-wave interaction in the Mississippi-Atchafalaya river plume on the Texas-Louisiana shelf', Ocean Modeling, vol. 84, pp. 67-83.

Samarasinghe, J, Bode, L and Mason, L 2003 'modeled response of Gulf St. Vincent (South Australia) to evaporation, heating and winds', Continental Shelf Research, vol. 23, pp. 1285-1313.

Schahinger, R 1987 'Structure of coastal upwelling events observed off the south-east coast of South Australia during February 1983-April 1984' Australian Journal of Marine and Freshwater Research, vol. 38, pp. 439-459

Schlag, Z and North, E 2012 'Lagrangian TRANSport model (LTRANS) v.2 User's Guide', University of Maryland Centre for Environmental Science, Cambridge, Maryland USA

Sharobeam, A and Sag, T 1977 'Numerical simulation of circulation in Gulf St. Vincent due to an idealized storm', Australian Journal of Marine and Freshwater Research, vol. 28, pp. 775–791.

Shchepetkin, A and McWilliams, J 2003 'A Method for Computing Horizontal Pressure-Gradient Force in an Oceanic Model with a Non-Aligned Vertical Coordinate', Journal of Geophysical Research, vol. 108, pp. 1-35.

Shchepetkin, A and McWilliams, J 2005 'The regional oceanic modeling system (ROMS): a split explicit, free-surface, topography-following-coordinate oceanic model', Ocean Modeling, vol. 9, no. 4, pp. 347-404.

Shchepetkin, A 2007 '10 Years of ROMS project: An overview with emphasis of what is overlooked, overdue or missing' Notes presented at: 2007 ROMS workshop (UCLA), University of Los Angeles, California USA

Signell, R, Beardsley, R, Graber, H and Capotondi, A 1990 'Effect of wave-current interaction on wind-driven circulation in narrow, shallow embayments', Journal of Geophysical Research, vol. 95, pp. 9671-9678.

de Silva Samarasinghe, J, Bode, L, and Mason, L 2003 'modeled response of Gulf St. Vincent (South Australia) to evaporation, heating and winds', Continental Shelf Research, vol. 23, no. 14, pp. 1285-1313.

Spitz, Y and Klinck, J 1998 Estimate of bottom and surface stress during a spring-neap tidal cycle by dynamical assimilation of tide guage observations in the Chesapeake Bay, Journal of Geophysical Research, vol. 103, pp. 761-782

Stammer, D, Ray, R, Andersen, O, Arbic, B, Bosch, W, Carrère, L, Cheng, Y, Chinn, D, Dushaw, B, Egbert, G, Erofeeva, S, Fok, H, Green, J, Griffiths, S, King, M, Lapin, V, Lemoine, F, Luthcke, S, Lyard, F, Morison, J, Müller, Padman, L, Richman, J, Shriver, J, Shum, C , Taguchi, E and Yi, Y 2014, ' Accuracy assesment of global barotropic ocean tide models', Reviews of Geophysics, vol. 52, pp. 243-282

Stephens, G 2005, Cloud feedbacks in the climate system: A critical review, Jounral of Climate, vol. 18, pp. 237–273

Stewart, R 2006 Light in the Ocean and Absorbtion of Light, viewed 15/04/2016, updated 15/09/2006, www.oceanworld.tamu.edu

Stocker, T and Schmitter, A 1997 'Influence of CO2 emission rates on the stability of the thermohaline circulation', Nature, vol. 388, pp. 862-865.

Stouffer, R, Yin, J, Gregory, J, Dixon, K, Spelman, M, Hurlin, W, Weaver, A, Eby, M, Flato, G, Hasumi, H, Hu, A, Jungclaus, J, Kamenkovich, I, Leverman, A, Montoya, M, Murakami, S, Nawrath, S, Oka, A, Peltier, W, Robitaille, D, Sokolov, A, Vettoretti, G and Weber, S 2006 'Investigating the Causes of the Response of the Thermohaline Circulation to Past and Future Climate Changes', Journal of Climate, vol. 19, pp. 1365-1387.

Tanner, J 2005 Three decades of habitat change in Gulf St. Vincent, South Australia, Transactions of the Royal Society of South Australia, vol. 129, pp. 65-73.

Teixeira, C 2010, 'Ocean Dynamics of Spencer Gulf: a numerical study' PhD Thesis, University of New South Wales

Tronson, K 1974 'The Hydraulics of the South Australian Gulf System. I Circulation', Australian Journal of Marine and Freshwater Research, vol. 25, pp. 413-426.

Ullman, S and Wilson, R 1998 Model parameter estimation from data assimilation modeling: Temporal and spatial variability of the bottom drag coefficient, Journal of Geophysical Research, vol. 103, pp. 5531-5549.

Umlauf, L and Burchard, H 2003 'A generic length-scale equation for geophysical turbulence models', Journal of Marine Research, vol. 61, pp. 235-265

UNESCO 1983 'Algorithms for computation of fundamental properties of seawater, 1983' UNESCO technical paper in: Marine Sciences, vol. 44, pp. 53

Valle-Levinson, A 2008 'Density-driven exhange flow in terms of the Kelvin and Ekman numbers', Journal of Geophysical Research, vol. 113, C04001

Wang, D 1975 'Wind-Driven Circulation in the Chesapeake Bay, Winter 1975', Journal of Physical Oceanography, vol. 9, pp. 564-572.

Warner, J C, Sherwood, C R, Arango, H G and Signell, R P 2005 'Performance of four turbulence closure models implemented using a generic length scale method', Ocean modeling, vol. 8, pp. 81-113

Wijesekera, H, Allen, J and Newberger, P 2003 'Modeling study of turbulent mixing over the continental shelf: Comparison of turbulent closure schemes', Journal of Geophysical Research, vol. 108, issue c3

Winsor, P and Chapman C 2004 'Pathways of Pacific water across the Chukchi Sea: A numerical model study' Journal of Geophysical Research, vol. 109, C03002

Woodson, C 2009 Oceanographic Models and Larval Dispersal, viewed 14/01/2015, www.piscoweb.org

Zhang, L, Xianqing, L, Ping, W and Ya Ping, W 2011 'Study on linear and nonlinear bottom friction parameterizations for regional tidal models using data assimilation' Continental Shelf Research, vol. 31, pp. 555-573

Zijl, F, de Lima Rego, J, Groeneweg, J, Dijkstra, J, Chatelain, M, de Kluijver, A and van Gils, J 2014 'Adelaide Receiving Environment Model: Pilot Model set-up and evaluation', DELTARES